Seismic Soil-Structure Interaction

by

ZHAO Xingquan

A thesis submitted in partial fulfilment of the requirements for the Degree of Doctor of Philosophy at the University of Canterbury

December 1989

Abstract

A time domain analysis procedure and computational models for seismic soil-structure interaction are presented in this work. The time domain analysis technique makes it possible to take the nonlinearity of the soil and the upper structure into account in the soil-structure interaction analysis.

The boundary element method has been used to model the far-field soil which has been shown to be very effective for a surface foundation or an embedded foundation in a linearly elastic half space. A simplified vertical energy transmitting boundary has been developed for a large near-field in which nonlinear finite elements are used. This simplified vertical boundary requires much less computational effort than that required by the boundary element method because no numerical transformation is required.

The bounding surface plasticity model has been implemented for the solid finite elements of the near-field soil and the beam elements of the upper structure. This model can also be used in the free field analysis.

An approximate model for the far-field dynamic stiffness matrix has been proposed for the time domain analysis. By specifying the dynamic stiffness matrix of the far-field at the fundamental frequency of the soil-structure system, a nonlinear analysis of the near-field and the upper structure can be performed. Techniques to avoid the unstable solution of the approximate model are also given.

Various partitioned analysis procedures are discussed and a numerical evaluation of the stabilities and their accuracies are presented.

An primary investigation of the soil-structure interaction effects is performed for two sites. Period shift due to the presence of the flexible soil has a very strong influence on the structural responses and the large structural displacements relative to the free field caused by the soil-structure interaction were found to be responsible for the pounding of adjacent structures. The soil nonlinearity has been found to be an important factor for the foundation failure under seismic loading.

Acknowledgement

This research was carried out at the Department of Civil Engineering, University of Canterbury under the overall guidance of Professor R. Park, the Head of the Department.

I wish to thank Dr. A.J. Carr, the main supervisor of the research project, and Dr. P.J. Moss, the co-supervisor of the project, for their invaluable advice and encouragement which have been of fundamental importance in completing this work.

Thanks are due to Dr. A. Bhimaraddi and Dr. R.O. Davis for their invaluable discussions.

Thanks are also due to Professor Gao Boyang (高伯扬) and Professor Shen Shizhao (沈世钊) of the Harbin Architectural and Civil Engineering Institute, Harbin, for their support and encouragement.

Grateful thanks are extended to the academic staff and fellow post-graduate students for their assistance. Special thanks are given to Mr. B. Hutchison for his assistance on the computer work and Mrs. V. Grey for her drawing.

I am very grateful to the Sisters in Villa Maria for their generous support, especially to Sisters Anne McLaughlin, Murry George, Marian Maxwell, Joan Kinney, Juliana Gallagher, Liguori Fox and Benedict Mcquillan.

I express my sincerest gratitude to Mr. J.B. Dunne for his most generous support and the arrangement of the accommodation.

Special thanks are due to Dr. Yan Hui Wang for her invaluable support and a great deal of encouragement.

The deepest gratitude is given to my parents for their precious support and constant encouragement.

Table of Contents

Table of Principal Symbols

$\{\ \}$	Column vector.
$[\ ]$	Matrix or submatrix.
$< >$	Step function operator.
α	Constant for the Newmark numerical integration.
δ	Constant for the Newmark numerical integration.
γ	Shear strain.
δ_{ij}	Kronecker delta symbol.
ϵ^e	Elastic strain
ϵ^p	Plastic strain
ϵ_{ij}	Strain tensor.
σ_{ij}	Stress tensor.
τ	Shear stress or time in a convolution integral.
λ	Lame constant or the slope of the normal consolidation line of soils.
κ	The slope of the swelling line of soils
υ	Poisson's ratio.
ρ	Mass density.
ζ	Damping ratio.
ϕ	Curvature.
(ϕ)	Modal shapes.
(Φ)	Modal shapes for a fixed base structure.
θ	Beam end rotation.
ω	Circular frequency.
Δt	Time increment.
∂	Partial differential operator.
∇^2	Laplacian differential operator.
Ω	Rotation strain.
η	Stress invariant ratio.
A_p	The amplitude of incident dilatational wave.
B_p	The amplitude of reflected dilatational wave.
A_{sv}	The amplitude of incident shear wave.
B_{sv}	The amplitude of reflected shear wave.
$[C]$	Damping matrix
c	Phase velocity.
c_s	Shear wave velocity.

c_p	Dilatational wave velocity.
d	The depth of a layer or the prefix for incremental quantities.
D_{ijkl}	Forth order tensor for the elastic material's property.
[D]	Constitutive matrix.
e	Void ratio.
EI	Flexural stiffness of a beam section.
E^h	Material parameter of a beam section.
E^p	Plastic modulus of a beam section.
E^p_o	Slope of the bounding line for a beam section.
e^p	Plastic void ratio.
f	Mode of the normal vector of a yielding function.
[F]	Flexibility matrix.
{F}	Nodal forces in the frequency domain.
F( )	Yielding function.
F_f( )	Fourier transform operator.
$[F^g_{bb}]$	Flexibility matrix of the ground.
$[g_u]$	Green's function for displacement.
$[g_t]$	Green's function for surface traction.
G	Shear modulus.
H	Plastic modulus.
H^b	Plastic modulus of the bounding surface.
h	Material parameter of soils.
i	Imaginary unit, ie., $\sqrt{-1}$.
J_o	Hardening parameter of soils.
J_1	The first stress invariant.
J_2	The deviatoric stress invariant.
J_3	The determinant of the deviatoric stress matrix.
k	Wave number.
K	Bulk modulus for soils, or plastic modulus for beam elements.
[K]	Static stiffness matrix.
L	Loading function.
{L}	Dilatational wave propagating direction vector.
[L]	Load shape function.
m	Material parameter for soils.
M	Material parameter for soils.
[M]	Mass matrix.
{M}	Shear wave propagating direction vector.
n_{ij}	Unit normal vector.
N	Material parameter of soils.

[N]	Displacement shape functions.
p	Mean normal effective stresses of soils.
{p}	Loads in the x-direction.
P	Surface traction in the x-direction
q	Deviatoric effective stress.
{q}	Beam end displacement vector.
{Q}	Beam end force vector.
r	Tangent of the incident angle for dilatational waves.
{r}	Load vector in the z-direction or nodal displacement vector in the time domain.
R	Surface traction in the z-direction.
{R}	Nodal force vector in the time domain.
s	Tangent of the incident angle for shear waves.
[S]	Dynamic stiffness matrix.
$[S^{e}_{bb}]$	Dynamic stiffness matrix of the ground with excavation.
$[S^{f}_{bb}]$	Dynamic stiffness matrix of the free field.
$[S^{n}_{bb}]$	Dynamic stiffness matrix of the bounded near-field soils.
t	Surface traction or time.
u	Displacement function for the x-direction in the frequency domain.
{U}	Nodal displacement vector in the frequency domain.
v	Displacement function for the y-direction in the frequency domain.
w	Displacement function for the z-direction in the frequency domain.
{W}	Nodal displacement vector in the z-direction in the frequency domain.
{z}	Modal displacement vector.

Chapter 1

Introduction

1.1 Soil-Structure Interaction Effects in a Seismic Environment

In recent years, much research has been carried out in the field of dynamic soil-structure interaction, especially where this has been concerned with the design of massive civil engineering structures such as nuclear power plants and cooling towers (L4, L5, W8, W12). The soil-structure interaction effect is also recognized as being important for everyday building structures (L4, L5, W8). The presence of the deformable soil modifies the response of the structure in two aspects. Firstly, the free-field ground motion at the site without the structure is strongly affected (O1, S7, S8). Secondly, the presence of the structure creates another source due to the structure interaction with the surrounding soil, ie., the incident seismic waves impinging on the base of the structure will be reflected and the actual base motion of the structure is different from the free-field motion at the site.

Since the late 1950's, it has been noticed that the soil conditions at the site have a strong influence on the ground motion during an earthquake (S7, S8). The maximum ground accelerations developed at two sites at about equal distances from the zone of energy release could be considerably different from each other due to the different soil deposits. Furthermore, the response spectrum from the two sites could have different characteristics. The reason for this phenomenon is that the seismic waves travel in a different manner in different media. For example, at two sites with the same bed-rock but different soil deposits on them, the seismic waves travel towards the sites from a source and impinge the surface of the bed rock. Because the two soil systems have different natural frequencies, it is very likely that low frequency components of the seismic wave will be amplified by the softer soil site while the high frequency component is amplified at the stiffer soil site.

Thus a structure with a low fundamental frequency may be severely affected where it rests on the soft soil deposits but adjacent stiffer structures on the same deposits may be hardly affected at all. Conversely, the structures with low fundamental frequency on stiffer soil deposits may be only slightly affected while adjacent stiff structures are subjected to large inertial loading (S7, S8).

The multiple reflections of seismic waves in a soil medium make it very difficult to describe the seismic wave mathematically. In most seismic engineering analyses, the soil deposits of the site are usually assumed to be much stiffer than the structure resting on the soil. The reflected waves from the structure's base are ignored. The motion that the structure's base is subjected to is assumed to be the same as the free-field ground motion and all of the input energy from the seismic excitation has to be dissipated by the inelastic deformation within the structure. This is called a single source problem. For most kinds of soil medium, the above assumption is far from realistic. The reflected waves from the structure carry a considerable amount of energy away and this is referred to as the radiation damping effect. In a layered or irregular soil medium, some secondary waves may be produced from the reflected wave and they may strike the structure again. Thus the response of the structure may be very different from the expected one.

Due to the presence of a deformable soil, the dynamic characteristics of a structure change. For example, the resonant frequency is no longer the natural frequency of the fixed base structure but the natural frequency of the soil-structure system. Usually, the natural frequency of the soil-structure system is much lower than the natural frequency of the fixed base structure. In general, the presence of deformable soil will result in a reduction of the maximum structural distortion in a seismic environment if the fundamental period of the soil-structure system is larger than the fundamental period of the site.

Because the rocking is permitted by a deformable soil, the vibration modes of the structure are different from those of the fixed base structure. For a nonlinear frame, the change of vibration modes may result in a different plastic hinge distribution. Some of the plastic hinges originally designed to dissipate the input energy may never be formed. The ductility demand may be greatly reduced for some structures and may be too high for others.

example, for the bounded near-field soil and upper structure, finite element models can be used. For the unbounded far-field soil, some other model, such as the boundary element model may be used to incorporate the energy radiation. The different parts of the soil-structure system can be discretized differently according to their accuracy requirements. For example, the upper structure is usually required to be analyzed with much more detail than the soil and thus a finer model can be used for the upper structure (W8). When the upper structure is modified during the design process or the system is analyzed under a different seismic excitation, the dynamic stiffness matrix of the far-field soil does not have to be recalculated.

If the non-linearity is restricted to the near-field and the upper structure, the substructure procedure can still give a good approximation when the total displacements are used as the basic unknowns (L5, W8). For most engineering applications, the non-linearity of the far-field soil may not affect the response of the structure very much and can be taken into account by the free-field analysis. Since seismic wave equations derived under the assumption of an elastic soil medium do not hold, the wave incidence and reflection mechanism in a nonlinear soil medium is different from that in elastic soil medium. In order to perform a nonlinear analysis by using the substructure procedure, the same incidence and reflection mechanism has to be assumed, ie., the seismic waves impinge and are reflected on the boundary between the elastic soil medium and nonlinear medium in the same manner as between two elastic regions. If the boundary used in the analysis can absorb all kinds of impinging wave completely, this assumption is realistic, because the distorted wave impinging on the boundary from the nonlinear soil region can be decomposed into the components in the form of the elastic waves with different frequencies. Thus there will be no waves reflected into the nonlinear soil region.

The maximum displacement relative to the free-field may increase if soil-structure interaction is taken into account. The seismic energy may be transferred among adjacent structures, especially where the dynamic characteristics are different, and the structure-structure interaction effects may be quite large (W13).

1.2 General Analysis Procedure

Theoretically, the easiest and most logical way to perform an analysis of soil-structure interaction in a seismic environment is to model a significant part of the soil around the structure and to apply the free-field motion at the artificial boundary (L5, W7). This direct procedure allows for nonlinear soil behaviour and can result in a true nonlinear analysis if the modelled part of soil is large enough. This problem is referred to as a source problem with the source being the external boundary. The direct procedure is not practical because the number of dynamic degrees of freedom is too great for most available programs and the computational cost can be very large. Because only a limited part of the soil can be modelled in this direct procedure, the superposition law is often assumed to be valid. In this case, a substructure procedure, which is computationally more efficient, can be employed (L5, W7).

If the motion of the soil-structure system is assumed to consist of two parts, a free-field motion and the interaction motion, the analysis can be performed by the following procedure (W8). In the first step, the free-field motion on the interface between the structure or near-field soil, which is the boundary of the soil being modelled, has to be computed and the analysis of the unbounded far-field soil is carried out without the presence of the structure. In the second step, the unbounded soil is modelled as a subsystem. The dynamic stiffness matrix of the degrees of freedom on the interface is determined. Then the interaction motion can be calculated by exerting the interaction forces resulting from the free-field motion on the interface nodes. This is a source problem and can be solved relatively easily.

The advantage of the substructure procedure is that the upper structure, near-field soil and far-field soil can be modelled by different methods. For

1.3 The Basic Governing Equation of Equilibrium of the Soil-Structure System

In order to facilitate the nonlinear dynamic soil-structure interaction analysis, the total displacement is used in the basic governing equations. At first, the formulae are given in the frequency domain and then transformed into the time domain.

In the following context, the near-field soil is regarded as an expanded part of the structure.

The equilibrium equations of the structure can be expressed in the frequency domain as (B4, L5, W8)

$$\begin{bmatrix} [S_{ss}] & [S_{sb}] \\ [S_{bs}] & [S_{bb}] \end{bmatrix} \begin{Bmatrix} (U_s^t) \\ (U_b^t) \end{Bmatrix} = \begin{Bmatrix} (F_s) \\ (F_b) \end{Bmatrix} \tag{1.1}$$

where S represents the dynamic stiffness matrix, U represents the displacement and F represents the forces applied on the structure. The superscript t stands for the total motion, the subscript s stands for the structure and the subscript b stands for the nodes on the boundary between the near-field and far-field.

The dynamic stiffness matrix [S] of the structure can be calculated from

$$[S] = -\omega^2 [M] + i\omega[C] + [K] \tag{1.2a}$$

if viscous damping is introduced, or

$$[S] = -\omega^2 [M] + (1 + 2\zeta i) [K] \tag{1.2b}$$

if hysteretic damping is introduced. Here [M], [C] and [K] represent the mass, viscous damping and static stiffness matrices, ω is the frequency and

ζ is the hysteretic damping ratio. $[S_{aa}]$, $[S_{ab}]$, $[S_{ba}]$ and $[S_{bb}]$ are submatrices of $[S]$.

In Eq. 1.1, $[F_b]$ is the interaction forces applied at the boundary and depends on the structure boundary motion relative to (U_b^g), the motion of the boundary nodes of the ground in which the near-field soil and the structure are absent. Thus it can be shown that

$$[F_b]=[S_{bb}^g]\ ((U_b^t)-(U_b^g)) \tag{1.3}$$

where $[S_{bb}^g]$ is the dynamic stiffness matrix of the ground without the near-field soil and cannot usually be written in the form of Eq. 1.2.

Substituting Eq. 1.3 into Eq. 1.1, the equilibrium equation of the soil-structure system is

$$\begin{bmatrix} [S_{bb}] & [S_{ab}] \\ [S_{ba}] & [S_{bb}]+[S_{bb}^g] \end{bmatrix} \begin{Bmatrix} (U_a^t) \\ (U_b^t) \end{Bmatrix} = \begin{Bmatrix} (F_a) \\ [S_{bb}^g](U_b^g) \end{Bmatrix} \tag{1.4}$$

In the analysis of soil-structure interaction under earthquake excitation, the only loaded nodes are often those on the interface of the far-field and near-field. Often $[F_a]$ is equal to zero and the typical form of the equation of motion is

$$\begin{bmatrix} [S_{bb}] & [S_{ab}] \\ [S_{ba}] & [S_{bb}]+[S_{bb}^g] \end{bmatrix} \begin{Bmatrix} (U_a^t) \\ (U_b^t) \end{Bmatrix} = \begin{Bmatrix} (0) \\ [S_{bb}^g](U_b^g) \end{Bmatrix} \tag{1.5}$$

The dynamic stiffness matrix of the far-field $[S_{bb}^g]$ is complex and frequency dependent. Its real part can be interpreted as generalized spring coefficients and imaginary part as generalized damping coefficients. It can be written as

$$[S_{bb}^g(\omega)] = [K_b^g b(\omega)] + i\omega[C_{bb}^g(\omega)] \tag{1.6}$$

Substituting Eq. 1.2a and Eq. 1.6, Eq. 1.5 may be written in the frequency domain as

$$(-\omega^2 \begin{bmatrix} [M_{ss}] & [M_{sb}] \\ [M_{bs}] & [M_{bb}] \end{bmatrix} + i\omega \begin{bmatrix} [C_{ss}] & [C_{sb}] \\ [C_{bs}] & [C_{bb}]+[C^g_{bb}(\omega)] \end{bmatrix}$$

$$+ \begin{bmatrix} [K_{ss}] & [K_{sb}] \\ [K_{bs}] & [K_{bb}]+[K^g_{bb}(\omega)] \end{bmatrix}) \begin{Bmatrix} (U^t_s) \\ (U^t_b) \end{Bmatrix} =$$

$$\begin{Bmatrix} (0) \\ (i\omega[C^g_{bb}(\omega)]+[K^g_{bb}(\omega)])(U^g_b) \end{Bmatrix} \tag{1.7}$$

Because the dynamic stiffness matrix is frequency dependent, the classical modes of the soil-structure system do not exist even in a entirely linear system. It is still possible however to transform the structure displacements into the modal displacements of the structure fixed at its boundary by the following transformation (W7):

$$(U^t_b) = (U^g_b) + (U_b) \tag{1.8a}$$

$$(U^t_s) = [T_{sb}](U_b) + (U^d_s) \tag{1.8b}$$

$$(U^d_s) = [\Phi](z) \tag{1.8c}$$

$$[T_{sb}] = -[K_{ss}]^{-1}\ [K_{sb}] \tag{1.8d}$$

where (U_b) is the nodal displacement on the near-field boundary relative to the ground motion, (U^d_s) is the structural displacement relative to the motion of the structure when the boundary nodal displacements are applied statically. $[T_{sb}]$ is the quasi-static transformation matrix, $[\Phi]$ is the modal shape of the soil-structure system fixed at its boundary nodes and (z) is the modal displacement. Eq. 1.7 may be rewritten in the frequency domain as

$$\left(- \omega^2 \begin{bmatrix} [I] & [\Phi]^T[M_{ss}][T_{sb}] \\ [T_{sb}]^T[M_{ss}][\Phi] & [M_{bb}]+[T_{sb}]^T[M_{ss}][T_{sb}] \end{bmatrix} \right.$$

$$\left. + i\omega \begin{bmatrix} 2[\zeta][\Omega]^{1/2} & [0] \\ [0] & [C^{\xi}_{bb}(\omega)] \end{bmatrix} + \begin{bmatrix} [\Omega] & [0] \\ [0] & [K^{\xi}_{bb}(\omega)] \end{bmatrix} \right) \begin{Bmatrix} (z) \\ (U_b) \end{Bmatrix}$$

$$= - \omega^2 \begin{Bmatrix} [\Phi]^T[M_{ss}][T_{sb}] \\ [M_{bb}]+[T_{sb}]^T[M_{ss}][T_{sb}] \end{Bmatrix} (U^{\xi}) \qquad (1.9)$$

where [I] is an identity matrix, $[\Omega]=[\Phi]^T[K_{ss}][\Phi]$, and $[\zeta]$ is a diagonal matrix whose elements are modal damping ratios if viscous damping is introduced.

Eq. 1.7 can be transformed into the time domain by the inverse Fourier transformation involving a convolution integral (W7):

$$\begin{bmatrix} [M_{ss}] & [M_{sb}] \\ [M_{bs}] & [M_{bb}] \end{bmatrix} \begin{Bmatrix} (\ddot{r}^t_s) \\ (\ddot{r}^t_b) \end{Bmatrix} + \begin{bmatrix} [C_{ss}] & [C_{sb}] \\ [C_{bs}] & [C_{bb}] \end{bmatrix} \begin{Bmatrix} (\dot{r}^t_s) \\ (\dot{r}^t_b) \end{Bmatrix}$$

$$+ \begin{bmatrix} [K_{ss}] & [K_{sb}] \\ [K_{bs}] & [K_{bb}] \end{bmatrix} \begin{Bmatrix} (r^t_s) \\ (r^t_b) \end{Bmatrix} + \begin{Bmatrix} (0) \\ (R_b) \end{Bmatrix} = \begin{Bmatrix} (0) \\ (0) \end{Bmatrix} \qquad (1.10)$$

where

$$(R_b) = \int_0^t ([K^{\xi}_{bb}(t-\tau)]((r^t_b(\tau)) - (r^{\xi}_b(\tau)))$$

$$+[C^{\xi}_{bb}(t-\tau)]((\dot{r}^t_b(\tau)) - (\dot{r}^{\xi}_b(\tau)))) d\tau \qquad (1.11)$$

where r is the displacement in the time domain and $[K^{\xi}_{bb}(t)]$ and $[C^{\xi}_{bb}(t)]$ are the dynamic stiffness matrices of a linear far-field soil with the excavation of the near-field soil in the time domain.

In most analyses, it is more convenient to use the ground motion of the free-field to evaluate the interaction forces. Eq. 1.11 can be rewritten as (W7)

$$\{R_b\} = \int_0^t (\,[K^g_{bb}(t-\tau)]\{r^t_b(\tau)\}+[C^g_{bb}(t-\tau)]\{\dot{r}^t_b(\tau)\}$$

$$-[K^f_{bb}(t-\tau)]\{\dot{r}^f_b(\tau)\}-[C^f_{bb}(t-\tau)]\{\ddot{r}^f_b(\tau)\})\,d\tau \qquad (1.12)$$

where the superscript f stands for the free-field. By using Eq. 1.12, the scattering motion does not have to be calculated, but the relationship can be found from the following equation in the frequency domain (W7),

$$[S^g_{bb}] + [S^n_{bb}] = [S^f_{bb}] \qquad (1.13)$$

$$[S^f_{bb}]\{U^f_b\} = [S^g_{bb}]\{U^g_b\} \qquad (1.14)$$

where $[S^n_{bb}]$ is the dynamic stiffness matrix of the near-field soil with only the degrees of freedom on the interface that contacts the far-field. These equations can be derived by using a sub-structure analysis on the soil system without the upper structure. Because the near-field soil is a bounded domain, its dynamic stiffness matrix can be calculated using the finite element method.

1.4 Modelling of the Near-Field Soil and the Upper structure

In the dynamic analyses of civil engineering structures, several discretized models, such as the finite difference, the finite element and the boundary element methods, have been successfully employed (B3, B10, C2, Z2). It appears that the finite element method is the most powerful one. During the design process, the structures are usually analyzed under static loading by the finite element method. During a dynamic analysis, an additional matrix, which takes the inertial effect into account, is needed. After introducing a corresponding damping mechanism, a damping matrix can be

derived. The dynamic characteristics of a structure can be fully determined by the mass, damping and static stiffness matrices and a dynamic analysis can be performed under any kind of dynamic loading. Due to its simplicity and accuracy, this procedure is superior to the "true dynamic" finite element analysis in which a dynamic element stiffness matrix is derived from the dynamic differential equilibrium equations in the frequency domain and the mass and stiffness matrices are coupled (C2).

For the mass matrix, a different set of displacement shape functions from those used in the derivation of the static stiffness matrix can be used as long as all significant inertial loading can be represented and this usually results in the lumped mass matrix. The damping matrix may be constructed on an element level in order to introduce different damping ratios for the different elements or on the structure level using Rayleigh or proportioned damping for simplicity (I1).

Often a coarser dynamic model than the static model may be preferred because the computational cost for a dynamic analysis is too high or the static model can not capture all essential dynamic responses and the dynamic model has to be established by a direct discretization (W7). In all circumstances, the discretization procedure for the near-field and the upper structure in a dynamic analysis is very similar to that used for a static analysis.

For the upper structure, many different models can be used. For a structure with a simple geometry, a shear beam model may be used when all the vertical and twisting displacements are restrained and rigid floors are assumed. For a three dimensional frame, the rigid floor assumption can still apply and result in a small dynamic system. For more complex structures, the plate element, shell element and curved beam element, or combination with some other simple element types can be used.

When a more complicated model is used, it is still possible to restrict some less important degrees of freedom or to distribute the structural mass to some master degrees of freedom to reduce the number of dynamic degrees of freedom. The simplest way may be to assume zero mass on certain degrees of freedom and use static condensation to eliminate these degrees of freedom (B3, C2). This reduction procedure does not apply to nonlinear systems where a finer model is usually required in the nonlinear region.

For the near-field soil, many kinds of elements can be used to discretize the domain. For example, in two dimensional analyses, even the combination of a simple shear beam or truss element can be used which is very simple to implement even for nonlinear analyses but may give coarse results. Usually, two or three dimensional isoparametric finite elements are recommended in which some sophisticated nonlinear constitutive law may be introduced.

It is worth noting that in certain linear soil-structure interaction analyses, the use of global generalized displacements to define the structural displacement may result in a smaller dynamic system than the finite element model. For example, in the analysis of a tall chimney, only the first 5 or 6 modes are needed to represent the structure reasonably well (L4).

1.5 Modelling of the Far-field Soil ——Energy Transmitting Boundary

In soil-structure interaction analyses, the most important and difficult task is the modelling of the far-field soil because of its unbounded nature. If a significant part of the soil is included in the model, the nature of the boundary is not important because the amplitudes of the interaction waves will be quite small when impinging on the boundary due to the material and geometry damping. From the aspect of computational cost, only a very small part of soil can be modelled. As described in Section 1.1, all of the outgoing waves from the interaction between the soil medium and the structure must travel through the artificial boundary without any significant reflection. In previous research, many different kinds of boundaries have been employed to incorporate the energy radiation and they can be catalogued into three types: elementary boundary, local boundary and consistent boundary.

In the early research on soil-structure interaction, the boundary of the model was assumed to be either fixed or totally free. All impinging waves were reflected back into the model and the reflection resulted in a distorted structural response. To improve the results, the boundary is usually located far away from the structure and high artificial material damping is introduced in order to ensure that when the reflected waves strike the base of the

structure their amplitudes are small enough to give a reasonably accurate structural response. The model leads to high computational cost and the abnormal material damping results in erroneous responses.

In order to take the energy radiation into account, another type of boundary has been used. Usually, the boundary consists of a series of dash pots and springs which are coupled only between the adjacent nodes (L6, W1). This kind boundary is called a local boundary and usually absorbs only part of the impinging waves. For example, a frequency independent viscous boundary has been extensively used in soil-structure analysis (B4, L5, S5). Infinite elements have been developed as an energy absorbing device (M1). Many other types of local boundary have been employed in the literature (L2, S11). The advantage of local boundaries is that they are easy to implement with the finite element method because they couple only the adjacent nodes on the boundary. It can be shown that the local boundaries can completely absorb only certain types of impinging waves from some angles.

In recent years, the boundary element method, a powerful numerical method to deal with an unbounded domain, has been applied to structural dynamics (B10, S12, W3, W4, W6). The boundary element model in the time domain for an uniform half space has been used in soil-structure interaction analyses (S12). The boundary element model developed by Wolf is suitable for a horizontally layered half space and can be attached to surface foundations, embedded foundations and finite element meshes (W7). It can completely absorb all kinds of impinging waves with varying angles of incidence. In the boundary element model, the dynamic stiffness matrix can be evaluated in the frequency domain or directly in the time domain and nonlinear analysis can be performed.

For comparison, the fundamental concept in both the finite element and the boundary element method will be given. In the finite element analysis, a given domain is discretized into finite number of elements and then the displacement field is constructed by using certain interpolation functions with nodal displacements as the unknown parameters. Next the boundary conditions are imposed on the constructed displacement function. Finally, the original differential equilibrium equations are satisfied by applying the principle of virtual work (B3). In the boundary element analysis, the displacement fields constructed are required to satisfy the differential equilibrium equations of a given domain and some boundary conditions under some loadings. These functions are usually referred as Green's functions.

The original differential equilibrium equations are transformed into a set of boundary integral equations by using Green's functions. Now the only requirement is that all boundary conditions have to be satisfied. The same discretization procedure can be used for the boundary of the given domain. Shape functions are used to construct the displacement on the boundary and then the boundary condition is imposed in some average sense. The interior displacement can be evaluated after all boundary unknowns are solved (B10, W7, W8).

For an unbounded domain, the boundary element method is superior to the finite element method. For wave propagation problems, it is impossible to exclude the incoming waves by the artificial boundary of a truncated finite element mesh. Conversely, it is quite easy to derive analytical solutions which satisfy all differential equations exactly in addition to the radiation condition when the soil system is under certain types of dynamic loadings. These analytical solutions can be used as the weighting functions in the indirect boundary element procedure (W7, W8). In a horizontally layered half space, the discrete form of the wave equations can be used to derive the analytical solutions under some fictitious loads with unknown amplitudes acting on the exterior of the interface between the near-field soil and far-field soil. These analytical solutions will satisfy all of the boundary conditions between the adjacent layers and free surface except those on the interface. The interface boundary conditions can be imposed in some average sense by adjusting the unknown amplitudes of the fictitious loads. Thus the displacement and force relationship on the interface can be determined. It is worth noting that for a horizontally layered half space, the analytical solution for the boundary element has to be constructed numerically.

If the near-field is modelled by finite elements and the number of the elements on the vertical boundary is large, the efficiency of the boundary element may be impaired because the Green's functions for all nodes have to be stored and a numerical transform has to be performed. The computer storage requirement increases dramatically with the increase of the number of the boundary elements on the vertical boundary. The required accuracy is hard to achieve because of error accumulation in the numerical transformation. In this case, some other kind of energy transmitting boundaries may be preferred. For example, for a horizontally layered half space, surface wave modes may be used to construct the transmitting boundary since most energy is carried away by surface waves (L5,T2). The exact modal shapes of the wave equations may

be used and the error due to discretization can be minimized. The computational cost for this boundary is much less than that for the boundary element because no numerical transformation from the wave number domain to the spatial domain is required. The boundary is considered as a special case of the boundary element for the vertical boundary in the sense of the weighting technique and numerical procedure and will be referred to as a simplified vertical boundary in what follows.

In conclusion the boundary element method may be the best way of modelling the unbounded domain when a linear elastic far-field is assumed. When the discrete form of the wave equations are used, the boundary element method can also be used for a horizontally layered half space. If linear soil is assumed, boundary elements can be directly attached to the foundation of the upper structure and thus no finite element model is needed for soils. When a large part of the soil is modeled by a finite element model to take into account the nonlinear behaviour of the soils, the partial reflection of the outgoing waves may not induce significant error in the response of the upper structure because of the material damping of the soil. In this case, a frequency independent viscous boundary may be preferred for a homogenous half space because of its simplicity and the simplified vertical boundary for a horizontally layered half space.

1.6 Prospects for a Feasible Analysis Procedure on Available Computers

In a dynamic soil-structure interaction analysis, the main computational effort is the evaluation of the dynamic properties of the upper structure and near-field soil, the calculation of the dynamic stiffness matrix of the far-field soil and the solution of the system equations. Because of the presence of the soil, the resultant dynamic system will be much larger than that for a fixed base structure. The memory required in a computer program will be greatly increased. In the evaluation of the dynamic stiffness matrix of far-field soil a substantial part of the computational effort has to be devoted to the complex transformation between the different domains, the calculation of discrete forms of the wave equations and the evaluation of Green's functions if the boundary elements are used. The boundary element

method can be used either in the frequency domain or directly in the time domain, but some of the quantities have to be computed in the frequency domain first and then transformed into the time domain. For example, if a time domain boundary element is applied, the Green's function has to be computed in the frequency domain first, as all of the discrete forms of wave equation are valid only for harmonic motions, then transformed into the time domain (W10, W11). The convolution integrals require a considerable amount of computational effort and memory. For a realistic engineering problem, it may not be practical to use the time domain boundary element for a horizontally layered half space on current computers, or at least not a practical way during the design process. It may be preferable to use the boundary element method in the frequency domain.

For a linear system, the transient analysis may be achieved by the frequency domain analysis for some initial conditions. For a nonlinear system, the analysis can only be performed by employing convolution integrals because the dynamic stiffness matrix is frequency dependent. The dynamic stiffness matrix has to be computed in the frequency domain first and then transformed into the time domain. This computation procedure reported earlier proved to be very time consuming and the transformation was numerically very difficult (Z2). It is attractive to develop an approximate model based on the frequency domain boundary element for far-field soil applicable to nonlinear structural analysis but with less computation effort than that associated with the frequency domain solution.

When the boundary elements are used to model a far-field soil, the resultant dynamic stiffness matrix has a different form from that of the near-field and upper structure. The finite element discretization results in strongly banded and sparse mass, damping and stiffness matrices. The dynamic stiffness matrix from the boundary element is a fully populated matrix but with a smaller number of degrees of freedom than for the finite element procedure. In the solution procedure, it may be not very efficient to solve the combined system equations because the resultant system have mixed characteristics. It may be more effective to use a partitioned analysis procedure which has been used successfully in fluid-structure interaction analysis (F2, P5). When an approximate model is used for the far-field soil, the partitioned analysis procedure is very easy to implement.

Chapter 2

The Theoretical Development of an Energy Transmitting Boundary —— Boundary Element Method

2.1 The Basic Wave Equation in an Infinite Domain

Wave propagation in an elastic medium is the fundamental problem of dynamic soil-structure interaction. For the sake of completeness and readability, the three dimensional wave equations in cartesian coordinates are given below (W7).

In the following expressions Cartesian tensor notation is used because of its simplicity in writing. The subscript indices (1,2,3,) represent (x,y,z) respectively.

The Kronecker delta symbol will be used,

$$\delta_{ij} = \begin{cases} 1 & \text{if } i=j \\ 0 & \text{otherwise} \end{cases}$$

The summation convention will apply, ie.,

$$a_{ii} = a_{11} + a_{22} + a_{33}$$

and

$$a_i a_i = a_1^2 + a_2^2 + a_3^2$$

When a body is under a harmonic excitation with frequency ω, the equilibrium equation of an infinitesimal rectangular parallelepiped surrounding a given point within the body is equal to

$$\sigma_{ij,j} = - \rho\omega^2 u_i \qquad (2.1)$$

where no external body forces are assumed to act on, σ is the amplitude of the stress tensor components as shown in Fig. 2.1 and the space derivatives are indicated by a comma, ie., $\sigma_{ij,j} = \partial\sigma_{ij}/\partial x_j$, ρ is the mass density and u represents displacement.

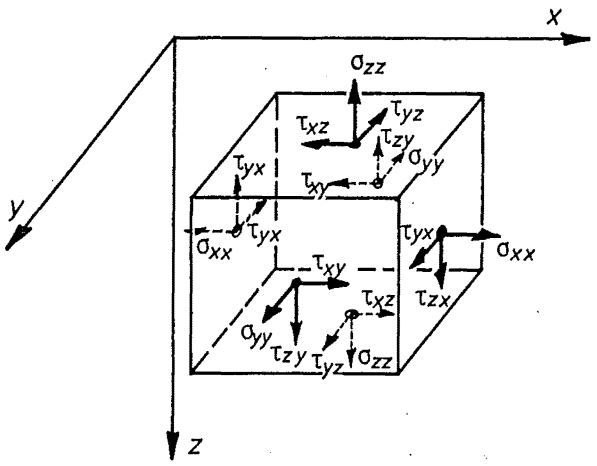

Fig. 2.1 Stress Components

The strain-displacement transformation can be written as:

$$\epsilon_{ij} = \frac{1}{2} (u_{i,j} + u_{j,i}) \qquad (2.2)$$

The constitutive equation for an elastic isotropic material is

$$\sigma_{ij} = \lambda \epsilon_{kk} \delta_{ij} + 2 G \epsilon_{ij} \qquad (2.3)$$

where λ is the Lamé constant, G is the shear modulus of the body and ϵ is the amplitude of the strain tensor components.

The surface traction vector with the amplitude t expressed in the global coordinate system acting on an infinitesimal element can be related to the element stress by the unit normal vector of the surface, ie.,

$$t_i = n_j \sigma_{ij} \qquad (2.4)$$

Substituting Eq. 2.2 and Eq. 2.3 into Eq. 2.1, the following equation can be obtained,

$$(\lambda+G) u_{k,ki} + G u_{i,kk} = - \rho \omega^2 u_i \qquad (2.5)$$

Now three displacement components can be solved by taking the boundary conditions into account. The prescribed surface traction can be enforced by using Eq. 2.4.

To solve Eq. 2.5, two displacement components have to be eliminated and the resulting differential equation is, however, of fourth order. An alternative way of solving for the displacement is to introduce new variables: the volumetric strain with amplitude e and the rotation strain vector $\{\Omega\}$ with the amplitude components Ω_1, Ω_2 and Ω_3. They are defined as

$$e = \epsilon_{ii} \tag{2.6}$$

$$\Omega_1 = \frac{1}{2} (u_{3,2} - u_{2,3}) \tag{2.7a}$$

$$\Omega_2 = \frac{1}{2} (u_{1,3} - u_{3,1}) \tag{2.7b}$$

$$\Omega_3 = \frac{1}{2} (u_{2,1} - u_{1,2}) \tag{2.7c}$$

The four unknowns can be uncoupled by a simple elimination procedure. It can be shown that the following two equations are achieved,

$$\nabla^2 e = - \frac{\omega}{c_p} e \tag{2.8}$$

$$\nabla^2 \{\Omega\} = - \frac{\omega}{c_s} \{\Omega\} \tag{2.9}$$

where ∇^2 is the Laplacian operator , c_p is called the dilatational wave velocity and is specified as

$$c_p = \left[\frac{\lambda + 2G}{\rho} \right]^{1/2} \tag{2.10}$$

c_s is called the shear wave velocity and is specified as

$$c_s = \left[\frac{G}{\rho} \right]^{1/2} \tag{2.11}$$

The wave equations Eq. 2.8 and Eq. 2.9 are linear partial differential equations of the second order.

To solve Eq. 2.8, the following trial function can be used,

$$e = - A_p \frac{i\omega}{c_p} \exp\left(- \frac{i\omega}{c_p} s_p \right) \exp(i\omega t) \tag{2.12}$$

$$s_p = (L)^T (X) \tag{2.13}$$

where $(L)^T = [L_x, L_y, L_z]$, $(X)^T = [x, y, z]$, s_p is the coordinate measured along a straight line in the propagating direction and A_p is a constant.

It can be verified that the trial solution satisfies Eq. 2.8 if the following condition holds,

$$(L)^T(L) = 1 \tag{2.14}$$

The three scalars can be considered as the direction cosines of the straight line along which s_p is measured.

The corresponding amplitudes of the displacement components are

$$U_{pj} = L_j A_p \exp\left[i\omega \left(t - \frac{s_p}{c_p}\right)\right] \tag{2.15}$$

where the subscript $j = x, y, z$ indicates the direction.

From Eq. 2.15 and Eq. 2.14 it can be shown that

$$U_{pj} U_{pj} = A_p^2 \exp\left[2i\omega \left(t - \frac{s_p}{c_p}\right)\right] \tag{2.16}$$

Eq. 2.16 represents a scalar wave propagating in the positive s_p-direction with the velocity c_p and amplitude A_p. Its displacement vector coincides with the direction of propagation. At a given time $t = t_o$, the displacement vector is constant if s_p is constant, ie., on a plane perpendicular to the propagating direction, the displacement vector is constant. The wave represented by Eq. 2.15 is called a dilatational wave or P-wave and subscript p has been introduced to indicate the wave type.

The following analogous trial solution can be used for Eq. 2.9,

$$(\Omega) = - (C) \frac{i\omega}{2c_s} \exp\left(- \frac{i\omega}{c_s} s_s \right) \exp(i\omega t) \tag{2.17}$$

$$s_s = (M)^T(X) \tag{2.18}$$

where $(M)^T = [M_x, M_y, M_z]$, $(C)^T = [C_x, C_y, C_z]$ and s_s is the coordinate measured along a straight line in the propagating direction.

The condition for Eq. 2.17 to satisfy Eq. 2.9 is

$$(M)^T (M) = 1 \tag{2.19}$$

$$(M)^T (C) = 0 \tag{2.20}$$

The three components of (M) are the direction cosines of propagation and (C) contains the amplitudes of the rotation strains.

The corresponding displacement components are

$$U_{sj} = A_{sj} \exp\left[i\omega \left(t - \frac{s_s}{c_s}\right)\right] \quad (j = x, y, z) \tag{2.21}$$

in which

$$A_{sx} = \frac{M_x M_z A_{sv} - M_y A_{sh}}{(M_x^2 + M_y^2)^{1/2}} \tag{2.22a}$$

$$A_{sy} = \frac{M_y M_z A_{sv} - M_x A_{sh}}{(M_x^2 + M_y^2)^{1/2}} \tag{2.22b}$$

$$A_{sz} = -(M_x^2 + M_y^2)^{1/2} A_{sv} \tag{2.22c}$$

$$A_{sh} = \frac{C_z}{(M_x^2 + M_y^2)^{1/2}} \tag{2.22d}$$

$$A_{sv} = \frac{M_x C_y - M_y C_x}{(M_x^2 + M_y^2)^{1/2}} \tag{2.22e}$$

where A_{sh} is the amplitude of the horizontal component and A_{sv} is the amplitude of the component lying in a plane determined by the vertical axis z and the direction of propagation. It can be shown that Eq. 2.21 represents a wave whose displacement vector lies in a plane perpendicular to the direction of

propagation with the constant velocity c_s. This type of wave is referred to as a shear wave or S-wave.

In most engineering applications, it is reasonable to assume that the P-wave and S-wave propagate in the x-z plane. Substituting $L_y = M_y = 0$ in Eq. 2.15 and Eq. 2.21 and adding the displacement caused by the P-wave and the S-wave, the total displacement components are

$$u = u(x,z) \exp(i\omega t) \tag{2.23a}$$

$$v = v(x,z) \exp(i\omega t) \tag{2.23b}$$

$$w = w(x,z) \exp(i\omega t) \tag{2.23c}$$

$$u(x,z) = L_x A_p \exp\left(-i\omega \frac{s_p}{c_p}\right) + M_z A_{sv} \exp\left(-i\omega \frac{s_s}{c_s}\right) \tag{2.23d}$$

$$v(x,z) = A_{sh} \exp\left(-i\omega \frac{s_s}{c_s}\right) \tag{2.23e}$$

$$w(x,z) = L_z A_p \exp\left(-i\omega \frac{s_p}{c_p}\right) + M_x A_{sv} \exp\left(-i\omega \frac{s_s}{c_s}\right) \tag{2.23f}$$

$$L_x^2 + L_z^2 = 1 \tag{2.23g}$$

$$M_x^2 + M_z^2 = 1 \tag{2.23h}$$

$$s_p = L_x x + L_z z \tag{2.23i}$$

$$s_s = M_x x + M_z z \tag{2.23j}$$

where u, v and w are the displacement components in x, y and z direction respectively. The in-plane and out-of-plane motions are uncoupled.

2.2 Dynamic Stiffness Matrix for Soil Element —— Discrete Form of Wave Equations

In a horizontally layered half space, the displacement solution has to satisfy all of the boundary conditions between the adjacent layers and at the free surface. This requirement makes it impractical to derive an analytical solution for the layered half space. Instead, each layer can be treated as a single element and the solution can be constructed for each element and the boundary conditions can be imposed in the same way as in the finite element method.

In the following sections, only the in-plane motion is considered because the out-of-plane motion is much simpler and the further details may be found in the reference (W7, K1).

The general definition of the stiffness matrix is the transformation matrix relating the force components and their corresponding displacement components. The dynamic stiffness matrix of a soil element will relate the stress amplitudes on the boundary to the corresponding displacement components. To enforce the boundary conditions at the top and bottom of the layer, the following condition has to be satisfied (K1, W7)

$$\frac{L_x}{c_p} = \frac{M_x}{c_s} \tag{2.24}$$

ie., the P-wave and the S-wave have the same variation in the x-direction. To solve for L_z and M_z from Eq. 2.23g and Eq.2.23h when L_x, which equals the cosine of the P-wave incidence angle, M_x, which equals the cosine of the S-wave incidence angle, are known, two roots with opposite signs for L_z and M_z can be found. They represent the waves travelling in the opposite direction. All of these waves have to be included in the solution of the wave equations.

The following notation can be defined

$$c = \frac{c_p}{L_x} = \frac{c_s}{M_x} \tag{2.25a}$$

$$k = \frac{\omega}{c} \tag{2.25b}$$

$$r = - i \left(1 - \frac{1}{L_x} \right)^{1/2} \tag{2.25c}$$

$$s = - i \left(1 - \frac{1}{M_x} \right)^{1/2} \tag{2.25d}$$

where c and k are the phase velocity and wave number, respectively. Substituting Eq. 2.25 into Eq. 2.23d and Eq. 2.23f and including the reflected waves travelling in the positive z-direction, it can be shown that

$$u(z,x) = u(z) \exp (-ikx) \tag{2.26a}$$

$$w(z,x) = w(z) \exp (-ikx) \tag{2.26b}$$

$$\begin{Bmatrix} u(z) \\ w(z) \end{Bmatrix} = \begin{bmatrix} Le^{ikrz} & Le^{-ikrz} & -Mse^{iksz} & Mse^{-iksz} \\ -Lre^{ikrz} & Lre^{-ikrz} & -Me^{iksz} & -Me^{-iksz} \end{bmatrix} \begin{Bmatrix} A_p \\ B_p \\ A_{sv} \\ B_{sv} \end{Bmatrix} \tag{2.26c}$$

where L and M are L_x and M_x , respectively. A_p, B_p, A_{sv} and B_{sv} are the amplitudes of the corresponding waves. Eq. 2.26c can be written symbolically as

$$\{U(z)\} = [GU(z)]\{A\} \tag{2.26d}$$

Substituting Eq. 2.26 into Eq. 2.2 and Eq. 2.3, the stress functions σ_{zz} and τ_{xz} can be derived as

$$\sigma_{zz}(z,x) = \sigma_{zz}(z) \exp (-ikx) \tag{2.27a}$$

$$\tau_{xz}(z,x) = \tau_{xz}(z) \exp (-ikx) \tag{2.27b}$$

$$\begin{Bmatrix} \sigma_{zz}(z) \\ \\ \tau_{xz}(z) \end{Bmatrix} = ikG \begin{bmatrix} L(1-s^2)e^{ikrz} & L(1-s^2)e^{-ikrz} & -2Mse^{iksz} & 2Mse^{-iksz} \\ \\ 2Lre^{ikrz} & -2Lre^{-ikrz} & M(1-s^2)e^{iksz} & M(1-s^2)e^{-iksz} \end{bmatrix}$$

$$\begin{Bmatrix} A_p \\ B_p \\ A_{sv} \\ B_{sv} \end{Bmatrix} \tag{2.27c}$$

ie.,

$$\{\sigma_h(z)\} = [GG_h(z)]\{A\} \tag{2.27d}$$

Setting $u(z) = U_1$ and $w(z) = W_1$ when $z = 0$ and $u(z) = U_2$ and $w(z) = W_2$ when $z = d$ where d is the depth of the layer, and substituting these into Eq. 2.26c then

$$\begin{Bmatrix} U_1 \\ iW_1 \\ U_2 \\ iW_2 \end{Bmatrix} = \begin{bmatrix} L & L & -Ms & Ms \\ -iLr & iLr & -iM & -iM \\ Le^{ikrd} & Le^{-ikrd} & -Mse^{iksd} & Mse^{-iksd} \\ -iLre^{ikrd} & iLre^{-ikrd} & -iMe^{iksd} & -iMe^{-iksd} \end{bmatrix} \begin{Bmatrix} A_p \\ B_p \\ A_{sv} \\ B_{sv} \end{Bmatrix} \tag{2.28a}$$

ie.

$$\{U^L\} = [GA]\{A\} \tag{2.28b}$$

and

$$\{U(z)\} = [GU(z)]\,[GA]^{-1}\,\{U^L\} \tag{2.28c}$$

The stresses are then determined from

$$\{\sigma^h(z)\} = [GG_h(z)][GA]^{-1}\{U^L\} \tag{2.29}$$

Applying the same procedure to Eq. 2.27c but setting $P_1 = -\tau_{xz1}$, $R_1 = -\sigma_{zz1}$ at z = 0 and $P_2 = \tau_{xz2}$, $R_2 = \sigma_{zz2}$ at z = d leads to

$$\begin{Bmatrix} P_1 \\ iR_1 \\ P_2 \\ iR_2 \end{Bmatrix} = ikG \begin{bmatrix} -2Lr & 2Lr & -M(1-s^2) & -M(1-s^2) \\ -iL(1-s^2) & -iL(1-s^2) & i2Ms & -i2Ms \\ 2Lre^{ikrd} & -2Lre^{-ikrd} & M(1-s^2)e^{iksd} & M(1-s^2)e^{-iksd} \\ iL(1-r^2)e^{ikrd} & iL(1-r^2)e^{-ikrd} & -i2Mse^{iksd} & i2Mse^{-iksd} \end{bmatrix} \begin{Bmatrix} A_p \\ B_p \\ A_{sv} \\ B_{sv} \end{Bmatrix} \qquad (2.30a)$$

i.e.,

$$\{P\} = [PA]\ \{A\} \qquad (2.30b)$$

After solving Eq. 2.28b for {A} and then substituting {A} into Eq. 2.30b, the dynamic stiffness matrix of the soil element can be obtained where

$$\{P\} = [S_{p\text{-}sv}^{L}]\ \{U^{L}\} \qquad (2.31)$$

$$[S_{p\text{-}sv}^{L}] = [PA]\ [GA]^{-1} \qquad (2.32)$$

The matrix inverse in Eq. 2.32 may be performed analytically and the explicit form of the dynamic stiffness matrix of a soil layer for in-plane motion is given in the appendix with some special cases.

The above procedure is very similar to the finite element procedure and the function

$$[N_u(z,x)] = \int_{-\infty}^{+\infty} [GU(z)]\ [GA]^{-1}\ e^{-ikx}\ dk \qquad (2.33)$$

may be interpreted as a displacement shape function which satisfies the differential equilibrium equations exactly.

For a half space, applying loads at the free surface will only develop the waves travelling in the positive z-direction. The radiation condition requires that no waves come toward the free surface from infinity. Setting A_p and A_{sv} equal zero in Eq. 2.26c and using the similar procedure eliminating B_p and B_{sv} lead to the dynamic stiffness matrix of the half space, $[S_{p\text{-}sv}^{H}]$. The

B_p and B_{sv} lead to the dynamic stiffness matrix of the half space, $[S_{p\text{-}sv}^{H}]$. The complete form is given in the appendix.

For a loaded horizontal layer, the equilibrium equation of an infinitesimal element can be expressed as (W7)

$$(\lambda + G)\, u_{k,ki} + G\, u_{i,kk} = -\rho\omega^2 u_i - p_i \tag{2.34}$$

where p_i is the loading function. For in-plane motion, all of the variables concerned with the y-direction can be omitted. If the following loading expressions are assumed

$$\begin{Bmatrix} p(z,x) \\ r(z,x) \end{Bmatrix} = \begin{Bmatrix} p(z) \\ r(z) \end{Bmatrix} e^{-ikx} \tag{2.35a}$$

and the load is linearly distributed in the vertical direction

$$\begin{Bmatrix} p(z) \\ r(z) \end{Bmatrix} = \begin{bmatrix} 1 - \frac{z}{d} & 0 & \frac{z}{d} & 0 \\ 0 & -i\left(1 - \frac{z}{d}\right) & 0 & -i\frac{z}{d} \end{bmatrix} \begin{Bmatrix} p_1 \\ ir_1 \\ p_2 \\ ir_2 \end{Bmatrix} \tag{2.35b}$$

the particular displacement solution of Eq. 2.34 is (W7)

$$\begin{Bmatrix} u^p(z) \\ w^p(z) \end{Bmatrix} = \frac{1}{k^2 G} \begin{bmatrix} -\frac{c_s^2}{r^2 c_p^2}\left(1 - \frac{z}{d}\right) & \frac{1}{kdr^2 s^2}\left(1 - \frac{c_s^2}{c_p^2}\right) \\ \frac{i}{kdr^2 s^2}\left(1 - \frac{c_s^2}{c_p^2}\right) & \frac{i}{s^2}\left(1 - \frac{z}{d}\right) \end{bmatrix}$$

$$\begin{bmatrix} -\frac{zc_s^2}{dr^2 c_p^2} & -\frac{1}{kdr^2 s^2}\left(1 - \frac{c_s^2}{c_p^2}\right) \\ -\frac{i}{kdr^2 s^2}\left(1 - \frac{c_s^2}{c_p^2}\right) & \frac{iz}{s^2 d} \end{bmatrix} \begin{Bmatrix} p_1 \\ ir_1 \\ p_2 \\ ir_2 \end{Bmatrix} \tag{2.36a}$$

where p_1 and p_2 are the load amplitudes at z = 0 and z = d acting in the x-direction, respectively, and r_1 and r_2 are the load amplitudes at z = 0 and z = d in the z-direction respectively, ie.,

$$\{U^p(z)\} = [PU(z)]\ \{p\} \tag{2.36b}$$

Substituting Eq. 2.36 into Eq. 2.3, letting $P_1 = -\tau_{xz1}$, $R_1 = -\sigma_{zz1}$, $P_2 = \tau_{xz2}$ and $R_2 = \sigma_{zz2}$, the dynamic stiffness matrix for the linearly distributed loading is

$$[SP] = \frac{G}{d}\begin{bmatrix} 1 & kd & -1 & 0 \\ kd(2-c_s^2/c_p^2) & c_s^2/c_p^2 & 0 & -c_s^2/c_p^2 \\ -1 & 0 & 1 & -kd \\ 0 & -c_s^2/c_p^2 & -kd(2-c_s^2/c_p^2) & c_s^2/c_p^2 \end{bmatrix} \tag{2.37a}$$

and

$$\{P^p\} = [SP]\{U^p\} \tag{2.37b}$$

Material damping can be taken into account by introducing complex material properties, ie., hysteretic or viscous damping is assumed. As a result G , c_p and c_s may be replaced in all of equations by (L5, S2, W7)

$$G^* = G\ (1 + 2\zeta_s) \tag{2.38a}$$

$$c_s^* = c_s\ (1 + 2\zeta_s)^{1/2} \tag{2.38b}$$

$$c_p^* = c_p\ (1 + 2\zeta_p)^{1/2} \tag{2.38c}$$

for hysteretic damping and

$$G^* = G\ (1 + 2\omega\zeta_s) \tag{2.38d}$$

$$c_s^* = c_s\ (1 + 2\omega\zeta_s)^{1/2} \tag{2.38e}$$

$$c_p^* = c_p\ (1 + 2\omega\zeta_p)^{1/2} \tag{2.38f}$$

for viscous damping, where ζ_p and ζ_s are damping ratio for the P-wave and the S-wave, respectively.

2.3 Boundary Element Method Based on Green's Function

In an elastic domain where no body forces are assumed to act, which satisfies the differential equilibrium equation Eq. 2.5, the displacement solution under a set of loads which satisfies all boundary conditions is a Green's function for this set of loads.

To present the principle of the indirect boundary element method used in the following section, a one-dimensional problem shown in Fig. 2.2 is taken as an illustration.

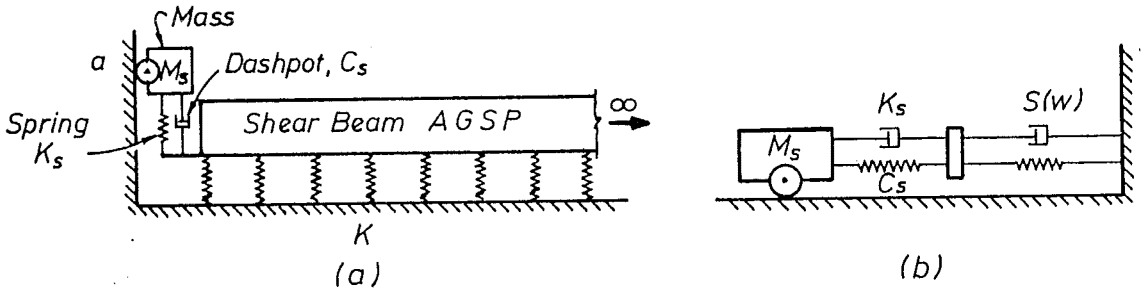

Fig. 2.2 a. Mass connected shear beam b. Dynamic model

A mass is connected through a spring K_s and a dashpot C_s with a semi-infinite shear beam with shear area A, shear modulus G, cross section area S and mass density ρ resting horizontally on an elastic foundation with spring constant k. If the shear beam is under a harmonic excitation at its end (x = 0) with amplitude P, the equilibrium equation in the vertical direction is represented by

$$W_{,xx} - \frac{k}{GA} W + \frac{\omega^2}{c_s^2} W = 0 \qquad (2.39a)$$

$$Q = GA\, W_{,x} \qquad (2.39b)$$

$$c_s = \left[\frac{GA}{\rho S}\right]^{1/2} \tag{2.39c}$$

where Q is the shear force in the beam. The solution of Eq. 2.39a which satisfies the boundary condition $W(x) = 0$ at $x = \infty$ is

$$W(x) = a \exp(-i\omega x/c) \tag{2.39d}$$

where c is the wave velocity, i.e.

$$c = \omega \left[\frac{GA}{k(a_o - 1)}\right]^{1/2} \tag{2.39e}$$

$$a_o = \frac{\omega\, GA}{c_s\, k} \tag{2.39f}$$

$$\frac{\partial W}{\partial x} = \frac{-ia}{c} \exp(-i\omega x/c) \tag{2.39g}$$

$$Q(x) = -iGA\omega\, a/c \exp(-i\omega x/c) \tag{2.39h}$$

If $W(x) = W_o$ at $x = 0$ then

$$Q(x) = -iGA\omega/c\, W_o \exp(-i\omega x/c) \tag{2.39i}$$

The dynamic stiffness coefficient of the shear beam under a point load is

$$S = (GAk(1-a_o^2))^{1/2} \tag{2.39j}$$

For an infinite beam with the same properties under a point load with an unknown amplitude q at $x = -e$, the equilibrium equation is

$$W_{,xx} - \frac{k}{GA} W + \frac{\omega^2}{c_s^2} W = q\, \delta(x+e) \tag{2.40a}$$

The solution is

$$W(x) = i \frac{qc}{2GA\omega} \exp(-i\omega e/c) \exp(-i\omega x/c) \tag{2.40b}$$

$$Q(x) = - \frac{q}{2} \exp(-i\omega e/c) \exp(-i\omega x/c) \tag{2.40c}$$

which can be referred to as the Green's functions. By enforcing the displacement $W(x) = W_o$ at $x = 0$, the unknown load amplitude can be solved from Eq. 2.40b.

$$q = -2(GAk(1-a_o^2))^{1/2} \exp(i\omega e/c)\, W_o \tag{2.40d}$$

Substituting Eq. 2.40d into Eq. 2.40c and setting $x = 0$, the relationship of the force and the displacement at the end can be specified as

$$P = (GAk(1-a_o^2))^{1/2} W_o \tag{2.40e}$$

$$S = (GAk(1-a_o^2))^{1/2} \tag{2.40f}$$

The stiffness coefficient of the beam is identical with the analytical solution because in enforcing displacement boundary conditions, no approximation is introduced.

For a three dimensional half space, the stiffness matrix of the far-field soil can be derived using the indirect boundary element method in a similar procedure to that for the semi-infinite shear beam. Firstly, distributed loads with initially unknown intensities are assumed to act on a source boundary S′ which is offset toward the far-field soil in the semi-infinite domain without excavation because the analytical solutions are available for this domain (W3, W4, W7). In the limit, the source boundary can be moved toward the interface S between near-field and far-field up to an infinitesimal distance. Because only a finite number of loads can be chosen, an interpolation function [L(s′)] has to be selected and an approximation is introduced. The distributed load can be expressed as a function of unknown nodal values {p},

$$\{p(s')\} = [L(s')] \{p\} \tag{2.41a}$$

where s' is the coordinate measured along the source boundary S'. The displacement and surface traction on the interface S for the semi-infinite domain under the load p(s') can be calculated,

$$\{U_p(s)\} = [g_u(s)]\{p\} \tag{2.41b}$$

$$\{T_p(s)\} = [g_t(s)]\{p\} \tag{2.41c}$$

where s is the coordinate measured along the interface S and $g_u(s)$, $g_t(s)$ contain the elements of Green's function.

Secondly, the prescribed displacements on the interface can be constructed as

$$\{U(s)\} = [N(s)]\{U_b\} \tag{2.41d}$$

where [N(s)] is the interpolation function and $\{U_b\}$ is the nodal displacement vector.

Finally, the displacement boundary condition on the interface S has to be enforced by the weighted-residual technique

$$\int_S [W(s)]^T(\{U(s)\} - \{U_p(s)\})\, ds \tag{2.41e}$$

where $[W(s)]^T$ contains the weighting functions. From Eq. 2.41e the unknown loads at all nodes can be determined. The weighting functions can be chosen in different possible form according to the different error distribution mechanisms. Here the matrix of the Green's functions $[g_t(s)]$ is chosen as the weighting function. From Eq. 2.41e, following equations result in

$$[G]\{p\} = [T]\{U_b\} \tag{2.41f}$$

$$[G] = \int_S [g_t(s)]_T[g_u(s)]ds \tag{2.41g}$$

$$[T] = \int_S [g_t(s)]^T[N(s)]ds \tag{2.41h}$$

The concentrated nodal forces on the interface can be obtained as

$$\{P_b\} = \int_S [N(s)]^T \{T_p(s)\} ds \tag{2.41i}$$

Substituting Eq. 2.41c and Eq. 2.41f into Eq. 2.41i the force-displacement relationship can be found as

$$\{P_b\} = [T]^T [G]^{-1} [T] \{U_b\} \tag{2.41j}$$

The stiffness matrix of the far-field is

$$[S^f_{bb}] = [T]^T [G]^{-1} [T] \tag{2.41k}$$

It can be verified that matrix [G] is symmetric and that the stiffness matrix is always symmetric.

The stiffness matrix of the free-field can be calculated by a similar procedure. Now the source boundary S' has to coincide with the interface S. In Eq. 2.41i $\{T_p(s)\}$ is replaced by $\{p(s)\}$. In order to keep the symmetry of the stiffness matrix, the weighting function is chosen as [L(s)] in Eq. 2.41e and the resultant matrices are

$$[T] = \int_S [L(s)]^T [N(s)] ds \tag{2.42a}$$

$$[G] = \int_S [L(s)]^T [g_u(s)] ds \tag{2.42b}$$

$$[S^f_{bb}] = [T]^T [G]^{-1} [T] \tag{2.42c}$$

A major point is that only one Green's function is needed and $[S^f_{bb}]$ can be calculated from Eq. 1.13 while $[S^n_{bb}]$ can be calculated by the finite element method. No significant error would be introduced by this simplified procedure except at the natural frequencies of the bounded near-field soil built in along its boundary (W7). In the case of the earthquake induced dynamic soil-structure interaction problems, the frequencies of the waves of

the interests are much lower than the natural frequencies of the near-field soil built in along its boundary.

2.4 Derivation of the Green's Function for a Two Dimensional Surface Foundation Resting on a Horizontally Layered Half Space

For a surface structure, the Green's function is easy to calculate. Firstly, the load must be transformed into the wave number domain by the Fourier transform

$$\{p(k)\} = F_t([L(x)])\ \{p\} \tag{2.43a}$$

where k is the wave number, x is the coordinate in the horizontal direction, $F_t(\ )$ stands for the Fourier transform operator, [L(x)] is the interpolation function and {p} is the unknown load parameter vector. For the out-of-plane motion, the loads will act on each element only in the y-direction and for the in-plane motion, the loads will act on each element in both the x-direction and the z-direction. Secondly, the displacement solution of the site under the loading {p(k)} is calculated by the direct-stiffness approach, ie., calculating the dynamic stiffness matrix of each layer and the half space and assembling all matrices into the global dynamic stiffness matrix resulting in the dynamic equilibrium equation (W7)

$$[S_s]\{U\} = \{Q\} \tag{2.43b}$$

where $[S_s]$ is the global stiffness matrix of the site, {U} is the displacement vector and {Q} is loading vector in which the elements corresponding to the displacements on the free surface are the loads contained in {p(k)} and all other elements are zero. The displacements at the free surface can be solved as

$$\{U_f(k)\} = [F]\{p(k)\} \tag{2.43c}$$

where [F] is the flexibility matrix corresponding to the displacements at the free surface. Finally, the inverse Fourier transform is performed on the displacements

$$\{U_f(x)\} = F_f^{-1}(\{U(k)\}) \tag{2.43d}$$

$\{U_f(x)\}$ contains the Green's function corresponding the surface displacements and can be used to calculate the dynamic stiffness matrix of the horizontally layered half space.

2.5 Derivation of the Green's Function for a Two Dimensional Foundation Embedded in a Horizontally Layered Half Space

A linearly distributed load with intensity (p) is assumed to act on a vertical line of a layer with depth d at an arbitrary depth in a horizontally layered half space. If a local x-z coordinate system is chosen for the layer, the loads at x = 0 corresponding to in-plane motion can be expressed as

$$\begin{Bmatrix} p(z,x) \\ \\ r(z,x) \end{Bmatrix} = \begin{Bmatrix} p(z) \\ \\ r(z) \end{Bmatrix} \delta(x) \tag{2.44}$$

where $\delta(x)$ is the Dirac delta function. After performing a Fourier transform, the loads have the form of Eq. 2.35 in the wave number domain. The particular solution of the displacement is given by Eq. 2.36. The global reactions can be calculated from Eq. 2.37b. In Eq. 2.36, setting z = 0 and z = d the following equation can be derived if the constant 2π in the Fourier transform is omitted

$$\begin{Bmatrix} U_1^p \\ iW_1^p \\ U_2^p \\ iW_2^p \end{Bmatrix} = \frac{1}{k^2 G} \begin{bmatrix} -\frac{c_s^2}{r^2 c_p^2} & \frac{1}{kdr^2 s^2}\left(1-\frac{c_s^2}{c_p^2}\right) & 0 & -\frac{1}{kdr^2 s^2}\left(1-\frac{c_s^2}{c_p^2}\right) \\ \frac{-1}{kdr^2 s^2}\left(1-\frac{c_s^2}{c_p^2}\right) & -\frac{1}{s^2} & \frac{1}{kdr^2 s^2}\left(1-\frac{c_s^2}{c_p^2}\right) & 0 \\ 0 & \frac{1}{kdr^2 s^2}\left(1-\frac{c_s^2}{c_p^2}\right) & -\frac{c_s^2}{r^2 c_p^2} & -\frac{1}{kdr^2 s^2}\left(1-\frac{c_s^2}{c_p^2}\right) \\ \frac{-1}{kdr^2 s^2}\left(1-\frac{c_s^2}{c_p^2}\right) & 0 & \frac{1}{kdr^2 s^2}\left(1-\frac{c_s^2}{c_p^2}\right) & -\frac{1}{s^2} \end{bmatrix}$$

$$\begin{Bmatrix} p_1 \\ ir_1 \\ p_2 \\ ir_2 \end{Bmatrix} \tag{2.45a}$$

ie.,

$$(U^p) = [UP]\ (p) \tag{2.45b}$$

Substituting Eq. 2.45b into Eq. 2.37b, the global reactions can be expressed as

$$(P^p) = [SP][UP]\ (p) \tag{2.46}$$

In the procedure similar to that used in reducing the distributed loads to nodal loads in a finite element analysis, the fixed boundary conditions at the two interfaces have to be imposed. Imposing the negative displacement from Eq. 2.45b, the reaction can be found as (W3)

$$(P^h) = -\ [S^L]\ [UP]\ (p) \tag{2.47}$$

where $[S^L]$ is the dynamic stiffness matrix of the layer. To achieve the same global displacement, the following external loads have to be applied to the soil system.

$$\{P\} = - \{P^p\} - \{P^h\} \tag{2.48a}$$

Substituting Eq. 2.46 and Eq. 2.47 into Eq. 2.48a, the total reaction of the system due to the load (p_i) applied on the ith element of the boundary is

$$\{P_i\} = [GE_i] \{p_i\} \tag{2.48b}$$

$$[GE_i] = ([S_i^L] - [SP_i]) [UP_i] \tag{2.48c}$$

where and in the following section the repeated indices do not mean summation. The global displacement field of the system (U^s) caused by the external load can be solved from

$$\{U^s\} = [F^s] \begin{Bmatrix} \{0\} \\ \{P\} \\ \{0\} \end{Bmatrix} \tag{2.49a}$$

where $[F^s]$ is the dynamic flexibility matrix of the system and equals to the inverse of the dynamic stiffness matrix of the system $[S_s]$. The displacement of the jth element on the boundary is

$$\{U_j^s\} = [F_{ji}^s] \{P_i\} \tag{2.49b}$$

where $[F_{ji}^s]$ is a submatrix from the system flexibility matrix $[F^s]$. Substituting Eq. 2.49b into Eq. 2.28c, the displacement function in the element j due to the loading on the element i is

$$\{U(z)_j\} = [GU(z)_j] [GA_j]^{-1} [F_{ji}^s] [GE_i] \{p_i\} \qquad (i \neq j) \tag{2.50}$$

For the ith element, the local response due to the particular solution has to be added. Substituting Eq. 2.36b into Eq. 2.28c, the local response is

$$\{U(z)_i^h\} = - [GU(z)_i] [GA_i]^{-1} \{U_i^p\} \tag{2.51}$$

where the negative sign is due to the imposition of the fixed interface boundary conditions. Substituting Eq. 2.45b into Eq. 2.51 and adding Eq. 2.36b, the local response is determined from

$$\{U(z)_i^L\} = ([PU(z)_i] - [GU(z)_i] [GA_i]^{-1} [UP_i]) \{p_i\} \tag{2.52}$$

Finally, adding the local response to Eq. 2.50, the total displacement due to the linearly distributed load on the element is found

$$\{U(z)_i\} = \{[GU(z)_i][GA_i]^{-1}([F_{sii}][GE_i]-[UP_i])+[PU(z)_i]\}\ \{p_i\} \qquad (2.53)$$

Eq. 2.50 and 2.53 are implicit functions of the wave number k and have to be transformed into the spatial domain by the inverse Fourier transform.

$$\{U(z,x)_i\} = F_f^{-1}\ (\{U(z)_i\}) \qquad (2.54)$$

Eq. 2.54 contains the elements of the Green's function for the displacement field in the frequency domain.

The Green's function for the surface traction on the interface of the near-field and far-field can be derived analogously. From Eq. 2.4, the components of the surface traction can be related to the stress components by a unit normal vector of the interface. The stress field can be derived from the corresponding displacement field by substituting Eq. 2.2 into Eq. 2.3

$$\sigma_{ij} = \lambda\ u_{k,k}\ \delta_{ij} + G\ (u_{i,j} + u_{j,i}) \qquad (2.55)$$

For the in-plane motion only σ_{xx} and τ_{zx} are needed on the vertical boundary and σ_{zz} and τ_{xz} are needed on the horizontal boundary. If a linearly distributed loading acts on the ith element on the vertical boundary, the stress components on the jth element on the vertical boundary are

$$\begin{Bmatrix}\sigma_{xx}(z)\\ \tau_{zx}(z)\end{Bmatrix} = ikG \begin{bmatrix} L(2r^2-s^2-1)e^{ikrz} & L(2r^2-s^2-1)e^{-ikrz} \\ 2Lre^{ikrz} & -2Lre^{-ikrz} \end{bmatrix}$$

$$\begin{bmatrix} 2Mse^{iksz} & -2Mse^{-iksz} \\ M(1-s^2)e^{iksz} & M(1-s^2)e^{-iksz} \end{bmatrix} \begin{Bmatrix} A_p \\ B_p \\ A_{sv} \\ B_{sv} \end{Bmatrix} \qquad (2.56a)$$

ie.,

$$\{\sigma_v\} = [GG_v(z)]\ \{A\} \qquad (2.56b)$$

From Eq. 2.28, the constant vector (A) can be solved for and then substituted into Eq. 2.56b

$$(\sigma_v) = [GG_v(z)]\ [GA]^{-1}\ (U^L) \tag{2.57}$$

Finally, substituting Eq. 2.49 into Eq. 2.57, the stress function of the jth element due to the loading on the ith element is

$$(\sigma_{vj}) = [GG_v(z)]\ [GA_j]^{-1}[F^s_{ji}][GE_i]\ (p_i) \qquad (i \neq j) \tag{2.58}$$

For the ith element the local response due to the imposition of fixed interface boundary conditions and the particular solution has to be taken into account. Substituting Eq. 2.36 into Eq. 2.55, it can be shown that

$$\begin{Bmatrix} \sigma^p_{xx}(z) \\ \tau^p_{zx}(z) \end{Bmatrix} = \begin{bmatrix} \frac{i}{kr^2}(1 - \frac{z}{d}) & -\frac{i}{k^2s^2d}[(\frac{c_s^2}{c_p^2} - 1)(\frac{1}{r^2} + 1) - 1] \\ \frac{1}{k^2r^2d}[\frac{c_s^2}{c_p^2}(1 - \frac{1}{s^2}) + \frac{1}{s^2}] & \frac{1}{ks^2}(1 - \frac{z}{d}) \end{bmatrix}$$

$$\begin{bmatrix} \frac{iz}{kr^2d} & \frac{i}{k^2s^2d}((\frac{c_s^2}{c_p^2} - 1)(\frac{1}{r^2} + 1) - 1) \\ -\frac{1}{k^2r^2d}[(\frac{c_s^2}{c}(1 - \frac{1}{s^2}) + \frac{1}{s^2}] & \frac{z}{ks^2d} \end{bmatrix} \begin{Bmatrix} p_1 \\ ir_1 \\ p_2 \\ ir_2 \end{Bmatrix} \tag{2.59a}$$

ie.

$$(\sigma^p_v(z)) = [GP_v(z)](p) \tag{2.59b}$$

Similarly, the stress function of the ith element due to the loading on itself can be derived as

$$(\sigma_v(z)_i) = ([GG_v(z)_i][GA_i]^{-1}([F^s_{ii}][GE_i] - [UP_i]) + [GP_v(z)_i])\ (p) \tag{2.60}$$

The stress function can be transformed into the spatial domain by an inverse Fourier transform

$$\{\sigma_v(z,x)_i\} = F_f^{-1}\ (\{\sigma_v(z)_i\}) \tag{2.61}$$

The Green's function for the surface traction can be calculated by Eq. 2.4 and Eq. 2.61.

2.6 An Alternative Approach to Evaluate the Global Nodal Forces and the Local Response

The nodal forces for the global response can be evaluated directly from the displacement functions of the layer fixed at the top and the bottom boundaries and the local responses under the loading can be derived analytically instead of by the numerical procedure given in the previous section.

For convenience and simplicity, the origin is located at the centre of the layer with depth d and its boundaries at the top and the bottom are fixed. The load can be expressed as

$$p(z) = (\frac{1}{2} - \frac{z}{d})p_1 + (\frac{1}{2} + \frac{z}{d})p_2 \tag{2.62a}$$

$$r(z) = (\frac{1}{2} - \frac{z}{d})r_1 + (\frac{1}{2} + \frac{z}{d})r_1 \tag{2.62b}$$

Substituting Eq. 2.10, 2.11, 2.25c and 2.25d into Eq. 2.5 and adding the external loads of Eq. 2.62, the governing differential equations can be written as

$$k^2r^2 \frac{c_p^2}{c_s^2} u - ik(\frac{c_p^2}{c_s^2} - 1)\, w_{,z} + u_{,zz} = \frac{p(z)}{G} \tag{2.63a}$$

$$k^2s^2w - ik\left(\frac{c_p^2}{c_s^2} - 1\right) u_{,z} + \frac{c_p^2}{c_s^2} w_{,zz} = \frac{r(z)}{G} \tag{2.63b}$$

Assuming a linear variation with z as the particular solution of Eq. 2.63 for u and w then

$$w^p(z) = a + b\,\frac{z}{d} \tag{2.64a}$$

$$w^p(z) = e + f\,\frac{z}{d} \tag{2.64a}$$

where a, b, e and f are constants. Substituting Eq. 2.62 and 2.64 into Eq. 2.63, the constants can be solved as

$$\begin{Bmatrix} a \\ b \\ e \\ f \end{Bmatrix} = \frac{1}{k^2G} \begin{bmatrix} -\frac{c_s^2}{2r^2c_p^2} & \frac{1}{kdr^2s^2}\left(1-\frac{c_s^2}{c_p^2}\right) & -\frac{c_s^2}{2r^2c_p^2} & -\frac{1}{kdr^2s^2}\left(1-\frac{c_s^2}{c_p^2}\right) \\ \frac{c_s^2}{r^2c_p^2} & 0 & -\frac{1}{r^2c_p^2} & 0 \\ \frac{i}{kdr^2s^2}\left(1-\frac{c_s^2}{c_p^2}\right) & \frac{i}{2s^2} & -\frac{i}{kdr^2s^2}\left(1-\frac{c_s^2}{c_p^2}\right) & \frac{i}{2s^2} \\ 0 & -\frac{i}{s^2} & 0 & \frac{i}{s^2} \end{bmatrix} \begin{Bmatrix} p_1 \\ ir_1 \\ p_2 \\ ir_2 \end{Bmatrix} \tag{2.64b}$$

If the load p(z) and r(z) are zero, the complementary solution is given by Eq. 2.26c and can be rewritten as (see the appendix)

$$U(z) = A\cos(krz) + iB\sin(krz) - s[iC\sin(ksz) + D\cos(ksz)] \qquad (2.65a)$$

$$W(z) = -r[iA\sin(krz) + B\cos(krz)] - C\cos(ksz) - iD\sin(ksz) \qquad (2.65b)$$

where A, B, C and D are the constants determined from the boundary conditions. Adding the particular solution of Eq. 2.64 to the complementary solution Eq. 2.65 and imposing the zero displacements boundary condition at z = -d/2 and z = d/2 the constants A, B, C and D can be found as

$$A = \frac{-2a\sin(ksd/2) - isf\cos(ksd/2)}{D_1} \qquad (2.66a)$$

$$B = \frac{ib\cos(ksd/2) + 2se\cos(ksd/2)}{D_2} \qquad (2.66b)$$

$$C = \frac{-ibr\cos(krd/2) + 2e\sin(krd/2)}{D_2} \qquad (2.66c)$$

$$D = \frac{2ra\cos(ksd/2) - if\cos(ksd/2)}{D_1} \qquad (2.66d)$$

where

$$D_1 = 2[\cos(krd/2)\sin(ksd/2) + rs\sin(krd/2)\cos(ksd/2)] \qquad (2.66e)$$

$$D_2 = 2[\sin(krd/2)\cos(ksd/2) + rs\cos(krd/2)\sin(ksd/2)] \qquad (2.66f)$$

Substituting Eq. 2.66 into Eq. 2.65 the local responses of the layer can be derived as

$$u^L(z) = aC_1^u(z) + bC_2^u(z) + eC_3^u(z) + fC_4^u(z) \qquad (2.67a)$$

$$w^L(z) = aC_1^w(z) + bC_2^w(z) + eC_3^w(z) + fC_4^w(z) \qquad (2.67b)$$

where

$$C_1^u(z) = \frac{D_1 - 2[\sin(ksd/2)\cos(krz) + rs\sin(krd/2)\cos(ksz)]}{D_1} \qquad (2.67c)$$

$$C_2^u(z) = \frac{D_2 z - d[\cos(ksd/2)\sin(krz) + rs\cos(krd/2)\sin(ksz)]}{D_2 d} \tag{2.67d}$$

$$C_3^u(z) = \frac{2is[\sin(ksd/2)\sin(krz) - \sin(krd/2)\sin(ksz)]}{D_2} \tag{2.67e}$$

$$C_4^u(z) = \frac{is[-\cos(ksd/2)\cos(krz) + \cos(krd/2)\cos(ksz)]}{D_1} \tag{2.67f}$$

$$C_1^v(z) = \frac{2ir[\sin(ksd/2)\sin(krz) - \sin(krd/2)\sin(ksz)]}{D_1} \tag{2.67g}$$

$$C_2^v(z) = \frac{ir[-\cos(ksd/2)\cos(krz) + \cos(krd/2)\cos(ksz)]}{D_2} \tag{2.67h}$$

$$C_3^v(z) = \frac{D_2 - 2[\sin(krd/2)\cos(ksz) + rs\sin(ksd/2)\cos(krz)]}{D_2} \tag{2.67i}$$

$$C_4^v(z) = \frac{D_1 z - d[\cos(krd/2)\sin(ksz) + rs\cos(ksd/2)\sin(krz)]}{D_1 d} \tag{2.67j}$$

From Eq. 2.2 and 2.3 the local stress responses can be derived as

$$\frac{\sigma_z}{G} = -ik\left(\frac{c_p^2}{c_s^2} - 2\right)[aC_1^u(z) + bC_2^u(z) + eC_3^u(z) + fC_4^u(z)]$$

$$+ \frac{c_p^2}{c_s^2}[aD_1^v(z) + bD_2^v(z) + eD_3^v(z) + fD_4^v(z)] \tag{2.68a}$$

$$\frac{\tau_{xz}}{G} = aD_1^u(z) + bD_2^u(z) + eD_3^u(z) + fD_4^u(z)$$

$$-ik[aC_1^v(z) + bC_2^v(z) + eC_3^v(z) + fC_4^v(z)] \tag{2.68b}$$

where

$$D_1^u(z) = \frac{2kr[\sin(ksd/2)\sin(krz) + s^2\sin(krd/2)\sin(ksz)]}{D_1} \tag{2.68c}$$

$$D_2^u(z) = \frac{D_2 - dkr[cos(ksd/2)cos(krz) + s^2cos(krd/2)cos(ksz)]}{D_2 d} \quad (2.68d)$$

$$D_3^u(z) = \frac{2iks[rsin(ksd/2)cos(krz) - ssin(krd/2)cos(ksz)]}{D_2} \quad (2.68e)$$

$$D_4^u(z) = \frac{iks[rcos(ksd/2)sin(krz) - scos(krd/2)sin(ksz)]}{D_2} \quad (2.68f)$$

$$D_1^v(z) = \frac{2ikr[rsin(ksd/2)cos(krz) - ssin(krd/2)cos(ksz)]}{D_1} \quad (2.68g)$$

$$D_2^v(z) = \frac{ikr[rcos(ksd/2)sin(krz) - scos(krd/2)sin(ksz)]}{D_2} \quad (2.68h)$$

$$D_3^v(z) = \frac{2ks[sin(krd/2)sin(ksz) + r^2sin(ksd/2)cos(krz)]}{D_2} \quad (2.68i)$$

$$D_4^v(z) = \frac{D_1 - dks[cos(krd/2)cos(ksz) + r^2cos(ksd/2)cos(krz)]}{D_1 d} \quad (2.68j)$$

The functions D(z) represent the derivative of the corresponding functions C(z) with respect to z.

The nodal loads at the top and the bottom of the layer can be obtained by substituting z = -d/2 and z = d/2 into Eq. 2.68a and 2.68b for P_1, R_1 and P_2, R_2 respectively but with a negative sign for computing the global responses. Noticing that the functions C(z) in Eq. 2.67 vanish at the boundaries of the layer and the nodal loads are

$$\begin{Bmatrix} P_1 \\ iR_1 \\ P_2 \\ iR_2 \end{Bmatrix} = G \begin{bmatrix} D^u_{11} & D^u_{21} & D^u_{31} & D^u_{41} \\ i\frac{c_p^2}{c_s^2}D^v_{11} & i\frac{c_p^2}{c_s^2}D^v_{21} & i\frac{c_p^2}{c_s^2}D^v_{31} & i\frac{c_p^2}{c_s^2}D^v_{41} \\ D^u_{11} & -D^u_{21} & -D^u_{31} & D^u_{41} \\ -i\frac{c_p^2}{c_s^2}D^v_{11} & i\frac{c_p^2}{c_s^2}D^v_{21} & i\frac{c_p^2}{c_s^2}D^v_{31} & -i\frac{c_p^2}{c_s^2}D^v_{41} \end{bmatrix} \begin{Bmatrix} a \\ b \\ e \\ f \end{Bmatrix} \tag{2.69a}$$

where

$$D^u_{11} = -\frac{2kr(1+s^2)sin(krd/2)sin(ksd/2)}{D_1} \tag{2.69b}$$

$$D^u_{21} = \frac{D_2 - kdr(1+s^2)cos(krd/2)cos(ksd/2)}{D_2 d} \tag{2.69c}$$

$$D^u_{31} = \frac{2iks[rcos(krd/2)sin(ksd/2) - ssin(krd/2)cos(ksd/2)]}{D_2} \tag{2.69d}$$

$$D^u_{41} = \frac{-iks[rcos(ksd/2)sin(krd/2) - scos(krd/2)sin(ksd/2)]}{D_1} \tag{2.69e}$$

$$D^v_{11} = \frac{2ikr[rcos(krd/2)sin(ksd/2) - ssin(krd/2)cos(ksd/2)]}{D_1} \tag{2.69f}$$

$$D^v_{21} = \frac{-ikr[rcos(ksd/2)sin(krd/2) - scos(krd/2)sin(ksd/2)]}{D_2} \tag{2.69g}$$

$$D^v_{31} = -\frac{2ks(1+r^2)sin(krd/2)sin(ksd/2)}{D_2} \tag{2.69h}$$

$$D^v_{41} = \frac{D_1 - kds(1+r^2)cos(krd/2)cos(ksd/2)}{D_1 d} \tag{2.69i}$$

The global response due to the linearly distributed loads on the ith element can be computed by substituting the Eq. 2.69a into Eq. 2.49a and Eq. 2.28c. For the ith element the local response from Eq. 2.67 has to be added.

By this procedure, the global nodal loads and the local responses are determined analytically and a better accuracy may be achieved than the numerical procedure described in the previous section.

For a higher order displacement shape function and load function or an inclined boundary, a similar procedure can be followed to derived the local response and the global nodal loads.

2.7 A Simplified Vertical Boundary for the Finite Element Model in the Near-Field

If the boundary element is connected with a finite element mesh on a vertical boundary, more than ten boundary elements may have to be chosen for a realistic size of the nonlinear near-field. The data stored for the numerical transformation will dramatically increase with the increase in the number of elements. This will impair the efficiency of the boundary element method and even make the computer implementation impractical. On the other hand, when the near-field is reasonably large and the material damping is present, the partial reflection of the out-going waves may not affect the response of the upper structure because the reflected waves may be damped out before they reach the structure. A simplified energy transmitting boundary may be used in this case.

It has been recognized that most of the energy in a half space is carried away by surface waves (L6). This is also the case for a layered half space in a soil-structure interaction. If the surface waves generated by the structure are properly modelled, the responses of the upper structure may be well predicted. When the soil layers are underlain by a rigid base, such as hard rock, the energy can be only radiated away in the horizontal direction. The waves travelling in the layers can be synthesized from the mode shapes of the layered system. There are an infinite number of modes for soil layers

underlain by rigid base. For layers on a half space, the energy will be also radiated into the half space but there are only a finite number of modes. For both systems, the surface waves can be completely prescribed by these mode shapes. The stresses in the layers can also be constructed from the mode shape functions.

The weighting technique used to derive the boundary element formula can also be used to develop an energy transmitting boundary for surface waves. The weighting function in Eq. 2.41e can be chosen as the surface traction on the boundary due to the surface waves developed in the layer. The prescribed displacement shape function is the shape function used for the finite elements connected to the boundary. Eq. 2.41e can be written as

$$\int_S \{T(s)\}^T(\{U(s)\} - \{U_p(s)\})\, ds \tag{2.70a}$$

where the surface traction is

$$\{T(s)\} = [g_t(s)]\{f\} \tag{2.70b}$$

and the boundary displacement is

$$\{U(s)\} = [g_u(s)]\{f\} \tag{2.70c}$$

$$\{U_p(s)\} = [N(s)]\{U_b\} \tag{2.70d}$$

where $[g_u(s)]$ and $[g_t(s)]$ depend on the mode shape function of the layers. Vector $\{f\}$ contains the mode participation factors and $[N(s)]$ is the shape function for the finite elements. Vector $\{f\}$ can be solved from Eq. 2.70a as

$$\{f\} = [V]^{-1}[H]\{U_b\} \tag{2.70e}$$

where

$$[V] = \int_S [g_t(s)]^T[g_u(s)]ds \tag{2.70f}$$

$$[H] = \int_S [g_t(s)]^T[N(s)]ds \tag{2.70g}$$

The surface traction on the boundary can be solved by substituting Eq. 2.70e into Eq. 2.70b and can be lumped into nodal forces using Eq. 2.41i. The dynamic stiffness matrix is derived in the same manner as the boundary element and is defined as

$$[S^{\S}_{bb}] = [H]^T[V]^{-1}[H] \qquad (2.70h)$$

It will be noted that Eq. 2.70h has the same form as Eq. 2.41k does but Eq. 2.70h is much easier to compute if only a few mode shapes are used. The computationally expensive transformation between the wave number domain and the spatial domain is not needed. Since only the surface wave modes are used to construct the displacements in the far-field, the boundary has to be located far away enough that the surface waves generated by the structure can be developed. Three times the half width of the foundation from the centre of the foundation may be adequate for the layers underlain by rigid rock and six times for the layers on a flexible half space. For a half space, only one Rayleigh mode can be used and the Rayleigh boundary by Lysmer and Kuhlemeyer (L6) can be considered as a special case in which the displacement compatibility requirement between the finite element mesh and the far-field is relaxed. The boundary was also used for the layers on rigid rock by Tzong and Penzien (T2) in which it was referred to as a boundary solution method. In their approach, the mode shapes were obtained by using the transfer matrix of each layer which is slightly easier than the determinant searching method. Numerical experiment has shown that the mode shapes obtained by using transfer matrices can not usually satisfy the zero external loading condition if there are more than four layers due to numerical and computational errors.

The boundary is a global boundary in the sense of integration over the boundary. For a near-field with two vertical boundaries and a horizontal boundary, it is easier to treat each boundary individually, ie., ignoring the coupling effects between them. The horizontal boundary can be further simplified by assuming that all waves impinge on it in a vertical direction and the viscous boundary for the corresponding layer can be adopted. This will introduce very small errors because surface waves usually decay rapidly with depth and the modelling of the horizontal boundary at a certain depth is not as critical as that for the vertical ones.

The mode shapes of the layered system can be obtained by solving the system equilibrium equation with zero amplitudes of interface loading, ie.,

setting the determinant of the dynamic stiffness matrix of the layered system to zero. The wave number is the only variable for a given frequency and may be real or complex depending on the material properties of the layers. To solve this problem, a determinant search technique has to be used and Muller's method has been proved to be very efficient (T1). Because the waves travelling away from the site are modelled and the displacements must not monotonically increase in the direction away from the site, a mode with the wave number whose real part is positive and imaginary part is negative can be used. The displacement shape function and the surface traction of mode j of a layer for the vertical boundary along z-direction at x_o can be defined as

$$\{g_u(z)\}_j = [N'_j(z)]\{\phi_j\}e^{-ikx_o} \tag{2.71a}$$

$$\{g_t(z)\}_j = [P_j(z)]\{\phi_j\}e^{-ikx_o} \tag{2.71b}$$

where $\{\phi_j\}$ is the corresponding subvector for the layer from mode j, ie. the modal displacements of the top and the bottom surfaces of the layer. The functions [N'(z)] and [P(z)] can be obtained from Eq. 2.28c and Eq. 2.57 with a proper change of signs for the surface traction. The analytical formulae are derived here for a better numerical accuracy though the numerical procedure described in the previous sections can be used to construct these functions.

The complementary solution of the system, Eq. 2.65a and 2.65b, can be rewritten in the term of the displacements at the top and bottom surfaces of the layer as

$$u(z) = E_1^u(z)U_1 + E_2^u(z)W_1 + E_3^u(z)U_2 + E_4^u(z)W_2 \tag{2.72a}$$

$$w(z) = E_1^w(z)U_1 + E_2^w(z)W_1 + E_3^w(z)U_2 + E_4^w(z)W_2 \tag{2.72b}$$

where the shape functions can be solved by setting $z = -d/2$, $u(z) = U_1$, $w(z) = W_1$ and $z = d/2$, $u(z) = U_2$, $w(z) = W_2$ in Eq. 2.65a and Eq. 2.65b and are given as

$$E_1^u = N_1 - N_2 \tag{2.72c}$$

$$E_2^u = N_3 + N_4 \tag{2.72d}$$

$$E_3^u = N_1 + N_2 \tag{2.72e}$$

$$E_4^u = - N_3 + N_4 \tag{2.72f}$$

$$E_1^v = N_5 + N_6 \tag{2.72g}$$

$$E_2^v = - N_7 + N_8 \tag{2.72h}$$

$$E_3^v = N_5 - N_6 \tag{2.72i}$$

$$E_4^v = N_7 + N_8 \tag{2.72j}$$

$$N_1 = \frac{sin(ksd/2)cos(krz) + rssin(krd/2)cos(ksz)}{D_1} \tag{2.72k}$$

$$N_2 = \frac{cos(ksd/2)sin(krz) + rscos(krd/2)sin(ksz)}{D_2} \tag{2.72l}$$

$$N_3 = \frac{is[-cos(ksd/2)cos(krz) + cos(krd/2)cos(ksz)]}{D_1} \tag{2.72m}$$

$$N_4 = \frac{is[-sin(ksd/2)sin(krz) + sin(krd/2)sin(ksz)]}{D_2} \tag{2.72n}$$

$$N_5 = \frac{ir[-sin(ksd/2)sin(krz) - sin(krd/2)sin(ksz)]}{D_1} \tag{2.72p}$$

$$N_6 = \frac{ir[-cos(ksd/2)cos(krz) + cos(krd/2)cos(ksz)]}{D_2} \tag{2.72q}$$

$$N_7 = \frac{cos(krd/2)sin(ksz) + rscos(ksd/2)sin(krz)}{D_1} \tag{2.72r}$$

$$N_8 = \frac{sin(krd/2)cos(ksz) + rssin(ksd/2)cos(krz)}{D_2} \tag{2.72s}$$

These shape functions are the components of the displacement shape function in Eq. 2.71a which may be written as

$$[N'(z)] = \begin{bmatrix} E_1^u & E_2^u & E_3^u & E_4^u \\ E_1^w & E_2^w & E_3^w & E_4^w \end{bmatrix} \tag{2.72t}$$

The function for the surface traction on the boundary can be obtained by substituting the displacement derivatives into Eq. 2.2, 2.3 and 2.4. For the vertical boundary located at x_o the surface traction components are

$$(T(z)) = \begin{Bmatrix} -\sigma_{xx} \\ -\tau_{xz} \end{Bmatrix} \tag{2.73a}$$

and for mode j the shape function for the surface traction in Eq. 2.71b is

$$(P_j(z)) = G \begin{bmatrix} ik\frac{c_p^2}{c_s^2}E_1^u - \left(\frac{c_p^2}{c_s^2} - 2\right)\frac{\partial E_1^w}{\partial z} & ik\frac{c_p^2}{c_s^2}E_2^u - \left(\frac{c_p^2}{c_s^2} - 2\right)\frac{\partial E_2^w}{\partial z} \\ ikE_1^w - \frac{\partial E_1^u}{\partial z} & ikE_2^w - \frac{\partial E_2^u}{\partial z} \\ ik\frac{c_p^2}{c_s^2}E_3^u - \left(\frac{c_p^2}{c_s^2} - 2\right)\frac{\partial E_3^w}{\partial z} & ik\frac{c_p^2}{c_s^2}E_4^u - \left(\frac{c_p^2}{c_s^2} - 2\right)\frac{\partial E_4^w}{\partial z} \\ ikE_3^w - \frac{\partial E_3^u}{\partial z} & ikE_4^w - \frac{\partial E_4^u}{\partial z} \end{bmatrix} \tag{2.73b}$$

where

$$\frac{\partial E_1^u}{\partial z} = \frac{\partial N_1}{\partial z} - \frac{\partial N_2}{\partial z} \tag{2.74a}$$

$$\frac{\partial E_2^u}{\partial z} = \frac{\partial N_3}{\partial z} + \frac{\partial N_4}{\partial z} \tag{2.74b}$$

$$\frac{\partial E_3^u}{\partial z} = \frac{\partial N_1}{\partial z} + \frac{\partial N_2}{\partial z} \tag{2.74c}$$

$$\frac{\partial E_4^u}{\partial z} = -\frac{\partial N_3}{\partial z} + \frac{\partial N_4}{\partial z} \tag{2.74d}$$

$$\frac{\partial E_1^v}{\partial z} = \frac{\partial N_5}{\partial z} + \frac{\partial N_6}{\partial z} \tag{2.74e}$$

$$\frac{\partial E_2^v}{\partial z} = -\frac{\partial N_7}{\partial z} + \frac{\partial N_8}{\partial z} \tag{2.74f}$$

$$\frac{\partial E_3^v}{\partial z} = \frac{\partial N_5}{\partial z} - \frac{\partial N_6}{\partial z} \tag{2.74g}$$

$$\frac{\partial E_4^v}{\partial z} = \frac{\partial N_7}{\partial z} + \frac{\partial N_8}{\partial z} \tag{2.74h}$$

and

$$\frac{\partial N_1}{\partial z} = \frac{-kr[sin(ksd/2)sin(krz) + s^2 sin(krd/2)sin(ksz)]}{D_1} \tag{2.75a}$$

$$\frac{\partial N_2}{\partial z} = \frac{kr[cos(ksd/2)cos(krz) + s^2 cos(krd/2)cos(ksz)]}{D_2} \tag{2.75b}$$

$$\frac{\partial N_3}{\partial z} = \frac{iks[rcos(ksd/2)sin(krz) - scos(krd/2)sin(ksz)]}{D_1} \tag{2.75c}$$

$$\frac{\partial N_4}{\partial z} = \frac{iks[-rsin(ksd/2)cos(krz) + ssin(krd/2)cos(ksz)]}{D_2} \tag{2.75d}$$

$$\frac{\partial N_5}{\partial z} = \frac{ikr[-rsin(ksd/2)cos(krz) + ssin(krd/2)cos(ksz)]}{D_1} \tag{2.75e}$$

$$\frac{\partial N_6}{\partial z} = \frac{ikr[rcos(ksd/2)sin(krz) - scos(krd/2)sin(ksz)]}{D_2} \tag{2.75f}$$

$$\frac{\partial N_7}{\partial z} = \frac{ks[r^2 cos(ksd/2)cos(krz) + cos(krd/2)cos(ksz)]}{D_1} \tag{2.75g}$$

$$\frac{\partial N_8}{\partial z} = \frac{-ks[r^2 sin(ksd/2)sin(krz) + sin(krd/2)sin(ksz)]}{D_2} \qquad (2.75h)$$

D_1 and D_2 are defined in Eq. 2.66e and 2.66f.

Once the displacement shape functions [N'(z)] and the surface traction shape functions [P(z)] at the vertical boundary for the corresponding wave numbers are obtained from Eq. 2.72t and Eq. 2.73b, the dynamic stiffness matrix of the boundary can be found from Eq. 2.70. In the case of a layered soil system on a rigid base where the soil properties of the left hand side far-field are different from those of the right hand side far-field, the dynamic stiffness matrix of the left hand side far-field has to be evaluated using the corresponding properties. The out-going waves transmitted by the left hand side boundary propagate in the opposite direction to those transmitted by the right hand side boundary. Thus a periodical function exp(ikx) has to be used to describe the waves in the left hand side far-field instead of exp(-ikx) in Eq. 2.26a and Eq. 2.26b. A proper change of signs in Eq. 2.73b has also to be carried out and the surface traction shape functions for the left hand side vertical boundary at $x = -x_o$ can be derived as

$$(P_j(z)) = G \begin{bmatrix} ik\frac{c_p^2}{c_s^2}E_1^u + (\frac{c_p^2}{c_s^2} - 2)\frac{\partial E_1^v}{\partial z} & ik\frac{c_p^2}{c_s^2}E_2^u + (\frac{c_p^2}{c_s^2} - 2)\frac{\partial E_2^v}{\partial z} \\ ikE_1^v + \frac{\partial E_1^u}{\partial z} & ikE_2^v + \frac{\partial E_2^u}{\partial z} \\ ik\frac{c_p^2}{c_s^2}E_3^u + (\frac{c_p^2}{c_s^2} - 2)\frac{\partial E_3^v}{\partial z} & ik\frac{c_p^2}{c_s^2}E_4^u + (\frac{c_p^2}{c_s^2} - 2)\frac{\partial E_4^v}{\partial z} \\ ikE_3^v + \frac{\partial E_3^u}{\partial z} & ikE_4^v + \frac{\partial E_4^u}{\partial z} \end{bmatrix} \qquad (2.76)$$

The displacement shape functions for the z-direction for both sides are the same.

2.8 Summary

The theoretical development of the indirect boundary element method has been presented in this chapter. The boundary element model based on the Green's functions for the semi-infinite horizontally layered half space automatically satisfies the radiation condition and the traction free condition on the surface of the half space and thus only the interface between the far-field and the near-field or the base of the upper structure needs to be modelled.

The numerical procedure deriving the Green's functions for a horizontally layered half space has been given in detail for a surface foundation and embedded foundation. An analytical procedure to compute the displacement and the stress field due to a linearly distributed load on an element has been derived. A better accuracy can be achieved by the analytical procedure than by the numerical procedure.

To overcome the large computer storage requirement of the boundary element if a large near-field soil has to be modelled, using an approximate model, a simplified vertical boundary has been derived. Because the surface wave modes of the horizontally layered half space are used to construct the displacement field for the far-field, the advantage of the boundary element model is preserved. The computational effort and computer storage requirements are very small when compared with the boundary element model because the computationally expensive numerical transformation is not needed.

Chapter 3

Modelling Of the Near-Field Soil and Upper Structure

3.1 Basic Formulation for the Finite Element Analysis

The finite element method has been proved as the most efficient method for discretizing a bounded domain for either static or dynamic problems (B3, Z2). For dynamic problem, the acceleration and velocity fields are interpolated in the same way as the displacement field and the static stiffness matrix of the domain can be used as a part of the dynamic stiffness of the domain. The dynamic equilibrium equation of an infinitesimal element in the domain can be written as

$$\sigma_{ij,j} + b_i = - \rho \ddot{u}_i - \zeta \dot{u}_i \tag{3.1}$$

where b, ρ and ζ represent the body force, mass density and damping property parameters respectively. By constructing approximate displacement, velocity and acceleration fields using interpolation functions and then approximating Eq. 3.1 by a weighting technique, the dynamic equilibrium equation of a system can be expressed as

$$[M]\{\ddot{r}\} + [C]\{\dot{r}\} + [K]\{r\} = \{R\} \tag{3.2a}$$

where [M], [C] and [K] are the mass, damping and stiffness matrices respectively, {r}, {r} and {r} are the nodal acceleration, velocity and displacement vectors and {R} is the applied load vector. For a system of m finite elements they are defined as

$$M_{ij} = \sum_{m} \int_{V_m} p \, N_{ki} N_{kj} \, dv \tag{3.2b}$$

$$C_{ij} = \sum_{m} \int_{V_m} z\, N_{ki} N_{kj}\, dv \qquad (3.2c)$$

$$K_{ij} = \sum_{m} \int_{V_m} B_{ki} D_{kl} B_{lj}\, dv \qquad (3.2d)$$

$$u_i = N_{ij} r_j \qquad (3.2e)$$

where N is the displacement interpolation function matrix, B is the transformation matrix which relates the strain field to the nodal displacement of the domain and D is the constitutive matrix which relates the stress field to the strain field of the domain. (R) depends on the type of the applied load and the body force.

For the upper structure, beam, plate, shell and solid elements can be used depending on the type of the structural members, but for the near-field soil only a solid element can be used. An 8-node isoparametric finite element is adopted to model the near-field for a two dimensional plane strain problem.

If only small displacements are considered, the nonlinearity arises only from the material properties, ie., matrix [D] is dependent on the stress and strain amplitudes and the loading history. The constitutive matrix in Eq. 3.2d has to be evaluated by the means of the theory of plasticity.

The modelling of the upper structure is relatively simple when compared with that of the soil. Even though the main interest in the study of soil-structure interaction is the response of the upper structure, the modelling of the near-field soil is a very important aspect because erroneous responses of the structure will inevitably be produced if the model of the soil fails to properly predict the response of the near-field. Due to the complex behaviour, soil can not be modelled properly under earthquake loading by simple elastic or nonlinear elastic theories.

3.2 Basic Formulation of the Theory of Plasticity

For completeness, some basic formulae of the theory of plasticity are given. It is usually assumed that a strain increment can be decomposed as (D1, D9)

$$d\epsilon_{ij} = d\epsilon^e_{ij} + d\epsilon^p_{ij} \tag{3.3}$$

where the superscripts e and p represent elastic and plastic strains respectively and the stress increment is related to the elastic strain increment by the generalized Hook's law

$$d\sigma_{ij} = D_{ijkl} d\epsilon^e_{kl} \tag{3.4a}$$

$$D_{ijkl} = (K-2G/3)\delta_{ij}\delta_{kl} + G(\delta_{ik}\delta_{jl} + \delta_{il}\delta_{jk}) \tag{3.4b}$$

where K is the bulk modulus and G is the shear modulus. δ_{ij} is the Kronecker delta symbol. The yield condition specifying the stress state at which plastic flow occurs is defined as

$$F(\sigma_{ij}, k(\epsilon^p_v)) = 0 \tag{3.5a}$$

where k is a hardening parameter defining the isotropic hardening rule and ϵ^p_v is the plastic volumetric strain. The flow rule relating the plastic strain increment vector with the stress and stress increment vector is defined as

$$S(\sigma_{ij}, k) = 0 \tag{3.5b}$$

When an associated flow rule is specified F = S. If an anisotropic hardening rule is introduced, σ_{ij} in the function F and S can be replaced with $\sigma_{ij}-\alpha_{ij}$ where α_{ij} denotes the translation of the surface centre in the stress space. When plastic flow takes place, the plastic strain increment for the associated flow rule may be given as (D1, P9)

$$d\epsilon^p_{ij} = \langle L \rangle n_{ij} \tag{3.6a}$$

$$L = \frac{1}{H} d\sigma_{kl} n_{kl} \tag{3.6b}$$

$$n_{ij} = \frac{\partial F}{\partial \sigma_{ij}} \frac{1}{f} \quad \text{and} \quad f = \left[\frac{\partial F}{\partial \sigma_{ij}} \frac{\partial F}{\partial \sigma_{ij}} \right]^{1/2} \tag{3.6c}$$

where $< >$ is a operator defined as

$$<L> = L \quad \text{if } L > 0 \text{ (Loading)} \tag{3.6d}$$

$$<L> = L \quad \text{if } L = 0 \text{ (Neutral loading)} \tag{3.6e}$$

$$<L> = 0 \quad \text{if } L < 0 \text{ (unloading)} \tag{3.6f}$$

H is the plastic modulus and can be obtained from the consistency condition that the stress state must always lie within or on the yield surface, ie., F = 0 and dF = 0 and then

$$H = - \frac{n_{ij}}{f} \frac{\partial F}{\partial k} \frac{\partial k}{\partial \epsilon_v^p} \tag{3.6g}$$

Substituting Eq. 3.6a into Eq. 3.3 and Eq. 3.4 it follows that

$$d\sigma_{ij} = D_{ijkl}(d\epsilon_{kl} - <L> n_{kl}) \tag{3.7a}$$

$$L = \frac{D_{rspq} n_{rs} d\epsilon_{pq}}{H + D_{abcd} n_{ab} n_{cd}} \tag{3.7b}$$

Substituting Eq. 3.4b into Eq. 3.7, then

$$d\sigma_{ij} = 2G d\epsilon_{ij} + (K-2G/3)\delta_{ij} d\epsilon_{kk} - [2G n_{ij} + (K-2G/3) n_{kk} \delta_{ij}] <L> \tag{3.8a}$$

$$L = \frac{2G n_{kl} d\epsilon_{kl} + (K-2G/3) n_{ss} d\epsilon_{kk}}{H + (K-2G/3) n_{rr} + 2G} \tag{3.8b}$$

For the undrained case, $d\epsilon_{kk} = 0$ and for an ideal elastic-plastic material, H is zero.

3.3 Constitutive Law for the Near-field Soil

Soils exhibit a strong non-linear behaviour even for a small strain amplitude. Many attempts have been made to develop a model predicting the soil behaviour. The critical state concept has been widely accepted in soil mechanics and many sophisticated soil models based on the critical state concept have been developed (A2, B1, B11, D4, M4, P9, R2, R3). A brief introduction to the theory and some soil models based on it is given below (A2, D9).

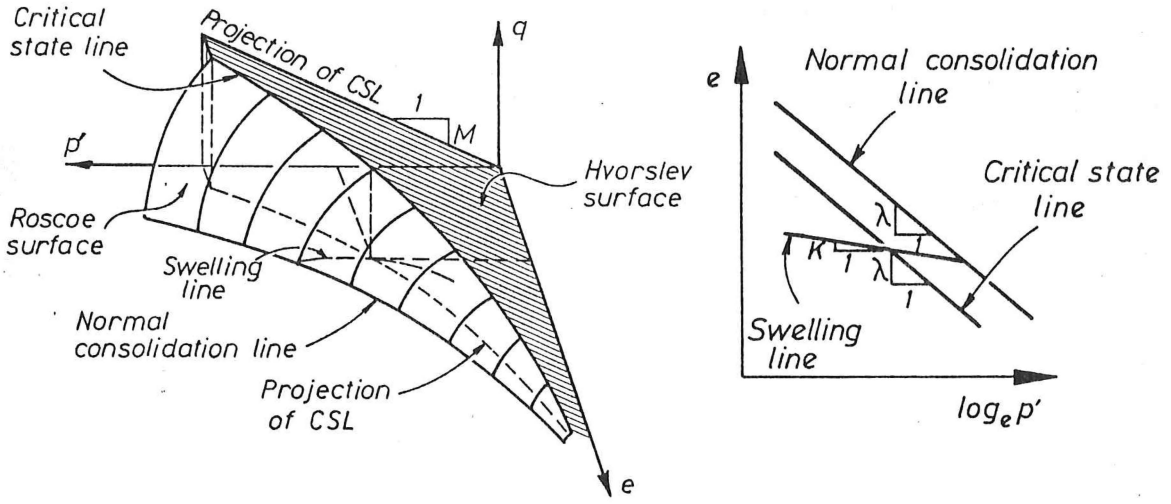

Fig. 3.1 The Critical State Line and Its Projection

In the following section, the stress parameters in the triaxial space are defined as

$$p' = \frac{1}{3}(\sigma_1 + 2\sigma_3) \tag{3.9a}$$

$$q = \sigma_1 - \sigma_3 \tag{3.9b}$$

where σ_1 and σ_3 are the axial and radial effective stresses and $\sigma_2 = \sigma_3$.

In the triaxial test of a virgin soil sample under a drained condition, the mean effective normal stress p' and the void ratio e are related by a simple function when the deviatoric stress q is absent. On the plot of void ratio e versus logarithm of the mean effective normal stresses p', the test results can be approximated by a straight line with a slope λ for loading and κ for unloading, and they are referred to as the normal consolidation line (NCL) and the swelling line respectively as shown in Fig. 3.1. If q is not zero, at failure, p', q and e are related by a unique function referred to as the critical state line (CSL) in p'-q-e space. The projection of CSL on the p'-q plane is a straight line with a slope M while on the e-lnp' plane it is a straight line parallel to the normal consolidation line. These relationships for all normally consolidated soils are valid under both drained and undrained tests and λ, κ and M are constants for the same soil. In the p'-q-e space, the continuous surface connecting NCL and CSL is referred to as a Roscoe surface under which over-consolidated states are defined and above which are impossible states. The soil states under the Roscoe surface are described as 'wet' because the soil has a higher water content than at the critical state. On the other side of the CSL, a surface which intersects with the Roscoe surface along the CSL is called a Hvorslev surface along which the heavily over-consolidated clay sample reaches the critical state. Soil states under the Hvorslev surface are described as 'dry'. These surfaces and drained and undrained test planes are shown in Fig. 3.1 and Fig. 3.2.

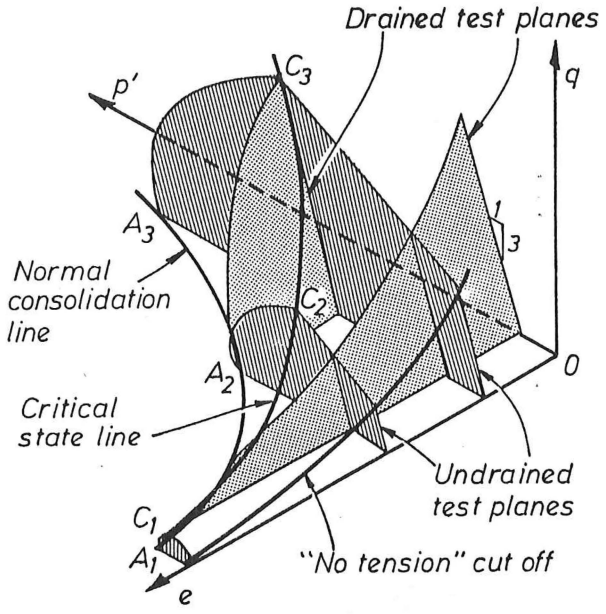

Fig. 3.2 The State Boundary Surface

Based on the critical state concept, various plasticity models for soil have been developed. In the Cam Clay model and the modified Cam Clay model (R3,B11,R2), the projection of the CSL in the p'-q plane is adopted as a fixed yield surface and another surface is adopted as a moving yield surface to implement the hardening behaviour of the soil. In the Cap Model (D10), the

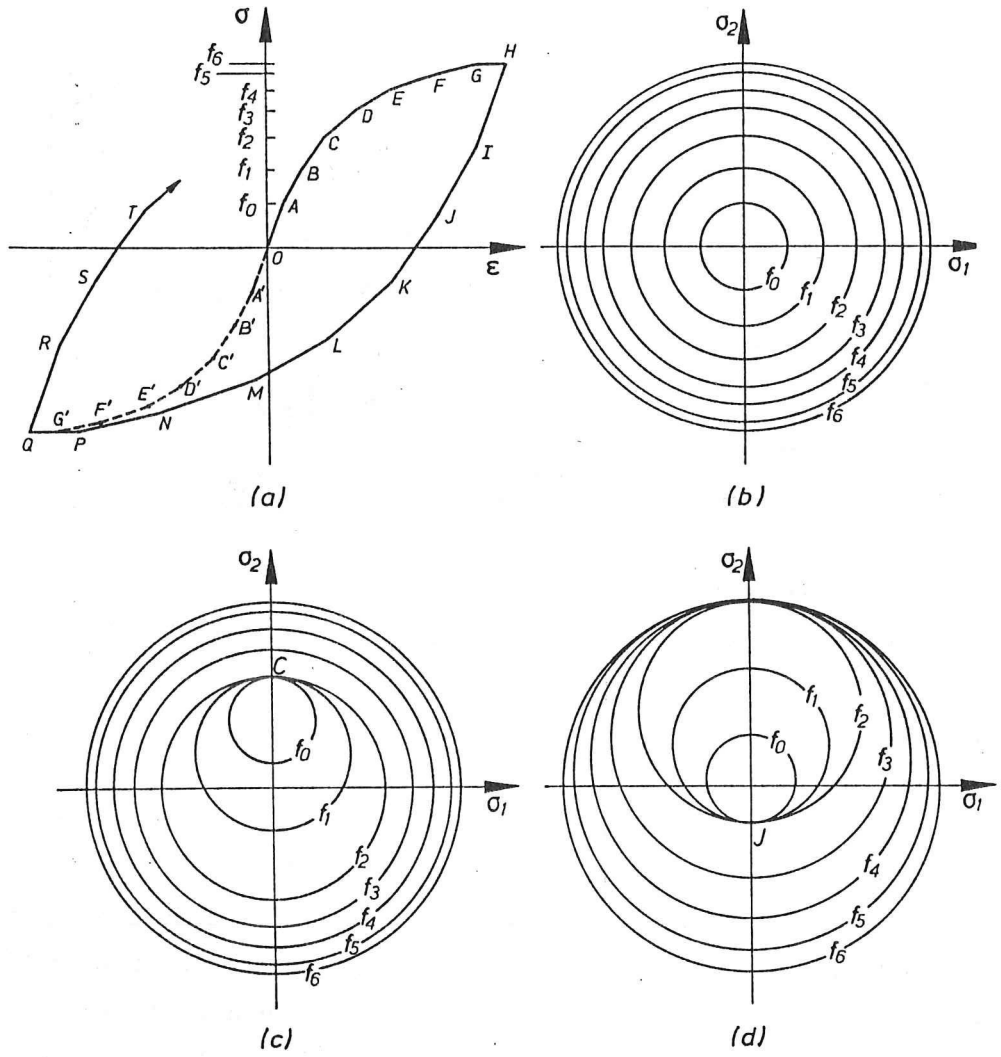

Fig. 3.3 Nested Surface Model:(a) Stress-strain Curve; (b) Before Loading; (c) Loading Behaviour; (d) Unloading Behaviour

yield surface consists of a fixed surface and a moving cap connected smoothly with the fixed yield surface. It has been recognized that these models can represent most of the important aspects of the soil under monotonic loading and are relatively simple to implement in the finite element method (D9). For cyclic loading, these models usually fail to satisfactorily predict some of the important aspects of soil behaviour. Because only an isotropic hardening rule is adopted, when the loading is reversed plastic strain can not be induced before the previously applied load is removed completely and the stress state point touches the yield surface again in the opposite side in the stress space. Soil usually does not behave elastically under cyclic loading within the yield surface defined in these models. In recent years, more sophisticated models have been developed for soil under cyclic loading (D3, M3, P9). They are usually very complex mathematically and involve more

parameters. A critical review on these models has been given by Pande and Pietruszczak (P1).

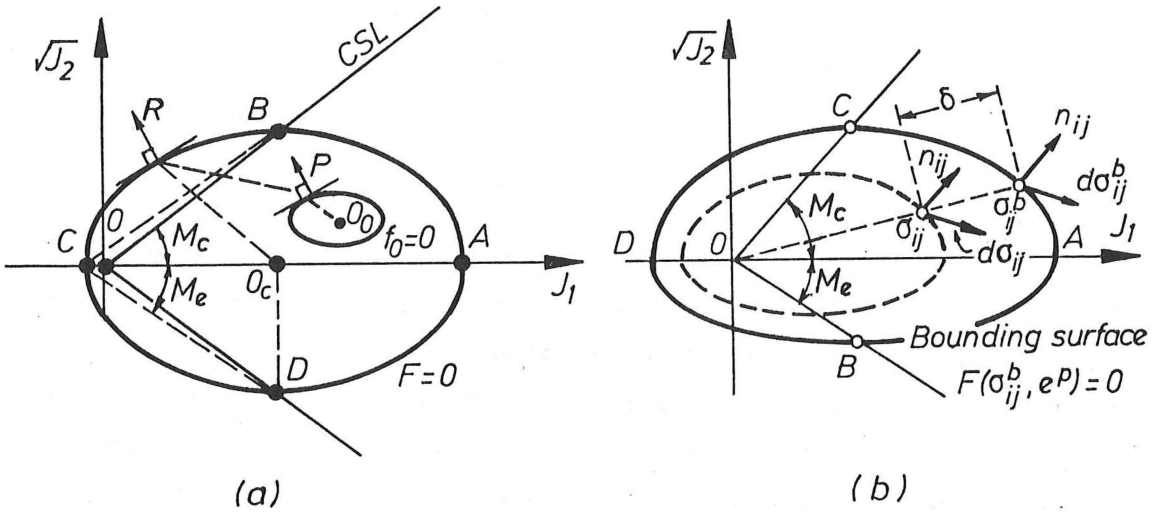

Fig. 3.4 Bounding Surface Model: (a) Two Surfaces; (b) One Surface

In 1967, Moroz introduced the nested surface model into the theory of plasticity (M3). Since then this model has been developed to predict soil behaviour and some modification has been done to model the important aspects of soil under cyclic loading by Prevost (P9), and Morz, Norris,and Zienkiewicz (M4). This model introduces a series of yield surfaces which can translate with no rotation and change their sizes in the stress space during the loading and unloading procedure as illustrated in Fig. 3.3, ie., kinematic and isotropic hardening rules are used. In this model, both origin anisotropy and plastic strain induced anisotropy behaviour can be described adequately and accuracy to a required level can be achieved by introducing the necessary number of the yield surfaces. The disadvantage of the model is the extensive memory requirement in a numerical implementation. To overcome the shortcomings of the model, a bounding surface model was proposed by Dafalias and Popov (D6) and Krieg (K3) and introduced into soil mechanics by Dafalias and Herrmann (D4, D5) and Mroz, Norris and Zienkiewicz (M4). Instead of individually defining a series of yield surfaces, a bounding surface and a yield surface are introduced to define the direction of plastic strain increment. The yield surface defines the elastic region and translates without rotation within the bounding surface from the current stress state to the image point on the bounding surface, at which the outward normal vector has the same direction as that of the current stress state on the yield surface, as illustrated in Fig. 3.4a. Both surfaces can expand or contract simultaneously under the isotropic hardening rule. The amplitude of the plastic strain increment due to a stress increment is computed by defining a

plastic modulus interpolation function in terms of the position of current stress state and the yield surface relative to the bounding surface. As a result, the model is considerably simplified and much less storage is required as compared to the nested surface model and the capability of predicting anisotropic and hysteresis behaviour of the soil is retained. The model has been extended to soil mechanics in the frame work of critical state soil theory by Mroz, Norris and Zienkiewicz (M4).

Dafalias and Herrmann proposed a simpler model in which only the bounding surface was explicitly defined (D3). In this model, the yield surface is reduced to a surface which is indirectly defined in the stress space to have the same incremental stress direction as at the corresponding point on the bounding surface and whose size increases during the loading and decreases during unloading procedure as shown in Fig. 3.4b. The region defined by the reduced yield surface is no longer an elastic region because its size decreases during unloading and the plastic deformation occurs once the loading procedure reverses. The surface is not a yield surface since no consistency condition is required. As a result, no translation rule has to be defined and the model loses the capability of predicting anisotropic behaviour of the soil. Unloading is a elastic procedure and loading is inelastic at the very beginning of the procedure. These limitations are considered insignificant in an engineering application at the current stage of knowledge and the model prediction is considered very good when compared with experimental results under monotonic and cyclic loading (D2, D3, D4). The model has been applied to the analysis of piles in nonlinear soils (C1).

The formulation outlined in 3.2 is applied to the bounding surface model except that the bounding surface is defined by

$$F(\sigma^b_{ij},\ J_o(\epsilon^p_v)) = 0 \tag{3.10a}$$

where the superscript b stands for the bounding surface.

$$L = \frac{1}{H} d\sigma_{kl} n_{kl} = \frac{1}{H^b} d\sigma^b_{kl} n^b_{kl} \tag{3.10b}$$

where H^b is defined by Eq. 3.6g.

$$n_{ij} = \frac{\partial F}{\partial \sigma^b_{ij}} \frac{1}{f} \quad \text{and} \quad f = \left[\frac{\partial F}{\partial \sigma^b_{ij}} \frac{\partial F}{\partial \sigma^b_{ij}}\right]^{1/2} \tag{3.10c}$$

If a radial mapping rule is applied, σ^b_{ij} can be expressed as

$$\sigma^b_{ij} = \alpha \sigma_{ij} \tag{3.10d}$$

where α can be found by substituting Eq. 3.10d into Eq. 3.10a.

The plastic modulus H can be interpolated as (D4)

$$H = H^b + hp_a[1 + |N/\eta|^m)(9Q^2+2J_2'V^2/3)/f^2] \frac{\delta}{\delta_o - \delta} \tag{3.10e}$$

where H^b is the plastic modulus of the bounding surface, h and m are material parameters, and p_a is the atmospheric pressure to provide correct dimensions. δ is the distance between the current stress state and the image stress state on the bounding surface defined by the mapping rule and δ_o is a reference point in the stress space. The other variables in Eq. 3.10e are defined as

$$\eta = \frac{\sqrt{J_2}}{J_1} \tag{3.10f}$$

$$J_1 = \sigma_{ii} \quad \text{and} \quad J_2 = s_{ij}s_{ij} \tag{3.10g}$$

$$s_{ij} = (\sigma_{ij} - \frac{J_1}{3}\delta_{ij}) \tag{3.10h}$$

$$J^b_1 = \sigma^b_{ii} \quad \text{and} \quad J^b_2 = s^b_{ij}s^b_{ij} \tag{3.10i}$$

$$s^b_{ij} = (\sigma^b_{ij} - \frac{J^b_1}{3}\delta_{ij}) \tag{3.10j}$$

$$Q = \frac{\partial F}{\partial J_1^b} \quad \text{and} \quad V = 2\,\frac{\partial F}{\partial J_2^b} \tag{3.10k}$$

In the radial mapping rule, δ can be defined as

$$\delta = [(\sigma^b_{ij} - \sigma_{ij})(\sigma^b_{ij} - \sigma_{ij})]^{1/2} = (\alpha - 1)[\sigma_{ij}\sigma_{ij}]^{1/2} \tag{3.10l}$$

Various shapes of bounding surface can be defined to match the behaviour of particular soils. Dafalias and Herrmann choose the following bounding surface (D3)

$$F = (J_1^b - \frac{2}{R} J_o)J_1^b + \left[\frac{R-1}{N}\right]^2 J_2^b + \frac{2-R}{R} J_o^2 = 0 \tag{3.11a}$$

for $0 \le \eta \le N$ and

$$F = (J_1^b - \frac{2}{R} J_o)J_1^b - \frac{J_2^b}{N^2} + 2J_o(\frac{1}{R} + \frac{A_c}{N_c})\frac{\sqrt{J_2^b}}{N} - \frac{2}{R}\frac{A_c}{N_c} J_o^2 = 0 \tag{3.11b}$$

for $\eta > N$, where R, A_c and N_c are material parameters and J_o is a hardening parameter which is the intersection point of the current elastic wall with the isotropic consolidation line. J_o can be calculated from the bounding surface equation for the normal consolidate state and its increment can be calculated by the following equation for the over-consolidated state

$$dJ_o = \frac{(1+e_o)J_o}{\lambda-\kappa}\,\frac{3Q}{f}\,\langle L\rangle \tag{3.11c}$$

L is defined in Eq. 3.6b. N depends on the Load angle θ

$$N(\theta) = \frac{2n_N N_c}{1 + n_N - (1 - n_N)\sin(3\theta)} \tag{3.11d}$$

$$\sin(3\theta) = 3\sqrt{6}\, J_3^b/(J_2^b)^{3/2} \quad \text{and} \quad -30^\circ \le \theta \le 30^\circ \tag{3.11e}$$

$$n_N = N_e/N_c \tag{3.11f}$$

where J_3 is the determinant of the deviatoric stress tensor s_{ij} and N_e and N_c are the values of N specified for triaxial compression and extension tests and are related to the slope of the isotropic consolidation line in the e-lnp' plot

$$N_e = \frac{\sqrt{2}}{3\sqrt{3}} M_e \tag{3.11g}$$

$$N_c = \frac{\sqrt{2}}{3\sqrt{3}} M_c \tag{3.11h}$$

R is a function of the Load angle and can be written as (D5)

$$R(\theta) = \frac{2n_R R_c}{1 + n_R - (1 - n_R)\sin(3\theta)} \tag{3.11i}$$

and similarly $n_R = R_e/R_c$ where R_e and R_c are material parameters.

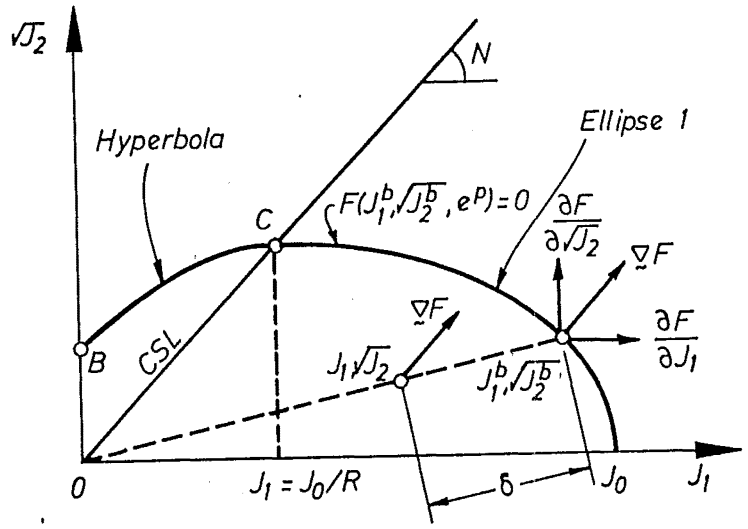

Fig. 3.5 The Bounding Surface in the Space of Stress Invariants

The bounding surface in the stress invariants space is shown in Fig. 3.5.

3.4 Finite Element Implementation of the Soil Model

In the finite element formulation, a tangent stiffness matrix as defined in Eq. 3.2d is required for a nonlinear problem. The D matrix in Eq. 3.2d is a transformation matrix mapping the quantity from the strain space into the stress space. The formulation outlined in Section 3.2 has to be rewritten to match the finite element formula.

Eq. 3.9a can be rewritten as

$$\{d\sigma\} = [D]\{d\epsilon\} \tag{3.12a}$$

where

$$\{d\sigma\} = \begin{Bmatrix} d\sigma_x \\ d\sigma_y \\ d\sigma_z \\ d\tau_{xy} \\ d\tau_{xz} \\ d\tau_{yz} \end{Bmatrix} \quad \text{and} \quad \{d\epsilon\} = \begin{Bmatrix} d\epsilon_x \\ d\epsilon_y \\ d\epsilon_z \\ d\gamma_{xy} \\ d\gamma_{xz} \\ d\gamma_{yz} \end{Bmatrix} \tag{3.12b}$$

$$[D] = [D^e] - [D^p] \tag{3.12c}$$

$$[D^e] = \begin{bmatrix} K+G4/3 & K-2G/3 & K-2G/3 & 0 & 0 & 0 \\ K-2G/3 & K+4G/3 & K-2G/3 & 0 & 0 & 0 \\ K-2G/3 & K-2G/3 & K+4G/3 & 0 & 0 & 0 \\ 0 & 0 & 0 & G & 0 & 0 \\ 0 & 0 & 0 & 0 & G & 0 \\ 0 & 0 & 0 & 0 & 0 & G \end{bmatrix} \tag{3.12d}$$

$$[D^p] = \frac{1}{T}\begin{bmatrix} D_1^2 & D_1D_2 & D_1D_3 & 2Gn_{12}D_1 & 2Gn_{13}D_1 & 2Gn_{23}D_1 \\ D_1D_2 & D_2^2 & D_2D_3 & 2Gn_{12}D_2 & 2Gn_{13}D_2 & 2Gn_{23}D_2 \\ D_1D_3 & D_2D_3 & D_3^2 & 2Gn_{12}D_3 & 2Gn_{13}D_3 & 2Gn_{23}D_3 \\ 2Gn_{12}D_1 & 2Gn_{12}D_2 & 2Gn_{12}D_3 & 4G^2n_{12}^2 & 4G^2n_{12}n_{13} & 4G^2n_{12}n_{23} \\ 2Gn_{13}D_1 & 2Gn_{13}D_2 & 2Gn_{13}D_3 & 4G^2n_{13}n_{12} & 4G^2n_{13}^2 & 4G^2n_{13}n_{23} \\ 2Gn_{23}D_1 & 2Gn_{23}D_2 & 2Gn_{23}D_3 & 4G^2n_{23}n_{12} & 4G^2n_{13}n_{23} & 4G^2n_{23}^2 \end{bmatrix} \tag{3.12e}$$

$$T = H + 2G + 9(K-2G/3)Q^2/f^2 \tag{3.12f}$$

$$D_1 = 2Gn_{11} + 3(K-2G/3)Q/f \tag{3.12g}$$

$$D_2 = 2Gn_{22} + 3(K-2G/3)Q/f \tag{3.12h}$$

$$D_3 = 2Gn_{33} + 3(K-2G/3)Q/f \tag{3.12i}$$

where i,j,k has been set equal to 1, 2, 3 (x, y, z) and the repeated numeral indices do not mean summation.

By applying the chain rule of differentiation to Eq. 3.10c means that

$$n_{ij} = [Q\delta_{ij} + \alpha Vs_{ij} + (X_NW_N + X_RW_R)C_{ij}]/f \tag{3.12j}$$

where

$$X_N = N\frac{\partial F}{\partial N}\ ,\ X_R = R\frac{\partial F}{\partial R}\ ,\ W_N = \frac{\partial N}{N\ \partial[\sin(3\theta)]}\ ,\ W_R = \frac{\partial R}{R\ \partial[\sin(3\theta)]}$$

$$\text{and}\quad C_{ij} = \frac{\partial[\sin(3\theta)]}{\partial\sigma_{ij}^b} \tag{3.12k}$$

and that

$$f^2 = 3Q^2 + \alpha^2V^2J_2 + 9(X_NW_N + X_RW_R)^2[1 - \sin^2(3\theta)] \tag{3.12l}$$

Substituting Eq. 3.11d and Eq. 3.11i and Eq. 3.11e into Eq. 3.12k leads to

$$W_N = \frac{1 - n_N}{1 + n_N - (1 - n_N)\sin(3\theta)} \tag{3.12m}$$

$$W_R = \frac{1 - n_R}{1 + n_R - (1 - n_R)\sin(3\theta)} \tag{3.12n}$$

$$C_{ij} = \frac{3\sqrt{6}}{\alpha J_2}\left[\frac{1}{\sqrt{J_2}}s_{ik}s_{kj} - \frac{1}{3}\sqrt{J_2}\delta_{ij} - \frac{s_{ij}}{\sqrt{6}}\sin(3\theta)\right] \tag{3.12q}$$

The coefficients α, V, X_N, X_R and H^b depend on the bounding surface and are derived by substituting Eq. 3.10d, Eq. 3.10k, Eq. 3.12k and Eq. 3.6g into the bounding surface equation Eq. 3.11a and Eq. 3.11b

$$\alpha = \frac{-B + (B^2 - 4AC)^{1/2}}{2A} \tag{3.13a}$$

for $0 \le \eta \le N$

$$A = J_1^2 + \left[\frac{R-1}{N}\right]^2 J_2, \quad B = -\frac{2J_oJ_1}{R}, \quad C = \frac{2 - R}{R} \tag{3.13b}$$

$$V = 2\left[\frac{R-1}{N}\right]^2 \tag{3.13c}$$

$$X_N = -2\alpha^2 J_2\left[\frac{R-1}{N}\right]^2 \tag{3.13d}$$

$$X_R = 2\left[\frac{J_o(\alpha J_1 - J_o)}{R} + \alpha^2 J_2\frac{R(R-1)}{N^2}\right] \tag{3.13e}$$

$$H^b = \frac{6}{R}\left[\alpha J_1 - (2 - R)J_o\right]\left[\frac{1+e_o}{\lambda-\kappa}\right]J_o\frac{Q}{f^2} \tag{3.13f}$$

and for $\eta > N$

$$A = J_1^2 - \frac{J_2}{N^2},\quad B = 2J_o\left[\frac{1}{R} + \frac{A_c}{N_c}\right]\frac{\sqrt{J_2}}{N} - \frac{2J_oJ_1}{R},\quad C = -\frac{2J_o^2}{N}\frac{A_c}{N_c} \tag{3.13g}$$

$$V = \frac{2}{N}\left[\frac{J_o}{\alpha\sqrt{J_2}}\left(\frac{1}{R} + \frac{A_c}{N_c}\right) - \frac{1}{N}\right] \tag{3.13h}$$

$$X_N = \frac{2\alpha^2 J_2}{N}\left[\frac{1}{N} - \frac{J_o}{\alpha\sqrt{J_2}}\left(\frac{1}{R} + \frac{A_c}{N_c}\right)\right] \tag{3.13i}$$

$$X_R = \frac{2J_o}{R}\left[\alpha\left(J_1 - \frac{\sqrt{J_2}}{N}\right) + \frac{A_c}{N_c}J_o\right] \tag{3.13j}$$

$$H^b = \frac{6}{R}\left[\alpha J_1 - \left(1 + R\frac{A_c}{N_c}\right)\frac{\alpha\sqrt{J_2}}{N} + \frac{2A_c}{N_c}J_o\right]\left[\frac{1+e_o}{\lambda-\kappa}\right]J_o\frac{Q}{f^2} \tag{3.13k}$$

For simplicity, Dafalias and Herrmann (D3) took the reference point δ_o as the distance between the image point on the boundary, σ_{ij}^b, and the origin. Thus the interpolation function in Eq. 3.10e becomes

$$\frac{\delta}{\delta_o - \delta} = \alpha - 1 \tag{3.13l}$$

The pore water pressure under the undrained condition can be approximately taken into account by adding the apparent bulk modulus of the pore water, K_a, to the constitutive matrix by the following formula

$$d\sigma_{ij}^t = d\sigma_{ij} + du\delta_{ij} \tag{3.14a}$$

$$du = K_a d\epsilon_{ii} \tag{3.14b}$$

$$K_a = \frac{1+e}{e}K_w \tag{3.14c}$$

where σ^t is the total stress, u is pore water pressure and K_w is the bulk modulus of the water and may be chosen as 10^5 kN/m^2 (G3). Eq. 3.12a can be rewritten as

$$\{d\sigma^t\} = [D^t]\{d\epsilon\} \tag{3.14d}$$

$$[D^t] = [D^e] - [D^p] + [D^v] \tag{3.14e}$$

$$[D^v] = \begin{bmatrix} K_a & K_a & K_a & 0 & 0 & 0 \\ K_a & K_a & K_a & 0 & 0 & 0 \\ K_a & K_a & K_a & 0 & 0 & 0 \\ 0 & 0 & 0 & 0 & 0 & 0 \\ 0 & 0 & 0 & 0 & 0 & 0 \\ 0 & 0 & 0 & 0 & 0 & 0 \end{bmatrix} \tag{3.14f}$$

Because K_a is much larger than the bulk modulus of the soil skeleton, the volumetric strain of a soil element is nearly zero under an undrained condition. As recommended by Naylor (N1), the reduced integration scheme is preferred and averaging the calculated stresses from integration points is taken as the element stress to reduce the stress error.

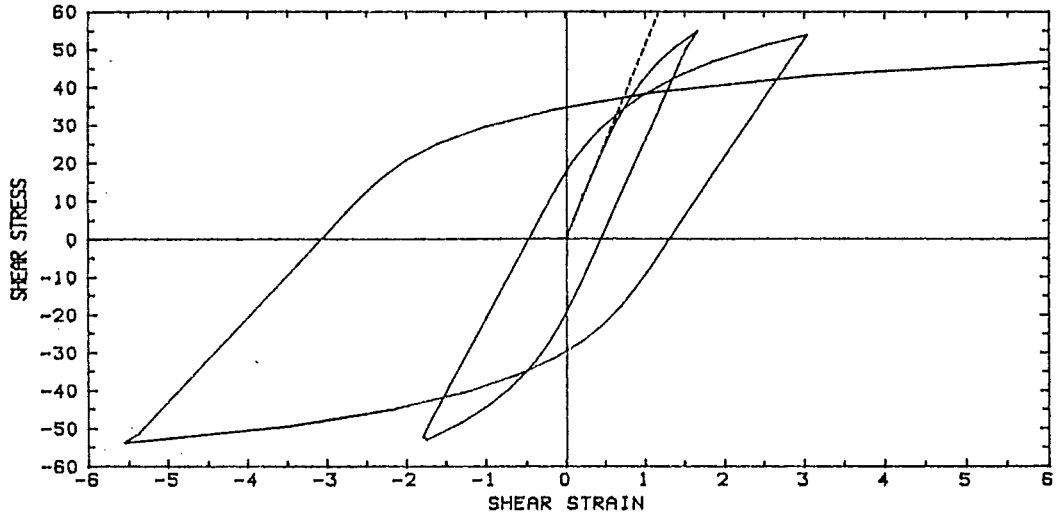

Fig. 3.6 Response of Undrained Simple Shear Model Problem

Many engineering applications can be idealized as plane strain problems. The constitutive matrix of the bounding surface soil model for plane strain problem can be derived by deleting the columns corresponding $d\epsilon_z$, $d\gamma_{xz}$ and $d\gamma_{yz}$ and setting the corresponding shear stresses zero in Eq. 3.12.

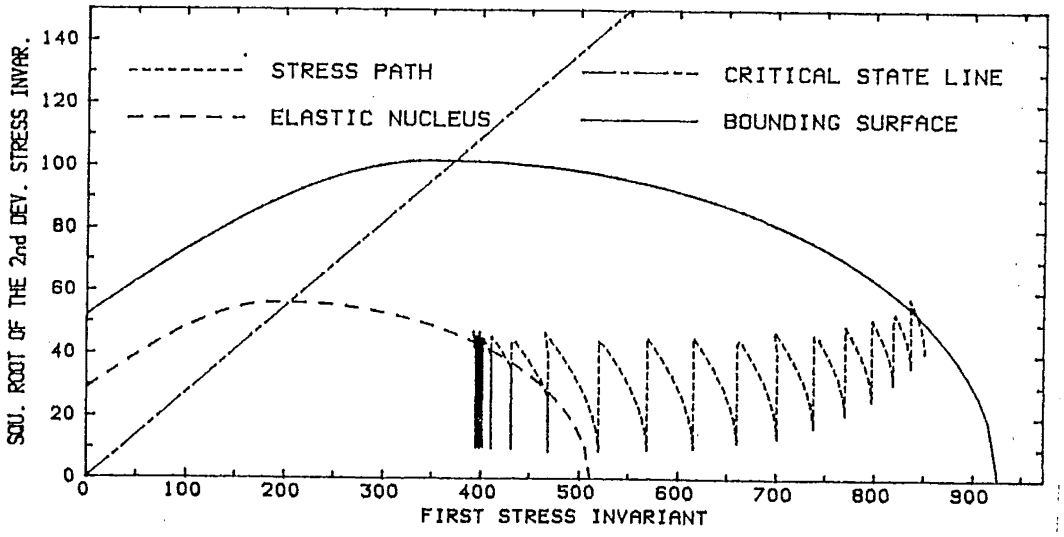

Fig. 3.7 Elastic Nucleus and Cyclic Stability

A simple shear problem was modelled by one 8-node isoparametic plane strain finite element to show the behaviour of the model and to verify the computer program. The result is shown in Fig. 3.6.

It can be seen from Fig. 3.6 that the effective normal stress decreases during the shearing procedure because of the pore water pressure generation. A soil element can be brought to the critical state for any amplitude of deviatoric stress component if a sufficient number of cycles of loading is applied. It has been shown experimentally by Sangrey, Henkel and Espig that depending on the amplitude of the deviatoric stress component, the soil may fail or be brought to a non-linear equilibrium (D3). The accumulation of the normal strain due to the plastic deformation has to be eliminated for the load cycles with lower amplitude of the deviatoric stress component to terminate the cyclic mobility. An elastic nucleus has been suggested by Dalafias and Herrmann to remedy the deficiency of the model (D3, D4). The size of the elastic nucleus depends on the magnitude of the plastic volumetric strain so that the load cycles with lower amplitude of deviatoric stress component will eventually enter the elastic nucleus domain with full stabilization while the cycles with higher amplitude will still be brought to a critical state. This can be very easily incorporated into the model without explicitly defining the elastic nucleus. Defining an additional material parameter α_{max} such that when $\alpha > \alpha_{max}$, set $H^b = \infty$ so that only elastic deformation occurs. This is illustrated in Fig. 3.7. It can be seen from Fig. 3.7 that this model may not be used without modification for modelling cohesionless soil to predict the

liquefaction of the soil because in all circumstances the soil will fail at the critical state and the pore water pressure may be stabilized (P1).

3.5 Determination of the Model Parameters and the Model Prediction

The parameters of the bounding surface model are N_c, N_e, λ, κ, R_c, R_e, m, h and A_c. The determination of the first four parameters is well described in the literature on critical soil mechanics and will not be repeated here (A2, D9). After these four parameters are chosen, R_c and R_e can be determined from a triaxial test on the normally consolidated soil since no other unknown parameters are present in the bounding surface equation. Under an undrained condition, an analytical expression was given by Dalafias and Herrmann for a normally consolidated soil as (D5)

$$\frac{|q|}{p_o} = \frac{M}{R-1}\left\{\frac{2}{R}\left[\frac{p}{p_o}\right]^{(\lambda-2\kappa/\lambda-\kappa)} + \left[1-\frac{2}{R}\right]\left[\frac{p}{p_o}\right]^{(-2\kappa/\lambda-\kappa)} - \left[\frac{p}{p_o}\right]^2\right\}^{1/2} \qquad (3.15a)$$

where p_o is the initial isotropic consolidation pressure. It is possible to obtain R_c and R_e by fitting the experimentally determined undrained stress path, given the values of κ and λ, and M_c and M_e for compression and extension respectively. R_c will also determine the lateral stress coefficient under a laterally restrained condition for a normally consolidated soil. This is illustrated in Fig. 3.8 for the normally consolidated kaolin tested by Banerjee and Stipho (B1).

Parameter m in Eq. 3.10e has been taken as 0.2 to ensure H becomes singular when η approaches zero so that purely elastic loading results and it has been considered to be suitable for most soils. Parameter h can be chosen to depend on the Load angle θ as

$$h(\theta) = \frac{2n_h\, h_c}{1 + n_h - (1 - n_h)\sin(3\theta)} \qquad (3.15b)$$

where

$$n_h = h_e/h_c \qquad (3.15c)$$

The parameters h_c and h_e are determined from the compression and extension tests respectively and have to be determined by fitting the experimental data on the isotropically over-consolidated soil sample at an overconsolidation ratio between 1 and R_c or R_e. Then A_c can be determined by fitting the experimental data on a heavily over-consolidated soil sample at an overconsolidation ratio grater at least than 5 when all other parameters are known (D3, D4).

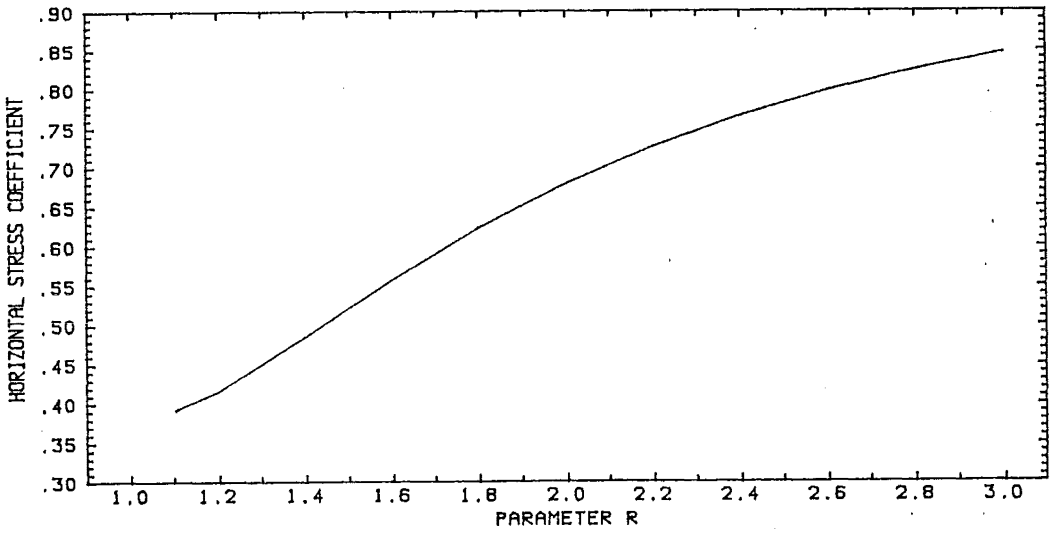

Fig. 3.8 Lateral Stress Coefficient Prediction for Kaolin

Table 3.1 Model Parameters for Kaolin

λ	0.14	N_c	0.286	R_e	2.45
κ	0.05	N_e	0.231	h_c	14.0
A_c	0.085	R_c	2.72	h_e	16.5

K and G can be chosen as

$$K = \frac{J_1(1+e_o)}{3\kappa} \qquad (3.15d)$$

$$G = \frac{3K(1-2\upsilon)}{2(1+\upsilon)} \qquad (3.15e)$$

where υ is the Poisson's ratio. An alternative way of defining the elastic parameters is to choose G as a constant depending on only the initial stress state and thus υ will vary with the stress state.

Table 3.2 Initial Conditions for Triaxial Compression on Kaolin

OCR	p_o (kpa)	p_i (kpa)	G (kpa)	e_i
1	366.0	366.0	10650.0	0.94
1.2	366.0	304.0	6350.0	0.95
5	380.0	76.0	2750.0	0.95
8	386.0	48.0	1670.0	0.95
12	413.0	35.0	1100.0	0.95

Table 3.3 Initial Conditions for Triaxial Extension on Kaolin

OCR	p_o (kpa)	p_i (kpa)	G (kpa)	e_i
1	414.0	414.0	11000.0	0.93
1.2	414.0	345.0	10150.0	0.93
6	551.0	92.0	3675.0	0.95
10	414.0	41.4	1932.0	0.95

For monotonic loading the test on kaolin reported by Benerjee and Stipho is simulated by the bounding surface model and the results are shown in Fig. 3.9 and Fig. 3.10. Very good agreement has been achieved. The model parameters are given in Table 3.1 and the initial conditions are given in Table 3.2 and Table 3.3 in which OCR is the overconsolidation ratio.

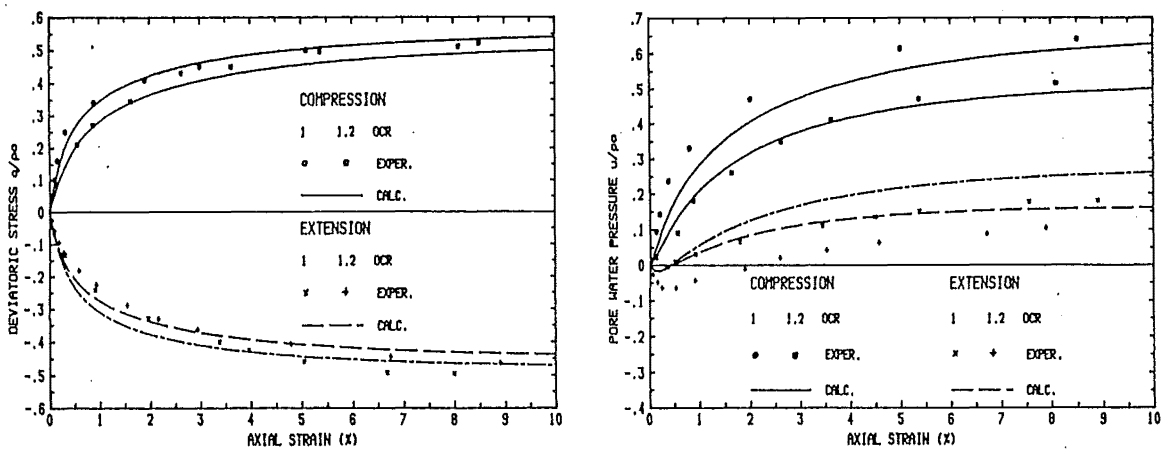

(a) (b)

Fig. 3.9 Simulation and Comparison of Normally Consolidated and Lightly Over-consolidated Soil

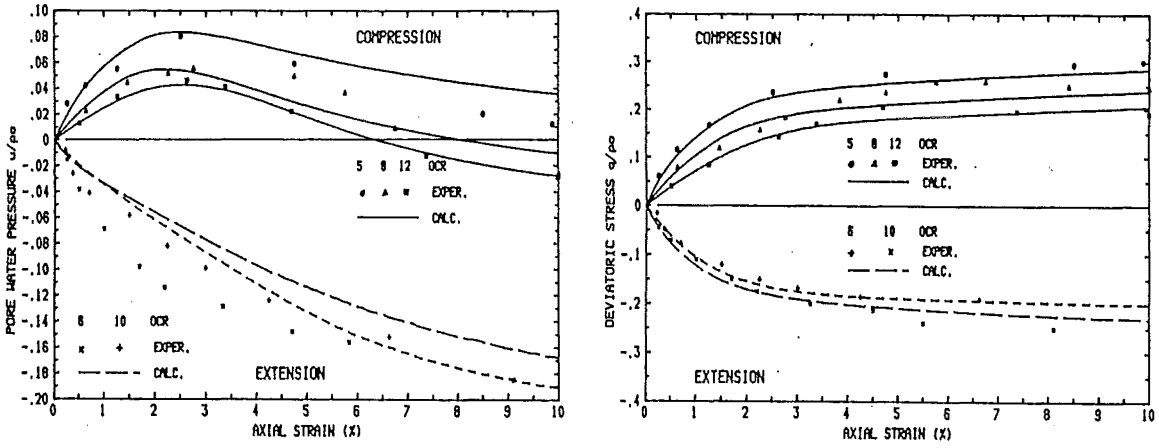

(a) (b)

Fig. 3.10 Simulation and Comparison of Heavily Over-consolidated Soil

For cyclic loading, the loading speed may affect the response of soil. Because there is no complete experimental data available, the original work for the comparison of cyclic loading given by Dafalias and Herrmann (D3, D4) is presented in Fig. 3.11 to demonstrate the model behaviour. The model predicts the loading and unloading path reasonably well in the first few cycles.

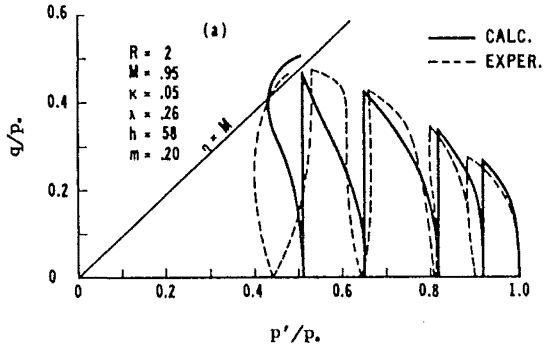

Fig. 3.11 Simulation and Comparison for Kaolin Under Cyclic Loading

3.6 The Bounding Surface Plasticity Model for the Beam Element

The bounding surface plasticity model can be applied to a beam element in which yielding is developed at certain sections of the beam. For example, if a beam element is assumed to yield only at the beam ends, the previous plasticity formulae can be extended as below. It is easier to use a vector notation for the beam element instead of tensor notation as for the solid element.

For a beam element, as shown in Fig. 3.12, plastic deformation is developed within the plastic hinges for either a finite small or infinite small length. For a dynamic beam model, the plastic hinges are assumed to be at the beam ends A and B. The yielding surfaces are defined as (K1)

$$F_A(Q_A, k_A) = 0 \tag{3.16a}$$

for end A and

$$F_B(Q_B, k_B) = 0 \tag{3.16b}$$

for end B, where Q is the force vector at the beam ends as shown in Fig. 3.12, k is a hardening parameter and the subscripts A and B indicate the quantity at end A and end B respectively. The interaction of beam end moment in different directions, torsion and axial forces can be included in the yield surface functions. The beam end incremental deformations corresponding to the forces shown in Fig. 3.12 consist of elastic and plastic parts and are defined as

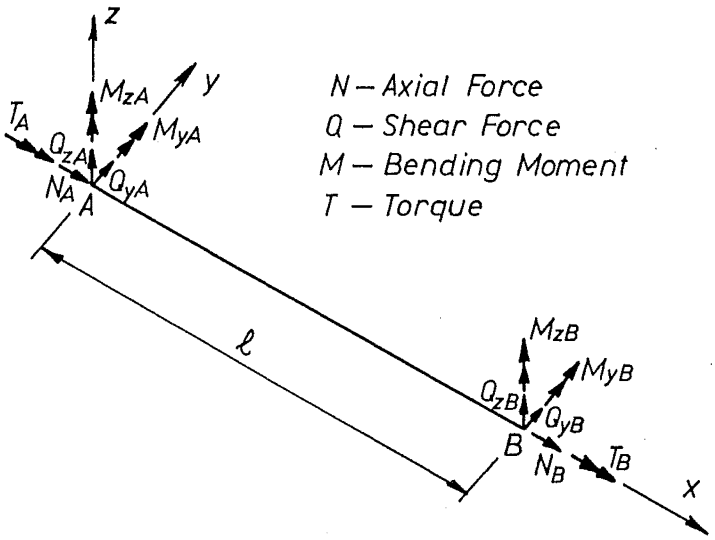

Fig. 3.12 Beam Element Model

$$dq_A = dq_A^e + dq_A^p \tag{3.16c}$$

$$dq_B = dq_B^e + dq_B^p \tag{3.16d}$$

where the superscripts e and p indicate elastic state and plastic state respectively.

The elastic part can be related to the incremental force vector by a stiffness matrix as

$$\begin{Bmatrix} dQ_A \\ dQ_B \end{Bmatrix} = \begin{bmatrix} S_{AA} & S_{AB} \\ S_{BA} & S_{BB} \end{bmatrix} \begin{Bmatrix} dq_A^e \\ dq_B^e \end{Bmatrix} \tag{3.16e}$$

The plastic deformation can be defined as

$$dq_A^p = \langle L_A \rangle f_A \tag{3.16f}$$

$$dq_B^p = \langle L_B \rangle f_B \tag{3.16g}$$

where f stands for the gradient of the yield surface F

$$f_A = \left\{ \frac{\partial F_A}{\partial Q_A} \right\} \tag{3.16h}$$

$$f_B = \left\{ \frac{\partial F_B}{\partial Q_B} \right\} \tag{3.16i}$$

and $< >$ is defined in Eq. 3.6d. L represents the loading function and is given as

$$L_A = \frac{f_A^T dQ_A}{K_A} \tag{3.16j}$$

$$L_B = \frac{f_B^T dQ_B}{K_B} \tag{3.16k}$$

where K represents plastic modulus and can be obtained from the consistency condition of Eq. 3.16a and 3.16b

$$K_A = - \frac{\partial F_A}{\partial k_A} \left\{ \frac{\partial k_A}{\partial q_A^p} \right\}^T f_A \tag{3.16l}$$

$$K_B = - \frac{\partial F_B}{\partial k_B} \left\{ \frac{\partial k_B}{\partial q_B^p} \right\}^T f_B \tag{3.16m}$$

If beam end A has yielded while end B is still elastic, $dq_B^p = \{0\}$ and from Eq. 3.16c to Eq. 3.16j L_A can be solved as

$$L_A = \frac{f_A^T (S_{AA} dq_A + S_{AB} dq_B)}{H_A} \tag{3.17a}$$

where

$$H_A = K_A + f_A^T S_{AA} f_A \tag{3.17b}$$

By substituting Eq. 3.17a into 3.16f, from Eq. 3.16c and 3.16e, the incremental forces of the beam element can be derived as

$$\begin{Bmatrix} dQ_A \\ \\ dQ_B \end{Bmatrix} = \begin{bmatrix} S_{AA} - \dfrac{S_{AA}f_A f_A^T S_{AA}}{H_A} & S_{AB} - \dfrac{S_{AA}f_A f_A^T S_{AB}}{H_A} \\ \\ S_{BA} - \dfrac{S_{BA}f_A f_A^T S_{AA}}{H_A} & S_{BB} - \dfrac{S_{BA}f_A f_A^T S_{AB}}{H_A} \end{bmatrix} \begin{Bmatrix} dq_A \\ \\ dq_B \end{Bmatrix} \tag{3.17c}$$

Similarly, if beam end B has yielded while end A is still elastic, $dq_A^P = (0)$ and from Eq. 3.16c to Eq. 3.16k L_B can be solved as

$$L_B = \frac{f_B^T(S_{BA}dq_A + S_{BB}dq_B)}{H_B} \tag{3.18a}$$

where

$$H_B = K_B + f_B^T S_{BB} f_B \tag{3.18b}$$

By substituting Eq. 3.18a into 3.16f, from Eq. 3.16c and 3.16e, the incremental forces and displacements at the ends of a beam element can be related by the tangent stiffness matrix as

$$\begin{Bmatrix} dQ_A \\ \\ dQ_B \end{Bmatrix} = \begin{bmatrix} S_{AA} - \dfrac{S_{AB}f_B f_B^T S_{BA}}{H_B} & S_{AB} - \dfrac{S_{AB}f_B f_B^T S_{BB}}{H_B} \\ \\ S_{BA} - \dfrac{S_{BB}f_B f_B^T S_{BA}}{H_B} & S_{BB} - \dfrac{S_{BB}f_B f_B^T S_{BB}}{H_B} \end{bmatrix} \begin{Bmatrix} dq_A \\ \\ dq_B \end{Bmatrix} \tag{3.18c}$$

When both ends of the beam element are yielding, the loading functions and the tangent stiffness matrix can be derived in a similar manner. The loading functions are obtained as

$$L_A = [(K_B T_{AA}^T + \alpha_{BB} T_{AA}^T - \alpha_{AB} T_{BA}^T)dq_A + (K_B T_{BA}^T + \alpha_{BB} T_{BA}^T - \alpha_{AB} T_{BB}^T)dq_B]/H \tag{3.19a}$$

$$L_B = [(K_A T_{AB}^T + \alpha_{AA} T_{AB}^T - \alpha_{BA} T_{AA}^T)dq_A + (K_A T_{BB}^T + \alpha_{AA} T_{BB}^T - \alpha_{BA} T_{BA}^T)dq_B]/H \tag{3.19b}$$

where

$$\alpha_{AA} = f_A^T S_{AA} f_A \tag{3.19c}$$

$$\alpha_{AB} = f_A^T S_{AB} f_B \tag{3.19d}$$

$$\alpha_{BA} = f_B^T S_{BA} f_A \tag{3.19e}$$

$$\alpha_{BB} = f_B^T S_{BB} f_B \tag{3.19f}$$

$$T_{AA} = S_{AA} f_A \tag{3.19g}$$

$$T_{AB} = S_{AB} f_B \tag{3.19h}$$

$$T_{BA} = S_{BA} f_A \tag{3.19i}$$

$$T_{BB} = S_{BB} f_B \tag{3.19j}$$

$$H = K_A K_B + K_A \alpha_{BB} + K_B \alpha_{AA} + \alpha_{AA}\alpha_{BB} - \alpha_{AB}\alpha_{BA} \tag{3.19k}$$

and $\alpha_{AB} = \alpha_{BA}$.

The incremental forces at the ends of a beam element can be found as

$$\begin{Bmatrix} dQ_A \\ dQ_B \end{Bmatrix} = \begin{bmatrix} S_{AA} - P_{AA} & S_{AB} - P_{AB} \\ S_{BA} - P_{BA} & S_{BB} - P_{BB} \end{bmatrix} \begin{Bmatrix} dq_A \\ dq_B \end{Bmatrix} \tag{3.20a}$$

where

$$P_{AA} = \frac{(K_B+\alpha_{BB})T_{AA}T_{AA}^T + (K_A+\alpha_{AA})T_{AB}T_{AB}^T - \alpha_{AB}(T_{AA}T_{AB}^T+T_{AB}T_{AA}^T)}{H} \tag{3.20b}$$

$$P_{AB} = \frac{(K_B+\alpha_{BB})T_{AA}T_{BA}^T + (K_A+\alpha_{AA})T_{AB}T_{BB}^T - \alpha_{AB}(T_{AA}T_{BB}^T+T_{AB}T_{BA}^T)}{H} \tag{3.20c}$$

$$P_{BA} = \frac{(K_B+\alpha_{BB})T_{BA}T_{AA}^T + (K_A+\alpha_{AA})T_{BB}T_{AB}^T - \alpha_{AB}(T_{BA}T_{AB}^T+T_{BB}T_{AA}^T)}{H} \tag{3.20d}$$

$$P_{BB} = \frac{(K_B+\alpha_{BB})T_{BA}T_{BA}^T + (K_A+\alpha_{AA})T_{BB}T_{BB}^T - \alpha_{AB}(T_{BA}T_{BB}^T+T_{BB}T_{BA}^T)}{H} \tag{3.20e}$$

For a beam element subjected to two dimensional loading, the force vector Q includes axial force, transverse force and moment. The interaction effects between these actions can be systematically incorporated into the yield surface function for each end. For example, the interaction of axial force and moment of a reinforced concrete beam can be taken into account by defining yielding surface functions Eq. 3.16a and 3.16b from experimental data as the bounding surfaces for each end and introducing a interpolation function for the plastic modulus K. Isotropic and kinematic hardening rules can also be introduced. As an illustration, the previously developed tangent stiffness matrix is formulated for a beam element subjected to moment without interaction with axial force, ie., the axial deformation is still elastic.

If Prager's kinematic hardening rule is introduced, Eq. 3.16a and 3.16b have the following form:

$$F = |M - k| - M_y = 0 \tag{3.21a}$$

$$dk = E_o^p d\phi^p \tag{3.21b}$$

where M is the moment at the end of a beam element, k is a hardening parameter, M_y is the yield moment, E_o^p is the stiffness of the section after yielding which for the bounding surface model is the slope of the bounding line in the moment-plastic-curvature plane and ϕ^p is the plastic curvature developed at the beam section. This model is usually referred to as a bi-linear model. If it is assumed that the plastic hinge has a finite length of l_p and the plastic curvature is constant within the plastic hinge, substituting Eq. 3.16j into Eq. 3.16f leads to

$$K = \frac{E^t}{l_p\left(1 - \frac{E^t}{EI}\right)} \tag{3.21c}$$

where E^t is the tangent stiffness of the beam section and EI is the initial elastic stiffness of the beam section.

Substituting Eq. 3.21a into Eq. 3.16h leads to

$$f = \text{Sign}\ (M - k) \tag{3.21d}$$

where the Sign function has the following definition:

$$\text{Sign}(x) = \begin{cases} 1 & \text{if } x \geq 0 \\ -1 & \text{if } x < 0 \end{cases} \tag{3.21e}$$

If end A is yielding while end B is still elastic, the beam end moments and rotations are related as

$$\begin{Bmatrix} dM_A \\ dM_B \end{Bmatrix} = \begin{bmatrix} S_{AA}\left(1 - \frac{S_{AA}}{H_A}\right) & S_{AB}\left(1 - \frac{S_{AA}}{H_A}\right) \\ S_{BA}\left(1 - \frac{S_{AA}}{H_A}\right) & S_{BB} - \frac{S_{BA}S_{AB}}{H_A} \end{bmatrix} \begin{Bmatrix} d\theta_A \\ d\theta_B \end{Bmatrix} \tag{3.22a}$$

where

$$H_A = K_A + S_{AA} \tag{3.22b}$$

and where θ represents the beam end rotation and S_{AA}, S_{AB}, S_{BA} and S_{BB} are the elements of the stiffness matrix for a linear elastic beam. For a uniform beam with a length of L, $S_{AA} = 4EI/L$, $S_{AB} = 2EI/L$, $S_{BA} = 2EI/L$ and $S_{BB} = 4EI/L$.

The loading function is

$$L_A = \text{Sign}(M_A - k_A) \frac{S_{AA}d\theta_A + S_{AB}d\theta_B}{H_A} \tag{3.22c}$$

and if $L_A > 0$

$$d\theta_A^p = \frac{S_{AA}d\theta_A + S_{AB}d\theta_B}{H_A} \tag{3.22d}$$

If end B is yielding while end A is still elastic, the beam end moments and rotations are related as

$$\begin{Bmatrix} dM_A \\ dM_B \end{Bmatrix} = \begin{bmatrix} S_{AA} - \frac{S_{AB}S_{BA}}{H_B} & S_{AB}\left(1 - \frac{S_{BB}}{H_B}\right) \\ S_{BA}\left(1 - \frac{S_{BB}}{H_B}\right) & S_{BB}\left(1 - \frac{S_{BB}}{H_B}\right) \end{bmatrix} \begin{Bmatrix} d\theta_A \\ d\theta_B \end{Bmatrix} \tag{3.23a}$$

where

$$H_B = K_B + S_{BB} \tag{3.23b}$$

$$L_B = \text{Sign}(M_B - k_B)\ \frac{S_{BA}d\theta_A + S_{BB}d\theta_B}{H_B} \tag{3.23c}$$

and if $L_B > 0$

$$d\theta_B^P = \frac{S_{BA}d\theta_A + S_{BB}d\theta_B}{H_B} \tag{3.23d}$$

If both ends are yielding, it can be shown that

$$\begin{Bmatrix} dM_A \\ dM_B \end{Bmatrix} = \frac{1}{H}\begin{bmatrix} \dfrac{(K_B+S_{BB})S_{AA} - S_{AB}S_{AB}}{K_B} & S_{AB} \\ S_{BA} & \dfrac{(K_A+S_{AA})S_{AA} - S_{AB}S_{AB}}{K_A} \end{bmatrix} \begin{Bmatrix} d\theta_A \\ d\theta_B \end{Bmatrix} \tag{3.24a}$$

where

$$H = \frac{K_AK_B + K_AS_{BB} + K_BS_{AA} + S_{AA}S_{BB} - S_{AB}S_{BA}}{K_AK_B} \tag{3.24b}$$

The loading functions are

$$L_A = \frac{\text{Sign}(M_A-k_A)}{H}[(K_BS_{AA} + S_{AA}S_{BB} - S_{AB}S_{BA})d\theta_A + K_BS_{AB}d\theta_B] \tag{3.24c}$$

$$L_B = \frac{\text{Sign}(M_B-k_B)}{H}[K_AS_{BA}d\theta_A + (K_AS_{BB} + S_{AA}S_{BB} - S_{BA}S_{AB})d\theta_B] \tag{3.24d}$$

If $L_A > 0$ then

$$d\theta_A^P = (K_BS_{AA} + S_{AA}S_{BB} - S_{AB}S_{BA})d\theta_A + K_BS_{AB}d\theta_B \tag{3.24e}$$

and if $L_B > 0$ then

$$d\theta_B^P = K_AS_{BA}d\theta_A + (K_AS_{BB} + S_{AA}S_{BB} - S_{BA}S_{AB})d\theta_B \tag{3.24f}$$

The tangent stiffness of the beam section can be calculated from

$$E^t = \frac{EIE^p}{EI + E^p} \tag{3.25a}$$

while the plastic modulus E^p is interpolated from

$$E^p = E_o^p + E_h \frac{\delta}{\delta_o - \delta} \tag{3.25b}$$

where E_h is a material parameter controlling the plastic deformation of the beam section within the bounding lines, δ is the distance from the current moment to the corresponding point on the bounding line, δ_o is the distance δ at first yield (the first yield moment is M_{yo}) and E_o is the slope of the bounding line as illustrated in Fig. 3.13. The detail of the interpolation function can be found from the reference by Dafalias and Popov (D6, D7).

The bounding surface model in one dimension has five parameters, EI, E_h, E_o^p, M_y and M_{yo}. A pure elastic range can be specified by M_{yo} and the model satisfies the Bauschinger effect. Unlike the widely used Ramberg-Osgood model, all parameters have their physical definitions and the model is more flexible. It may be easily extended to systematically take the inelastic interaction between the actions at the beam ends into account.

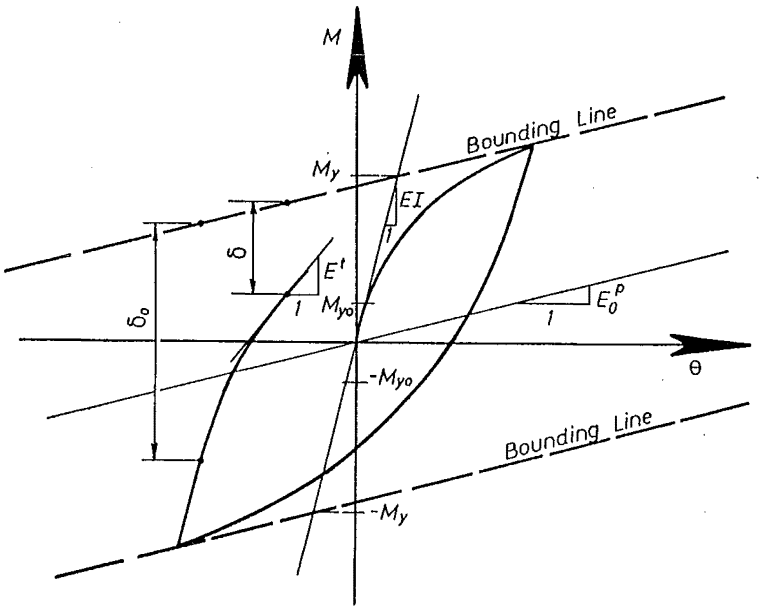

Fig. 3.13 The Bounding Surface Model for One Dimension Problem

3.7 Solution Techniques for the Dynamic Problems

The dynamic equilibrium equation of a system discretized by a finite element mesh can be written as (F1)

$$[M]\{\ddot{r}\} + [C]\{\dot{r}\} + [K]\{r\} + \{D(r,\dot{r})\} + \{S(r)\} = \{R(t)\} \qquad (3.26a)$$

where [M] represents mass matrix and [C] and [K] are the reference damping and stiffness matrices which may be taken as the initial ones or an updated ones during the iteration (F1). $\{D(r,\dot{r})\}$ and $\{S(r)\}$ are the forces generated from nonlinear damping and stiffness operators respectively and $\{R(t)\}$ is the applied force vector. Various solution techniques have been proposed in the literature (B3, F1, Z2). An efficient solution technique of such a problem may be the incremental method combined with the modified Newton-Raphson iteration. The scheme adopted here is the Newmark constant acceleration method due to its stability and accuracy for most engineering problems (N3).

Eq. 3.26a can be rewritten as (F1, S13)

$$[M]\{\ddot{r}\} + [C]\{\dot{r}\} + [K]\{r\} = \{R(t)\} - D'(r,\dot{r}) - S'(r) \qquad (3.26b)$$

where [C] and [K] may be chosen as other than the initial damping and stiffness matrices and may be updated when the rate of convergence of the iteration diminishes. The nonlinear forces $D'(r,\dot{r})$ and $S'(r)$ are computed from the system properties and the damping and stiffness matrices assigned for the left hand side of Eq. 3.26b. The details of solving Eq. 3.26a by the pseudo-force approach may be found in literature (F1,S13).

3.8 Material Assumptions and Other Available Models

The bounding surface model described in the previous sections is suitable for cohesive soils because it is developed in the frame work of

critical state soil mechanics. From the practical point of view it is reasonable to assume that the clay is saturated and subjected to undrained loading during an earthquake event because of the rapid loading and unloading. For cohesionless soil the parameters for the state boundary surface in the critical soil mechanics are difficult to determine because of its heavily over-consolidated state in both the natural and laboratory conditions and most of the soil models based on the critical soil mechanics will not be expected to predict the cohesionless soil behaviour well. However, it is possible to define a suitable type of bounding surface, mapping rule, interpolation function for plastic modulus and hardening parameters to predict the behaviour of a cohesionless soil using the bounding surface soil model. Such an attempt has been done by Aboim and Roth (A1). The extension has to be verified by reliable experiment for various stress paths under both drained and undrained conditions.

Other simple constitutive laws for soils have been used in finite element dynamic analyses. For example, the equivalent linear model has been successfully used to determine ground motion (I1, S3, S4, S6, S8). Variable modulus models which define the elastic modulus as a function of current stress or strain state and loading condition (loading and unloading) may also be used (N2, D9). Care and sound engineering judgement must be exercised when these simple models are adopted.

Chapter 4

Computer Implementation of the Energy Transmitting Boundaries and Numerical Considerations

4.1 The Boundary Element Formulation

The Green's function and the general formulae have been derived in Chapter 2. In the following sections, the detailed formulae will be derived for surface and embedded foundations.

For a surface foundation, the distributed loads can be chosen as being piece-wise constant and thus the interpolation function [L(s)] is an identity matrix. The advantage of choosing piecewise constant loads is that only one Green's function has to be calculated if all the elements are of equal size. The displacement can also be chosen as being piecewise constant and the displacement interpolation function [N(s)] is also an identity matrix. From Eq. 2.42a the matrix [T] is a diagonal matrix whose elements are the length of the corresponding element. All of the diagonal elements corresponding to the displacements in the same direction in matrix [G] in Eq.2.42b are identical and if the first two rows are calculated the other rows can be assigned the same elements in the same order as the first two rows.

For an embedded foundation, two vertical boundaries and a horizontal boundary at the bottom are chosen. This simple geometry of the boundary will result in less effort to compute the Green's function.

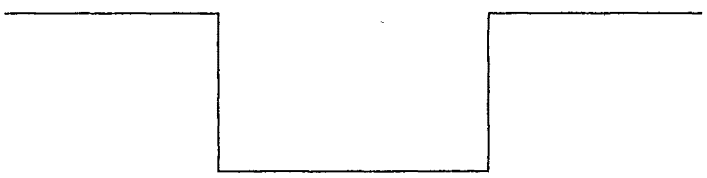

Fig. 4.1 The boundaries for an embedded foundation

For the vertical boundaries, the displacement shape function N(s) can be chosen as a piece-wise linear function. For the ith element in the local coordinate system, the displacement shape function is

$$[N_i(s)] = \begin{bmatrix} 1 - \frac{s}{b_i} & 0 & \frac{s}{b_i} & 0 \\ 0 & 1 - \frac{s}{b_i} & 0 & \frac{s}{b_i} \end{bmatrix} \tag{4.1}$$

where b_i is the length of the ith element and s is the local coordinate in the ith element.

For the source parameters, a discontinuity at each corner is introduced so that the matrices can be uncoupled into submatrices for the vertical and horizontal boundaries and the singularity at the corner can be avoided. The source shape function for an element on the vertical boundary is

$$[L_i(s)] = \begin{bmatrix} 1 - \frac{s}{b_i} & 0 & \frac{s}{b_i} & 0 \\ 0 & 1 - \frac{s}{b_i} & 0 & \frac{s}{b_i} \end{bmatrix} \tag{4.2}$$

and on the horizontal boundary

$$[L_i(s)] = \begin{bmatrix} 1 & 0 \\ 0 & 1 \end{bmatrix} \tag{4.3}$$

The source shape function of the whole system is

$$[L(s)] = \begin{bmatrix} [L(s)]_{LL} & [L(s)]_{LH} & [L(s)]_{LR} \\ [L(s)]_{HL} & [L(s)]_{HH} & [L(s)]_{HR} \\ [L(s)]_{RL} & [L(s)]_{RH} & [L(s)]_{RR} \end{bmatrix} \tag{4.4}$$

where $[L(s)]_{LL}$ - the shape function for the left hand side vertical boundary.
$[L(s)]_{HH}$ - the shape function for the horizontal boundary.

$[L(s)]_{RR}$ - the shape function for the right hand side vertical boundary.

The other submatrices are coupling terms and are null matrices here.

The Green's function of the system can be written as

$$[g_u(s)] = \begin{bmatrix} [g_u(s)]_{LL} & [g_u(s)]_{LH} & [g_u(s)]_{LR} \\ [g_u(s)]_{HL} & [g_u(s)]_{HH} & [g_u(s)]_{HR} \\ [g_u(s)]_{RL} & [g_u(s)]_{RH} & [g_u(s)]_{RR} \end{bmatrix} \tag{4.5}$$

where all subscripts have the same definition as in Eq. 4.4, each submatrix is in its own local coordinate system and contains the elements from Eq. 2.53 and Eq. 2.54. All elements are nonzero.

The generalized strain-displacement matrix [T] from Eq. 2.42a can be integrated analytically. Because the shape function for the displacement and the unknown loads are piece-wise functions, matrix [T] can be evaluated for each element and then assembled. For example, for the ith element on the vertical boundary

$$[T_i^v] = \begin{bmatrix} 1/3 & 0 & 1/6 & 0 \\ 0 & 1/3 & 0 & 1/6 \\ 1/6 & 0 & 1/3 & 0 \\ 0 & 1/6 & 0 & 1/3 \end{bmatrix} b_i^v \tag{4.6}$$

For the jth element on the horizontal boundary

$$[T_j^h] = \begin{bmatrix} 1 & 0 \\ 0 & 1 \end{bmatrix} b_j^h \tag{4.7}$$

where b_i^v and b_j^h are the length of the element on the vertical and horizontal boundaries respectively.

The flexibility matrix [G] can be written as

$$[G] = \begin{bmatrix} [G]_{LL} & [G]_{LH} & [G]_{LR} \\ [G]_{HL} & [G]_{HH} & [G]_{HR} \\ [G]_{RL} & [G]_{RH} & [G]_{RR} \end{bmatrix} \tag{4.8}$$

where all the subscripts in Eq. 4.8 have the same definition as previously. [G] is a symmetric matrix.

Because the off diagonal submatrices in Eq. 4.4 are null matrices, following equations can be derived

$$[G]_{LL} = \int_S [L(s)]_{LL}^T \, [g_u(s)]_{LL} \, ds \tag{4.9a}$$

$$[G]_{HL} = \int_S [L(s)]_{HH}^T \, [g_u(s)]_{HL} \, ds = \int_S [g_u(s)]_{HL} \, ds \tag{4.9b}$$

$$[G]_{HH} = \int_S [L(s)]_{HH}^T \, [g_u(s)]_{HH} \, ds = \int_S [g_u(s)]_{HH} \, ds \tag{4.9c}$$

$$[G]_{RL} = \int_S [L(s)]_{LL}^T \, [g_u(s)]_{RL} \, ds \tag{4.9d}$$

$$[G]_{HR} = \int_S [L(s)]_{HH}^T \, [g_u(s)]_{HR} \, ds = \int_S [g_u(s)]_{HR} \, ds \tag{4.9e}$$

$$[G]_{RR} = \int_S [L(s)]_{RR}^T \, [g_u(s)]_{RR} \, ds \tag{4.9f}$$

These integrations have to be performed numerically using the Gaussian quadrature. For the integration on the vertical boundaries, 4 integration points would be adequate. If the geometry of the boundary is as simple as that shown in Fig. 4.1, matrix $[G]_{LL}$ and $[G]_{RR}$ are related to each other by a simple transformation matrix which depends on the nodal numbering of the vertical boundary nodes, as are $[G]_{HR}$ and $[G]_{HL}$.

If the dynamic stiffness matrix of the far-field $[S^{\infty}_{bb}]$ is evaluated by Eq. 2.42, the Green's function $[g_t(s)]$ for the surface traction can still be decomposed into submatrices as

$$[g_t(s)] = \begin{bmatrix} [g_t(s)]_{LL} & [g_t(s)]_{LH} & [g_t(s)]_{LR} \\ [g_t(s)]_{HL} & [g_t(s)]_{HH} & [g_t(s)]_{HR} \\ [g_t(s)]_{RL} & [g_t(s)]_{RH} & [g_t(s)]_{RR} \end{bmatrix} \tag{4.10}$$

The matrices [G] and [T] have to be determined by integrating all coupling terms.

4.2 Transformation in the Wave Number Domain and the Spatial Domain

As described in Section 2.2, in order to enforce the displacement boundary conditions on the top and the bottom of each soil layer which corresponds to a boundary element, all quantities have to be assumed to vary in the x-direction as the function exp(ikx) does (Eq. 2.26a and El. 2.26b) and thus they are functions of the wave number k. For the unknown distributed loads, a transformation has to be performed before the displacement solution can be found. This is simple because the distribution function of the loads has a simple form and the transformation can be performed analytically. The transformation required in Eq. 2.54 are more difficult and has to be done using a numerical technique.

The Fourier transform can be written as

$$f(x) = \int_{-\infty}^{+\infty} F(k)\ \exp(ikx)\ dk \tag{4.11}$$

The nature of function F(k) has a very strong influence on the selection of the numerical technique. The most efficient method is the fast Fourier transform originally developed by Cooley and Turkey (C4) if a significant number of the transformed values of the function are required in the spatial

domain. The fast Fourier transform is actually an application of the trapezoidal rule and the nature of the periodical function exp(ikx) is employed. For the transformation in Eq. 2.54, the most significant computational effort does not lie in the transformation itself, but in the evaluation of the Green's function. On the other hand, for each Gaussian integration point in Eq. 4.9 for the vertical boundaries, the Green's function in the spatial domain is required only for two different values of x, ie., at x = 0 and x = 2b, where b is the half width of the foundation, if the origin of the coordinate system is selected at the top of the left hand side vertical boundary. The most effective method of performing the transformation would be to evaluate the integral in Eq. 4.11 directly by some numerical integration method. The Fourier transform of Eq. 4.11 can be decomposed into two integrals as

$$A(x) = \int_0^{+\infty} A(k)\,Sin(kx)\,dk \qquad (4.12a)$$

$$B(x) = \int_0^{+\infty} B(k)\,Cos(kx)\,dk \qquad (4.12b)$$

For x = 0 the integrals reduce to an ordinary integration with infinite limits. For x = 2b the integrals are decomposed into two integrals which contain sine and cosine functions respectively as shown in Eq. 4.12. The Green's function in the wave number domain does not decrease rapidly with the increase of wave number for small wave numbers and because of the dynamic nature of the soil system, the function gets very sharp peaks at the wave number corresponding to the natural frequencies of the soil system. These natural frequencies are difficult to estimate before carrying out the integration. These characteristics of the Green's function rule out higher order numerical quadrature such as Gauss-Laguerre and Gauss-Hermite expansion procedures (D8, P8). Some elementary numerical integration technique such as the trapezoidal rule and Filon quadrature may be preferred as long as the truncation error is small (D8). The Green's function in the wave number domain stands for the amplitude of a displacement component with a certain frequency and propagating in a certain direction. The wave number is proportional to the frequency of the component for a wave travelling in any direction in the half space except the vertically travelling wave for which

the wave number is zero. As is well known, a dynamic system is much less sensitive to an excitation whose frequency is much larger than the fundamental frequency of the system. This property will allow the truncation error in the integration to be treated very crudely. An uneven sampling rate can be chosen, ie., a bigger step size is used for higher wave numbers because the Green's function is relatively smooth when the wave number is large.

For the transformation of the Green's function related to the horizontal boundary, the fast Fourier transformation algorithm may be preferred since a large amount of data is required for each element in the integration in Eq. 2.42b. The upper integration limit for Eq. 4.12 is chosen as the wave number at which the symmetric part A(k) and the antisymmetric part B(k) of the function F(k) are sufficiently small. Then the chosen integration interval can be divided into a number of subintervals. The size of each subinterval depends on the wave number and the frequency. The subinterval is bigger for the large waver numbers. For small wave numbers, the size of the subintervals can be larger for high frequencies. The fast Fourier transformation is then performed on each subinterval and a bigger incremental wave number can be used for the larger wave numbers. Because the property of periodicity has been assumed for the function F(k) in the fast Fourier transform, the function to be transformed for one subinterval has to be assumed to be zero for all other subintervals.

The components of the Green's function with small wave numbers are very important in the accuracy of the dynamic stiffness matrix because these components correspond to either a vertically propagating wave or wave components with low frequency. A fine integration step is preferred for very small wave numbers and this can be achieved by the direct evaluation of the Fourier transform. Because a small number of pulses of the Green's function in the wave number domain are required to be transformed into the spatial domain for small wave numbers and a relative large number of values in the spatial domain are required, it is more economical to compute the contribution from each pulse directly.

4.3 The Implementation of the Simplified Vertical Energy Transmitting Boundary

The matrices [V] and [H] in Eq. 2.70h can be computed by substituting Eq. 2.71 into Eq. 2.70f and 2.70g with some proper arrangement of the different modes. It can be shown by the Maxwell-Betti reciprocity theorem that matrix [V] is symmetric and its components may be written as

$$V_{ij} = \{\phi_i\}^T \int_S [P_i(z)]^T [N'_j(z)] dz \{\phi_j\} \tag{4.13a}$$

where $\{\phi_i\}$ and $\{\phi_j\}$ are the ith and jth mode shapes respectively and the integration is performed over the vertical boundary. The order of [V] is m by m and m is the number of the modes used. For a n-layers system the integration of Eq. 4.13a can be performed on each layer and the summation is taken as

$$V_{ij} = \sum_{k=1}^{n} \exp(-ik_i x_o) \int_{d_k} \{\phi_i\}_k^T [P_i(z)]_k^T [N'_j(z)]_k dz \{\phi_j\}_k \exp(-ik_j x_o) \tag{4.13b}$$

where the subscript k indicates the kth layer in the system and k_i and k_j represent the wave number for the ith and jth mode respectively. The symbol i equals $\sqrt{-1}$ and x_o is the location of the boundary. The number of the layers can be chosen as few as the number of layers that have different material properties, but it is easier to implement if each finite element on the vertical boundary is taken as an individual layer. The mode shape vector for the layer is a subvector of the mode shape of the layered system taking the values at the top and the bottom surface displacements of the layer.

Similarly, matrix [H] can be computed for each layer (each finite element on the vertical boundary) and taking the summation over all layers. For example, the ith row of [H] may be written as

$$[H_i] = \sum_{k=1}^{n} \exp(-ik_i x_o) \{\phi_i\}_k^T \int_{d_k} [P_i(z)]_k^T [N(z)]_k dz \tag{4.13c}$$

The summation in Eq. 4.13c is not as simple as the summation in Eq. 4.13b and a finite element assemblage procedure has to be followed. The order of the matrix [H] is m by N and N = 4n + 2 for an 8 node finite element mesh.

The number of the mode shapes used depends on the material damping and the distance of the boundary from the foundation. In general, all modes whose wave number has a small negative imaginary part may have to be used. For a damped site, only a few modes are needed. For an undamped site, there are a finite number of modes with real wave number even if the layers are on a rigid base. These modes may have to be included.

4.4 Symmetric and Antisymmetric Foundation Systems

When a symmetric foundation system is under the excitation of a vertically or horizontally propagating seismic wave, symmetric or antisymmetric loading may arise for some wave patterns. In such circumstance, a more efficient solution strategy can be followed by taking the symmetry and antisymmetry into account.

Eq. 2.41f can be rewritten as

$$\begin{bmatrix} [G]_{11} & [G]_{12} & [G]_{13} \\ [G]_{21} & [G]_{22} & [G]_{23} \\ [G]_{31} & [G]_{32} & [G]_{33} \end{bmatrix} \begin{Bmatrix} (p_1) \\ (p_2) \\ (p_3) \end{Bmatrix} = \begin{bmatrix} [T]_{11} & [T]_{12} & [T]_{13} \\ [T]_{21} & [T]_{22} & [T]_{23} \\ [T]_{31} & [T]_{32} & [T]_{33} \end{bmatrix} \begin{Bmatrix} (U_{b1}) \\ (U_{b2}) \\ (U_{b3}) \end{Bmatrix} \tag{4.14}$$

where the subscript 2 indicates that these nodes are on the symmetric axis and the other subscripts indicate that the nodes are on the other part of the boundary. For a symmetric foundation system, the following transformation can be found

$$(p_3) = [T_p]\ (p_1) \tag{4.15a}$$

$$(U_{b3}) = [T_u]\ (U_{b1}) \tag{4.15b}$$

where $[T_p]$ and $[T_u]$ are transformation matrices which depend on the node numbering of the boundary. Substituting Eq. 4.15 into Eq. 4.14

$$\begin{bmatrix} [G]_{11}+[G]_{13}[T_p] & [G]_{12} \\ [G]_{21}+[G]_{23}[T_p] & [G]_{22} \end{bmatrix} \begin{Bmatrix} (p_1) \\ (p_2) \end{Bmatrix} = \begin{bmatrix} [T]_{11}+[T]_{13}[T_u] & [T]_{12} \\ [T]_{21}+[T]_{23}[T_u] & [T]_{22} \end{bmatrix} \begin{Bmatrix} (U_{b1}) \\ (U_{b1}) \end{Bmatrix} \tag{4.16}$$

For an antisymmetric foundation system

$$(p_3) = -[T_p]\ (p_1) \tag{4.17a}$$

$$(U_{b3}) = -[T_u]\ (U_{b1}) \tag{4.17b}$$

and

$$\begin{bmatrix} [G]_{11}-[G]_{13}[T_p] & [G]_{12} \\ [G]_{21}-[G]_{23}[T_p] & [G]_{22} \end{bmatrix} \begin{Bmatrix} (p_1) \\ (p_2) \end{Bmatrix} = \begin{bmatrix} [T]_{11}-[T]_{13}[T_u] & [T]_{12} \\ [T]_{21}-[T]_{23}[T_u] & [T]_{22} \end{bmatrix} \begin{Bmatrix} (U_{b1}) \\ (U_{b1}) \end{Bmatrix} \tag{4.18}$$

Now the boundary condition on the symmetric axis can be imposed by deleting the variables which will be zero in the solution. A new set of system equations can be derived from Eq 4.16 and Eq. 4.18. Symbolically, it can be written as

$$[G']\ (p') = [T']\ (U_b') \tag{4.19}$$

The dynamic stiffness matrix of the far-field is written as

$$[S_{bb}^{\infty\prime}] = [T']^T[G']^{-1}[T'] \tag{4.20}$$

Chapter 5

Time Domain Analysis and the Approximate Modelling of the Far-Field

5.1 Transformation of the Dynamic Stiffness Matrix

As described in Section 1.3, the dynamic stiffness matrix of the far-field is required in the time domain analysis. The dynamic stiffness matrix in Eq. 2.42m is a function of the frequency and has to be transformed into the time domain by a Fourier transformation. This transformation requires a considerable amount of computational effort. Furthermore, the elements in the dynamic stiffness matrix are unbounded in the frequency domain, ie., the stiffness will become infinite as the frequency tends to infinity.

By definition, the dynamic stiffness coefficient in the time domain is the force that produces a unit impulse displacement in the time domain on one node with zero displacements of the other nodes (W7, W8). The unit impulse displacements of a system in the time domain can be represented by the Dirac delta function $[I]\delta(t)$ mathematically, where $[I]$ is an identity matrix. This displacement field can be transformed into the frequency domain as

$$[U(\omega)] = F_f([I]\delta(t)) = [I] \tag{5.1}$$

The force in the frequency domain required for the displacement field is

$$[P(\omega)] = [S(\omega)]\ [U(\omega)] = [S(\omega)] \tag{5.2}$$

where $[S(\omega)]$ is the dynamic stiffness matrix of the system. Now an inverse transformation is applied

$$[P(t)] = F_f^{-1}([P(\omega)]) = F_f^{-1}([S(\omega)]) \tag{5.3}$$

ie.,

$$[S(t)] = F_f^{-1}([S(\omega)]) \tag{5.4a}$$

Alternatively, the dynamic flexibility matrix has the same transformation, ie.,

$$[F(t)] = F_f^{-1}([F(\omega)]) \tag{5.4b}$$

where $[F(\omega)] = [S(\omega)]^{-1}$.

Numerically, Eq. 5.4 is easier to perform because the flexibility matrix is bounded in the frequency domain.

For an unbounded function $S(\omega)$ in the frequency domain, the transformation is valid only in the sense of a distribution (W7, W8). The function $S(\omega)$ can be decomposed into a finite polynomial and a regular function for which the transformation can be performed (W7). For example,

$$S(\omega) = K + i\omega C - M\omega^2 - iN\omega^3 + s(\omega) \tag{5.5}$$

where K, C, M and N are constants and $s(\omega)$ is a bounded complex function in the frequency domain.

If the Delta function is represented by

$$\delta(t) = 1/2\pi \int_{-\infty}^{+\infty} \exp(i\omega t)\, d\omega \tag{5.6}$$

the transformation of Eq. 5.5 may be written as

$$S(t) = K\delta(t) + C\delta'(t) + M\delta''(t) + N\,\delta'''(t) + s(t) \tag{5.7}$$

where the prime indicates the order of the derivative with respect to time and $s(t)$ is the Fourier transform of $s(\omega)$ in the time domain.

From the definition of the dynamic stiffness, the forces R(t) in the time domain can be evaluated using a convolution integral assuming that $S(t) = 0$ and the displacement $r(t) = 0$ when $t < 0$

$$R(t) = \int_0^t S(t-\tau)\, r(\tau)\, d\tau \tag{5.8}$$

where r(t) is the displacement function in the time domain. Substituting Eq. 5.7 into Eq. 5.8 it can be found that

$$R(t) = K\, r(t) + C\, \dot{r}(t) + M\, \ddot{r}(t) + N\, \dddot{r}(t) + \int_0^t s(t-\tau)\, r(\tau)\, d\tau \tag{5.9}$$

where K, C and M can be interpreted as the static stiffness, viscous damping and mass coefficients, respectively. The transform of the polynomial part of the function is only valid on the sense of a distribution since the Delta function $\delta(t)$ has been introduced. However, the Fourier transform of the flexibility matrix in Eq. 5.4 can be performed directly because the bounded property of the flexibility function.

5.2 Computational Procedure for a Time Domain Analysis Using the Convolution Integral

In Eq. 1.10, the interactive force vector $\{R_b\}$ can be written in the time domain as

$$[R_b] = \int_0^t [S^g_{bb}(t-\tau)\, (\{r^t_b(\tau)\} - \{r^g_b(\tau)\})\, d\tau \tag{5.10}$$

If the flexibility matrix is used, the displacement can be written as

$$(r_b^t) - (r_b^s) = \int_0^t F_{bb}^s(t-\tau)]\ [R_b(\tau)]\ d\tau \tag{5.11}$$

Eq. 5.11 can be discretized at the nth time step as

$$(r_b^t)_n - (r_b^s)_n = \sum_{i=1}^{n-1} ([F_{bb}^s]_{n-i}(R_b)_i) + [F_{bb}^s]_o(R_b)_n \tag{5.12}$$

where a linear temporal variation of the concentrated interaction forces over the nth time step is assumed.

$$[F_{bb}^s]_{n-i} = \int_0^{\Delta t} \frac{\tau}{\Delta t}\ [F_{bb}^s((n+1-i)\Delta t - \tau)]d\tau$$

$$+ \int_0^{\Delta t} (1 - \frac{\tau}{\Delta t})\ [F_{bb}^s((n-i)\Delta t - \tau)]\ d\tau \tag{5.13a}$$

$$[F_{bb}^s]_o = \int_0^{\Delta t} \frac{\tau}{\Delta t}\ [F_{bb}^s(\Delta t - \tau)]\ d\tau \tag{5.13b}$$

If the trapezoidal rule is applied to the function $F_{bb}^s(t)$, Eq. 5.13 may be rewritten as

$$[F_{bb}^s]_{n-i} = \Delta t[F_{bb}^s((n-i)\Delta t)] \tag{5.14a}$$

$$[F_{bb}^s]_o = \frac{1}{2}\ \Delta t[F_{bb}^s(0)] \tag{5.14b}$$

$(R_b)_n$ can be then solved from Eq. 5.12 as follows

$$(R_b)_n = [F_{bb}^s]^{-1}((r_b^t)_n - (r_b^s)_n - \sum_{i=1}^{n-1} [F_{bb}^s]_{n-i}(R_b)_i) \tag{5.15}$$

After substituting Eq. 5.15 into Eq. 1.10 at time step $t = n\Delta t$, it can be shown that

$$\begin{bmatrix} [M_{ss}] & [M_{sb}] \\ [M_{bs}] & [M_{bb}] \end{bmatrix} \begin{Bmatrix} (\ddot{r}_s^t)_n \\ (\ddot{r}_b^t)_n \end{Bmatrix} + \begin{bmatrix} [C_{ss}] & [C_{sb}] \\ [C_{bs}] & [C_{bb}] \end{bmatrix} \begin{Bmatrix} (\dot{r}_s^t)_n \\ (\dot{r}_b^t)_n \end{Bmatrix} + \begin{bmatrix} [K_{ss}] & [K_{sb}] \\ [K_{bs}] & [K_{bb}]+[F_{bb}^g]_o^{-1} \end{bmatrix} \begin{Bmatrix} (r_s^t)_n \\ (r_b^t)_n \end{Bmatrix}$$

$$= \begin{Bmatrix} (0) \\ [F_{bb}^g]_o^{-1}((r)_n + \sum_{i=1}^{n-1} [F_{bb}^g]_{n-i}(R_b)_i) \end{Bmatrix} \qquad (5.16)$$

For a nonlinear analysis, it is desirable to rewrite Eq. 5.16 in an incremental form:

$$\begin{bmatrix} [M_{ss}] & [M_{sb}] \\ [M_{bs}] & [M_{bb}] \end{bmatrix} \begin{Bmatrix} (\Delta\ddot{r}_s^t) \\ (\Delta\ddot{r}_b^t) \end{Bmatrix} + \begin{bmatrix} [C_{ss}] & [C_{sb}] \\ [C_{bs}] & [C_{bb}] \end{bmatrix} \begin{Bmatrix} (\Delta\dot{r}_s^t) \\ (\Delta\dot{r}_b^t) \end{Bmatrix}$$

$$+ \begin{bmatrix} [K_{ss}] & [K_{sb}] \\ [K_{bs}] & [K_{bb}]+[F_{bb}^g]_o^{-1} \end{bmatrix} \begin{Bmatrix} (\Delta r_s^t) \\ (\Delta r_b^t) \end{Bmatrix} = \begin{Bmatrix} (0) \\ (\Delta R_b') \end{Bmatrix} \qquad (5.17a)$$

where

$$(\Delta R_b') = [F_{bb}^g]_o^{-1} \left((\Delta r_b^g) - \sum_{i=1}^{n-1} [F_{bb}^g]_{n-i}(R_b)_i + \sum_{i=1}^{n-2} [F_{bb}^g]_{n-1-i}(R_b)_i \right) \qquad (5.17b)$$

Eq. 5.17a can be solved by a standard solution procedure but care must be exercised in evaluating the interaction forces. Eq. 5.15 may not be used because of the accumulation of error. Instead, the incremental form of Eq. 1.10 may be employed

$$\begin{bmatrix} [M_{ss}] & [M_{sb}] \\ [M_{bs}] & [M_{bb}] \end{bmatrix} \begin{Bmatrix} (\Delta\ddot{r}_s^t) \\ (\Delta\ddot{r}_b^t) \end{Bmatrix} + \begin{bmatrix} [C_{ss}(t)] & [C_{sb}(t)] \\ [C_{bs}(t)] & [C_{bb}(t)] \end{bmatrix} \begin{Bmatrix} (\Delta\dot{r}_s^t) \\ (\Delta\dot{r}_b^t) \end{Bmatrix}$$

$$+ \begin{bmatrix} [K_{ss}(t)] & [K_{sb}(t)] \\ [K_{bs}(t)] & [K_{bb}(t)] \end{bmatrix} \begin{Bmatrix} (\Delta r_s^t) \\ (\Delta r_b^t) \end{Bmatrix} + \begin{Bmatrix} (0) \\ \Delta(R_b) \end{Bmatrix} = \begin{Bmatrix} (0) \\ (0) \end{Bmatrix} \qquad (5.18)$$

from which (ΔR_b) can be solved for as

$$\{\Delta R_b\} = -\left([M_{bs}]\{\Delta \ddot{r}_s^t\} + [M_{bb}]\{\Delta \ddot{r}_b^t\} + [C_{bs}]\{\Delta \dot{r}_s^t\} + [C_{bb}]\{\Delta \dot{r}_b^t\} \right.$$

$$\left. + [K_{bs}]\{\Delta r_s^t\} + [K_{bb}]\{\Delta r_b^t\} \right) \qquad (5.19a)$$

$$\{R_b\}_n = \{R_b\}_{n-1} + \{\Delta R_b\} \qquad (5.19b)$$

It has been shown that for certain problems, for example, a cantilever beam under a sinusoidal force, the acceleration may not be modelled properly by integration techniques such as the Newmark method (S10) and thus the interactive forces may contain larger errors than those found in the other terms. Due to the accumulation of error in Eq. 5.15, convergence may not be achieved. The backward difference formula may be employed to evaluate the velocity and acceleration as they depend only on the calculated displacement. For example, the Houbolt difference formula may be used (H2).

$$\{\ddot{r}\}_n = \frac{1}{\Delta t^2}\left(2\{r\}_n - 5\{r\}_{n-1} + 4\{r\}_{n-2} - \{r\}_{n-3} \right) \qquad (5.20a)$$

$$\{\dot{r}\}_n = \frac{1}{\Delta t}\left(11\{r\}_n - 18\{r\}_{n-1} + 9\{r\}_{n-2} - 2\{r\}_{n-3} \right) \qquad (5.20b)$$

Eq. 5.20 is used only for the computation of the interaction forces. In order to avoid the artificial high frequency components in the acceleration and velocity, the time step size in Eq. 5.20 may be larger than that used in solving Eq. 5.17.

An alternative way to perform the nonlinear analysis has been reported in the literature (K3). For a nonlinear soil-structure interaction problem, Eq. 1.10 may be written in the time domain as

$$\begin{bmatrix} [M_{ss}] & [M_{sb}] \\ [M_{bs}] & [M_{bb}] \end{bmatrix} \begin{Bmatrix} (\ddot{r}_s^t) \\ (\ddot{r}_b^t) \end{Bmatrix} + \begin{bmatrix} [C_{ss}^L] & [C_{sb}^L] \\ [C_{bs}^L] & [C_{bb}^L] \end{bmatrix} \begin{Bmatrix} (\dot{r}_s^t) \\ (\dot{r}_b^t) \end{Bmatrix}$$

$$+ \begin{bmatrix} [K_{ss}^L] & [K_{sb}^L] \\ [K_{bs}^L] & [K_{bb}^L] \end{bmatrix} \begin{Bmatrix} (r_s^t) \\ (r_b^t) \end{Bmatrix} = \begin{Bmatrix} (P_s(t)) \\ (P_b(t)) \end{Bmatrix} + \begin{Bmatrix} (0) \\ (R_b) \end{Bmatrix} \qquad (5.21)$$

where P represents the pseudo-force arising from the nonlinear material property of the structure and near-field soil and the superscript L represents the linear part of the stiffness and damping matrix. If the pseudo-forces are known, Eq. 5.21 can be transformed into the frequency domain as

$$\left(-\omega^2 \begin{bmatrix} [M_{ss}] & [M_{sb}] \\ [M_{bs}] & [M_{bb}] \end{bmatrix} + i\omega \begin{bmatrix} [C_{ss}^L] & [C_{sb}^L] \\ [C_{bs}^L] & [C_{bb}^L]+[C_{bb}^g(\omega)] \end{bmatrix} \right.$$

$$\left. + \begin{bmatrix} [K_{ss}^L] & [K_{sb}^L] \\ [K_{bs}^L] & [K_{bb}^L]+[K_{bb}^g(\omega)] \end{bmatrix} \right) \begin{Bmatrix} (U_s^t) \\ (U_b^t) \end{Bmatrix} = \begin{Bmatrix} (P_s(\omega)) \\ (P_b(\omega)) \end{Bmatrix} + \begin{Bmatrix} (0) \\ [S_{bb}^g](U_b^g) \end{Bmatrix} \qquad (5.22)$$

Because these pseudo-forces are dependent on the displacement field induced in the structure and near-field soil, an iteration procedure has to be used. At the nth step iteration, the pseudo forces calculated at (n-1)th step from the time domain displacement field can be transformed into the frequency domain and substituted into Eq. 5.22 to calculate the new state of the displacement field throughout the response time of interest. It has been reported that if the nonlinearity is not severe, this iteration procedure could be more economical than using the convolution integrals (W9).

5.3 Previously Proposed Frequency Independent Model

The evaluation of the displacement from Eq. 5.11 may not be very difficult or time consuming as for t larger than certain value, the flexibility function vanishes and the convolution integral does not have to be calculated starting from $\tau = 0$. However, the evaluation of the flexibility function in the time domain is very time consuming due to its frequency dependence. As described in section 1.6, it is desirable to develop an approximate model for the far field soil.

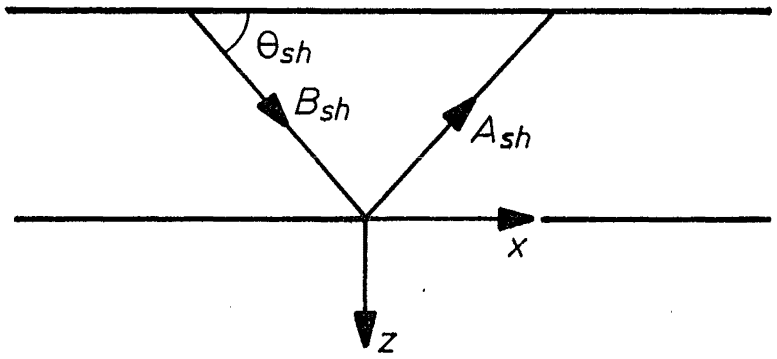

Fig. 5.1 Horizontal boundary for out-plane motion

A few approximate models have been developed in the literature. For the boundary of a finite element mesh in the near-field, a frequency independent dashpot boundary has been employed in soil-structure analysis (L5, L6). The viscous boundary is to create an medium outside the boundary which is governed by the following differential equations. For example, for a horizontal boundary shown in Fig 5.1

$$V_{,z} + V_{,t}/c_s = 0 \tag{5.23a}$$

for out-of-plane motion and

$$\lambda (U_{,x} + W_{,z}) + 2GW_{,z} + \rho c_p W_{,t} = 0 \tag{5.23b}$$

$$G (U_{,z} + W_{,x}) + \rho c_s U_{,t} = 0 \tag{5.23c}$$

for in-plane motion, where the comma indicates the derivative with respect to the spatial coordinates and time.

The advantage of the viscous boundary is its simplicity to implement. Only the adjacent nodes on the boundary are coupled and the resultant dynamic stiffness matrix has the same characteristics as that from the finite element procedure. It can be shown that to enforce the incoming wave amplitudes A_p and A_{sv} in Eq. 2.26 being zero from Eq. 5.23 the following condition must be held

$$(1 - M_x^2)^{1/2} = 1 \tag{5.24a}$$

$$(1 - L_x^2)^{1/2} = 1 \tag{5.24b}$$

ie., such a viscous boundary can only absorb vertically incident wave completely. The frequency independent viscous boundary has difficulty in transmitting surface waves in some cases (W8) but can work well in transmitting Rayleigh waves in a half space (C3). The viscous boundary may have to located far enough from the structure in order to minimize the effects of wave reflection.

Another type of energy absorbing boundary is called a paraxial element boundary which makes use of a more complicated differential equation to eliminate the incoming wave (C3). Interface elements are used to model the boundary. For example, for an out-of-plane motion the following differential equation can be adopted for the area below a horizontal boundary

$$c_s^2 V_{,xx} - 2c_s V_{,xt} - 2V_{,tt} = 0 \tag{5.25a}$$

instead of the original differential equation

$$c_s^2 (V_{,zz} + V_{,xx}) - V_{,tt} = 0 \tag{5.25b}$$

The solution of Eq. 5.25b representing a wave travelling in the positive x-direction is

$$V(x,z,t) = (A_{sh} \exp(iksz) + B_{sh} \exp(-iksz)) \exp[-i(kx-\omega t)] \tag{5.26}$$

where k and s is defined in Eq. 2.25. For a perfect energy transmitting boundary, the incoming wave amplitude A_{sh} must be zero. Substituting Eq. 5.26 into Eq. 5.25a, it can be shown that at the origin of the coordinate system which is located at the boundary

$$A_{sh} = \frac{\sqrt{(1 - M_x^2)} + \frac{1}{2}M_x^2 - 1}{-\sqrt{(1 - M_x^2)} + \frac{1}{2}M_x^2 - 1} B_{sh} \tag{5.27a}$$

Substituting Eq. 5.26 into Eq. 5.23a, for the viscous boundary it can be shown that

$$A_{sh} = \frac{\sqrt{(1 - M_x^2)} - 1}{\sqrt{(1 - M_x^2)} + 1} B_{sh} \tag{5.27b}$$

The ratio of reflected wave amplitude and incident wave amplitude $|A_{sh}|/|B_{sh}|$ is shown in Fig. 5.2. It is clearly shown that the paraxial element boundary is superior to the viscous boundary for absorbing an incident wave but for the incident wave with a small angle the reflected wave is not negligible. Because the parameter $V_{,zt}$ is involved, the corresponding matrix will no longer be symmetric and thus greater computational effort is required.

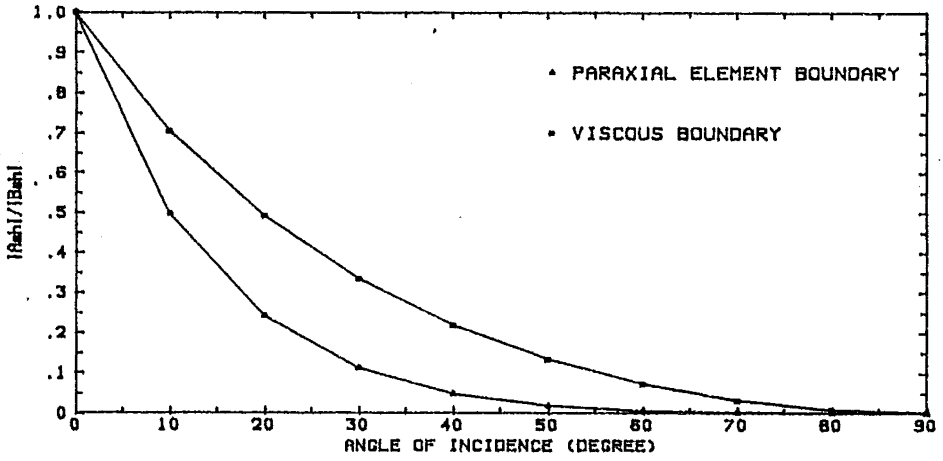

Fig. 5.2 Amplitude Ratio of Reflected and Incidence Wave

The reflected wave can be eliminated by a numerical simulation procedure. One of these models is a superposition boundary which uses two sets of elementary boundaries, ie., fixed and completely free (S11). The reflected waves from these two boundaries have the same amplitudes but with opposite sign. By averaging two solutions, the reflected waves are

eliminated. The boundary can absorb all type of waves, regardless of frequency or angle of incidence. The drawback to this method is that when multi-reflection from boundary to boundary is encountered, the computational cost is very large. Another numerical simulation is to predict the boundary motion from the nodal displacements of the interior nodes adjacent to the boundary at earlier time steps (L2). For example, for out-of-plane motion at a horizontal boundary, the following time and spatial extrapolation of the boundary displacement will eliminate the reflected waves

$$V_b(z,x,t) = \sum_{j=1}^{N} (-1)^{j+1} C_j^N V_i[z-jd,\ x,\ t-(j-1)\Delta t] \qquad (5.28a)$$

where the subscript b stands for boundary, i for the interior region adjacent to the boundary, d for the spatial interval and C_j^N for the binomial coefficients. Substitute Eq. 5.26 into Eq. 5.28a and for the displacement in the interior region setting $A_{sh} = 0$, at the boundary $z = 0$ it can be shown that

$$\left|A_{sh}/B_{sh}\right| = -1 + \sum_{j=1}^{N} (-1)^{j+1} C_j^N \exp\left[i\omega j\left(\frac{M_x d}{c_s} - \Delta t\right)\right] \qquad (5.28b)$$

Using the properties of the binomial coefficients, Eq. 5.28b can be written as

$$\left|A_{sh}/B_{sh}\right| = 2^{N/2}\left(1 - \cos\left[\omega\left(\frac{M_x d}{c_s} - \Delta t\right)\right]\right)^{N/2} \qquad (5.28c)$$

For $\omega d/c_s = \pi/4$ and $\omega\Delta t = \pi/25$, Eq. 5.28c is plotted in Fig. 5.3 for $N = 2$ and $N = 3$. It is shown that the numerical simulation is better than paraxial element boundary for the waves with small angle of incidence but for the waves with large angle of incidence the time step size has to be reduced to achieve better behaviour.

For surface foundations on a half space, frequency independent soil impedances formulae have been proposed. Evaluating soil impedances at the fundamental frequency of a soil-structure system and adding masses, springs and dashpots to the system may be the most attractive model (B4,W7).

The model proposed by Ghaffar-Zadeh and Chapel is suitable only for a uniform half space and it has not been shown if the higher modes and

nonlinearity of the structure are affected (G1). Another model proposed by Wolf and Somaini requires greater computation effort and for some problems the approximate dynamic stiffness of the soil is greatly different from the original one in the low frequency range (W5).

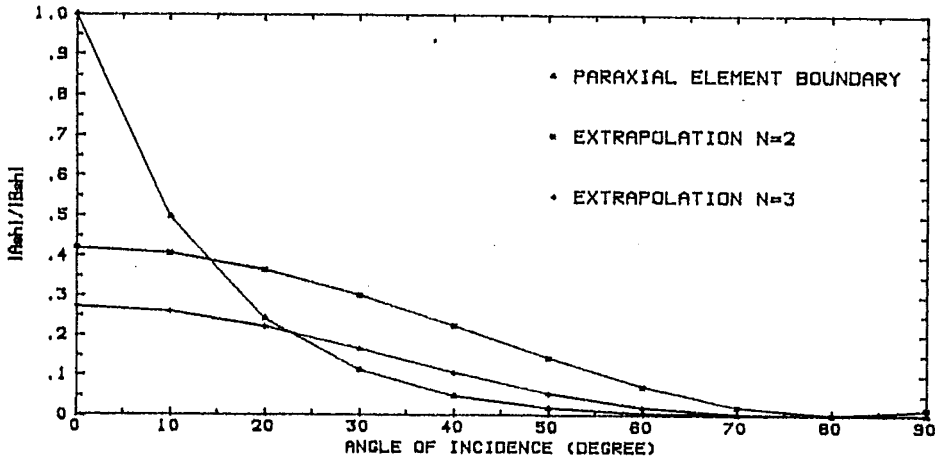

Fig. 5.3 Amplitude Ratio of Reflected and Incidence Wave

5.4 The Proposed Approximate Model and Its Numerical Verification

For civil engineering structures in a seismic environment, the structure and near field soil are sensitive only to the reflected waves from the boundary with the frequencies near to the fundamental frequency of the soil-structure system. It can be shown that if the far-field can be modelled well only in a small range around the fundamental frequency of the soil-structure system, the response of the structure will be very accurate. For example, for an oscillator with a strip foundation resting on a single horizontally layered half space, if the soil impedances are calculated only up to the fundamental frequency of the soil-structure system, there would be little difference for the structural response under an earthquake excitation from the response calculated exactly, even though the soil impedances are very strongly frequency dependent. It can be concluded that if the reflected waves with the frequencies in a small range around the fundamental frequency of the soil-structure system are eliminated completely, the structural response would

be very well predicted. The boundary element method for a layered half space would be ideal if some computational simplification can be achieved.

The approximation may start from the transformation of the dynamic stiffness matrix in Eq. 5.5. It has been shown that the frequency dependence of radiation damping has little effect on the structural response (B4). The imaginary part of the dynamic stiffness of the far field can be chosen as constant and the real part may be modelled as a quadratic function in the frequency domain. From Eq. 5.9, setting N = 0 results in constant mass, stiffness and radiation damping matrices and a convolution integral in the time domain. If these constant matrices are determined at the fundamental frequency of the soil-structure system, the contribution to the interaction forces from the convolution integral will not contain the frequency components to which the soil-structure system is sensitive and it can be treated very approximately. For example, it could simply be ignored.

The fundamental frequency of the soil-structure system is required in order to determine the constant matrices for the approximate model. From Eq. 1.7, the following eigenvalue problem arises

$$\left(-\omega^2 \begin{bmatrix} [M_{ss}] & [M_{sb}] \\ [M_{bs}] & [M_{bb}] \end{bmatrix} + \begin{bmatrix} [K_{ss}] & [K_{sb}] \\ [K_{bs}] & [K_{bb}]+[K^g_{bb}(\omega)] \end{bmatrix}\right) \begin{Bmatrix} (U^d_s) \\ (U_b) \end{Bmatrix} = \begin{Bmatrix} (0) \\ (0) \end{Bmatrix} \qquad (5.29a)$$

where

$$(U_b) = (U^t_b) - (U_g) \qquad (5.29b)$$

$$(U^d_s) = (U^t_s) - [T](U_g) \qquad (5.29c)$$

$$[T] = [K_{ss}]^{-1}[K_{sb}] \qquad (5.29d)$$

The fundamental frequencies have to be evaluated by iteration. First, starting from the fundamental frequency of the soil-structure system fixed at its boundary, calculate $[K(\omega)]$ and then substitute the calculated value into Eq. 5.29 to recompute the frequency. After only two or three iterations, the approximate fundamental frequency ω_1 can be obtained. The radiation damping matrix can be specified at the approximate fundamental frequency. The constant stiffness matrix may be the static stiffness matrix of the far-field

if it exists or specified at a frequency smaller than the approximate fundamental frequency.

Another more approximate method may be used to find the fundamental frequency of the soil-structure system. From Eq. 1.9 the eigenvalue problem may be written as

$$\left(- \omega^2 \begin{bmatrix} [I] & [\Phi]^T[M_{ss}][T_{sb}] \\ [T_{sb}]^T[M_{ss}][\Phi] & [M_{bb}]+[T_{sb}]^T[M_{ss}][T_{sb}] \end{bmatrix} \right.$$

$$\left. + \begin{bmatrix} [\Omega] & [0] \\ [0] & [K^g_{bb}(\omega)] \end{bmatrix} \right) \begin{Bmatrix} (z(\omega)) \\ (U_b(\omega)) \end{Bmatrix} = \begin{Bmatrix} (0) \\ (0) \end{Bmatrix} \tag{5.30}$$

Eq. 5.30 may result in a small system if only a few lower fixed boundary structural modes are introduced and can be used to find the approximate fundamental frequency of the soil-structure system as only an approximation to the fundamental frequency is required. The eigenvectors calculated from Eq. 5.29 and Eq. 5.30 represent the modal shapes based on different set of displacements. The difference between the fundamental frequencies calculated from Eq. 5.29 and Eq. 5.30 is very small.

If the static stiffness matrix, $[K^A_{bb}]$ is used, an added mass matrix and radiation damping matrix can be specified at the fundamental frequency ω_1 as follows:

$$[M^A_{bb}] = \frac{1}{\omega_1^2} ([K^A_{bb}] - [K^g_{bb}(\omega_1)]) \tag{5.31a}$$

$$[C^A_{bb}] = [C^g_{bb}(\omega_1)] \tag{5.31b}$$

Eq. 5.18 can be rewritten in the time domain in the incremental form

$$\begin{bmatrix} [M_{ss}] & [M_{sb}] \\ [M_{bs}] & [M_{bb}] \end{bmatrix} \begin{Bmatrix} (\Delta \ddot{r}^t_s) \\ (\Delta \ddot{r}^t_b) \end{Bmatrix} + \begin{bmatrix} [C_{ss}(t)] & [C_{sb}(t)] \\ [C_{bs}(t)] & [C_{bb}(t)]+[C^A_{bb}] \end{bmatrix} \begin{Bmatrix} (\Delta \dot{r}^t_s) \\ (\Delta \dot{r}^t_b) \end{Bmatrix}$$

$$+\begin{bmatrix}[K_{ss}(t)] & [K_{sb}(t)]\\ [K_{bs}(t)] & [K_{bb}(t)]+[K^{A}_{bb}]\end{bmatrix}\begin{Bmatrix}(\Delta r^{t}_{s})\\ (\Delta r^{t}_{b})\end{Bmatrix}=\begin{Bmatrix}(0)\\ (\Delta R_{b})\end{Bmatrix} \qquad (5.32a)$$

where

$$(\Delta R_{b}) = [M^{A}_{bb}](\Delta \ddot{r}^{g}_{b}) + [C^{A}_{bb}]\ (\Delta \dot{r}^{g}_{b}) + [K^{A}_{bb}](\Delta r^{g}_{b}) \qquad (5.32b)$$

Eq. 5.32 can then be solved using a direct integration scheme in the time domain.

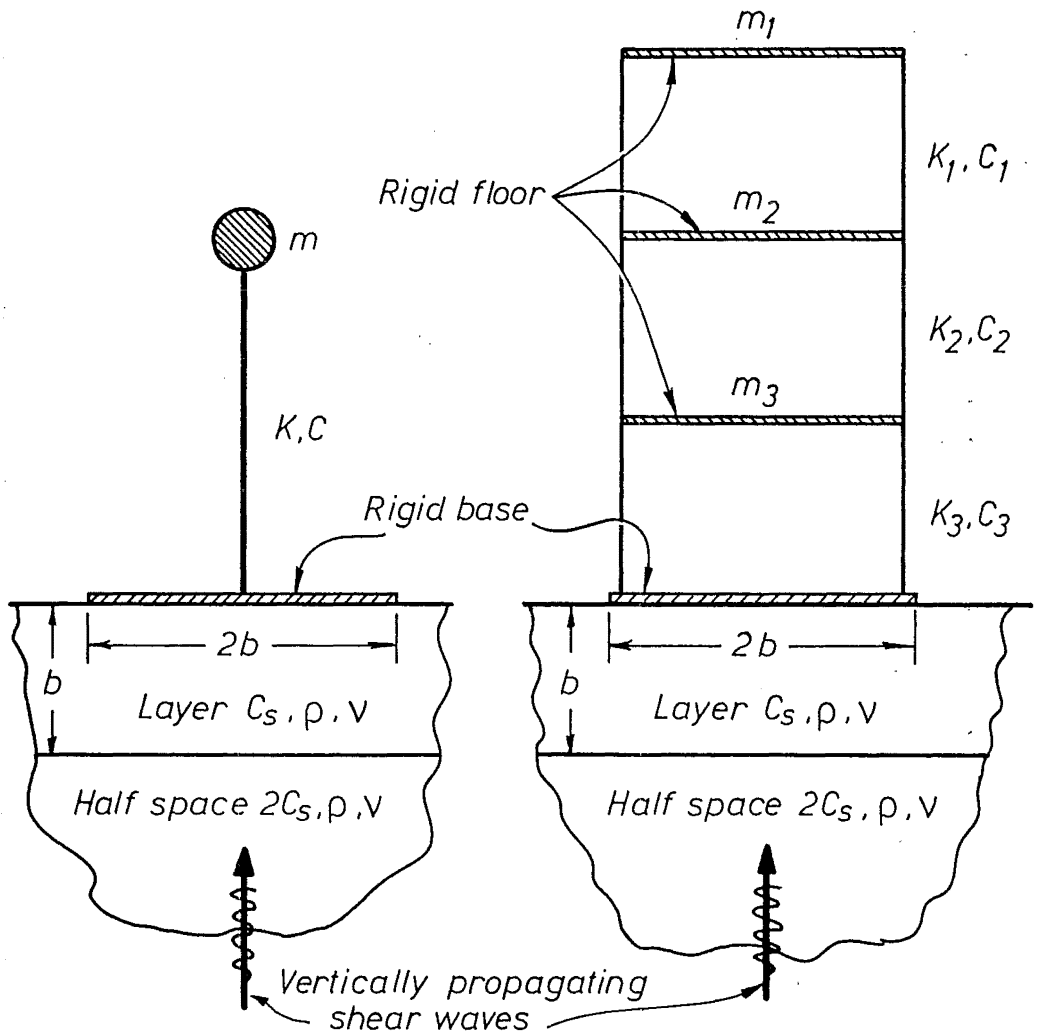

Fig. 5.4 The Model Problem of a Single Oscillator and a 3-Storey Rigid Floor Frame

As examples, a single degree of freedom oscillator and a 3-degree-of-freedom shear beam model with rigid strip foundation resting on a single horizontally layered half space are excited by the El Centro May 1940 earthquake (as shown in Fig. 5.4). A vertically propagating shear wave is assumed. The response is calculated in the frequency domain and the time domain for the linear system and in the time domain for a nonlinear system. The approximate models are compared with the convolution integral solution.

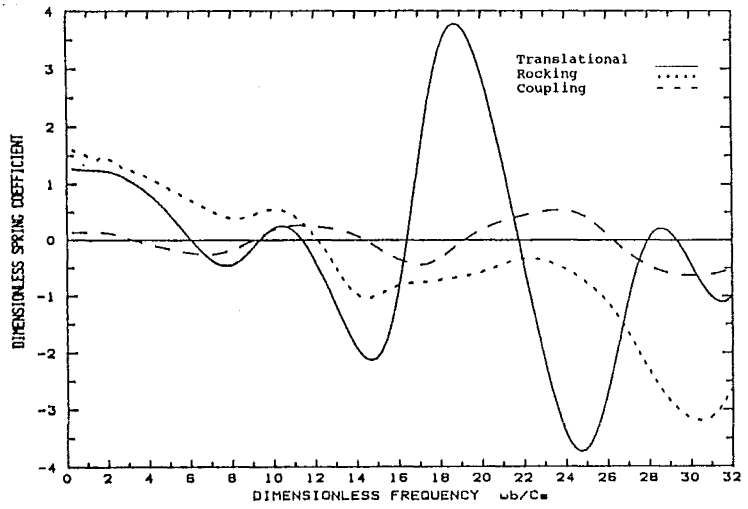

Fig. 5.5 Spring Coefficients for a Single Layer on Half Space

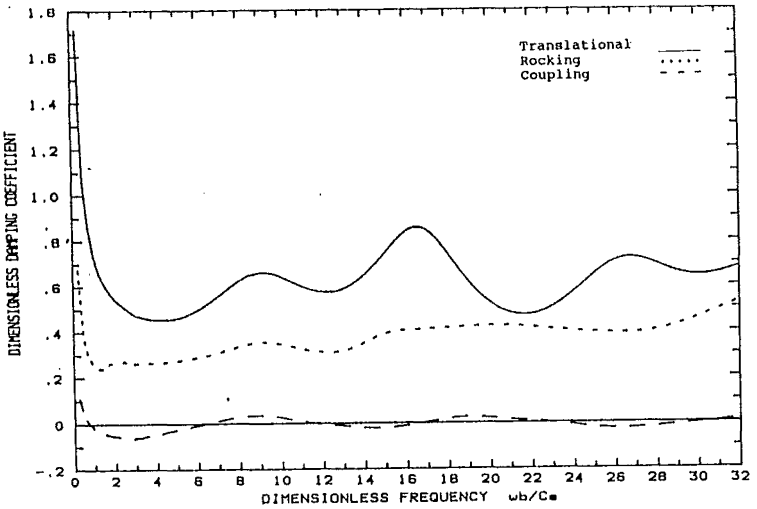

Fig. 5.6 Damping Coefficients for a Single Layer on Half Space

The shear wave velocity of the half space is twice that of the layer. A material damping ratio $\zeta = 0.05$ is introduced for both the layer and the half space with Poisson' ratio $\upsilon = 0.33$. The coefficients in the dynamic stiffness are strongly frequency dependent so that the effectiveness of the frequency dependent model can be verified. The soil impedances in the frequency domain are shown in Fig. 5.5 and Fig. 5.6. A bi-linear model is introduced for the nonlinear structure and the stiffness of the yielded structure is taken as 1/8 of the initial stiffness. The yielding strength F_y is 1/4 or 1/8 of the maximum internal force F_m developed in the linear model.

All parameters are chosen so that the soil-structure interaction effects are significant. A parameter study has been carried out and some of the results are shown in Fig. 5.7 — Fig. 5.16. The solid line is from the convolution integral analysis while the dotted line is from the proposed model.

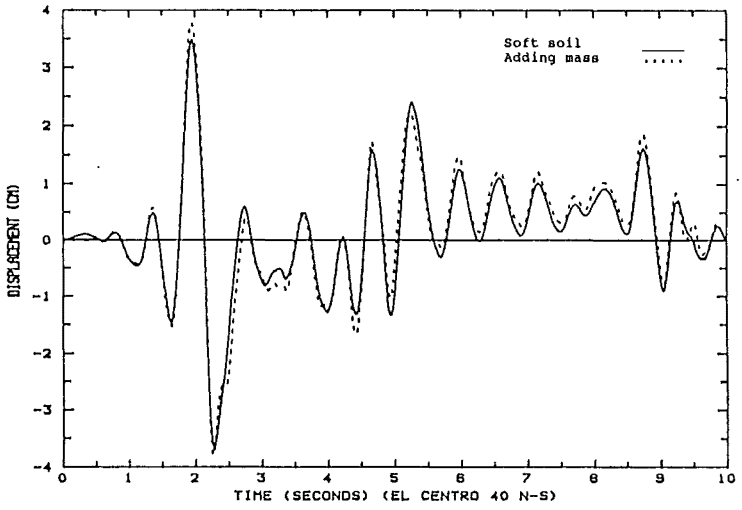

Fig. 5.7 Response of an Inelastic Oscillator on Soft Soil ($F_y/F_m = 1/4$)

For the single degree-of-freedom oscillator, the approximate model yields very good results for both the linear and nonlinear models. For the multi-degree-of freedom structure, all of fixed base modal responses are very well approximated (as shown in Fig. 5.11 — Fig. 5.13). This may be due to the fact that the frequencies of the higher fixed base modes are much less affected by the presence of the deformable soil. For the nonlinear structure, the classical modes and frequencies do not remain constant. But if a

linear system is assumed at each time step, the changing modes and frequencies can be found. For a softening structure, such instant frequencies will decrease when the structure starts yielding. How much the frequency changes in this case relative to the initial frequencies may be much less than that change of the fundamental frequency due to the presence of deformable soil.

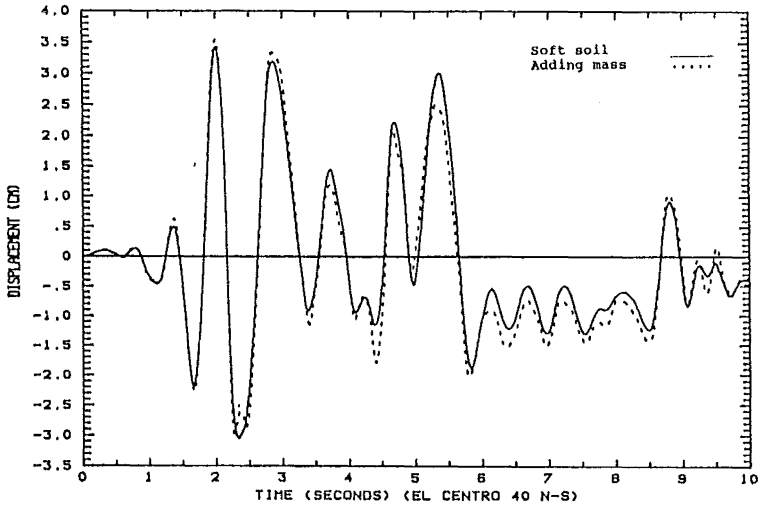

Fig. 5.8 Response of an Inelastic Oscillator on Soft Soil (F_y/F_m = 1/8)

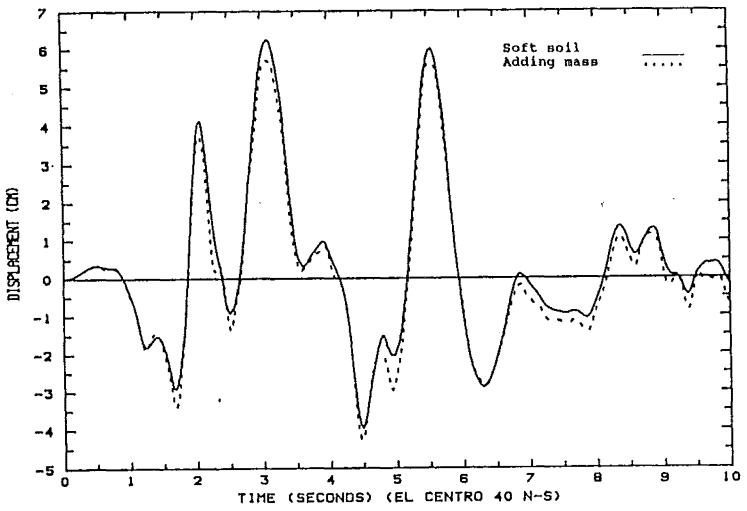

Fig. 5.9 Response of an Inelastic Oscillator on Soft Soil (F_y/F_m = 1/8)

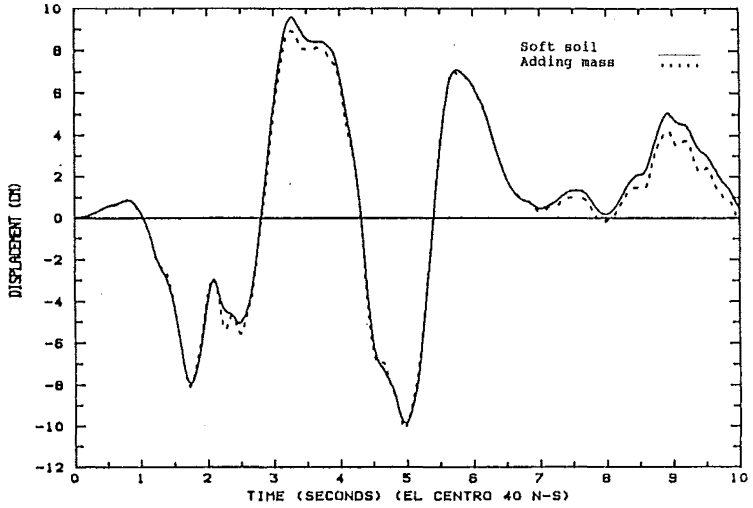

Fig. 5.10 Response of an Inelastic Oscillator on Soft Soil (F_y/F_m = 1/8)

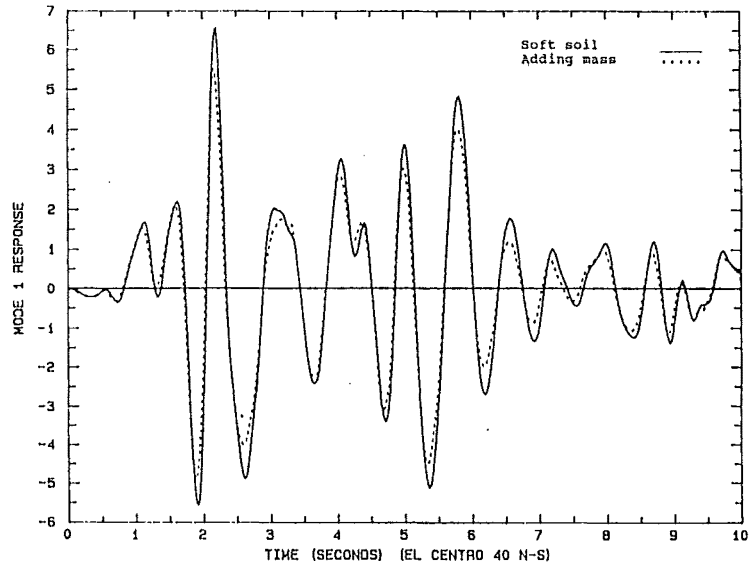

Fig. 5.11 Mode 1 Response for a Three Storey Frame

If the soil impedances are more strongly frequency dependent in the lower frequency range as shown in Fig.14, the proposed model still behaves very well. The responses are shown in Fig. 5.15-Fig. 5.16.

It is interesting to note that if the added masses are ignored, the higher modal response are affected.

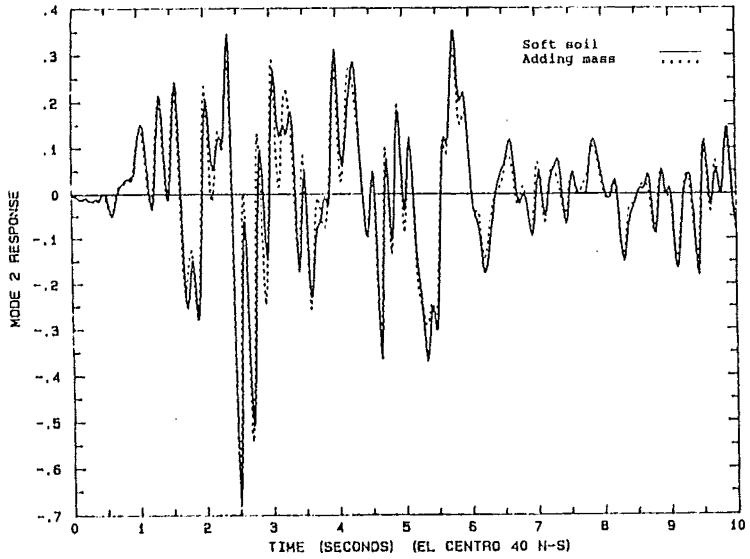

Fig. 5.12 Mode 2 Response for a Three Storey Frame

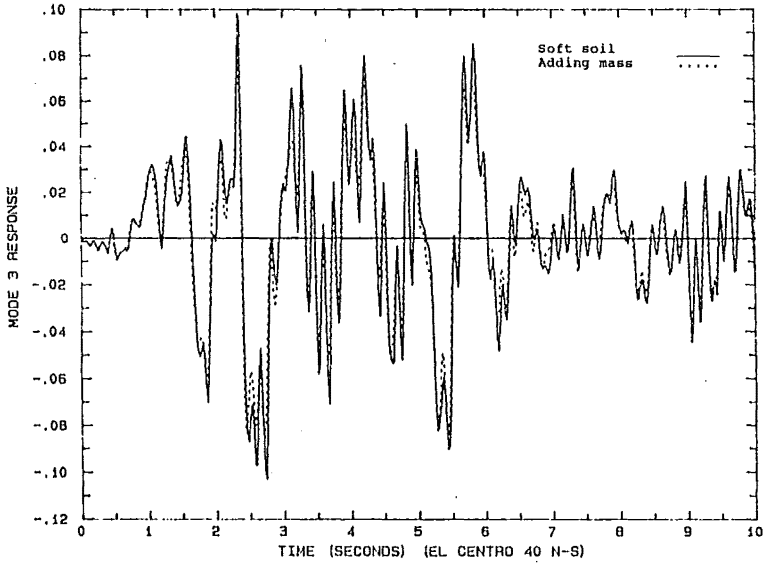

Fig. 5.13 Mode 3 Response for a Three Storey Frame

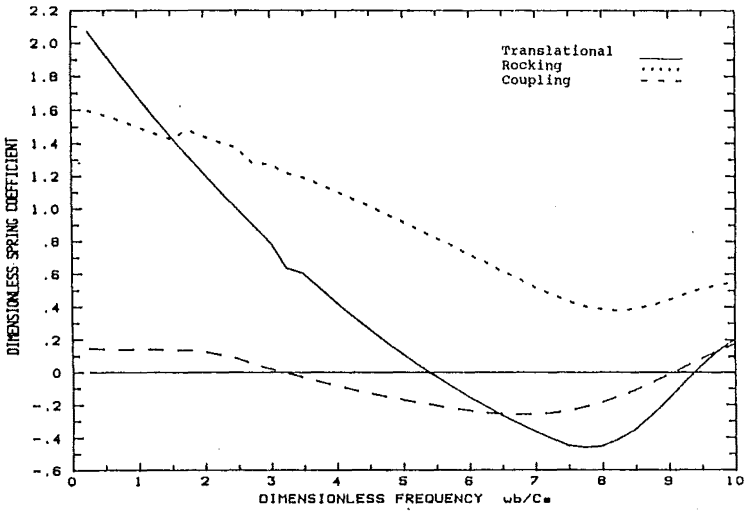

Fig. 5.14 Spring Coefficients for a Single Layer On Half Space

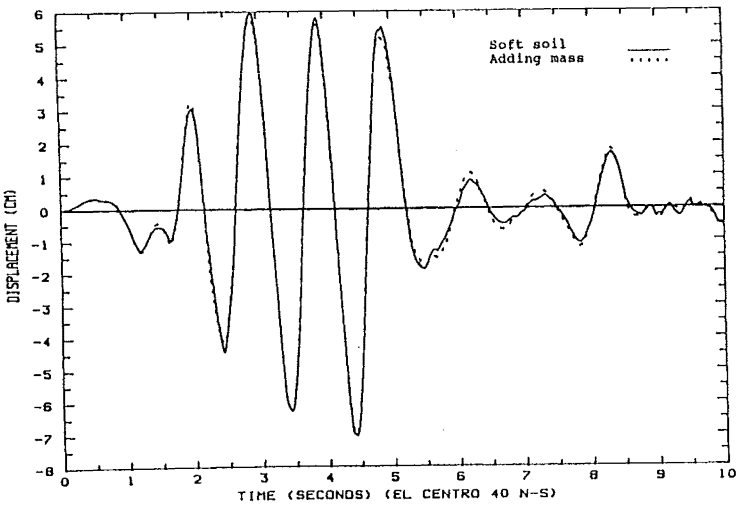

Fig. 5.15 Response of an Elastic Oscillator on Soft Soil

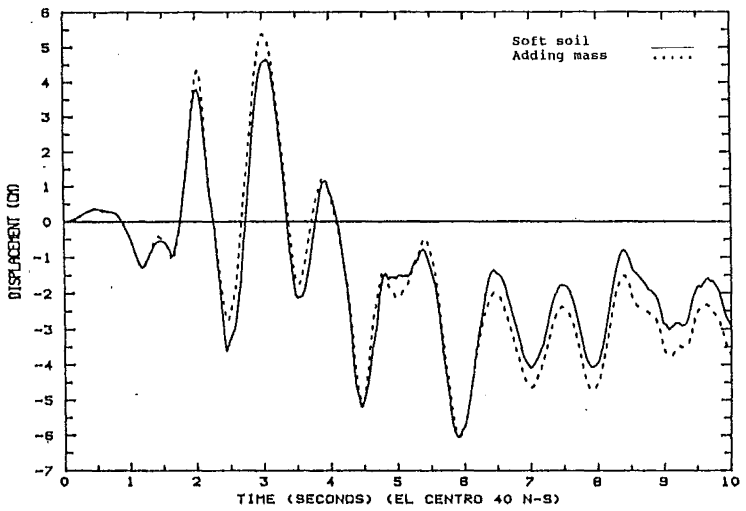

Fig. 5.16 Response of an Inelastic Oscillator Soft Soil (F_y/F_n = 1/4)

5.5 Numerical Results of the Simplified Vertical Boundary

A rigid strip foundation on a layer over a half space subjected to harmonic loading is modelled using finite elements and the vertical boundary derived in the previous chapters. The viscous boundary is adopted for the horizontal boundary because the horizontal boundary in a layered soil system is much less critical than the vertical boundary. An analytical solution is used to compare with the numerical results instead of the solution from the boundary element method because numerical errors may result from the Fourier transform. An 8-node two dimensional finite element model is used for the near-field soil and the vertical boundary is located at six times the half width of the foundation from the centre of the foundation and the horizontal boundary is at four times the half width of the foundation from the top surface as shown in Fig. 5.17. The maximum finite element dimension is defined as 1/3 of the shortest wave length transmitted by the mesh. Thus the minimum number of the elements per half width of the foundation is two if the waves with a dimensionless frequency up to three are properly modelled. The depth of the layer is chosen equal to the half width of the foundation. The mass densities of the layer and the half space are uniform and the material damping ratio is 0.05 of critical damping for both layer and the half

space. The shear modulus of the layer is 1/3 of the shear modulus of the half space and the surface wave velocities for the system are frequency dependent at the frequency range of interest.

The compliances of the foundation are shown in Fig. 5.18 and 5.19 which has been normalized by multiplying the translational and the vertical displacements by the shear modulus of the layer and the rocking displacement by the shear modulus and the square of the half width of the foundation. The solid line and two dashed lines in Fig. 5.18 and Fig. 5.19 are the analytical solutions from reference (T2) while the circles, triangles and the crosses are the corresponding results for the finite element model and the simplified vertical boundaries. A good agreement between the analytical solution and the numerical one can be seen.

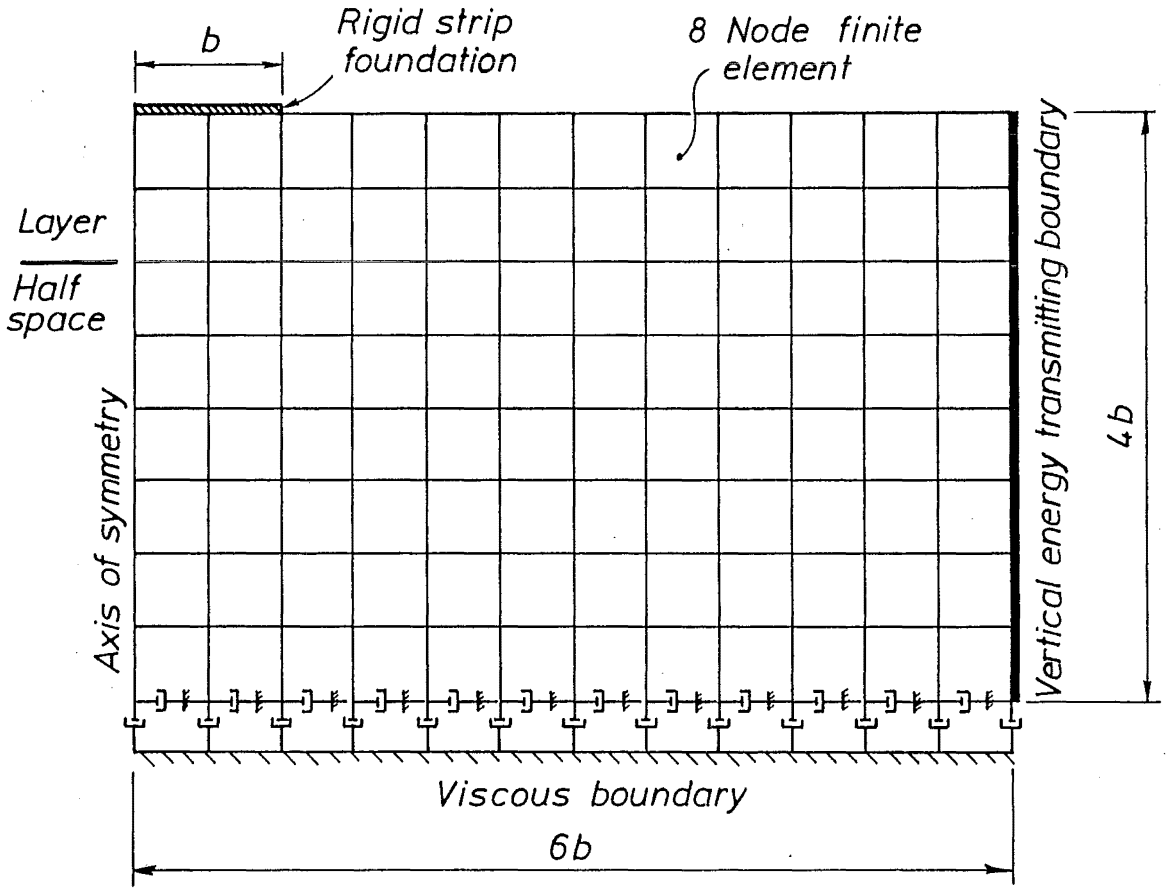

Fig. 5.17 The Strip Foundation and the Finite Element Mesh

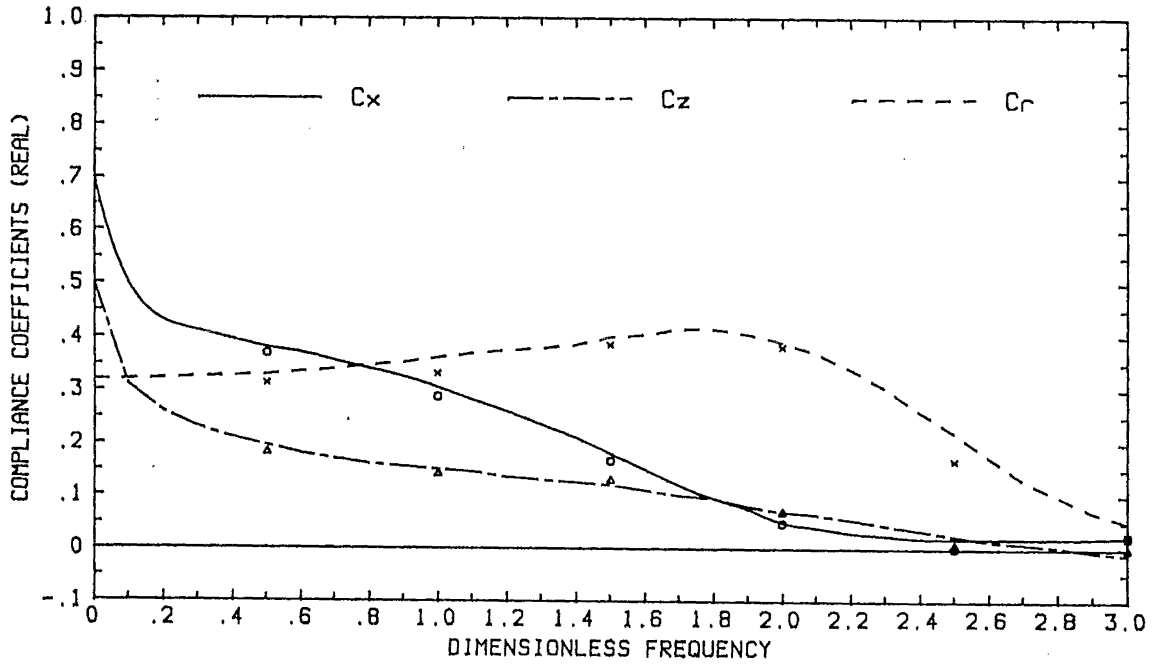

Fig. 5.18 Compliance of the strip Foundation (Real Part)

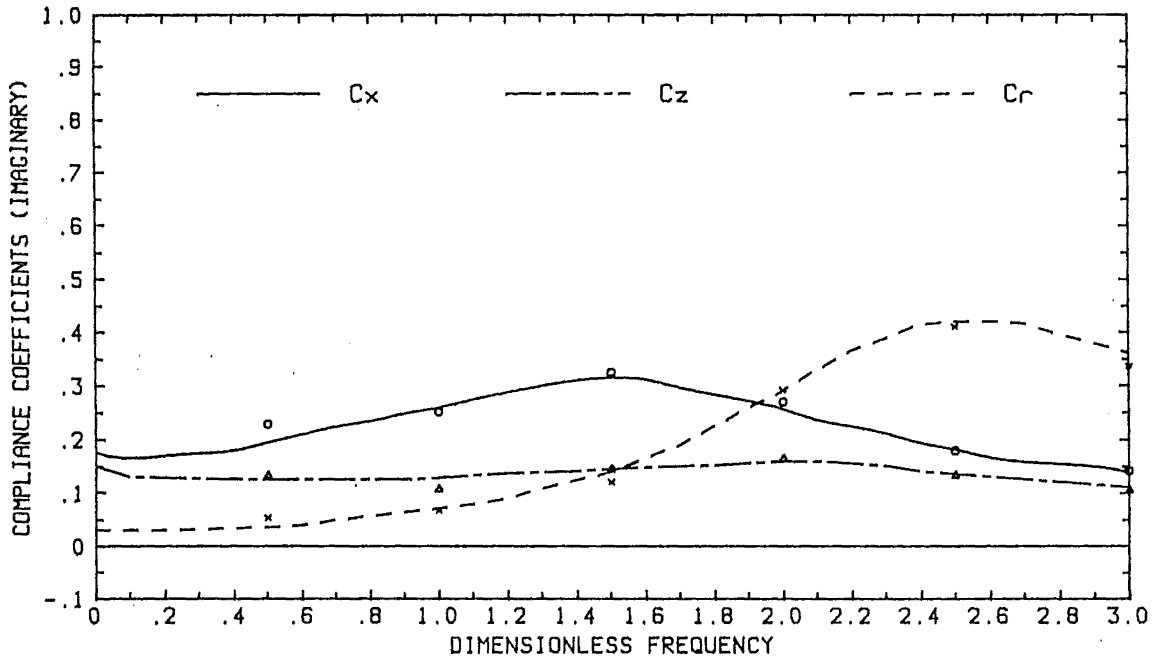

Fig. 5.19 Compliance of the strip Foundation (Imaginary Part)

For a layer on rigid rock, numerical results can be found in reference (T2). It has also been found that when the excitation frequency is high, for example, higher than the fundamental frequency of the vertically propagating shear waves, more accurate results can be obtained with only two or three modes if the viscous boundary is superimposed on the vertical boundary. This may be due to the fact that for high frequencies, the dynamic stiffness

coefficients of the soil converge to the damping coefficients of the viscous boundary.

There are some difficulties in using this boundary in the time domain by specifying the dynamic stiffness matrix of the far-field at the fundamental frequency of the soil structure system because the real or imaginary part of some diagonal elements in the dynamic stiffness matrix may be negative. If constant stiffness and damping matrices from the boundary are used in the time domain integration, the solution procedure will become unstable for the high frequency modes due to the negative diagonal elements. The negative diagonal elements in the real part of the far-field dynamic stiffness can be converted into positive ones by adding positive elements to the mass matrix at the corresponding degree of freedom for which the real parts of the diagonal elements of the dynamic stiffness matrix are negative. The added mass elements are determined in such a way that the real part of the dynamic stiffness does not change at the fundamental frequency of the soil-structure system. For the imaginary part which represents the damping coefficient, a positive element with the same order of the damping coefficient from a viscous boundary may be used to replace the negative imaginary part of the diagonal element in the far-field dynamic stiffness matrix. Because there are a small number of negative diagonal elements in the far-field dynamic stiffness matrix the modification hardly has any effects on the low frequency modes of the soil structure system which dominate the structural responses under seismic excitation. A single degree freedom oscillator on a layer underlain by rigid rock is analyzed. The layer is modelled by finite elements and the vertical boundary specified at the fundamental frequency of the soil-structure system. No visible difference on the response of the oscillator is observable due to the modification of the negative diagonal elements of the far-field dynamic stiffness matrix. The boundary is located at three times the half width of the foundation from the centre of the foundation.

5.6 Summary

It is concluded that the approximate boundary element model is the most effective model for seismic soil-structure interaction analyses. In particular, when a linear horizontally layered half space is assumed, the

artificial soil boundary can be attached directly to the foundation of the upper structure and finite elements are not needed to model the soil. This model may also be used as a transmitting boundary of the finite element mesh for the near-field soil in which nonlinearity is taken into account. If a large number of the finite elements are used on the vertical direction, the boundary element method becomes less efficient and even impossible to implement on computers because the large amount of storage required for the numerical transform. The simplified vertical boundary may be used as the energy transmitting boundary for the finite element mesh. This boundary is more accurate for the layers underlain by rigid rock than for the layers underlain by flexible soils because more energy is carried away by the surface waves in the former than in the latter site. When a relative large finite element mesh is used to model the nonlinear soil, partial reflection of the out-going waves may not have significant influence on the responses of the structure because of the material damping of the soil. In this case, a viscous boundary may be employed for a homogeneous half space because of its simplicity and less computer memory requirements than for the other models.

Numerical results have shown that the simplified vertical boundary and viscous boundary may be located at six times of the half width of the foundation from the centre of the foundation if the layers are underlain by flexible soils and the simplified vertical boundary may be located at three times of the half width of the foundation from the centre of the foundation if the layers are underlain by a rigid rock. The horizontal boundary may be located at a distance three times of the half width of the foundation to minimize the effects of wave reflection.

Chapter 6

Free Field Analysis and the Input Motion for Soil-Structure System

6.1 Free Field Analysis of a Linear Horizontally Layered Half Space

The free field analysis is a very important aspect of soil-structure interaction analyses because the interaction forces acting on the interface between the structure and far field soil have to be evaluated either from the scattered motion or from the free field motion directly. Ground motions are usually recorded on either the ground surface or the outcrop of the bed rock at the sites. The ground motion at a certain depth at a site has to be computed for the analysis of a soil-structure system. Because of the scope of this thesis, only some of the methods reported in the literature and the use of the models developed in the previous chapters on this topic are discussed.

For a given site, it is usually assumed, for the simplicity of analysis, that the profile of the site consists of a series of horizontally layered soil deposits. If a soil is assumed to have linear elastic properties, the propagation of a seismic wave in the soil can be approximately depicted by the wave equations derived in Chapter 2 under some assumption on the wave pattern. The displacements and the stress amplitudes on the boundaries of each layer are related to each other by the dynamic stiffness matrix of the layer defined in Eq. 2.32 in the frequency domain. To impose the boundary condition at the free surface and the continuity at each interface, the dynamic stiffness matrix of the site and the load vector have to be constructed. The dynamic stiffness matrix can be assembled from each layer in the same way as the finite element method does. The resultant relationship of the displacement and the load for the soil system is (W7)

$$\{F\} = [S_s]\{U\} \tag{6.1}$$

where $[S_s]$ is the dynamic stiffness matrix, $\{U\}$ is the displacement amplitude of the soil layer interfaces and the free surface and $\{F\}$ is the corresponding load vector. $[S_s]$ is a banded matrix and its maximum half band width is 4. The load vector $\{F\}$ depends on the location of the control motion and the wave pattern assumed.

If the control motion is at the free surface of the layered system, then all the elements of the load vector $\{F\}$ except the one corresponding to the interface between the last layer and the half space are zero. The displacements at the other interfaces of the site can be solved from Eq. 6.1 by setting the displacements at the free surface equal to the control motion and using Gaussian elimination. The dynamic stiffness of the site may not need to be constructed in this case because the displacements at the interfaces can also be solved for in each layer. Starting from the first layer at the ground surface, the displacements at the first interface (which is the bottom of the first layer) are determined only by the properties of the first layer and can be solved for from the dynamic equilibrium equation of that layer. For the second layer, the displacements at the second interface are determined by the properties of the first and the second layers. For the nth interface, only the dynamic stiffness matrices of the nth and (n-1)th layers need to be computed. This procedure is not valid for surface waves because of the implication of no incoming waves from infinity.

If the control motion is specified at the outcrop of the 'bed rock', the free-field analysis is a soil-structure interaction problem in which the layers correspond to the structure while the 'bed rock' or the half space corresponds to the soil in the analysis of soil-structure interaction. The control motion can be treated as input motion. From Eq. 1.5 the dynamic equilibrium equation for the soil system is

$$\begin{bmatrix} [S_{LL}] & [S_{LH}] \\ [S_{HL}] & [S^L_{HH}]+[S^b_{HH}] \end{bmatrix} \begin{Bmatrix} \{U_L\} \\ \{U_H\} \end{Bmatrix} = \begin{Bmatrix} \{0\} \\ [S^b_{HH}]\{U_c\} \end{Bmatrix} \tag{6.2}$$

where the subscript L represents the nodes connecting only the layers, H is for the node connecting the layer and the half space, the superscript L indicates that the contribution is from the layers and b indicates that the contribution is from the bedrock modeled by a half space. U_c is the control

motion measured at the outcrop of the bedrock, ie., the free-field motion without the presence of the layers. If a surface wave is assumed for the site, the control motion in the outcrop does not exist.

Because the continuity requires a constant phase velocity, the wave number defined in Eq. 2.25b has to be constant at the site and is determined only by the incidence angle of the incoming waves for a given frequency component at a given site. The cosine of the wave propagating direction in each layer is determined by the phase velocity and the corresponding wave speed of the layer as given in Eq. 2.25a and 2.25b.

For in-plane motion, the type of the wave assumed will affect the amplitudes of the vertical and horizontal displacements of the control motion. The free surface condition of the top layer or the half space will determine the reflected wave amplitudes from the incident wave amplitudes by setting the stresses σ_{zz} and τ_{xz} and z equal zero in Eq. 2.27c. The ratio of the horizontal and the vertical displacement amplitudes can then be solved for from Eq. 2.26c under the assumption of the corresponding wave pattern. For example, if a dilatational wave is assumed to be the incident wave in a half space, the incident shear wave amplitude A_{sv} in Eq. 2.26c and Eq. 2.27c can be set to zero and if this dilatational wave is assumed to propagate vertically at the site, the reflected shear wave amplitude B_{sv} can be set to zero as well.

For surface waves, the displacements at all nodes have to be determined from the eigenvalue problem arising from Eq. 6.1 because the load vector is a zero vector (W7). The displacement at each node is computed by scaling the 'eigenvector' corresponding to the wave number computed, a set of displacements determined from Eq. 6.1 with zero loading vector. This will lead to Rayleigh waves for in-plane motion and Love waves for the out-of-plane motion. The procedure to find the eigenvalues of the dynamic stiffness matrix was given in Chapter 2.

Once the displacements at the interfaces are obtained, the displacements and stresses at any point in any layer can be calculated from Eq. 2.28c, 2.29 and Eq. 2.57.

If a vertical propagating wave is assumed, the horizontal and the vertical displacements are uncoupled. The above equations will be simplified and reduced to wave equations derived by Schnabel et al. in which a transfer

function is developed for each layer (S2).

6.2 Nonlinear Analysis of a Horizontally Layered Half Space

At this stage, non-linear analysis of the free-field is only for vertically propagating waves which is a one dimensional problem. The most popular numerical method has been the equivalent linear method proposed by Seed et al.(S6) in which the properties of the soils are determined by the total stresses.

The equivalent linear method was applied to the vertically propagating wave problem described in Section 6.1 by Seed et al. (S6). The average shear moduli and damping ratio of each layer were determined from the corresponding shear strain level (S2). Iteration was used to determine the soil properties compatible with the shear strain induced. This method was successfully used to determine the relationship between the soil conditions and the ground motion in Mexico City in the Earthquake of September 19, 1985 (S8). Usually, at a site reasonably far away from the epicentre of the earthquake, the soil nonlinearity due to the free-field motion is small and the equivalent linear method can be justified for such a problem.

A finite element approach based on the equivalent linear method was also used to predict the ground motion (I1). A Rayleigh damping matrix was constructed at element level whose damping ratio was based on the strain amplitude of the element. A rigid base was assumed for the model but it may be possible for the flexibility of the base rock to be taken into account.

The shear beam model was used to perform the nonlinear free-field analyses (J1,L1). A viscous boundary was used to take the bedrock flexibility into account. The nonlinear analysis was based on the total stress and a simple soil model similar to that developed by Hardin (H1) was used.

More advanced finite element models for which the constitutive law was based on the theory of plasticity were employed in a free-field analysis (P1). Pore water generation during a earthquake was simulated and some of

these models were capable of predicting the liquefaction of sands in an earthquake (P1). Pore water pressure may be separated from the effective stresses and the partially drained problem may also be solved by these soil models.

The bounding surface soil model described in Chapter 3 may also be used to predict the effects of nonlinear soil on the ground motion, the pore water generation and the energy dissipation but the model may not be used to simulate soil liquefaction phenomena at this stage of the development.

At this stage, the nonlinear free field analysis is used mainly for the evaluation of ground surface motion. In soil-structure interaction analysis, the direct method may have to be employed to take the nonlinear free field motion into account.

6.3 Evaluation of the Scattered Motion

The scattered motion of a soil system is defined as the motion at the nodes (which will subsequently lie on the soil-structure interface) of the free-field soil with excavation (W7). The scattered motion is not very easy to determine. It may be determined by finite element analysis and usually a very large finite element mesh may be required. In this way, the advantage of the substructure method over the direct method may be impaired. As described in Chapter 1, the evaluation of the scattered motion has been avoided by introducing the dynamic stiffness matrix of the soil system without excavation and the interaction forces are determined from the free-field motion directly. In Chapter 5, an approximate model was proposed for the soil dynamic stiffness matrix. An approximation was also implicitly introduced to the evaluation of the scattered motion. From Eq. 1.14, it can be shown that

$$\{U_b^s\} = [T]\{U_b^f\} \tag{6.3}$$

where

$$[T] = [S_{bb}^s]^{-1}[S_{bb}^f] \tag{6.4}$$

for a flexible base and

$$[T] = [S^{s}_{bb}]^{-1}[A][S^{f}_{bb}] \qquad (6.5)$$

for a rigid base, where [A] is the transformation matrix used to impose the rigid body motion condition at the interface nodes. [T] is a function of the frequency. In the approximate model, if [T] is specified at the fundamental frequency of the soil structure system, the component of the scattered motion with the frequency of the fundamental frequency of the soil-structure system is accurately modelled but the other components are only approximated. This may induce some errors to the scattered motion which is not explicitly required in the soil-structure interaction analysis, but the response of the soil-structure system would be well represented. The scattered motion is not required for the finite element analysis of the near-field because the external loading for the soil-structure system can be computed directly from free-field motion and the procedure will be given in the next section.

If the scattered motion is required, the approximate method proposed by Wolf (W7) can be used for a surface foundation. By this method, the imaginary parts of $[S^{s}_{bb}]$ and $[S^{f}_{bb}]$ are omitted and the real parts are replaced by continuously distributed springs with constant values. This method has shown good agreement with the exact solution. Further details can be found in reference (W7).

6.4 The Seismic Loads for the Soil-Structure System with Energy Transmitting Boundaries

When the soil-structure system is equipped with an energy transmitting boundary, the loads on the system due to a seismic wave propagating towards the site have to be computed. The procedure used to specify the loads depends on the nature of the unknown displacements, ie., the total displacement or the displacement relative to the free-field motion or relative to the scattering motion. A number of different ways to specify the loading on the system

reported in the literature (L5, B4). The easiest way for a nonlinear problem assumes a horizontal rigid boundary at the bottom of the system and the input motion is specified at the boundary. The vertical boundaries are energy transmitting boundaries and the boundary forces depend on the relative motion. For a horizontally layered soil system underlain by a flexible half space, a rigid horizontal boundary may be also assumed for the case of vertically propagating waves provided that the boundary is located at such a depth that the amplitudes of the waves generated by the structure are very small at the boundary. This can be justified by the fact that most energy is carried away by the surface waves generated by the structure and the surface waves decay rapidly with depth. Nonlinear problems can be solved by this procedure because the inertial loading depends only on the mass matrix and the input acceleration at the rigid boundary.

If energy transmitting boundaries are used for all boundaries, the total displacement method is the only way to solve the nonlinear problem. The implicit assumption to use an energy transmitting boundary is that the nonlinearity is limited to the region modelled by the finite element mesh and the free-field motion does not induce any nonlinearity at the site. Without these assumptions the direct method has to be used. Under these assumptions, the motion and the stress at the boundary of the near-field can be decomposed into two parts, ie. the one induced by free field motion and the one induced by the motion relative to the free-field motion. The surface traction induced by the free field motion and by the energy transmitting boundaries at the boundary may be considered as external loads of the soil-structure system under a seismic excitation. If the body forces are neglected, the dynamic equilibrium of the soil-structure system can be expressed by the virtual work principle in the time domain as

$$\rho\int_V \{u'\}^T\{\ddot{u}\}dV + \zeta\int_V \{u'\}^T\{\dot{u}\}dV + \int_V \{\epsilon'\}^T\{\sigma\}dV =$$

$$\int_S \{u'\}^T\{t^f\}dS + \int_S \{u'\}^T\{t^b\}dS \qquad (6.6)$$

where ρ is the mass density, ζ is the damping coefficient, u, u and u are the actual total acceleration, velocity and displacement fields of the soil-structure system and t is the surface traction at the boundary of the near-field. The prime indicates that the quantity is associated with the virtual

displacement field. V and S denote the total volume of the system truncated at the near-field boundary and the area of the near-field boundary respectively. The superscripts f and b indicate the free field and the energy transmitting boundary respectively. An assumption has been made that the displacement shape functions for the near-field are frequency independent and the continuity requirements between the near-field and the far-field are relaxed. The surface traction due to the energy transmitting boundary depends on the motion relative to the free field motion because only the outgoing waves generated by the structure are permitted to pass through the boundary. After a finite element discretization of the upper structure and the near-field soil and performing the integration over each element, Eq. 6.5 can be written as

$$[M](\ddot{r}) + [C](\dot{r}) + [K](r) = (R^f) + (R^b) \tag{6.6}$$

where M, C and K represent the mass, damping and stiffness matrices respectively and R represents the equivalent nodal forces on the near-field boundary from the corresponding surface traction. (R^b) can be computed as

$$(R^b) = - [K^g_{bb}]((r^t_b) - (r^f_b)) - [C^g_{bb}]((\dot{r}^t_b) - (\dot{r}^f_b)) \tag{6.7}$$

where $[K^g_{bb}]$ and $[C^g_{bb}]$ are the real and imaginary parts of the dynamic stiffness matrix of the far-field respectively, specified at the fundamental frequency of the soil-structure system and they depend on the nature of the energy transmitting boundaries. The negative sign in Eq. 6.7 indicates that the surface traction on the finite element mesh and on the far-field are in the opposite directions. For a viscous boundary, $[K^g_{bb}]$ is a null matrix and the radiation damping matrix can be computed from

$$[C^g_{bb}] = \Sigma \rho c_s \int_s [N(s)]^T [N(s)] ds \tag{6.8}$$

where N(s) is the finite element displacement shape function along the boundary.

For the simplified vertical boundary the stiffness and the radiation damping matrix can be computed from Eq. 2.70h.

The surface traction on the boundary due to the free field motion is computed from the stress field of the free field motion. If the stress distribution of the free field is known at any time, the equivalent nodal forces can be obtained as

$$\{R^f\} = \Sigma \int_s [N(s)]^T [\sigma(s)]\{n\} ds \tag{6.9}$$

where $\{n\}$ is the unit normal vector of the surface.

Substituting Eq. 6.7 and 6.9 into Eq. 6.6, the dynamic equilibrium equation of the soil-structure system may be written in terms of the total displacement as

$$\begin{bmatrix} [M_{ss}] & \\ & [M_{bb}] \end{bmatrix} \begin{Bmatrix} \{\ddot{r}_s^t\} \\ \{\ddot{r}_b^t\} \end{Bmatrix} + \begin{bmatrix} [C_{ss}] & [C_{sb}] \\ [C_{bs}] & [C_{bb}]+[C_{bb}^g] \end{bmatrix} \begin{Bmatrix} \{\dot{r}_s^t\} \\ \{\dot{r}_b^t\} \end{Bmatrix} +$$

$$\begin{bmatrix} [K_{ss}] & [K_{sb}] \\ [K_{bs}] & [K_{bb}]+[K_{bb}^g] \end{bmatrix} \begin{Bmatrix} \{r_s^t\} \\ \{r_b^t\} \end{Bmatrix} = \begin{Bmatrix} \{0\} \\ \{R^f\} + [K_{bb}^g]\{\dot{r}_b^f\} + [C_{bb}^g]\{\dot{r}_b^f\} \end{Bmatrix} \tag{6.10}$$

where the subscript s indicates the upper structure and the near-field soil while b indicates the boundary. Once the boundary nodal forces due to the free field motion are determined, the displacement field can be solved for.

If the finite element mesh extends to infinity, the stress at any point can be computed from the element static stiffness matrix and the dynamic displacements of the free field motion. If the near-field soil is taken out from the fictitious finite element mesh as a substructure, the equivalent nodal forces on the near-field boundary are equal to the static stiffness matrix of the near-field multiplied by the nodal displacements from the free field motion because the surface tractions along the boundary between the near-field and the far-field are computed from the stresses which are due to the elastic deformation of the free-field. The nodal forces calculated are in equilibrium with the inertial and damping forces on the near-field. This requires that at any time, the free field motion of all nodes be known. In

fact, if the nodal displacements of the free field motion of the elements along the boundary are known, the equivalent nodal forces can be computed by imposing the free field motion on these elements statically. A relative smaller amount of computer memory for the input motion is required for this procedure.

For inclined input seismic waves, the stresses along the boundary can be obtained from Eq. 2.29 and 2.57 in the frequency domain if the free field motion is known. The integration in Eq. 6.8 can be also performed in the frequency domain and the equivalent nodal forces are then transformed into the time domain.

For vertical seismic waves, the free field analysis may be carried out by a finite element model in the time domain. The vertical and horizontal motion are uncoupled and the displacements vary only through the depth of the soil. The equivalent nodal forces due to the free field motion may be obtained by multiplying the static stiffness matrix of the elements along the boundary with the free field element nodal displacements and the Fourier transform can be avoided.

Chapter 7

Partitioned Analysis Procedure for the Soil-Structure System

7.1 The General Partitioned Analysis Procedure

An integrated treatment of coupled fields is often required in many engineering problems. For example, soil-structure interaction and fluid-structure interaction are typical coupled field problems. The coupled field problem is usually tackled by transforming it into an equivalent single field problem using analytical or numerical methods at the expense of very complicated, special purpose and large scale computer programming. Because each field has its own distinguished properties and a special treatment has to be used, such overall treatment may hardly satisfy the requirement of the most individual filed. On the other hand, the computer programming for the coupled field problem may be unreliable and very difficult to use.

For dynamic soil-structure interaction problems, two physically different fields are coupled together, the soil and the upper structure. The upper structure is often much stiffer than the soil medium. When a numerical integration scheme is employed, the time step size is restricted by stability, accuracy and economic considerations. For the upper structure, the stability consideration may require that an implicit integration algorithm be used even though the cost per time step and the storage requirements tend to increase dramatically with the number of the degrees of freedom. For the soil medium, an explicit integration scheme may be preferred because the explicit algorithm is inexpensive per time step and requires much less storage than the implicit algorithm but a small time step may be required for numerical stability considerations. Such contrary requirements make efficient soil-structure interaction analysis very difficult.

From computational grounds, the coupled subsystem can arise from a single physical field because different numerical models are used in different parts of the field. The near-field soil is usually modelled by the finite element method which results in a system of differential equations with a large and sparse stiffness matrix. When the equations are solved, the sparseness of the stiffness matrix is taken into account by using specially designed equation solver. The far-field is effectively modelled by the boundary element method which results in a relatively small, fully populated and sometimes nonsymmetric, dynamic stiffness matrix. The property of the dynamic stiffness matrix of the far-field impairs the efficiency of the equation solver if an equivalent single field problem has to be solved.

From considerations of accuracy, the time step size has to be smaller than a certain fraction of the shortest period of the response component which has to be integrated reasonably accurately. In most civil engineering structures, the high frequency components are more important for certain types of degree of freedom or certain parts of the structure than for the others. For example, the rotational degrees of freedom associated with a frame display higher frequencies than the translational degree of freedom. When a soil-structure system is excited by seismic waves, the high frequency components will be amplified in the upper structure while the low frequency components dominate the response of the soil medium. If an implicit integration scheme is employed, the time step size required from an accuracy consideration required in the upper structure would be much smaller than that in the soil medium. It is difficult to carry out the analysis using different time steps for different parts of the soil-structure system in an equivalent single field analysis.

Another feature of the modern structural dynamic analysis is the existing software. When a coupled field problem is tackled by transferring it into an equivalent single field problem, a considerably amount of modification has to be done on the software and this is not possible for most users (P5). In some cases this may result in as improper numerical model being used in some fields (P5).

In recent years, an alternative approach, the partitioned analysis procedure, has been introduced into structural dynamics (B5, B6, B7, L3, P2). In this approach, each field can be solved by a separate program module and the solution of the coupled field can be achieved by executing a set of

programs simultaneously and exchanging the interface data at each time step. This partitioned analysis procedure will overcome all of the difficulties mentioned above.

For example, a fully coupled and linear three-field system is governed by the following differential equations

$$\begin{bmatrix} [M_{xx}] & & \\ & [M_{yy}] & \\ & & [M_{zz}] \end{bmatrix} \begin{Bmatrix} (\ddot{r}_x) \\ (\ddot{r}_y) \\ (\ddot{r}_z) \end{Bmatrix} + \begin{bmatrix} [C_{xx}] & [C_{xy}] & [C_{xz}] \\ [C_{yx}] & [C_{yy}] & [C_{yz}] \\ [C_{zx}] & [C_{zy}] & [C_{zz}] \end{bmatrix} \begin{Bmatrix} (\dot{r}_x) \\ (\dot{r}_y) \\ (\dot{r}_z) \end{Bmatrix} +$$

$$\begin{bmatrix} [K_{xx}] & [K_{xy}] & [K_{xz}] \\ [K_{yx}] & [K_{yy}] & [K_{yz}] \\ [K_{zx}] & [K_{zy}] & [K_{zz}] \end{bmatrix} \begin{Bmatrix} (r_x) \\ (r_y) \\ (r_z) \end{Bmatrix} = \begin{Bmatrix} (R_x) \\ (R_y) \\ (R_z) \end{Bmatrix} \qquad (7.1)$$

where the subscripts x, y and z stand for field x, y and z respectively, M, C and K are the mass, damping and stiffness matrices of the system and r and R represent displacement and load respectively. Eq. 7.1 can be integrated by a direct numerical method.

The stiffness matrix can be decomposed into two matrices as

$$[K]^I = \begin{bmatrix} [K_{xx}] & [K_{xy}] & [K_{xz}] \\ [0] & [K_{yy}] & [K_{yz}] \\ [0] & [0] & [0] \end{bmatrix} \qquad (7.2a)$$

$$[K]^E = \begin{bmatrix} [0] & [0] & [0] \\ [K_{yx}] & [0] & [0] \\ [K_{zx}] & [K_{zy}] & [K_{zz}] \end{bmatrix} \qquad (7.2b)$$

where the superscripts I and E represent implicit and explicit respectively. If the damping matrix [C] is decomposed in the same way and predictors are introduced for some variables, Eq. 7.1 can be rewritten as

$$[M_{zz}](\ddot{r}_z) = (R_z) - [C_{zx}](\dot{r}_x^p) - [C_{zy}](\dot{r}_y^p) - [C_{zz}](\dot{r}_z^p) - [K_{zx}](r_x^p) - [K_{zy}](r_y^p) - [K_{zz}](r_z^p) \quad (7.3a)$$

from which $(\ddot{r}_z)$, $(\dot{r}_z)$ and (r_z) can be solved, then

$$[M_{yy}](\ddot{r}_y) + [C_{yy}](\dot{r}_y) + [K_{yy}](r_y) = (R_y) - [C_{yx}](\dot{r}_x^p) - [C_{yz}](\dot{r}_z) - [K_{yx}](r_x^p) - [K_{yz}](r_z) \quad (7.3b)$$

from which $(\ddot{r}_y)$, $(\dot{r}_y)$ and (r_y) can be solved, and finally,

$$[M_{xx}](\ddot{r}_x) + [C_{xx}](\dot{r}_x) + [K_{xx}](r_x) = (R_x) - [C_{xy}](\dot{r}_y) - [C_{xz}](\dot{r}_z) - [K_{xy}](r_y) - [K_{xz}](r_z) \quad (7.3c)$$

from which $(\ddot{r}_x)$, $(\dot{r}_x)$ and (r_x) are solved.

It can be seen that field z has to be solved first and in a fully explicit manner, then field y is solved in a mixed manner because the response on the interface with field x has to be extrapolated and field x can be solved in a fully implicit manner. This partition is called differential partitioning which requires predictors for both displacements and velocities (P5). An alternative way of partitioning can be achieved by integrating first, then partitioning and finally applying predictors to the partitioned equations. Without losing generality, the Newmark integration scheme is applied to Eq. 7.1, and it can be shown that (N3, B3)

$$[K]^* (r)_{n+1} = (R)^*_{n+1} \quad (7.4a)$$

where

$$[K]^* = a_0[M] + a_1[C] + [K] \quad (7.4b)$$

$$(R)^*_{n+1} = (R)_{n+1} + [M](\ddot{r})^*_n + [C](\dot{r})^*_n \quad (7.4c)$$

$$(\ddot{r})^*_n = a_0(r)_n + a_2(\dot{r})_n + a_3(\ddot{r})_n \quad (7.4d)$$

$$(\dot{r})^*_n = a_1(r)_n + a_4(\dot{r})_n + a_5(\ddot{r})_n \quad (7.4e)$$

The parameters a_0, a_1, a_2, a_3, a_4, a_5 are defined as

$$a_0 = \frac{1}{\alpha\Delta t^2}, \qquad a_1 = \frac{\delta}{\alpha\Delta t}, \qquad a_2 = \frac{1}{\alpha\Delta t},$$

$$a_3 = \frac{1}{2\alpha} - 1, \qquad a_4 = \frac{\delta}{\alpha} - 1, \qquad a_5 = \frac{\Delta t}{2}\left(\frac{\delta}{\alpha} - 2\right) \tag{7.4f}$$

where α and δ are the constants determining the stability and accuracy of the integration scheme. By decomposing the damping and stiffness matrices in Eq. 7.4b, Eq. 7.4a can be rewritten as

$$\begin{aligned} a_0[M_{zz}](r_z)_{n+1} = (R_z)^*_{n+1} &- (a_1[C_{yz}] + [K_{yz}])(r_z^p)_{n+1} \\ &- (a_1[C_{zy}] + [K_{zy}])(r_y^p)_{n+1} \\ &- (a_1[C_{zx}] + [K_{zx}])(r_x^p)_{n+1} \end{aligned} \tag{7.5a}$$

from which $(\ddot{r}_z)$, $(\dot{r}_z)$ and (r_z) can be solved, then

$$\begin{aligned} (a_0[M_{yy}] + a_1[C_{yy}] + [K_{yy}])(r_y)_{n+1} &= (R_y)^*_{n+1} \\ &- (a_1[C_{yz}] + [K_{yz}])(r_z)_{n+1} - (a_1[C_{yx}] + [K_{yx}])(r_x^p)_{n+1} \end{aligned} \tag{7.5b}$$

from which $(\ddot{r}_y)$, $(\dot{r}_y)$ and (r_y) can be solved, finally

$$\begin{aligned} (a_0[M_{xx}] + a_1[C_{xx}] + [K_{xx}])(r_x)_{n+1} &= (R_x)^*_{n+1} \\ &- (a_1[C_{xz}] + [K_{xz}])(r_z)_{n+1} - (a_1[C_{xy}] + [K_{xy}])(r_y)_{n+1} \end{aligned} \tag{7.5c}$$

This partition is called algebraic partitioning in which only a displacement predictor is required and the stability and accuracy depend on the computational sequences and the predictors (P5). When field y and x are solved, only the updated information on the previously solved fields is required in the differential partition analysis while the history information on the previously solved fields is still required in the algebraic partition analysis due to the presence of generalized load term $(R)^*$. Another disadvantage of the algebraic partition analysis is that the time step size has to be the same for all coupled fields.

For a finite element model, only the adjacent fields are coupled through a boundary and a simple three-field system arises from the two finite element meshes. Without loss of generality, this simple coupled system can be used as an illustration to present the different partition techniques.

The dynamic equilibrium equation of the system without damping is

$$\begin{bmatrix} [M_{xx}] & & \\ & [M_{yy}] & \\ & & [M_{zz}] \end{bmatrix} \begin{Bmatrix} (\ddot{r}_x) \\ (\ddot{r}_y) \\ (\ddot{r}_z) \end{Bmatrix} + \begin{bmatrix} [K_{xx}] & [K_{xb}] & [0] \\ [K_{bx}] & [K_{bb}] & [K_{by}] \\ [0] & [K_{yb}] & [K_{yy}] \end{bmatrix} \begin{Bmatrix} (r_x) \\ (r_b) \\ (r_y) \end{Bmatrix} = \begin{Bmatrix} (R_x) \\ (R_b) \\ (R_y) \end{Bmatrix} \quad (7.6)$$

The first partition analysis procedure is that proposed by Belytschko and Mullen called Node-by-Node I-E (Implicit-Explicit) partition (B5, B6). The stiffness matrix is partitioned as

$$[K]^I = \begin{bmatrix} [K_{xx}] & [K_{xb}] & [0] \\ [K_{bx}] & [K_{bb}] & [K_{by}] \\ [0] & [0] & [0] \end{bmatrix} \quad (7.7a)$$

$$[K]^E = \begin{bmatrix} [0] & [0] & [0] \\ [0] & [0] & [0] \\ [0] & [K_{yb}] & [K_{yy}] \end{bmatrix} \quad (7.7b)$$

The differential partitioning results in the equations

$$[M_{yy}](\ddot{r}_y) = (R_y) - [K_{yb}](r_b^p) - [K_{yy}](r_y^p) \quad (7.7c)$$

$$\begin{bmatrix} [M_{xx}] & \\ & [M_{bb}] \end{bmatrix} \begin{Bmatrix} (\ddot{r}_x) \\ (\ddot{r}_b) \end{Bmatrix} + \begin{bmatrix} [K_{xx}] & [K_{xb}] \\ [K_{bx}] & [K_{bb}] \end{bmatrix} \begin{Bmatrix} (r_x) \\ (r_b) \end{Bmatrix} = \begin{Bmatrix} (R_x) \\ (R_b) - [K_{by}](r_y) \end{Bmatrix} \quad (7.7d)$$

It can be seen that field y is solved in a fully explicit fashion, while field x is solved in a fully implicit fashion and the boundary is solved in a mixed fashion. On the right hand side of Eq. 7.7d, the coupled term $[K_{yb}](r_y)$ is required which is equal to the forces exerted on the boundary of the field x from field y. The stiffness term $[K_{bb}]$ consists of the contribution from field x and field y and thus a cross boundary stiffness matrix has to be assembled to solve field x and the boundary. To avoid this, an alternative partition,

called element-by-element I-E partition, was proposed by Hughes and Liu (H3, H4). In this partition analysis, the stiffness matrix can be partitioned as

$$[K]^I = \begin{bmatrix} [K_{xx}] & [K_{xb}] & [0] \\ [K_{bx}] & [K_{bb}^x] & [0] \\ [0] & [0] & [0] \end{bmatrix} \tag{7.8a}$$

$$[K]^E = \begin{bmatrix} [0] & [0] & [0] \\ [0] & [K_{bb}^y] & [K_{by}] \\ [0] & [K_{yb}] & [K_{yy}] \end{bmatrix} \tag{7.8b}$$

Eq. 7.6 can be solved in the following sequences,

$$[M_{yy}](\ddot{r}_y) = (R_y) - [K_{yb}](r_b^p) - [K_{yy}](r_y^p) \tag{7.8c}$$

$$\begin{bmatrix} [M_{xx}] & \\ & [M_{bb}] \end{bmatrix} \begin{Bmatrix} (\ddot{r}_x) \\ (\ddot{r}_b) \end{Bmatrix} + \begin{bmatrix} [K_{xx}] & [K_{xb}] \\ [K_{bx}] & [K_{bb}^x] \end{bmatrix} \begin{Bmatrix} (r_x) \\ (r_b) \end{Bmatrix}$$

$$= \begin{Bmatrix} (R_x) \\ (R_b) - [K_{bb}^y](r_b^p) - [K_{by}](r_y^p) \end{Bmatrix} \tag{7.8d}$$

One more term is present in the right hand side of Eq. 7.8d than that of Eq. 7.7d. If an extensive boundary is involved, the element-by-element partition will require more computational work than the node-by-node partition but no cross boundary stiffness matrix is required. A slight modification occurs if the stiffness matrix is partitioned as

$$[K]^I = \begin{bmatrix} [K_{xx}] & [K_{xb}] & [0] \\ [K_{bx}] & [K_{bb}^x] & [K_{by}] \\ [0] & [0] & [0] \end{bmatrix} \tag{7.8e}$$

$$[K]^E = \begin{bmatrix} [0] & [0] & [0] \\ [0] & [K^y_{bb}] & [0] \\ [0] & [K_{yb}] & [K_{yy}] \end{bmatrix} \tag{7.8f}$$

Eq. 7.8d can be rewritten as

$$\begin{bmatrix} [M_{xx}] & \\ & [M_{bb}] \end{bmatrix} \begin{Bmatrix} (\ddot{r}_x) \\ (\ddot{r}_b) \end{Bmatrix} + \begin{bmatrix} [K_{xx}] & [K_{xb}] \\ [K_{bx}] & [K^x_{bb}] \end{bmatrix} \begin{Bmatrix} (r_x) \\ (r_b) \end{Bmatrix}$$

$$= \begin{Bmatrix} (R_x) \\ (R_b) - [K^y_{bb}](r^p_b) - [K_{by}](r_y) \end{Bmatrix}. \tag{7.8g}$$

The updated (r_y) is used instead of the predictor.

The I-E partition can be carried out on each degree of freedom if the stiffness matrix is partitioned as (P3)

$$[K]^I = \begin{bmatrix} [K_{xx}] & [K_{xb}] & [0] \\ [K_{bx}] & [K_{bb}] & [K_{by}] \\ [0] & [K_{yb}] & [0] \end{bmatrix} \tag{7.9a}$$

$$[K]^E = \begin{bmatrix} [0] & [0] & [0] \\ [0] & [0] & [0] \\ [0] & [0] & [K_{yy}] \end{bmatrix} \tag{7.9b}$$

This partition is referred to as the DOF-by-DOF I-E partition in which it is impossible to solve the equations separately but has the advantage that some degrees of freedom can be treated explicitly while the others can be treated implicitly. The stiffness terms associated with the explicitly treated degrees of freedom do not have to be assembled into the global stiffness matrix.

When the stability requirement governs both fields, an implicit partition may be preferred. The stiffness matrix can be partitioned as

$$[K]^I = \begin{bmatrix} [K_{xx}] & [K_{xb}] & [0] \\ [K_{bx}] & [K_{bb}] & [K_{by}] \\ [0] & [0] & [K_{yy}] \end{bmatrix} \tag{7.10a}$$

$$[K]^E = \begin{bmatrix} [0] & [0] & [0] \\ [0] & [0] & [0] \\ [0] & [K_{yb}] & [0] \end{bmatrix} \tag{7.10b}$$

Eq. 7.6 can be solved as

$$[M_{yy}](\ddot{r}_y) + [K_{yy}](r_y) = (R_y) - [K_{yb}](r_b^p) \tag{7.10c}$$

and then

$$\begin{bmatrix} [M_{xx}] & \\ & [M_{bb}] \end{bmatrix} \begin{Bmatrix} (\ddot{r}_x) \\ (\ddot{r}_b) \end{Bmatrix} + \begin{bmatrix} [K_{xx}] & [K_{xb}] \\ [K_{bx}] & [K_{bb}] \end{bmatrix} \begin{Bmatrix} (r_x) \\ (r_b) \end{Bmatrix} = \begin{Bmatrix} (R_b) \\ (R_b) - [K_{by}](r_y) \end{Bmatrix} \tag{7.10d}$$

Compared with Eq. 7.7, field y is solved in a quasi-implicit fashion because the boundary value has to be predicted. A version of this implicit partition is the element-by-element I-I partition by which better accuracy can be achieved for some problems (P3, P4). The stiffness matrix is partitioned in the same way as in Eq. 7.8 but both fields are solved implicitly as

$$\begin{bmatrix} [M_{xx}] & \\ & [M_{bb}] \end{bmatrix} \begin{Bmatrix} (\ddot{r}_x) \\ (\ddot{r}_b) \end{Bmatrix} + \begin{bmatrix} [K_{xx}] & [K_{xb}] \\ [K_{bx}] & [K_{bb}^*] \end{bmatrix} \begin{Bmatrix} (r_x) \\ (r_b) \end{Bmatrix}$$

$$= \begin{Bmatrix} (R_x) \\ (R_b) - [K_{bb}^*](r_b^p) - [K_{by}](r_y^p) \end{Bmatrix} \tag{7.11a}$$

and

$$\begin{bmatrix} [M_{bb}] & \\ & [M_{yy}] \end{bmatrix} \begin{Bmatrix} (\ddot{r}_b) \\ (\ddot{r}_y) \end{Bmatrix} + \begin{bmatrix} [K^{\chi}_{bb}] & [K_{by}] \\ [K_{yb}] & [K_{yy}] \end{bmatrix} \begin{Bmatrix} (r_b) \\ (r_y) \end{Bmatrix}$$

$$= \begin{Bmatrix} (R_b) - [K_{bx}](r^p_x) - [K^{\chi}_{bb}](r^p_b) \\ (R_y) \end{Bmatrix} \qquad (7.11b)$$

The disadvantage of the partition is that the boundary values are solved twice, but then no boundary cross stiffness matrices are required. An alternative way of solving the partitioned equations is to replace (r^p_x) and (r^p_b) in Eq. 7.11b by the updated values determined from Eq. 7.11a, and at next time step solve Eq. 7.11b first and then solve Eq. 7.11a by using the updated values instead of the predictors for field y and the boundary (P3).

The stability consideration requires that the time step size be smaller than the critical one in an explicit integration scheme. This critical time step size could be much smaller than that required in the implicit integration scheme determined from an accuracy consideration. In a partitioned analysis procedure, it is possible that different time steps are employed in the different fields. A mixed time element-by-element partition, the mI-E partition, was proposed by Liu and Belytschko as follows (L3).

The time step size in the implicit field is $m\Delta t$ and is Δt in the explicit field. The predictor and corrector employed in the explicit field are:

$$(r^p_b)_{n+j} = (r_b)n + j\Delta t(\dot{r}_b)_n + (1/2 - \alpha)\,(j\Delta t)^2(\ddot{r}_b)_n \qquad (7.12a)$$

$$(\dot{r}^p_b)_{n+j} = (\dot{r}_b)_n + (1 - \delta)j\Delta t(\ddot{r}_b)_n \qquad (7.12b)$$

$$(r^p_y)_{n+j} = (r_y)_{n+j-1} + \Delta t(\dot{r}_y)_{n+j-1} + (1/2 - \alpha)\Delta t^2(\ddot{r}_y)_{n+j-1} \qquad (7.12c)$$

$$(\dot{r}^p_y)_{n+j} = (\dot{r}_y)_{n+j-1} + (1 - \delta)\Delta t(\ddot{r}_y)_{n+j-1} \qquad (7.12d)$$

$$(r_b)_{n+j} = (r^p_b)_{n+j} + \alpha(j\Delta t)^2(\ddot{r}_b)_{n+j} \qquad (7.12e)$$

$$(\dot{r}_b)_{n+j} = (\dot{r}^p_b)_{n+j} + \delta j\Delta t(\ddot{r}_b)_{n+j} \qquad (7.12f)$$

$$(r_y)_{n+j} = (r_y^p)_{n+j} + \alpha\Delta t^2(\ddot{r}_y)_{n+j} \tag{7.12g}$$

$$(\dot{r}_y)_{n+j} = (\dot{r}_y^p)_{n+j} + \delta\Delta t(\ddot{r}_y)_{n+j} \tag{7.12h}$$

where $j = 1, 2, \ldots\ldots, m$.

For $j = 1,2, \ldots\ldots, m$, solve

$$[M_{yy}](\ddot{r}_y)_{n+j} = (R_y)_{n+j} - [K_{yy}](r_y^p)_{n+j} - [K_{yb}](r_b^p)_{n+j} \tag{7.12i}$$

If $j = m$, solve

$$\begin{bmatrix} [M_{xx}] & \\ & [M_{bb}] \end{bmatrix} \begin{Bmatrix} (\ddot{r}_x)_{n+\alpha} \\ (\ddot{r}_b)_{n+\alpha} \end{Bmatrix} + \begin{bmatrix} [K_{xx}] & [K_{xb}] \\ [K_{bx}] & [K_{bb}^x] \end{bmatrix} \begin{Bmatrix} (r_x)_{n+\alpha} \\ (r_b)_{n+\alpha} \end{Bmatrix}$$

$$= \begin{Bmatrix} (R_x)_{n+\alpha} \\ (R_b)_{n+\alpha} - [K_{bb}^y](r_b^p)_{n+\alpha} - [K_{by}](r_y^p)_{n+\alpha} \end{Bmatrix} \tag{7.12j}$$

where the displacement vector on the left hand side can be written as

$$(r)_{n+\alpha} = (r)_n + m\Delta t(\dot{r})_n + (m\Delta t)^2[(1/2 - \alpha)(\ddot{r})_n + \alpha(\ddot{r})_{n+\alpha}] \tag{7.12k}$$

If the time step size limit arises from an accuracy consideration in the implicit integration scheme, this mixed time technique can be easily extended to an element-by-element mI-I partition by solving the following equations.

For $j = 1, 2, \ldots\ldots, m$, solve

$$\begin{bmatrix} [M_{bb}] & \\ & [M_{yy}] \end{bmatrix} \begin{Bmatrix} (\ddot{r}_b) \\ (\ddot{r}_y) \end{Bmatrix} + \begin{bmatrix} [K_{bb}^y] & [K_{by}] \\ [K_{yb}] & [K_{yy}] \end{bmatrix} \begin{Bmatrix} (r_b) \\ (r_y) \end{Bmatrix}$$

$$= \begin{Bmatrix} (R_b) - [K_{bx}](r_x^p) - [K_{bb}^x](r_b^p) \\ (R_y) \end{Bmatrix} \tag{7.12l}$$

where

$$(r_b^p)_{n+j} = (r_b)_{n+j-1} + \Delta t(\dot{r}_b)_{n+j-1} + (1/2 - \alpha)\Delta t^2(\ddot{r}_b)_{n+j-1} \qquad (7.12m)$$

$$(r_x^p)_{n+j} = (r_b)_n + j\Delta t(\dot{r}_b)_n + (1/2 - \alpha)(j\Delta t)^2(\ddot{r}_b)_n \qquad (7.12n)$$

and for j = m, solve

$$\begin{bmatrix} [M_{xx}] & \\ & [M_{bb}] \end{bmatrix} \begin{Bmatrix} (\ddot{r}_x)_{n+m} \\ (\ddot{r}_b)_{n+m} \end{Bmatrix} + \begin{bmatrix} [K_{xx}] & [K_{xb}] \\ [K_{bx}] & [K_{bb}^x] \end{bmatrix} \begin{Bmatrix} (r_x)_{n+m} \\ (r_b)_{n+m} \end{Bmatrix}$$

$$= \begin{Bmatrix} (R_x)_{n+m} \\ (R_b)_{n+m} - [K_{bb}^y](r_b^p)_{n+m} - [K_{by}](r_y^p)_{n+m} \end{Bmatrix} \qquad (7.12p)$$

7.2 Stability and Accuracy Evaluation

The factors governing an integration scheme are its stability and accuracy. The theoretical evaluations of the partitioned analysis procedures have been reported in literature (B6, B7, H3, L3, P3). It has been shown that a theoretical evaluation of the partitioned procedure is more difficult than that of the integration scheme for a single field and is limited to only a few of the partitioned procedures. Some criteria for the stability reported in the literature is based on numerical experiments (B6, B7, L3). Numerical experiment can not give a definitive conclusion but the limited detected will be applied to general problems. In this context, a numerical experiment is performed to evaluate the stability of each partitioned procedure given in the previous section and the accuracies of the different modes. The stability of an integration scheme for a given system depends on the highest frequency of the system and the accuracy depends on the

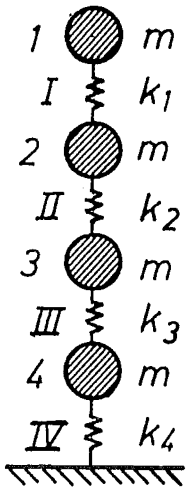

Fig. 7.1 Model Problem

mode frequency distribution of the system response as well as the integration scheme itself. For a single field problem, the response of the system can be decomposed into a number of equivalent single degree of freedom systems, one for each natural frequency, and the accuracy of an integration scheme can be assessed from the single degree of freedom systems (B3). For a partitioned analysis procedure, no such equivalent single degree of freedom systems can be derived for the dynamic system. For a partitioned analyses procedure the achieved accuracy may be different for each mode of the whole systems even when compared at the same sampling frequency in the time domain. If a large dynamic system is used to evaluate the accuracy of a partitioned analysis procedure, numerical errors are inevitably introduced into the modal responses which are computed from the overall responses of the system. From these above considerations the following 4-degree-of-freedom system is used to study the properties of the different integration schemes. The spring k_1 could represent the upper structure, k_2 and k_3 represent the near-field soil while k_4 is the far-field stiffness for a soil-structure interaction problem. Assume $K_1/k_2 = 2$, $k_2 = k_3$ and $k_3/k_4 = 1.5$. The mass for each degree of freedom is chosen as being the same. The ratio of the highest natural frequency to the lowest natural frequency is 7. In the Node-by-Node partition, node 1 and node 2 are in group 1 and node 3 and node 4 are in group 2. In the Element-by-Element partition, element 1 in is group 1 and element 2, 3 and 4 are in group 2.

The unconditional stability is achieved only for the Node-by-Node I-I partition. The predictor and integration formula used are the Newmark constant acceleration scheme. For the I-E partition, the critical sampling frequency is

$$\Omega_{crit} = (2/\delta)^{1/2} \qquad (7.13a)$$

$$\Delta t\omega^{E}_{max} \leq \Omega_{crit} \qquad (7.13b)$$

where ω^{E}_{max} is the maximum eigenvalue of the system

Table 7.1. Critical Time Step Size

Partition Method	Critical Time Step
Fully Explicit	0.0407
Element-by-Element I-E	0.0544
Element-by-Element I-I	0.0638
Element-by-Element I-I (Alternative Solving)	0.08948
Node-by-Node I-E	0.05122
Node-by-node I-I-E	0.1095
Element-by-Element mI-E (m = 2)	0.03298
Node-by-Node mI-E (m = 2)	0.0485

$$(-\omega^2[M] + [K]^E)\ (u) = (0) \qquad (7.13c)$$

as derived by Park, Hughes and Liu(P3, H3).

For an Element-by-Element I-I partition, only conditional stability is achieved for all of the predictors recommended by Park and Felippa (P5). The critical sample frequency strongly depends on the stiffness terms $[K^x_{bb}]$ and $[K^y_{bb}]$ for which the displacements have to be extrapolated. It seems that $\Delta t(K_{bb}/M_{bb})^{\frac{1}{2}}$ is roughly constant for this model problem as shown in Fig. 7.2. The critical sampling frequency depends much less on the other terms of the stiffness matrix. When $[K_{bb}]$ is very small compared with the other terms, the critical sample frequency is larger but still depends on $[K_{bb}]$.

For the mixed time step mI-E partition, the stiffness term for which the displacement has to be extrapolated has a significant effect on the stability. For m = 2 in the Element-by-Element mI-E partition, it can be seen from Fig. 7.3 that when the pseudo-frequency ratio $(k_2/m_2)^{1/2}/\omega_{max}{}^E$ is less than 0.31, the critical sample frequency is greater than 2, and when the pseudo-frequency ratio is greater than 0.48, the critical sample frequency drops quickly and this is in contrast with the formula proposed by Liu and Belytschko (L3). For the Node-by-Node mI-E partition, the same trend can be found but the critical frequency drops at a higher value of the pseudo-frequency ratio.

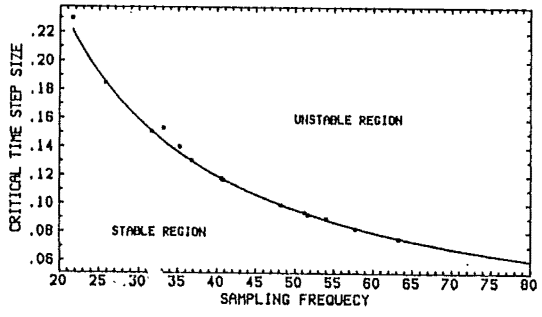

Fig. 7.2 Stability For Element-by -Element I-I Partition

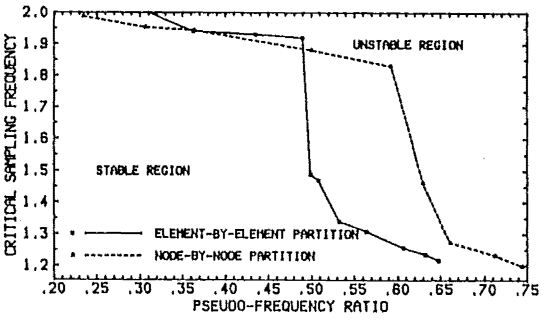

Fig. 7.3 Stability For Mixed Time Step I-E Partition

The accuracy of each algorithm can be estimated by the phase and amplitude error of each mode. The modal problem is integrated subjected to an unit initial displacement and then the modal displacement vector is calculated from

$$\{z(t)\} = [\phi]^T[M]\{r(t)\} \tag{7.14a}$$

$$\{z(0)\} = [\phi]^T[M]\{r(0)\} \tag{7.14b}$$

where $[\phi]$ are the mode shapes and [M] is the mass matrix of the system. The initial velocity and acceleration are zero and each modal displacement is a cosine function.

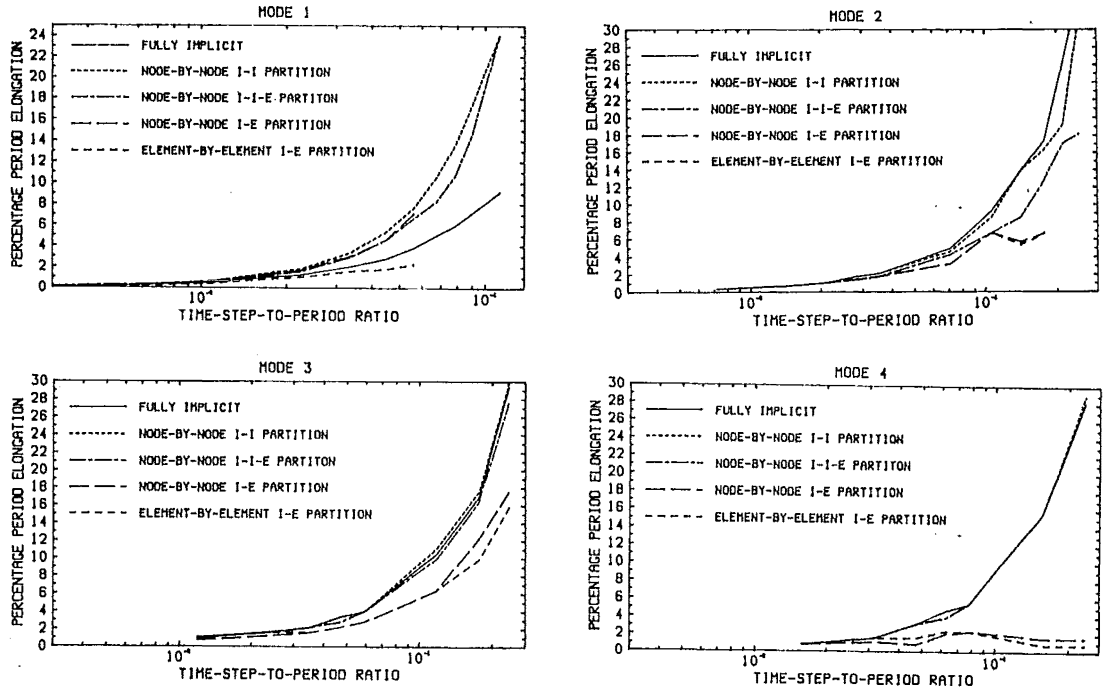

Fig. 7.4 Period Elongation of the Modal Problem

It can be seen from Fig. 7.4 that the period of the first mode is best predicted by the Element-by-Element I-E partition, followed by the fully implicit, the Node-by-Node I-E partition and the Node-by-Node I-I partition. In the Node-by-Node I-I partition, if element 4 is integrated explicitly (I-I-E partition), the period error is reduced before the critical time step size is reached. For mode 2, all partition procedures are more accurate than the fully implicit scheme and the two I-E partitions have the same accuracy. For mode 3, the fully implicit, the Node-by-Node I-I and the Node-by-Node I-I-E partitions are very similar, and the two I-E partitions are the same for small time steps. The I-E partitions are more accurate than the others. For mode 4, the I-E partitions introduce smaller period errors than do the other partitions.

The amplitude error can be found from Fig. 7.5. The Element-by-Element I-E partition, the Node-by-Node I-I partition and the fully implicit method introduce nearly the same amount of positive damping for mode 1 when the time step is large. The Node-by-Node I-E and the I-I-E partition introduce more positive damping to mode 1 before the critical time step is reached. All algorithms introduce positive damping to mode 2. When the time step is small, the Node-by-Node I-I partition introduces the smallest amount of damping. For large time steps, the most accurate is the fully implicit algorithm, followed by the Node-by-Node I-I partition, the Node-by-Node I-E partition, the Element-by-Element I-E partition and the Node-by-Node I-I-E partition. For mode 3, the most accurate method is the Node-by-Node I-I-E partition, followed by the fully implicit, the Element-by-Element I-E, the Node-by-Node I-E and the Node-by-Node I-I partition and positive damping is introduced. For mode 4, both the I-E partitions introduce negative damping and the others introduce positive damping. The Node-by-Node I-I partition gives more positive damping than the other algorithms.

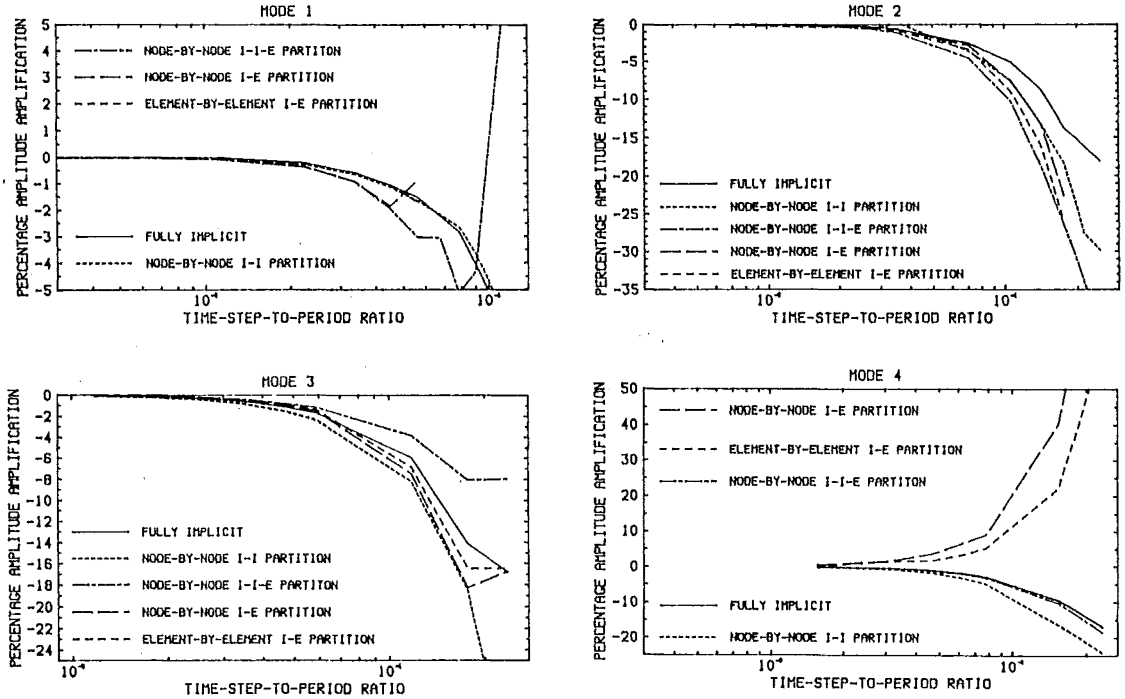

Fig. 7.5 Amplitude Amplification of the Modal Problem

If the time step size for the explicit part is reduced to half of the time step size for the implicit part, the period error is reduced for both the I-E partitions in all modes as is shown in Fig. 7.6. The Element-by-Element

mI-E partition is the most accurate for mode 1. The amplitude error is reduced for all modes, but for mode 1, the Node-by-Node mI-E partition tends to introduce negative damping when the time step is large.

It can be seen from Fig. 7.7 that the Node-by-Node I-I partition introduces nearly the same amount of period error for modes 2, 3 and 4, and larger error to mode 1. This partition introduces more positive damping for the higher modes. The Node-by-Node I-E partition introduces less period error for the higher modes, negative damping for mode 4 and nearly the same amount of positive damping for the first three modes.

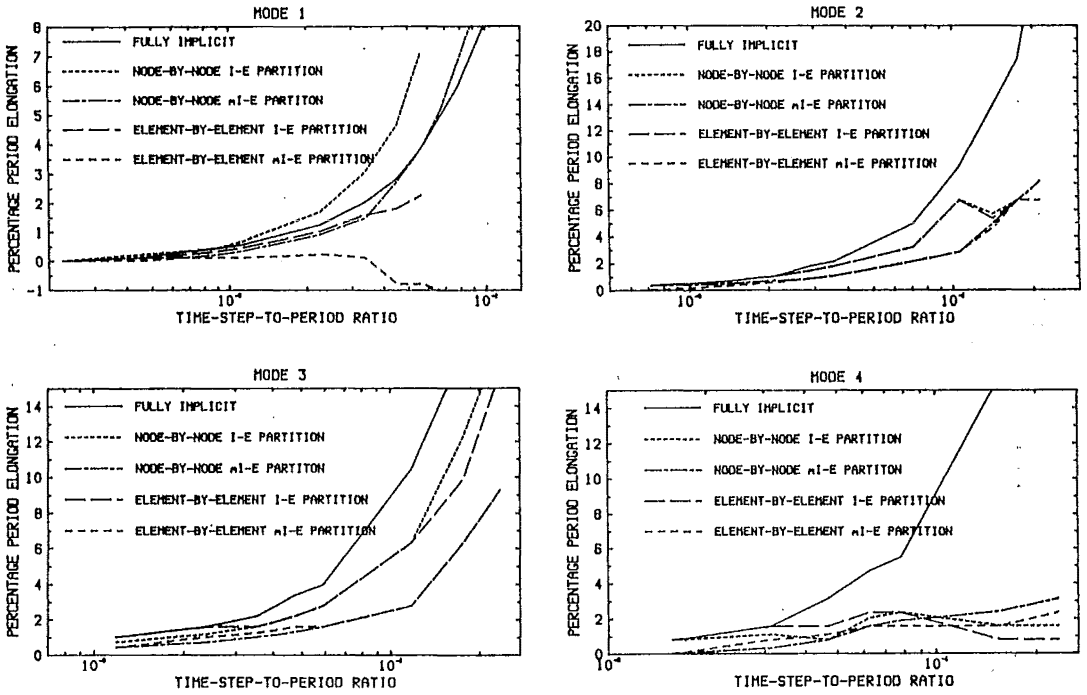

Fig. 7.6 Period Error for Mixed Time Step Partitions

It can be seen form Fig. 7.8 that the Element-by-Element I-E partition has similar properties for the different modes but introduces much less error for the first mode than does the Node-by-Node I-E partition.

For the Element-by-Element I-I partition, all modes have similar characteristics for the period elongation. This partition has a much better period accuracy for mode 1 than the Node-by-Node I-I partition. It possesses smaller amplitude error for all modes except mode 1 than the Node-by-Node I-

I partition and it introduces less positive damping in the higher modes.

As expected, the fully implicit method introduces the same amount error to all modes for the same ratio of time step size to the modal period.

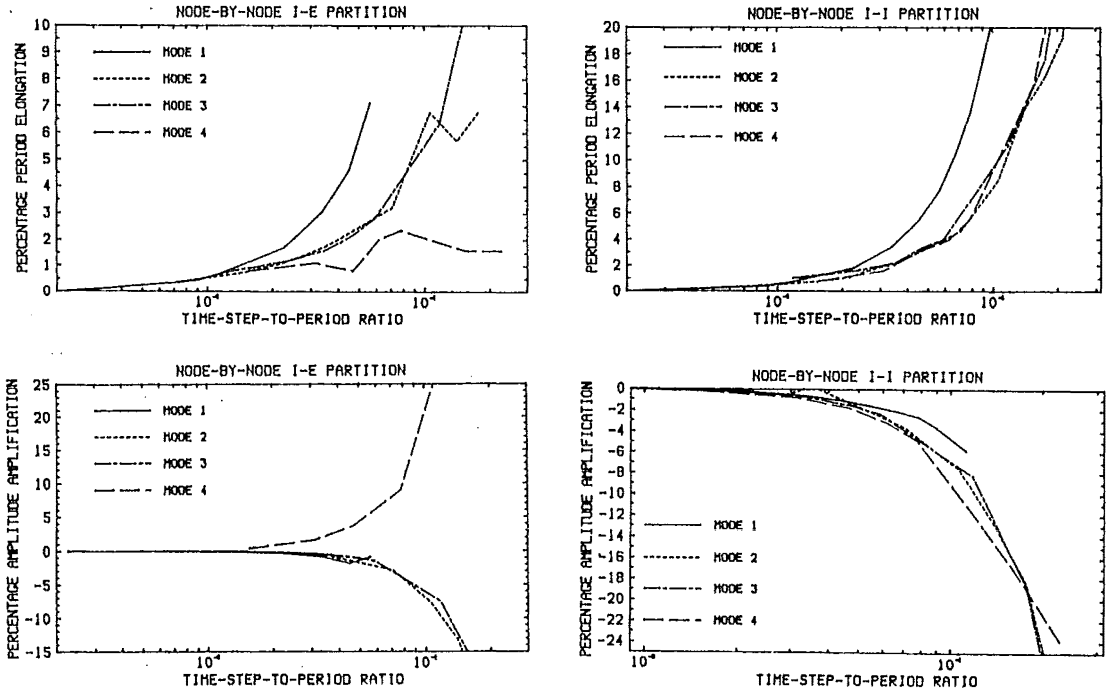

Fig. 7.7 Modal Error for Node-by-Node Partition

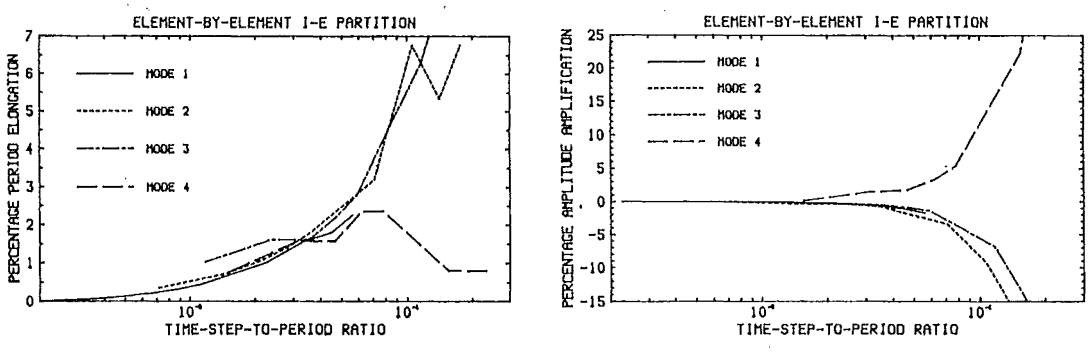

(a) (b)

Fig. 7.8 Modal Error for Element-by-Element I-E Partition

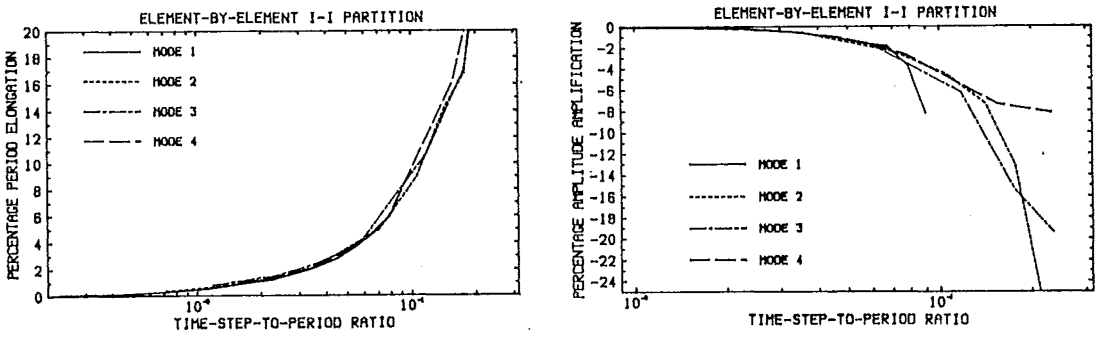

(a) (b)

Fig. 7.9 Modal Error of Element-by-Element I-I Partition

7.3 Summary

Among all of the partition procedures, unconditional stability can only be achieved for the Node-by-Node I-I partition. The critical time step size of the Element-by-Element partition depends on the maximum frequency of the explicit field and on the diagonal terms of the stiffness matrix for which the displacements are extrapolated. The critical time step size for the mixed time step Element-by-Element mI-E and Node-by-Node mI-E partition depends not only on the maximum frequency of the explicit element group but also depends on the stiffness of the elements for which the displacement is extrapolated. The Element-by-Element I-I partition introduces smaller period error than the fully implicit and the Node-by-Node I-I partition and a smaller amplitude error in the higher modes. The Element-by-Element I-E partition introduces smaller period and amplitude errors in the fundamental mode than do all other procedures. If the time step size is reduced for the explicit element group, the accuracy is improved for both the I-E partitions.

It appears that if the stability is a major concern, the Node-by-node I-I partition can be used for soil-structure interaction analyses and the time step size is determined by the accuracy requirements. A smaller time step size than that required by the fully implicit procedure may have to be chosen because of the larger period errors introduced for the lower frequency modes. Because an explicit procedure may have to be used for the far-field if the boundary element model is employed, the Element-by-Element I-E procedure may

be preferred in which case the near-field soil can be integrated explicitly. This would make it easier to take into account the uplift and slip between the soil and the base of the upper structure. A smaller time step may be used for the soil if necessary, ie., using the Element-by-Element mI-E partition procedure.

Chapter 8

A Primary Investigation of Soil Conditions and Soil-Structure Interaction During a Strong Earthquake

8.1 Soil Condition and Building Damage

As is described in Chapter 1, a soil deposit at a given site has a strong influence on the damage of structures. This has been one of the most dramatic aspects of the earthquake effects in Mexico City in the earthquake of September 19, 1985 (S8). The epicentre of the earthquake was about 350 kilometres away from the city. The earthquake with a Richter magnitude of 8.1 generated a seismic wave with peak ground acceleration of the order 0.04g (gravity acceleration) and peak spectral acceleration (5% damping) of 0.11g on the hard stiff soil deposits. However, the building damage due to the strong ground shaking had enormously different intensities in the different parts of the city. This difference in the damage intensities was attributed to the difference in the soil deposits at the different parts of the city (S8). For example, due to the soft soil deposits of 37m in depth at the SCT (Secretaria de Communicaciones y Transportes) site in the heavy damage area, the peak ground acceleration was about 0.17g and the spectral acceleration at 5% damping was 1.0g at a period of about 2 seconds which is the fundamental period of the site. The components of the seismic wave, with periods near to the fundamental period of the site, incident from the rock was significantly amplified by the soft soil. The amplification phenomena was also apparent in other parts of the city with soft soil deposits (S8). The accelerogram recorded at the SCT site in E-W direction is shown in Fig. 8.1. The spectral accelerations of the SCT site and a rock site (CUMV-Civdad Universitaria Mesa Vibradora) in Mexico City are shown in Fig. 8.2.

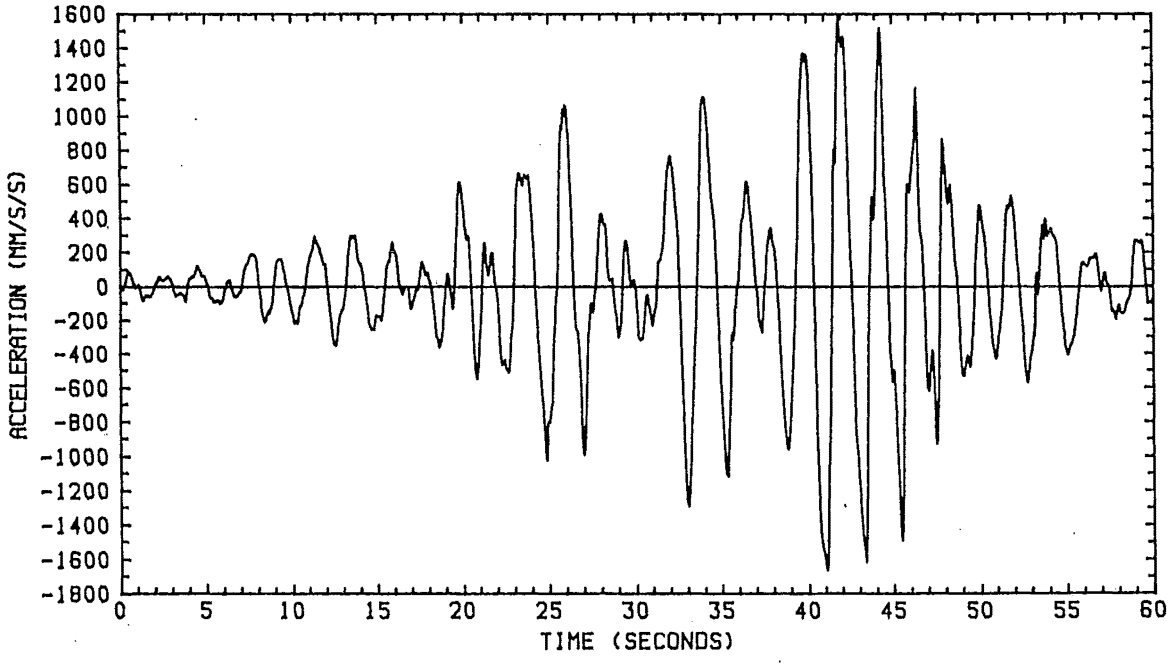

Fig. 8.1 East-West Ground Acceleration at SCT Site

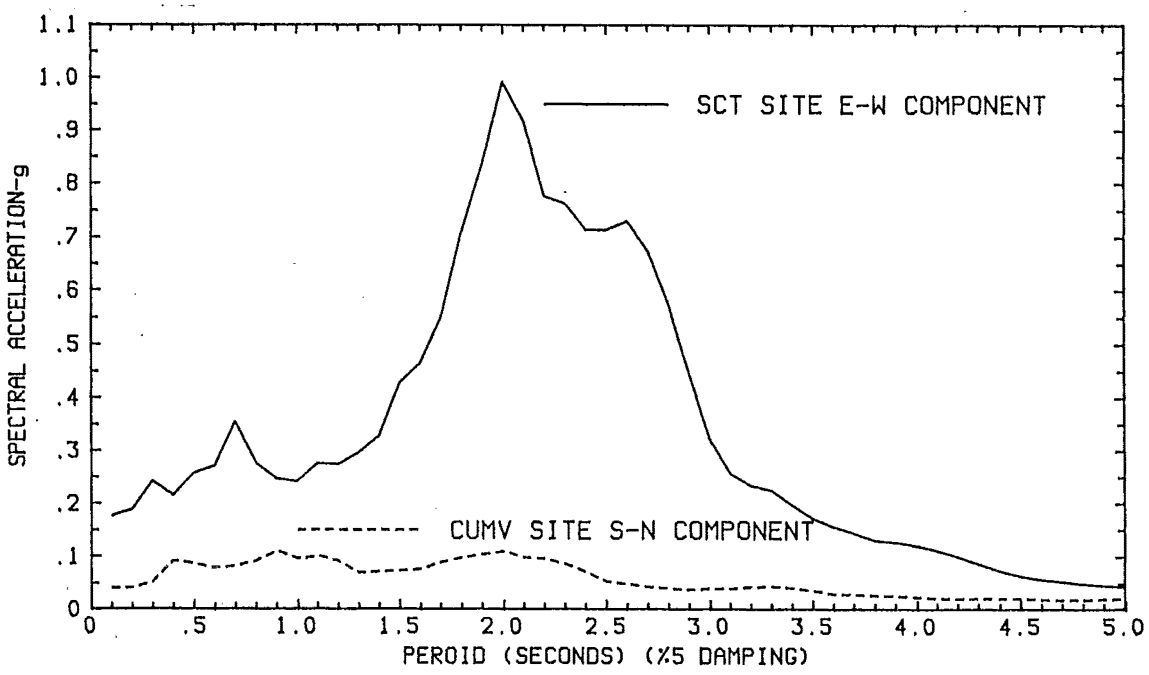

Fig. 8.2 Acceleration Spectra

The severely damaged buildings were mainly from 6 to 15 storeys high with fundamental period ranging from about 0.7 to 1.7 seconds (B9) and damage to 6 to 12 storey buildings was especially severe (S1). Concrete structures suffered major damage while only one 21-storey steel building with a fundamental period of about 2 seconds collapsed. Framed structures with deep beams and slabs or waffle slabs connected to the columns to form rigid frames were the major type of structures that were damaged. A large number of failures occurred in the upper or intermediate levels of these structures. In over 40% of the collapsed or severely damaged buildings, pounding between adjacent buildings occurred and in at least 15% the pounding was the primary cause of collapse (B8). Severe foundation damage was found in the area at which the thickness of the soft soil layer was from about 39 to 50m while little damage occurred in the other areas (G2). A large amounts of settlement and foundation rotation were found.

In such a flexible soil site, soil-structure interaction would have a major influence on the structural response. Due to the presence of the flexible soil, the dynamic characteristics of a structure would be different from that of the same structure on stiff soil. In general, the fundamental period of the structure would be larger and the radiation damping would also affect the response of the structure. The displacement of the building relative to the free-field may be much larger than that of a building on a stiff soil and this could make the pounding between adjacent buildings with different heights much more severe. An investigation of the soil-structure interaction effects at a site similar to the SCT site in Mexico City subjected to the east-west component of the ground acceleration recorded at the SCT site in the earthquake of Mexico City in September 19, 1985 is reported in this chapter. Instead of using a single-degree-of-freedom oscillator or a shear beam with lumped masses modelling the structure, several single bay frames with a different number of storeys will be used in the analyses. The frames are idealized with the dimensions similar to these used in a practical design but are expected to give some useful information on non-linear effects and soil-structure interaction effects on the response of the structures.

Five frames are used. The height of each storey is 3.25m, the span of the beam is 6.5m and the span in the direction perpendicular to the plane of frame is also 6.5m. The columns have a dimension of 0.8mx0.8m and the beams have a dimension of 0.4mx0.8m(bxh). The Young's modulus of the material is

taken as $2.6 \times 10^{10} N/M^2$ for the reinforced concrete. Lumped masses are used including rotational masses which are so assigned that the structures would have the same fundamental period as that if consistent masses were used. The total mass for each floor was determined from the pre-assigned fundamental period for each frame and the total weight for each floor is in the range of practical design. The period assigned for each frame was determined from the fundamental period to number of storey relationship reported for Mexico City by Scawthorn (S1). In order to minimize the effort of data processing, 12-storey frames were chosen for the long period structures. Neither rigid end-block nor shear deformation was taken into account. The fundamental period of each frame is shown in Table 8.1

Table 8.1 FRAME PROPERTIES

No. OF FRAME	1	2	3	4	5
No. OF STOREY	5	8	12	12	12
NATURAL PERIOD(S)	0.5	1.0	1.5	2.0	2.5

In the non-linear analysis, the bi-linear and the curvilinear models developed in Chapter 3 were used. The bi-linear ratio was 1% and the material parameter E_h (see Chapter 3) was 80% of the initial elastic stiffness. Plastic hinges were only allowed to form at the beam ends and the base ends of the ground floor columns and the plastic hinge length was calculated from the equation given by Park and Paulay (P7) to give 0.44m for the beams and 0.35m for the columns. The yield moments for each beam and column were determined by dividing the maximum elastic moments developed in the member subjected to the same earthquake excitation by a load factor. No interaction between the axial forces and bending moments was taken into account.

The Newmark constant acceleration integration scheme (N3) was employed and the time step for the structures whose fundamental period equals one seconds or smaller was 0.005 seconds and 0.01 seconds was used for the others. 60 seconds of the original earthquake record has been used in the analysis.

Rayleigh damping was assumed for all structures with the damping ratios being 5% for the first and fifth fixed base modes. The damping matrix was proportional to the initial elastic stiffness matrix and mass matrix and calculated from:

$$[C] = a_o[M] + a_1[K] \qquad (8.1a)$$

where

$$a_o = \frac{2\omega_1\omega_2(\zeta_2\omega_1 - \zeta_1\omega_2)}{\omega_1^2 - \omega_2^2} \qquad (8.1b)$$

$$a_1 = \frac{2(\omega_1\zeta_1 - \omega_2\zeta_2)}{\omega_1^2 - \omega_2^2} \qquad (8.1c)$$

and ω_1 and ω_2 are the circular frequencies for the first and fifth fixed base modes respectively and ζ_1 and ζ_2 are the corresponding damping ratios.

For the structures on soft soil, the damping coefficients a_o and a_1 are still calculated from Eq. 8.1b and 8.1c using the frequencies for the fixed base modes, ie., a_o and a_1 are the same as those for the corresponding structures on the stiff soil. The damping matrix is computed from Eq. 8.1a but the stiffness matrix [K] and mass matrix [M] include the contributions from the base nodes. When the soil stiffness becomes infinitely large, the computed damping matrices will cause the structure to have the same response as the corresponding structures do on stiff soil.

The structures on soft soil are assumed to have rigid base floors and this assumption will simplify the computational procedure while introducing little error.

All analyses were carried out on a Vax 750 Computer System using the programs developed by the author.

8.2 The Response of the Structures on Stiff Soil

Firstly, the structures described in the previous section are assumed to rest on stiff soil and subjected to the ground motion in the east-west direction at SCT site in Mexico City in the earthquake of September 19, 1985. An elastic analysis is carried out first. The top floor horizontal displacement-time histories for Frames 1 to 4 are shown in Fig. 8.3 to 8.6. The maximum responses are obtained at about 40 to 50 seconds for all

structures. It can be seen form Fig. 8.6 that the resonance has built up in frame 4.

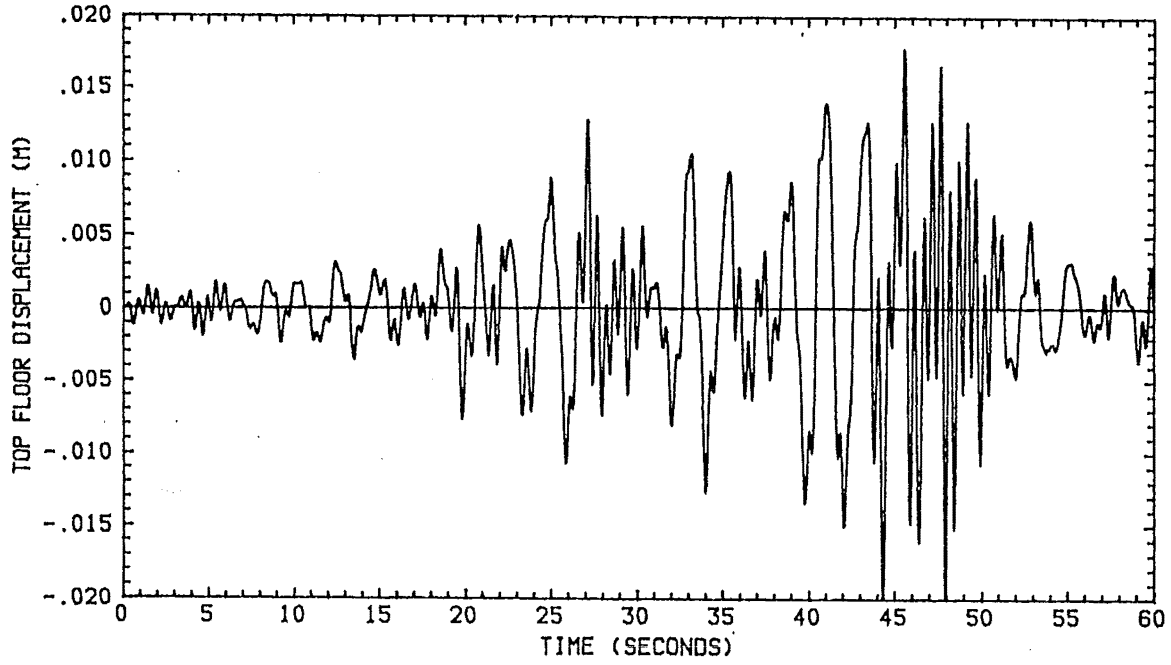

Fig. 8.3 5-Storey Frame 1 Elastic Response (Stiff Soil)

Secondly, load factors are assigned to each frame and the yield moments for each beam and ground floor column are determined by dividing the maximum elastic moments by the load factor. Nonlinear analyses are carried out for a bi-linear model and curvilinear model of the moment-curvature relationship. A typical bi-linear and curvilinear moment-curvature hysteresis loops are shown in Fig. 8.7. The energy dissipated by the plastic deformation is larger in the bi-linear model than in the curvilinear model for a complete loading cycle but energy can still be dissipated by plastic deformation when the moment is less than the yield moment in the curvilinear model. Ductility is defined as the ratio of the maximum curvature to the yield or equivalent yield curvature ϕ_y which is shown in Fig. 8.7. Curvature ductility demand is of important interest for a ductile structure. Four would be used for a load factor in a practical design and was chosen for all five frames but 2 and 1.5 were also used for frame 1 and frame 2. The top floor horizontal displacement-time histories of the bi-linear model for Frames 1 to 3 are shown in Fig. 8.8 to Fig. 8.10. The ductility demands are shown in Table 8.3 to 8.5 for the bi-linear model.

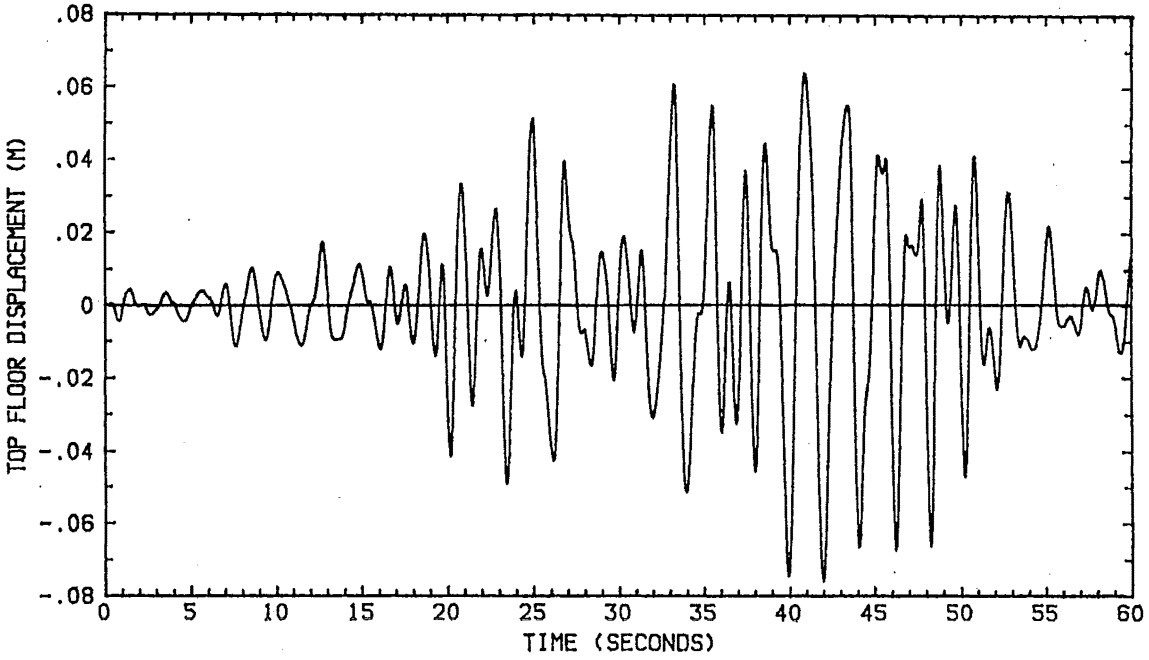

Fig. 8.4 8-Storey Frame 2 Elastic Response (Stiff Soil)

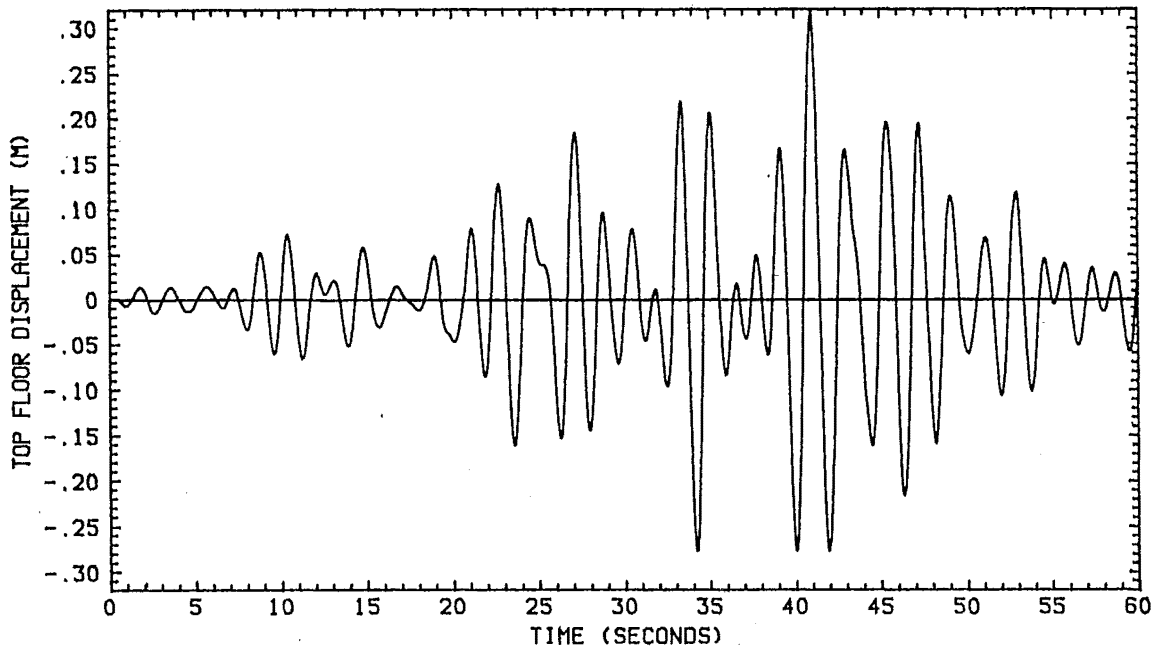

Fig. 8.5 12-Storey Frame 3 Elastic Response (Stiff Soil)

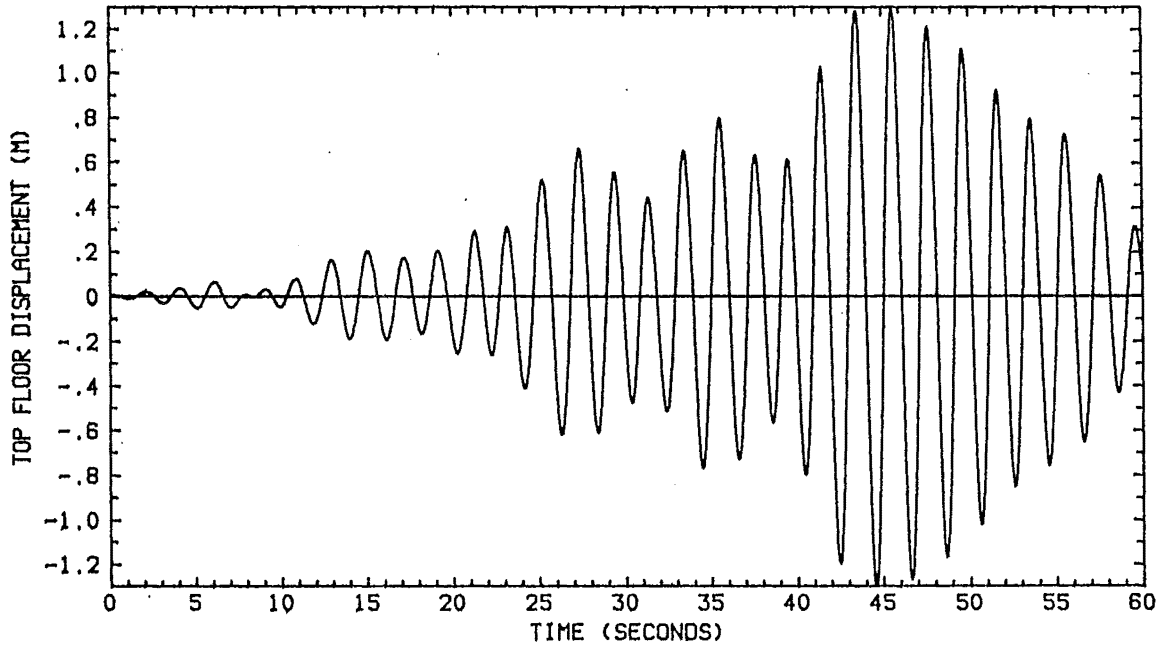

Fig. 8.6 12-Storey Frame 4 Elastic Response (Stiff Soil)

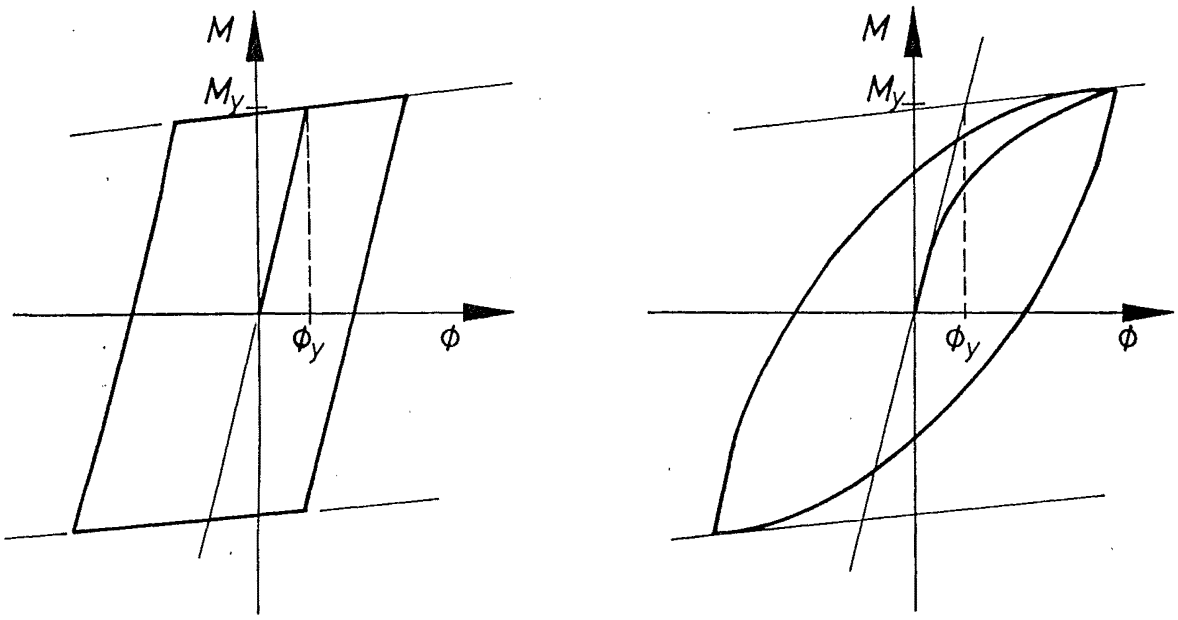

Fig. 8.7 Hysteresis Loop for Bi-linear and Curvilinear Model

Period elongation due to yielding is obvious in the inelastic responses of all the structures, especially at the time when the maximum responses are obtained and a pulse with a period of about 2 seconds is generated except for the 5-storey frame with a load factor of 1.5 (not shown). For the 5-storey frame and the 8-storey frame, a small load factor will lead to a large

amplification of displacement response. For example, if the load factor is 2, the maximum displacement (absolute value) for the 8-storey frame would be about 3.5 times as large as for the elastic case, and if the load factor is 4, about 10 fold displacement amplification is found for the 5-storey frame but only 4 fold for the 8-storey frame. For the 12-storey frame 3, the maximum top floor displacement is about the same for both elastic and inelastic response when the load factor is 4 while for the 12-storey frame 4 and frame 5, only half of the elastic top floor displacement has been developed in the inelastic response.

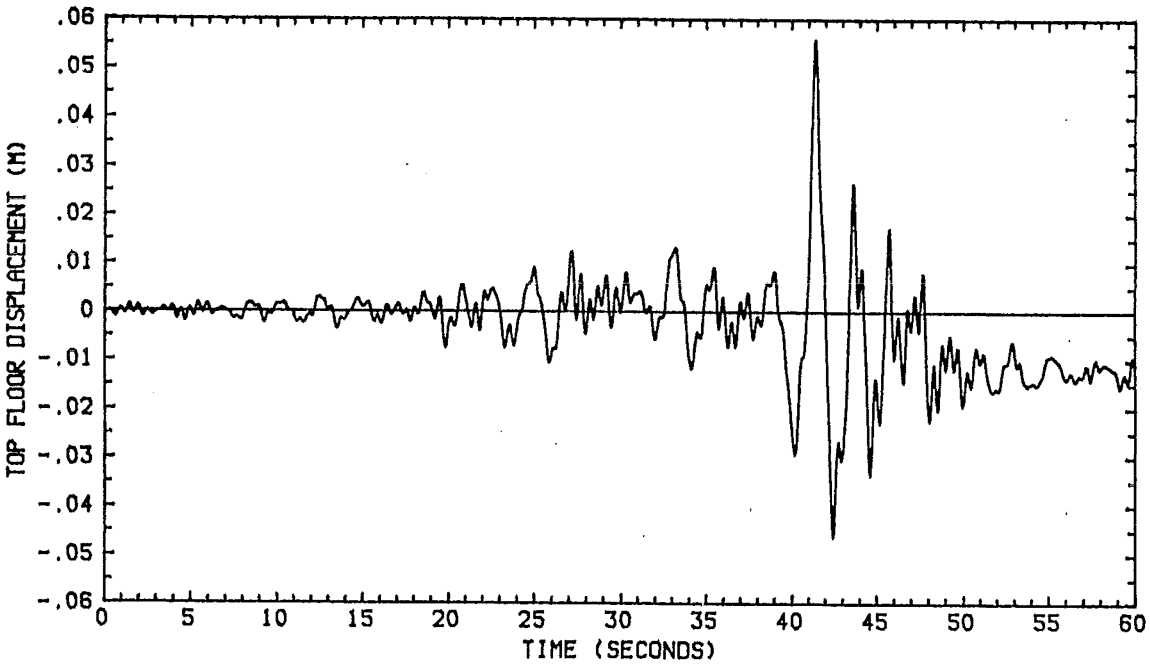

Fig. 8.8 5-Storey Frame Inelastic Response (Load Factor =2)

Table 8.2 THE MAXIMUM NUMBER OF THE PLASTIC HINGES DESIGNED

No. OF FRAME	1	2	3	4	5
No. OF THE DESIGNED PLASTIC HINGES	12	18	26	26	26

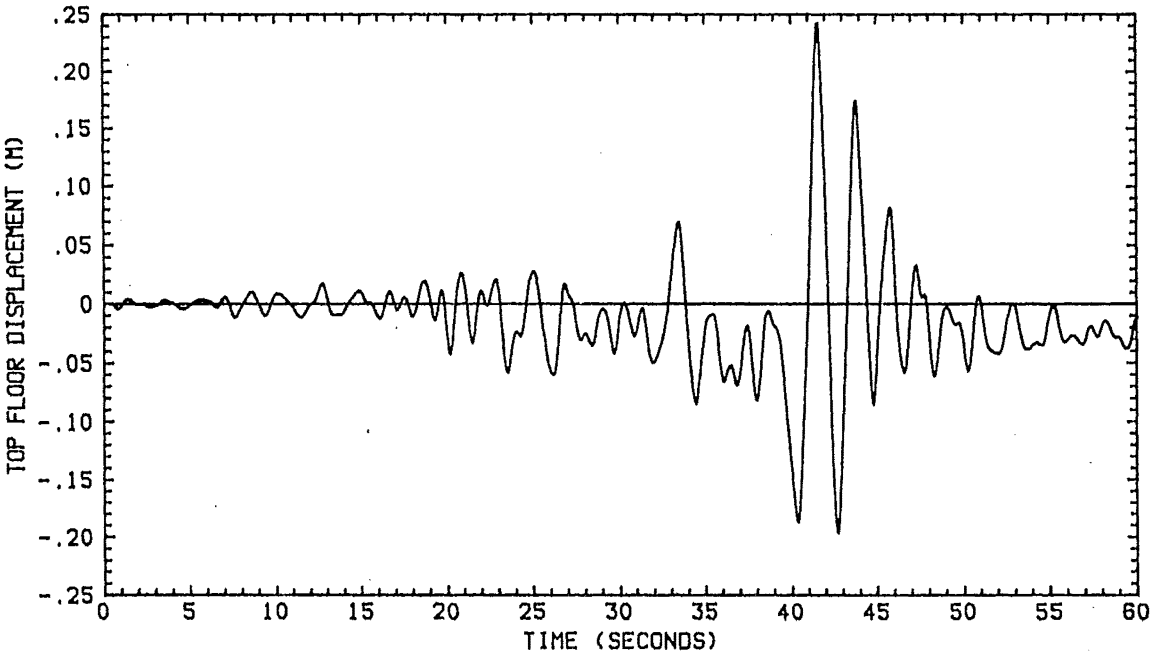

Fig. 8.9 8-Storey Frame Inelastic Response (Load Factor =2)

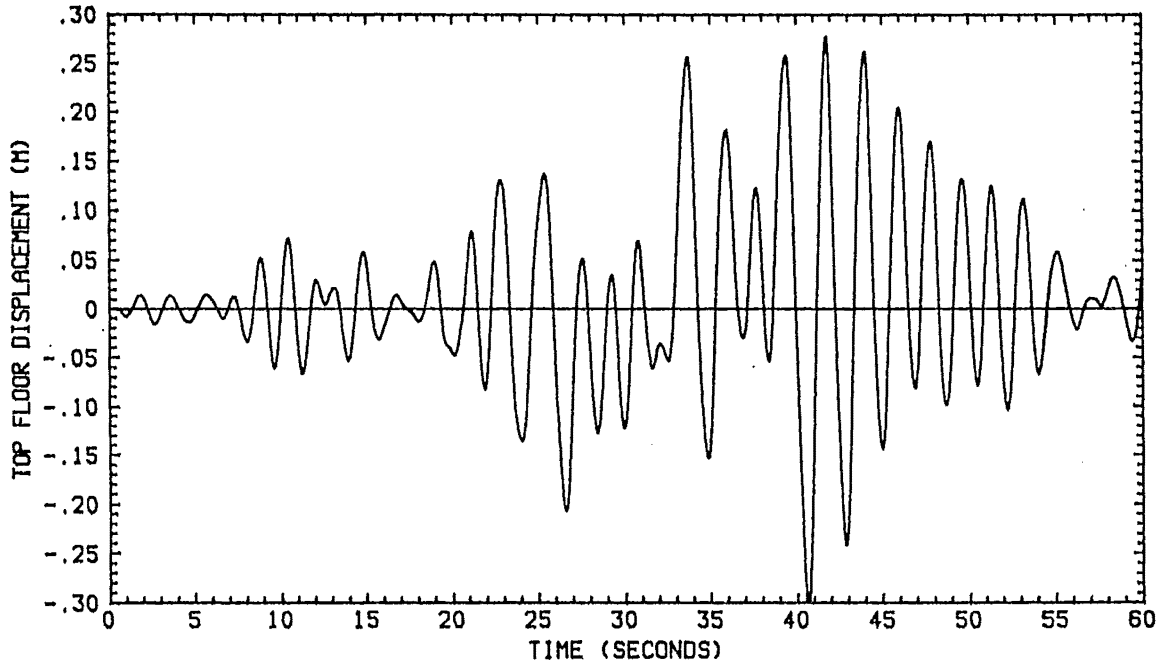

Fig. 8.10 12-Storey Frame 4 Inelastic Response (Load Factor =4)

For a strain softening nonlinear structure, two nonlinearity induced phenomena affect the response of the structure, ie., period elongation and energy dissipation. Energy dissipation due to plastic deformation will reduce the maximum response of the structure while the effect of the period elongation on the response depends on the frequency characteristics ofthe input motion. If the fundamental period shifts towards the predominant period of the input motion due to yielding, a large response would be developed due to the resonance build-up, while if the fundamental period shifts away from the period of the input motion, the response would be reduced. This can be better explained from the mismatch of the incident wave and the reflected wave. The mismatch of the incident wave and the reflected wave will prevent the resonance building up.

Table 8.3 CURVATURE DUCTILITY DEMAND OF 5-STOREY FRAME ON STIFF SOIL (BILINEAR MODEL)

NUMBER OF BEAM	LOAD FACTOR=4	LOAD FACTOR=2	LOAD FACTOR=1.5
1	301.1	77.3	14.4
2	183.8	45.1	9.2
3	129.9	32.3	7.0
4	110.0	27.4	6.5
5	119.0	25.0	7.4
BASE COL.	186.95	53.6	11.4

For the ground motion shown in Fig. 8.1, the period elongation may strongly affect the response of the structures because the ground motion is highly dominated by a component with a period of about 2 seconds. When plastic hinges develop, the fundamental period of the structure becomes larger than the initial one for the bi-linear model while the period keeps changing for the curvilinear model. The fundamental periods of the frames when all designed plastic hinges form are shown in Table 8.6.

Table 8.4 CURVATURE DUCTILITY DEMAND OF 8-STOREY FRAME ON STIFF SOIL (BILINEAR MODEL)

NUMBER OF BEAM	LOAD FACTOR=4	LOAD FACTOR=2	LOAD FACTOR=1.5
1	212.6	70.0	28.6
2	126.4	41.6	17.4
3	83.5	27.2	18.2
4	61.4	19.9	8.8
5	47.5	15.4	7.1
6	38.0	12.4	6.1
7	33.0	11.0	5.8
8	40.6	13.5	7.5
BASE COL.	57.7	17.7	10.2

Table 8.5 CURVATURE DUCTILITY DEMAND OF 12-STOREY FRAME (LOAD FACTOR=4) (BILINEAR MODEL)

BEAM No.	FRAME 3	FRAME 4	FRAME 5
1	52.0	9.4	11.3
2	30.3	5.9	7.1
3	19.2	4.4	4.8
4	13.6	3.8	3.6
5	11.2	3.4	3.0
6	10.3	3.3	2.8
7	10.2	3.3	2.7
8	10.6	3.4	3.4
9	10.7	3.4	4.1
10	10.9	3.4	4.8
11	11.6	3.4	5.5
12	14.8	4.1	7.1
BASE COL.	21.7	5.8	11.2

The ductility demand is much larger for the beams at the upper floor levels than the lower levels for all frames and this may help explain why considerable structural damage was found in the upper levels of buildings in Mexico City after the earthquake. For the 5-storey and 8-storey frames, a load factor of 4 leads to a enormous ductility demand which exceeds the realistic capacity of any structural member. The overall ductility demand of the 8-storey frame is smaller than that of the 5-storey frame for load factors of 4 and 2 but is larger for a load factor 1.5 because more plastic hinges are formed and the fundamental periods lengthen for the load factors of 4 and 2 compared with that for the load factor of 1.5. The overall ductility requirement for the 12-storey frame 3 is larger than that for the other 12-storey frames because the period shift of frame 3 means that larger inertial loads would be induced. The ductility demand for the 12-storey frame 4 is smaller than that of the other 12-storey frames because any period shift for frame 4 means that smaller inertial loads would be experienced by the frame than the inertial load experienced by the elastic one.

The ductility demands (the ductility factor are defined as the ratio of the maximum curvature developed to the equivalent yield curvature as shown in Fig. 8.7) are larger for the curvilinear model than that for the bi-linear model for all frames except for the 5-storey frame with the load factor of 1.5 and the 12-storey frame 5. The number of the plastic hinges formed in the frames for bi-linear model are shown in Fig. 8.11 to Fig. 8.13 and the maximum number of the designed plastic hinges are shown in Table 8.2.

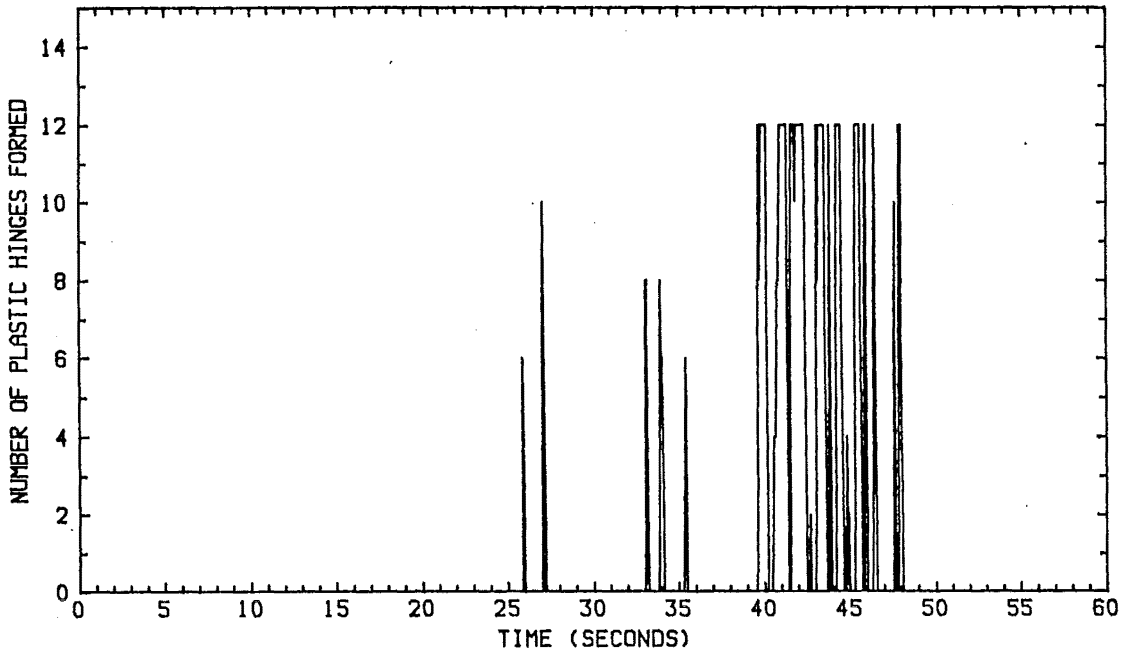

Fig. 8.11 Number of the Plastic Hinges Formed in the 5-Storey Frame (Load Factor = 2)

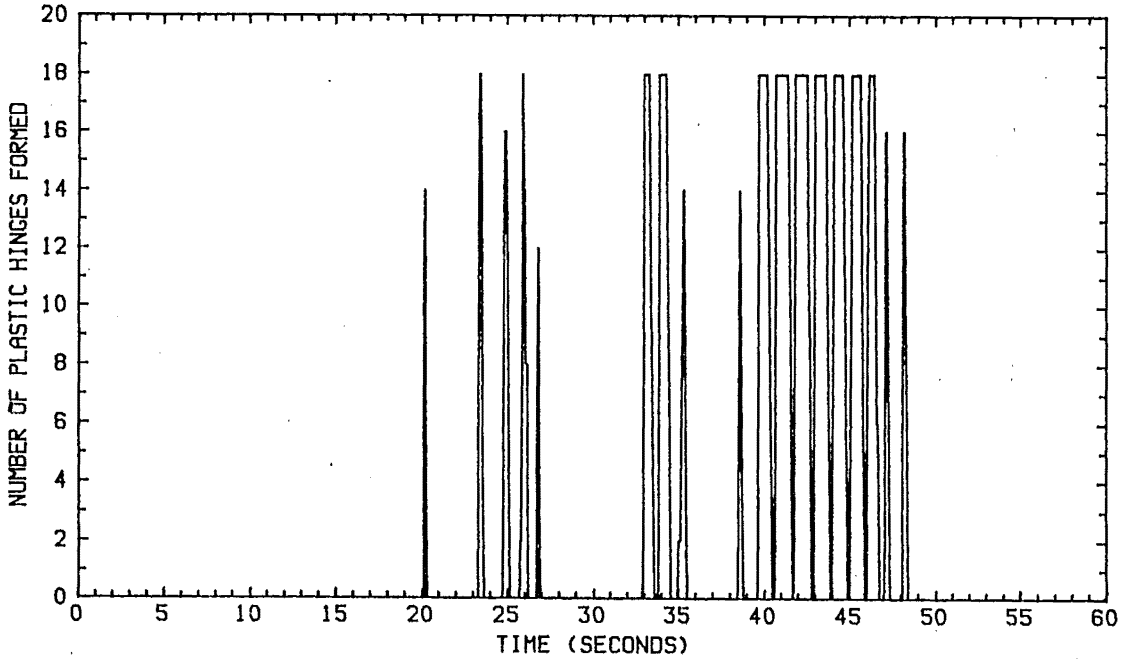

Fig. 8.12 Number of the Plastic Hinges Formed in the 8-Storey Frame (Load Factor = 2)

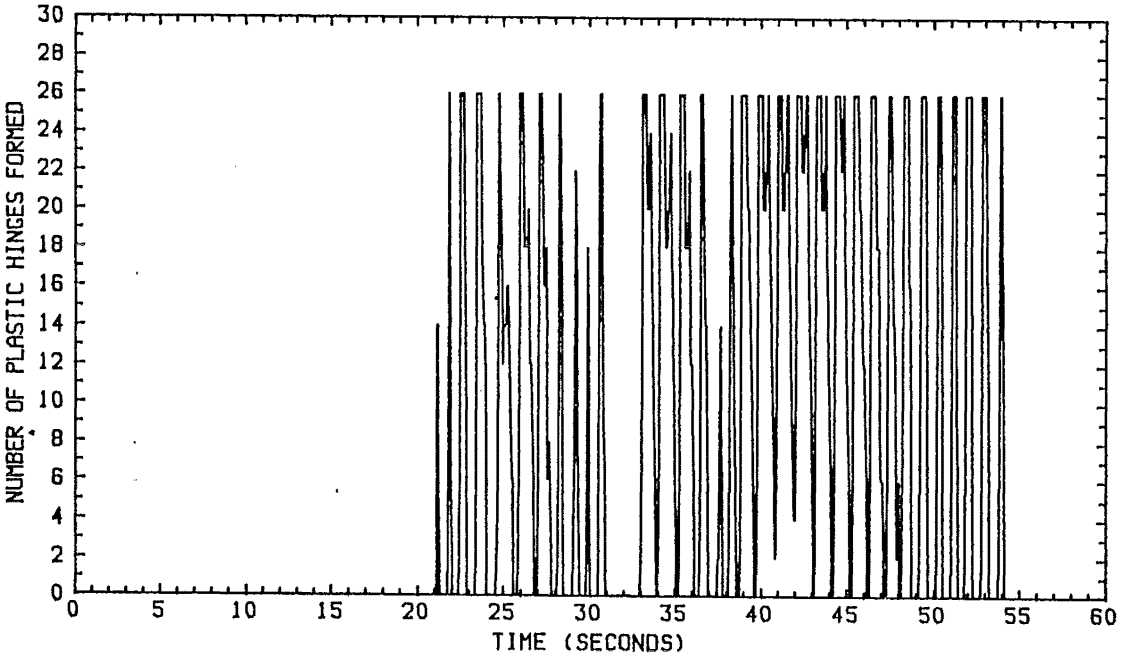

Fig. 8.13 Number of the Plastic Hinges Formed in the 12-Storey Frame 3 (Load Factor = 4)

Table 8.6 NATURAL PERIOD OF THE FRAMES WITH PLASTIC HINGES

No. OF FRAME	1	2	3	4	5
NATURAL PERIOD	2.745	5.300	7.624	10.167	12.715

8.3 The Response of the Structures on Soft Soil

A hypothetical site similar to the SCT site in Mexico City is assumed and the properties of the soil deposits are shown in Table 8.7. The fundamental period of the site is about 2 seconds. The Poisson's ratio is assumed to be 0.33 and the hysteretic damping ratio is assumed to be 5%.

Linear soil is assumed initially and 16 boundary elements were used to model the layers and the half space. A rigid foundation was assumed and the normalized spring and damping coefficients are shown in Fig. 8.14. The cut-off frequency (the natural frequency of the site for the fundamental wave

Table 8.7 PROPERTIES OF THE SOIL DEPOSITS

No. OF LAYER	DEPTH (M)	SHEAR WAVE SPEED (M/S)	MASS DENSITY (KG/M^3)
1	4	70	2200
2	27	75	2200
3	7	110	2200
HALF SPACE		900	2200

mode) exists less than which no radiation damping is present. The fundamental periods of the soil-structure systems were determined and are shown in Table 8.8 and the dynamic stiffness of the soil is specified at the fundamental frequency of the soil-structure system for each frame. Only frame 1 will benefit from radiation damping.

Table 8.8 FUNDAMENTAL PERIODS OF STRUCTURES

NUMBER OF FRAME	NUMBER OF STOREY	FIXED BASE PERIOD(SECONDS)	FLEX. BASE PERIOD(SECONDS)
1	5	0.5	1.07
2	8	1.0	1.95
3	12	1.5	3.13
4	12	2.0	4.17
5	12	2.5	5.20

The mode shapes were computed for each frame. The mode shapes of the horizontal displacement of each floor level for frames 3, 4 and 5 were very similar. The mode shapes of the horizontal displacement relative to the base are the displacement patterns which induce the internal forces while the total displacement mode shapes plus ground acceleration represent the inertial load distribution for the vertically travelling seismic waves if no damping is present. The first five modes are shown in Fig. 8.15 and Fig. 8.16. The mode shapes are normalized so that the maximum absolute value is unity. The values for the base in the total displacement mode shapes are set equal to zero because they are not of interest. It can be seen that the first and second relative displacement modes are little affected by the presence of soft soil but the higher modes are dominated by the rocking mode. The first total displacement modes are similar for all frames with or without the presence of the flexible soil.

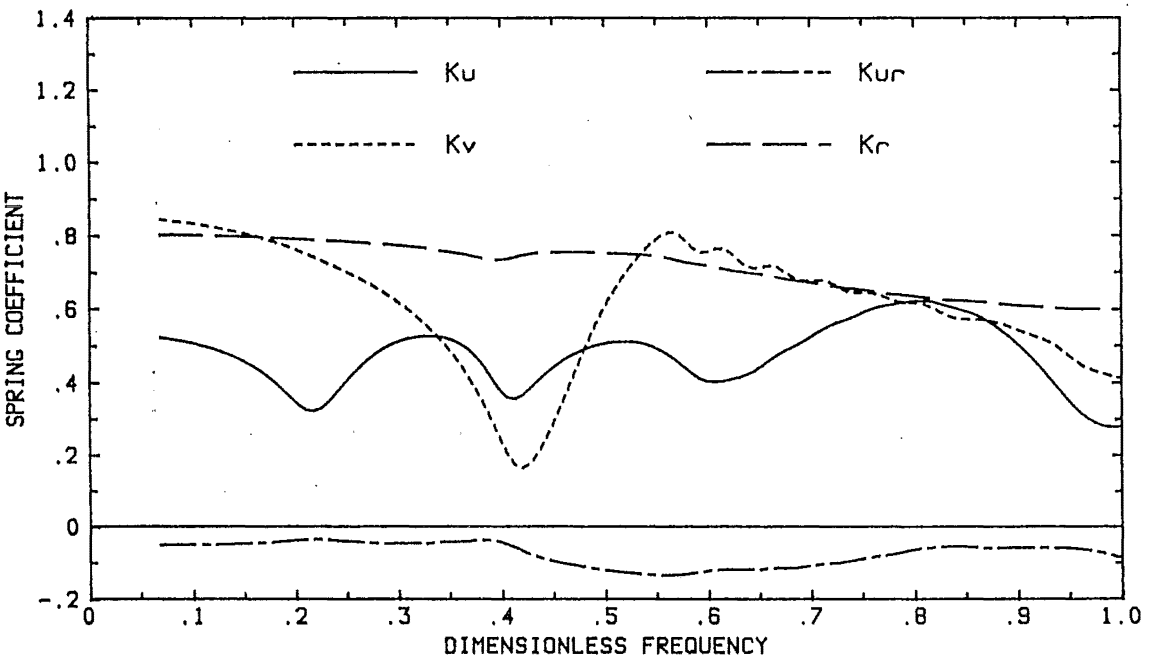

(a) Spring Coefficients

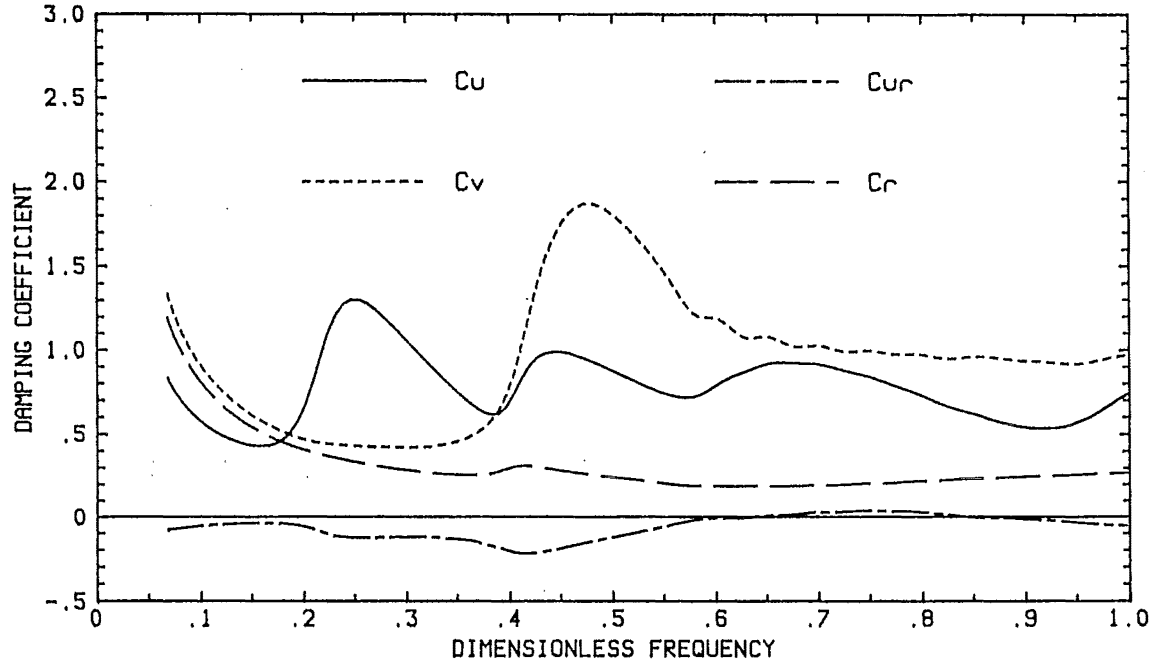

(b) Damping Coefficients

Fig. 8.14 Dynamic Stiffness of The Surface Foundation

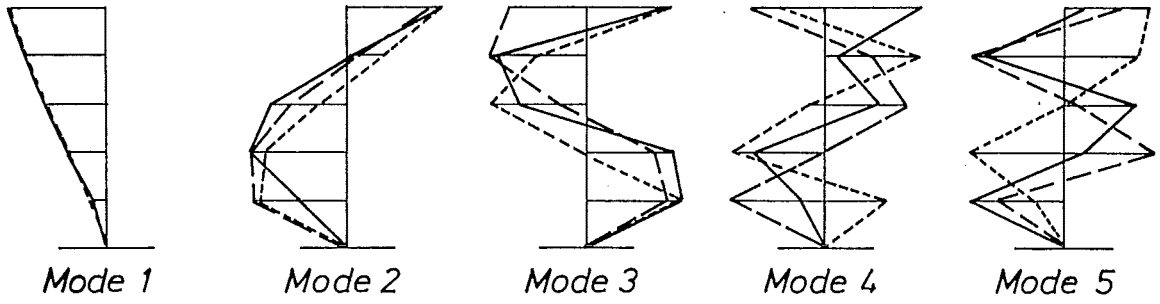

(a) 5-Storey Frame

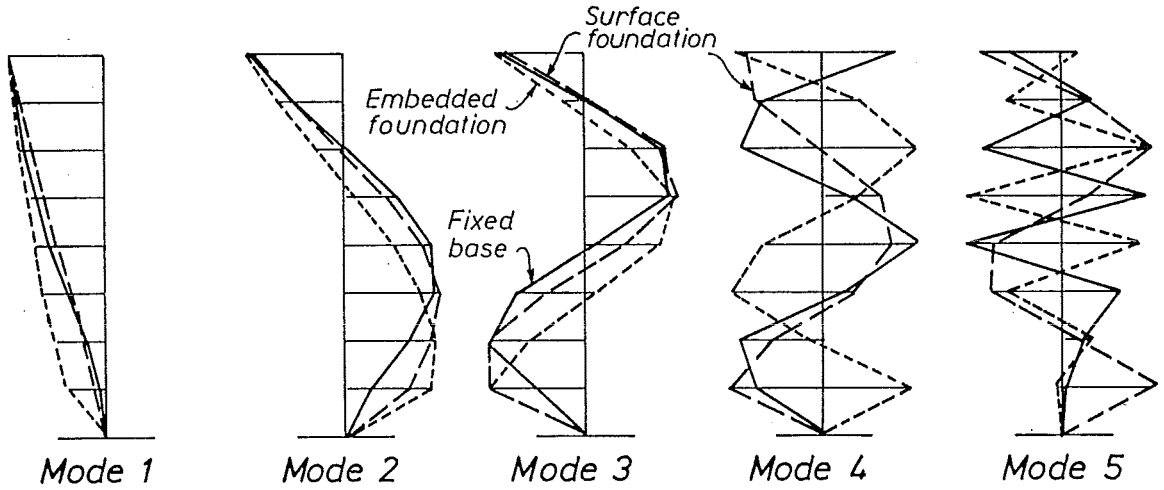

(b) 8-Storey Frame

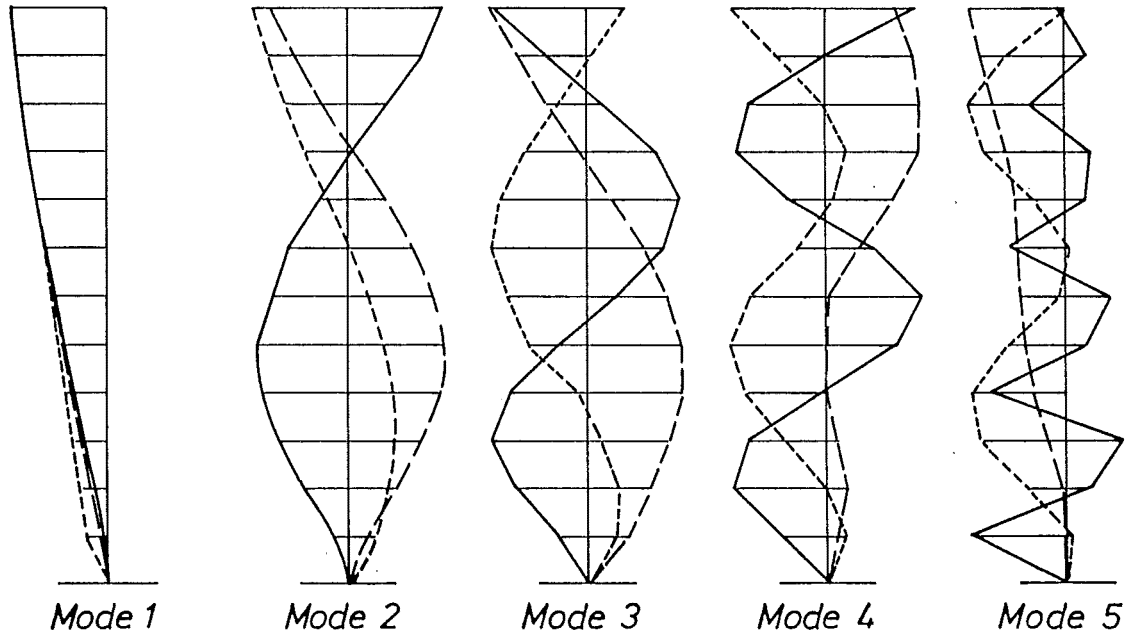

(c) 12-Storey Frame

Fig. 8.15 The Mode Shapes of the Displacement Relative to Base

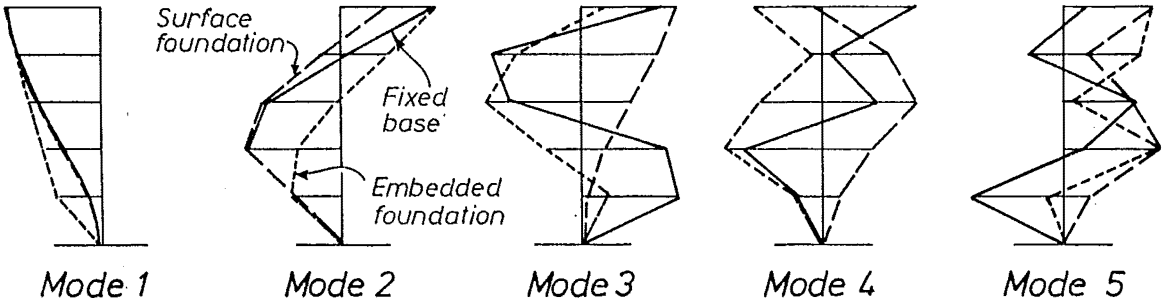

(a) 5-Storey Frame

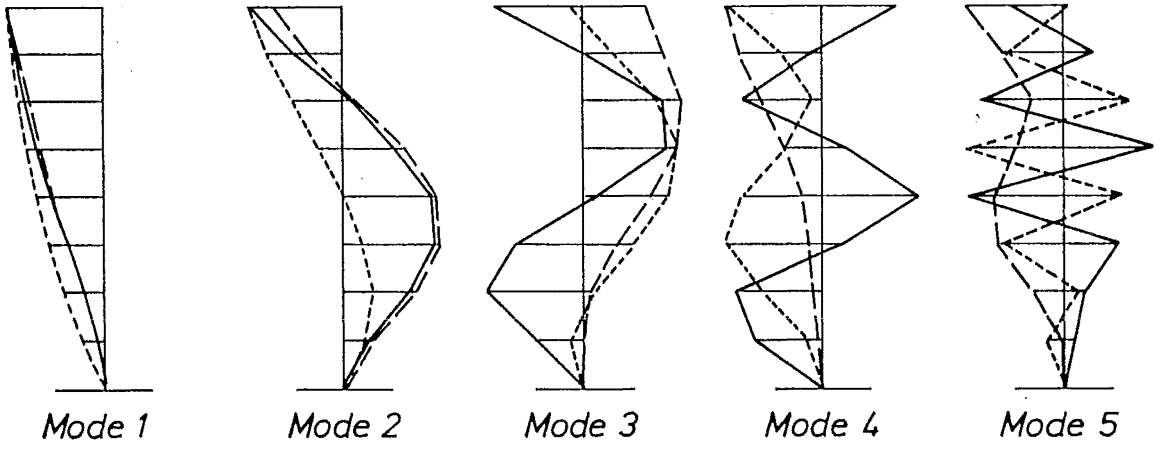

(b) 8-Storey Frame

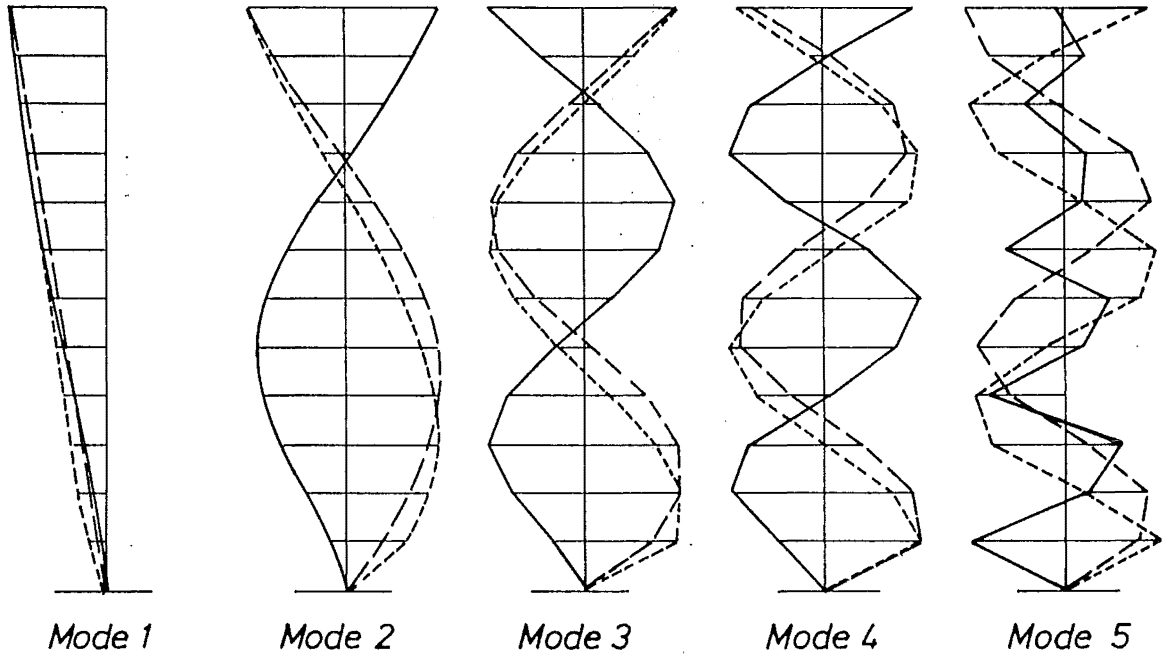

(c) 12-Storey Frame

Fig. 8.16 The Mode Shapes of Total Displacement

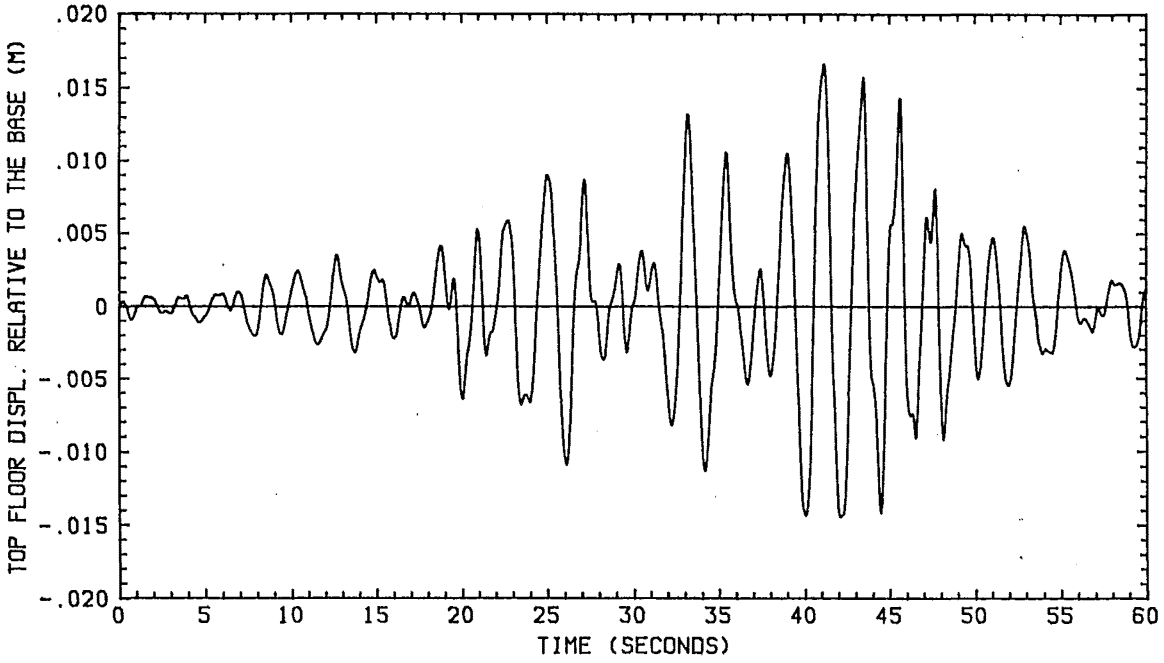

Fig. 8.17 5-Storey Frame 1 Elastic Response (Soft Soil)

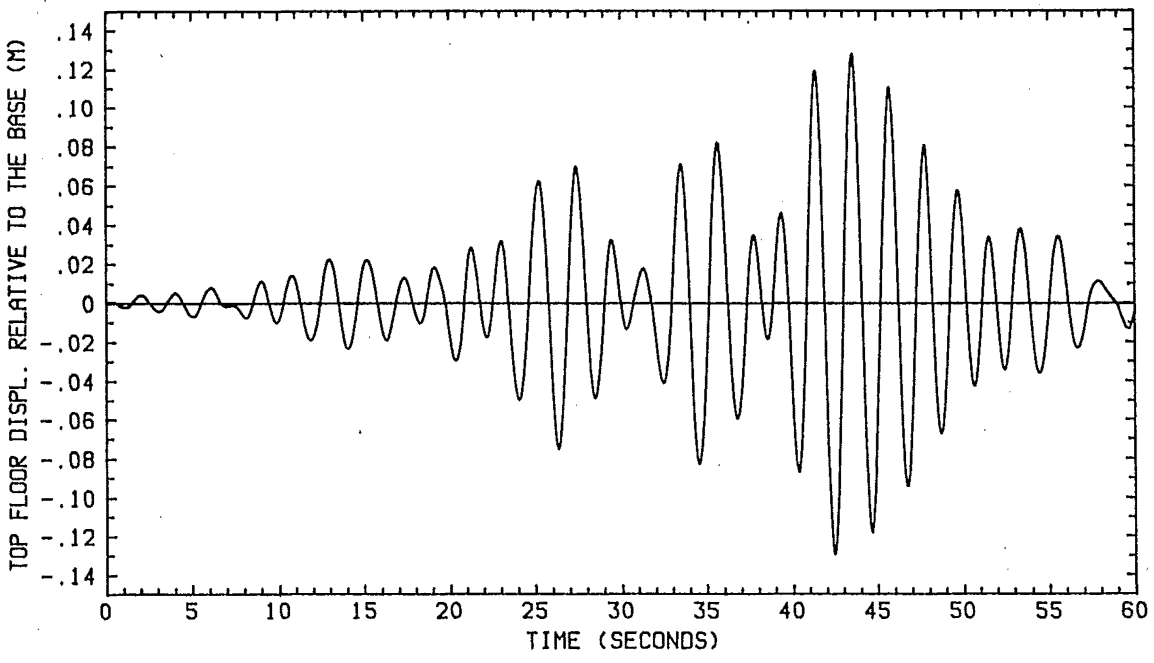

Fig. 8.18 8-Storey Frame 2 Elastic Response (Soft Soil)

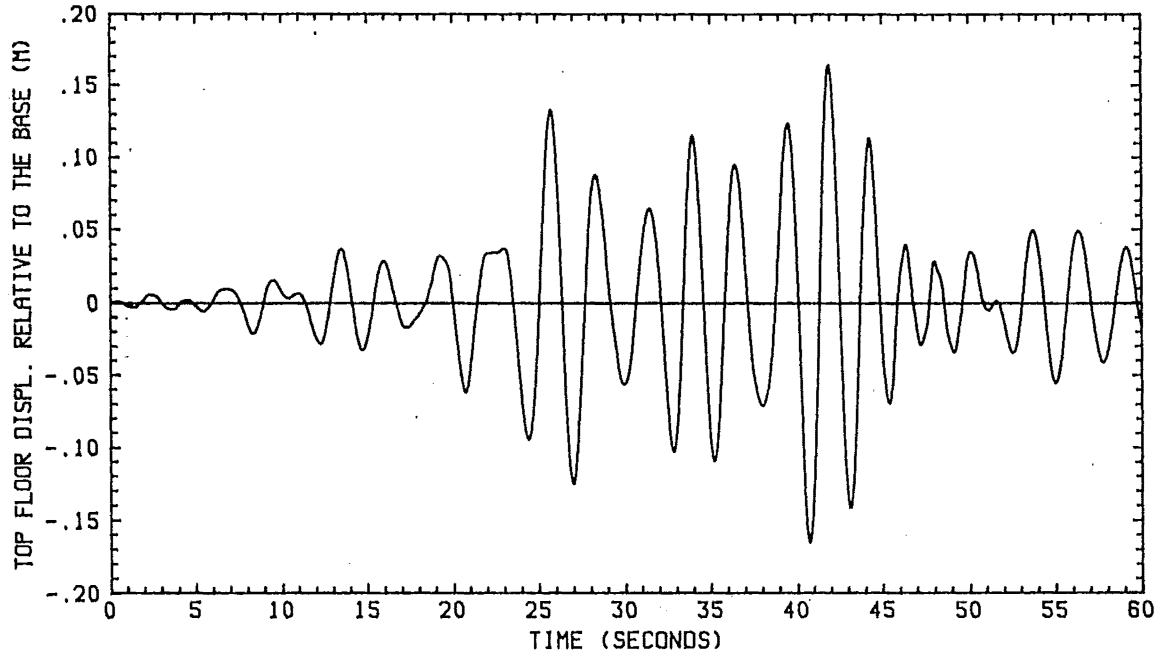

Fig. 8.19 12-Storey Frame 3 Elastic Response (Soft Soil)

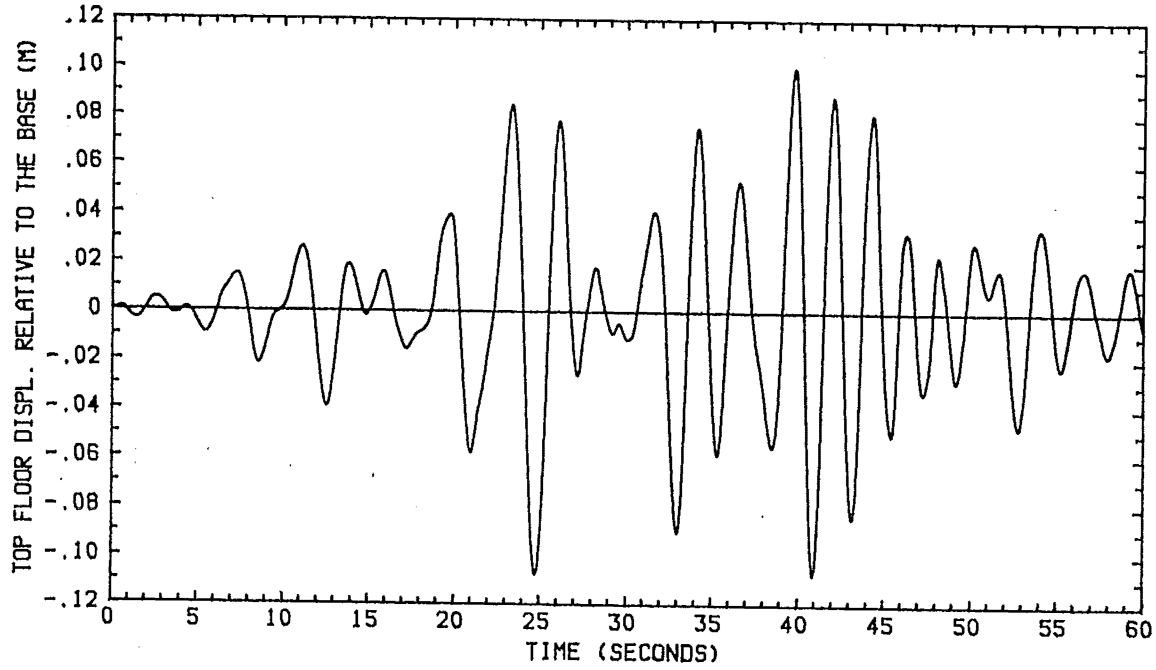

Fig. 8.20 12-Storey Frame 4 Elastic Response (Soft Soil)

Elastic analyses of the frames on soft soil were carried out at first. The 5-storey frame benefits from the radiation damping of the soil and the period shift barely affects the response and maximum response are slightly smaller than those of the frame on stiff soil while the response of the 8-storey frame increases considerably due to the period shift and little benefit from the radiation damping. All of the 12-storey frames benefit from the period shift and the maximum responses are considerably reduced. The time histories of the top floor displacement relative to the base of frames 1 to 4 are shown in Fig. 8.17 to Fig. 8.20 respectively and the periods shifts are obvious when compared with the response shown in Fig. 8.3 to Fig. 8.6.

Table 8.9 CURVATURE DUCTILITY DEMAND OF 5-STOREY FRAME ON SOFT SOIL (BILINEAR MODEL)

NUMBER OF BEAM	LOAD FACTOR=2	LOAD FACTOR=1.5
1	77.5	14.4
2	45.4	9.2
3	32.3	7.0
4	27.4	6.5
5	29.8	7.4
BASE COL.	53.6	11.4

Nonlinear analyses were carried out for the frames on the soft soil with the same yield moments as those for the frames on stiff soil. The ductility demands of each frame are shown in Table 8.9 to Table 8.11. The ductility requirements of the beams at the upper floor level are larger for the frames on soft soil than for those on the stiff soil because of the rotation of the foundation. It is interesting to notice that the ductility requirements for the 5-storey frame on soft soil is larger than those for the frame on the stiff soil even though the elastic response of the frame on soft soil is smaller than that of the frame on stiff soil. This may be due to the period shift and the fact that more plastic hinges developed in the frame on soft soil than in the frame on stiff soil. For the 8-storey frame, the ductility demands are larger for the frame on soft soil than for stiff soil. The ductility requirements at the upper floor level of the 12-storey frame 3 are twice those for the frame on stiff soil but smaller in the lower level of the frame because of the rocking motion of the foundation. Plastic hinges do not form in the 12-storey frame

Table 8.10 CURVATURE DUCTILITY DEMAND OF 8-STOREY FRAME ON SOFT SOIL (BILINEAR MODEL)

NUMBER OF BEAM	LOAD FACTOR=2	LOAD FACTOR=1.5
1	94.6	68.2
2	59.9	41.3
3	39.4	40.6
4	28.7	19.5
5	28.8	14.4
6	22.2	11.1
7	17.6	9.2
8	15.1	10.8
BASE COL.	21.8	14.5

4 and frame 5 on soft soil even when the load factor taken as 8.

Table 8.11 CURVATURE DUCTILITY DEMAND OF 12-STOREY FRAME 3 ON SOFT SOIL (LOAD FACTOR = 4)

No. OF BEAM	1	2	3	4	5	6	7
DUCT. DEMAND	91.5	53.9	32.4	21.6	16.0	11.9	9.5
No. OF BEAM	8	9	10	11	12	BASE COL.	
DUCT. DEMAND	8.4	7.2	6.4	6.3	6.4	16.4	

The time histories of the horizontal top floor displacement relative to the base for frames 1 to 4 are shown in Fig. 8.21 to Fig. 8.23. Compared with the corresponding elastic response, about the same order of period elongation has developed due to the frame plastic deformation for the frames on soft soil as for the frames on stiff soil. The time history of the top floor displacement relative to the free-field has the same shape as the displacement relative to the frame base does.

The number of the plastic hinges formed in the frames on soft soil are shown in Fig. 8.24 to Fig. 8.26. Compared with Fig. 8.11 to Fig 8.13 it can be seen that more plastic hinges were formed in the 5-storey and 8-storey frames on soft soil than on stiff soil but less in the 12-storey frame 3 on soft soil.

Table 8.12 FUNDAMENTAL PERIODS OF THE FRAMES WITH EMBEDDED FOUNDATIONS

NUMBER OF FRAME	NUMBER OF STOREYS	PERIODS (SECONDS)
1	5	0.72
2	8	1.41
3	12	1.84
4	12	2.39
5	12	2.96

The horizontal displacement relative to the free-field is a very important factor for the pounding of adjacent structures with different dynamic characteristics and this was one of the major causes of the structural damage in Mexico City. The horizontal displacement envelopes are shown in Fig. 8.27. It can be seen that the horizontal displacements relative to the free-field are much larger than the displacements of the frames on stiff soil for frame 1 to frame 3 but smaller for frame 4 and frame 5.

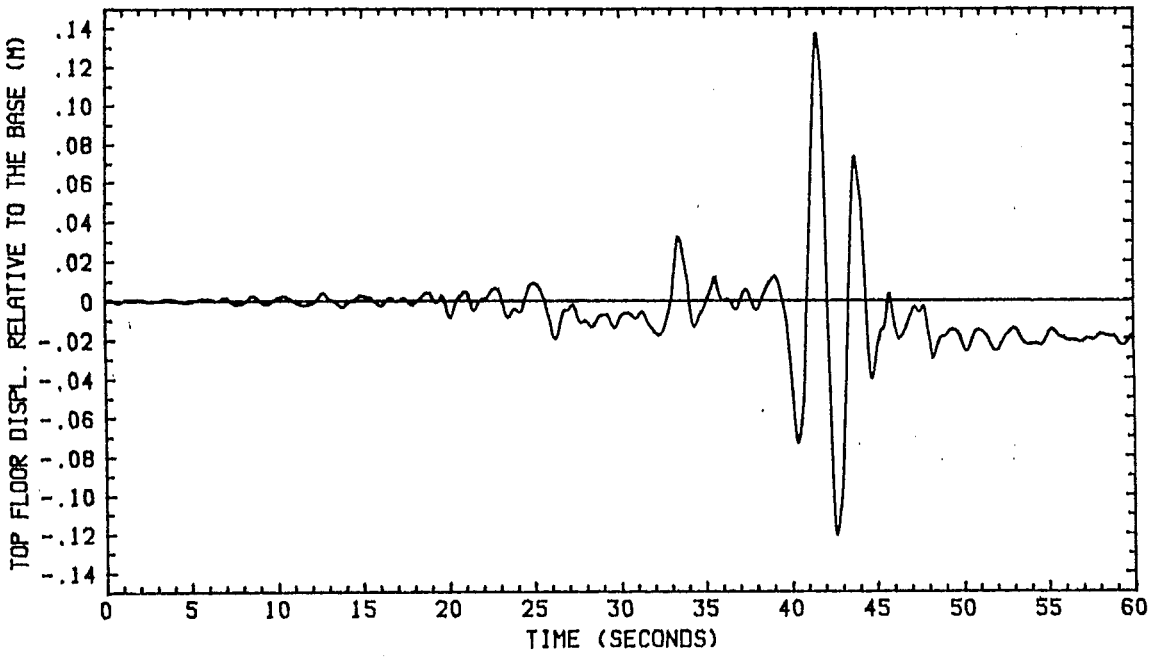

Fig. 8.21 5-Storey Frame Inelastic Response
(Soft Soil Load Factor = 2)

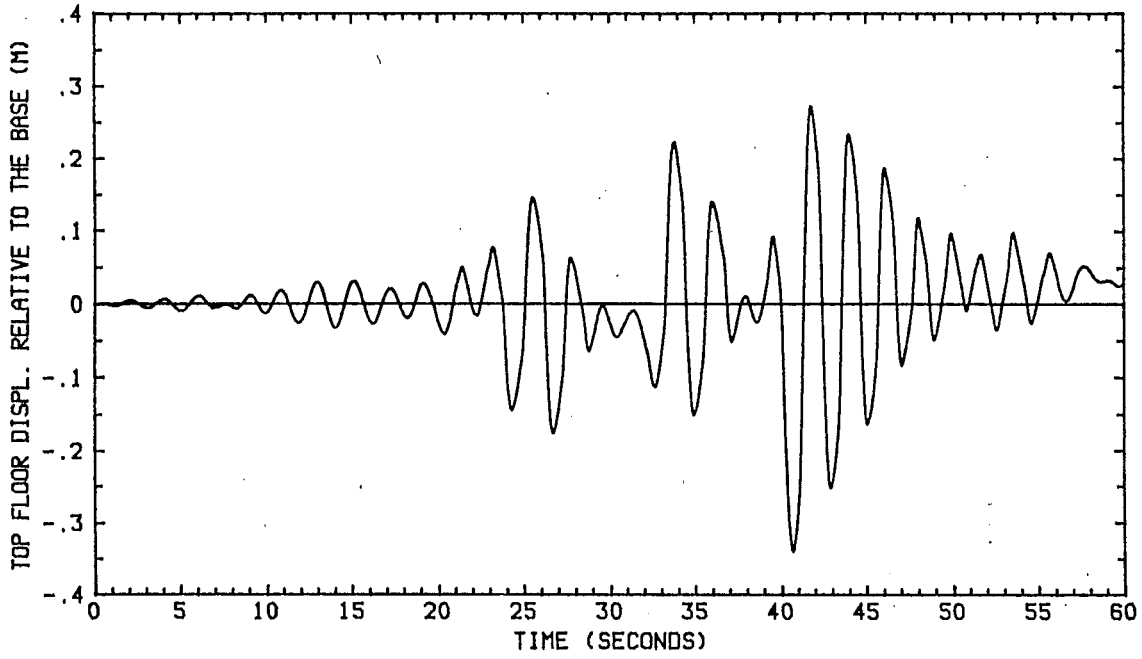

Fig. 8.22 8-Storey Frame Inelastic Response
(Soft Soil Load Factor = 2)

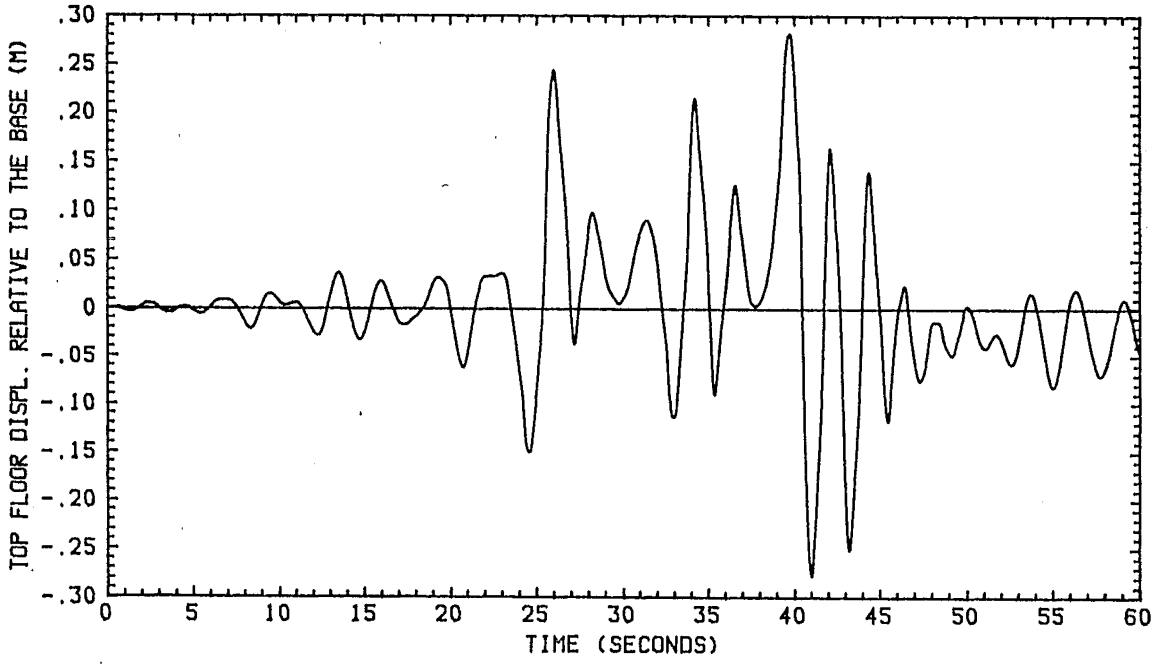

Fig. 8.23 12-Storey Frame 3 Inelastic Response (Soft Soil Load Factor = 4)

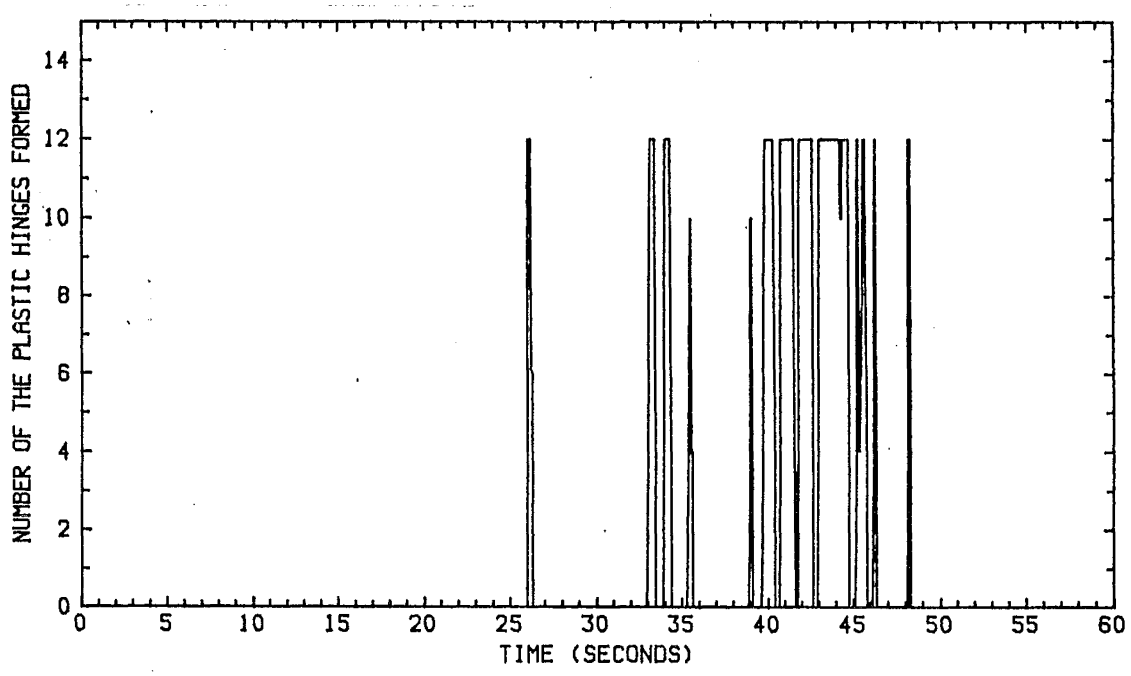

Fig. 8.24 Number of the Plastic Hinges Formed in the 5-Storey Frame (Soft Soil Load Factor = 2)

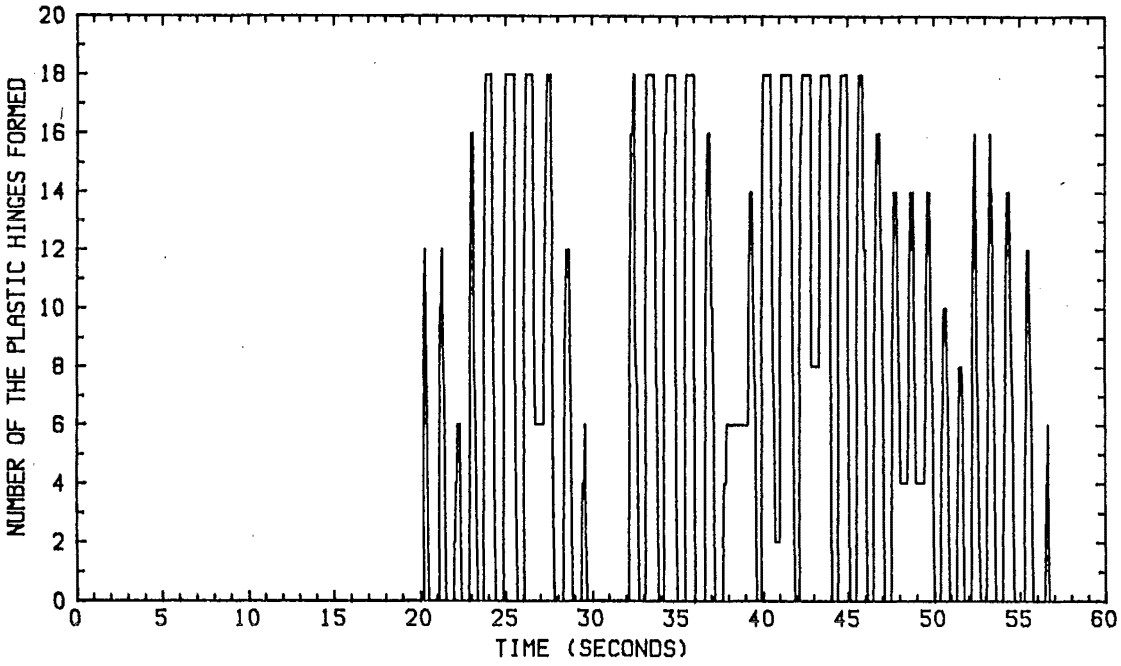

Fig. 8.25 Number of the Plastic Hinges Formed in the 8-Storey Frame (Soft Soil Load Factor = 2)

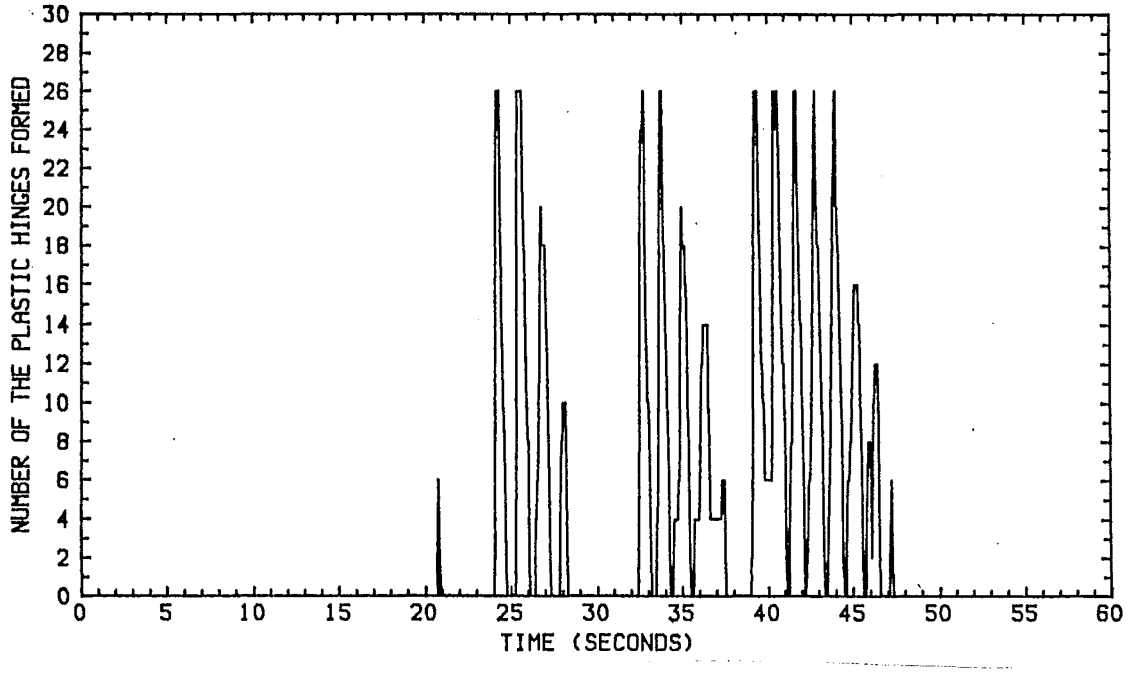

Fig. 8.26 Number of the Plastic Hinges Formed in the 12-Storey Frame 3 (Soft Soil Load Factor=4)

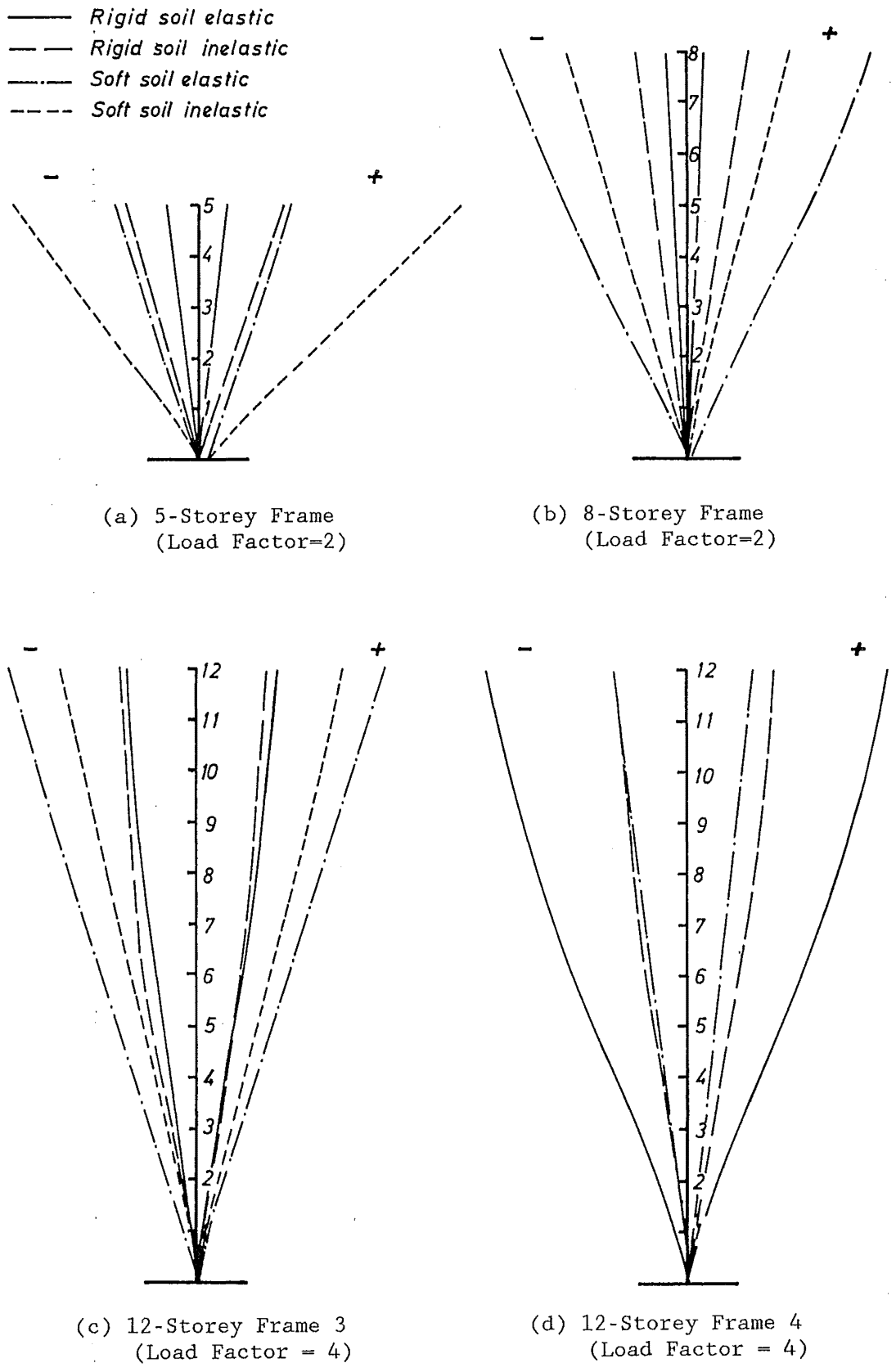

(a) 5-Storey Frame
(Load Factor=2)

(b) 8-Storey Frame
(Load Factor=2)

(c) 12-Storey Frame 3
(Load Factor = 4)

(d) 12-Storey Frame 4
(Load Factor = 4)

Fig. 8.27 Horizontal Displacement Envelopes

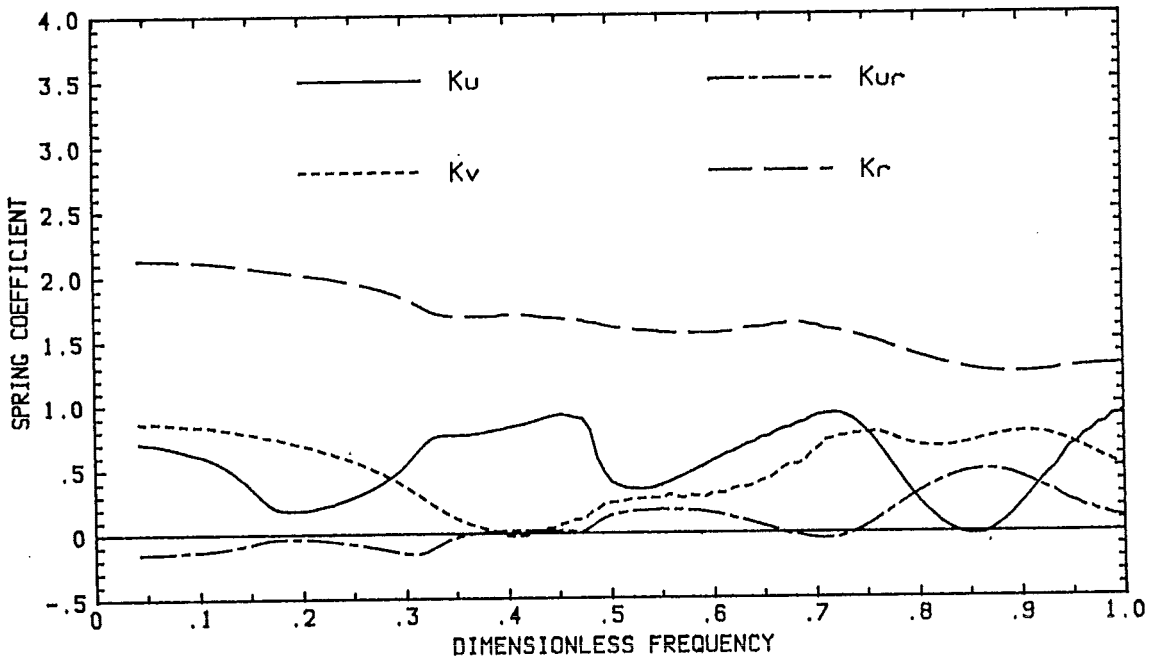

(a) Spring Coefficients

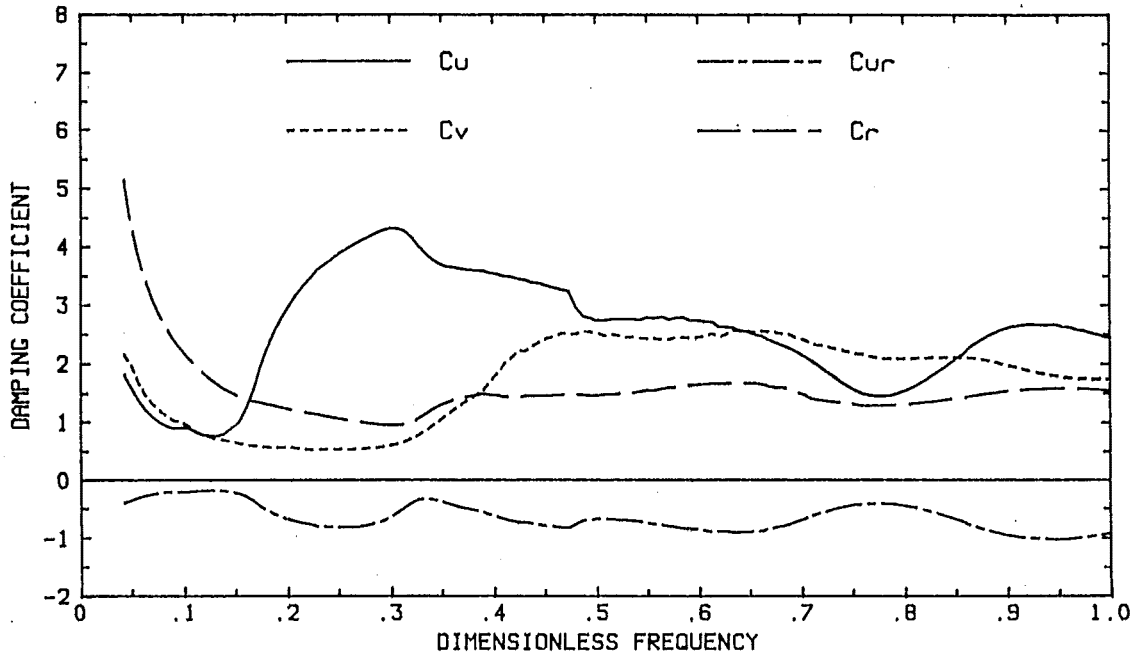

(b) Damping Coefficients

Fig. 8.28 Dynamic Stiffness of the Embedded Foundation

If the foundation of the frame is embedded in the soil, the stiffness and damping coefficients increase as shown in Fig. 8.28. The depth of the embedment of the foundation was one storey height of the frame. The fundamental periods of the soil-structure systems are shown in Table 8.12 and the mode shapes are shown in Fig. 8.15 and Fig. 8.16. The soil-structure system is stiffened by the foundation embedment and the rocking motion of the foundation would be smaller than that for a surface foundation. It would be expected that the elastic responses of frame 1, 2 and 3 would increase while the responses of frame 4 and 5 would decrease when compared with those of the corresponding fixed base frames under the earthquake excitation shown in Fig. 8.1.

8.4 Soil Nonlinearity and Foundation Failure

It seems impossible to properly predict a foundation failure by assuming elastic soil properties if the site is under excitation by a vertically propagating shear wave because the shear stresses induced in the elastic soil are relatively small compared with the confining stresses. The pore water pressure generated by the shear deformation in a nonlinear soil will reduce the confining stresses and the failure of the soil occurs progressively with increasing cycles of loading. The nonlinear soil model described in Chapter 3 was used to examine the effects of nonlinear soil behaviour on the soil-structure interaction.

For a nonlinear analysis, the finite element mesh has to be reasonably large so that the nonlinear behaviour of the soil can be limited to the near-field modelled by the finite element. The parameters of the soil have to be determined by complete laboratory testing. The solution procedure requires a few iterations per time step and the time step has to be smaller than that for a linear analysis. To carried out the iteration technique, the nonlinear stresses have to be evaluated for a number of subincrements per iteration step. These make the nonlinear analysis very time consuming. In order to reduce the computation effort, a simple site, i.e. a single layer on rigid rock, was chosen instead of the site used in the previous section. The depth of the layer was six meters which was equal to the width of the foundation.

A surface foundation was assumed and the soil parameters evaluated in Chapter 3 were adopted for the layer. The over consolidation ratio is chosen as 1.2 which would be a likely value for a natural soil. The fundamental period of the site for vertically propagating shear waves was 0.34 seconds. The El Centro earthquake with the maximum acceleration scaled to one-tenth of the original intensity was chosen as an input base motion and a vertically propagating shear wave was assumed. An average shear wave velocity of 70m/s was also assumed. A nonlinear free field analysis was carried out first using the finite element model described in Chapter 6 and very small nonlinearity was induced in the free field motion. The spectral acceleration of the base input motion and the surface motion are shown in Fig. 8.29. It can be seen the maximum amplification occurs at the fundamental period of the site.

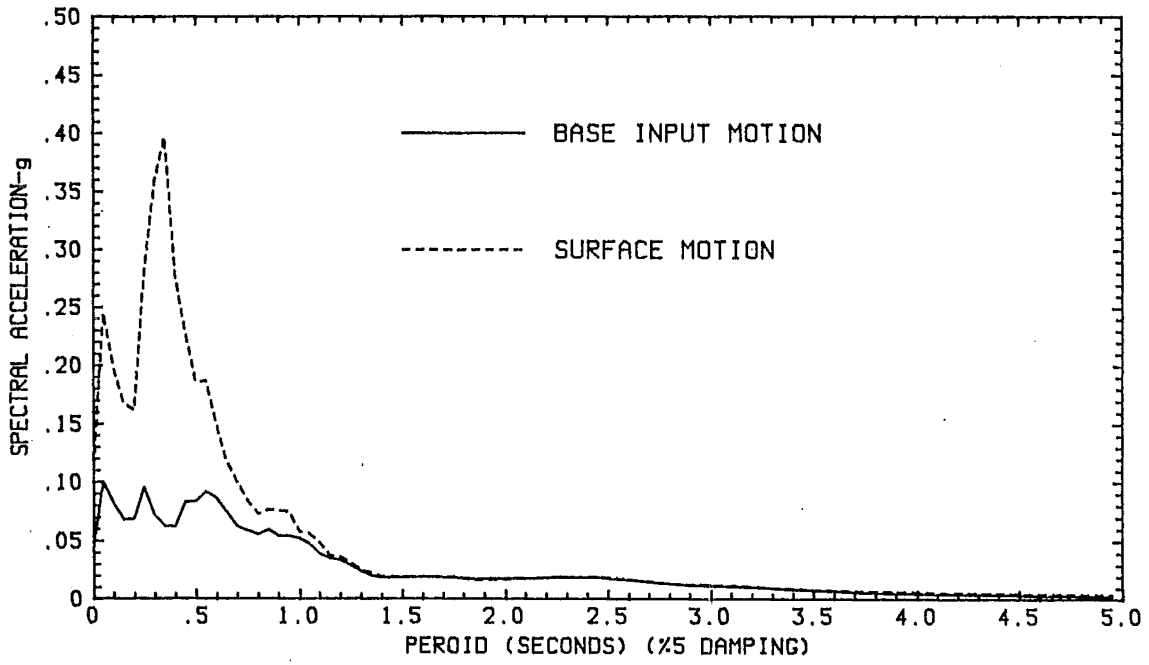

Fig. 8.29 Spectral Acceleration of the Site

A 4-storey frame with a fundamental period of 0.2 seconds was considered. 80 8-node finite elements were used to model the near-field soil. The energy transmitting boundary was constructed by using 12 surface wave modes and located at about 3.5 times of the half width of the foundation as shown in Fig.8.30. The finite element mesh is small for a nonlinear analysis but is adequate for the purpose of evaluating the effects of the nonlinear soil behaviour on soil-structure interaction. The fundamental period of the soil-structure system was 0.314 seconds. The properties of the frame were chosen in such a way that the soil-structure interaction was significant and the radiation damping was also present.

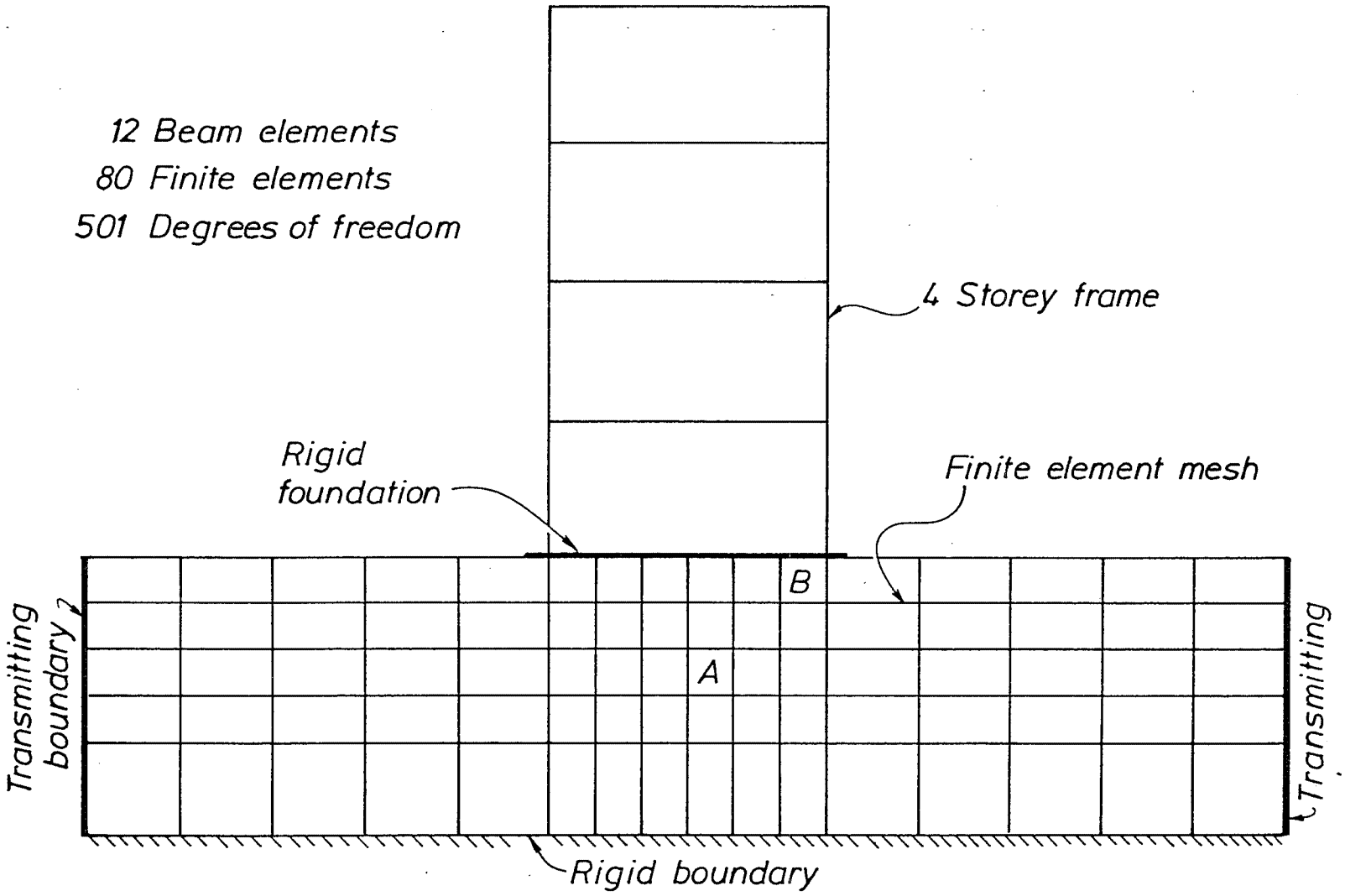

Fig. 8.30 A 4-storey Frame on a Single Layer

The responses of the structure on stiff soil are shown in Fig 8.31 for the case where the load factor of 4 were used and a bi-linear model were chosen for the inelastic behaviour. It can be seen that the inelastic response is larger than for the elastic case.

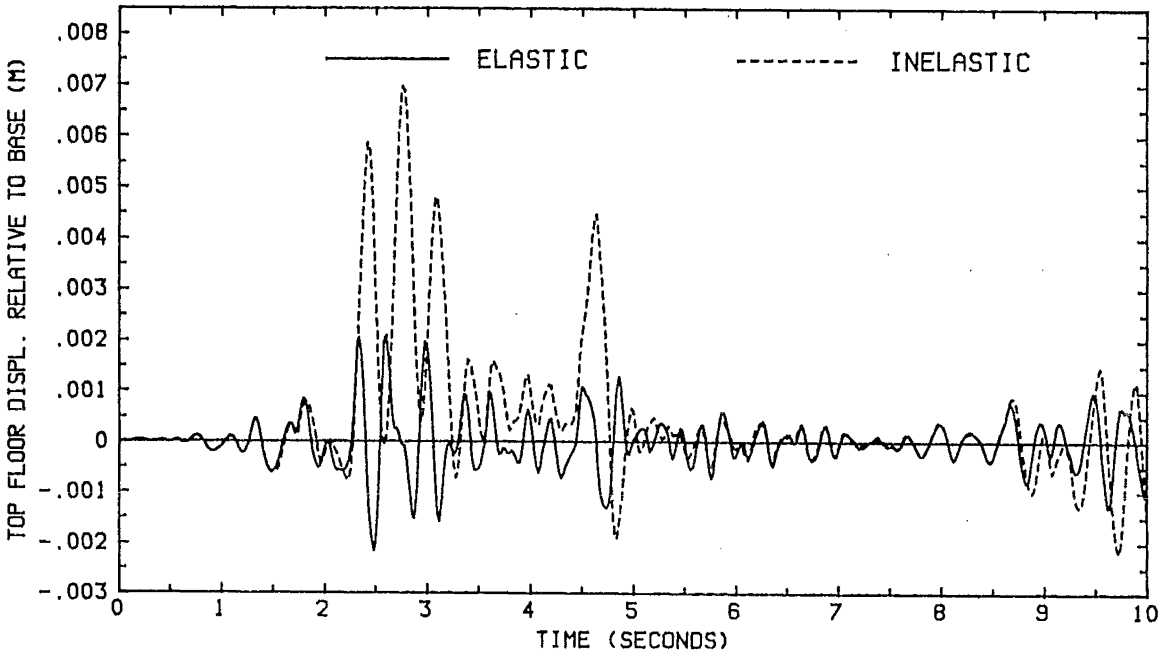

Fig. 8.31 Responses of the Structure on Stiff Soil

The elastic response of the frame on a linear elastic soil is shown in Fig. 8.32 together with the response of the frame on a stiff soil. It can be seen that the response of the frame on soft soil is amplified because of the period shift even though the radiation damping reduces the response. The high frequency component of the response disappears in the response of the frame on soft soil and this may be due to the radiation damping.

The response of the frame on a nonlinear soil is shown in Fig. 8.33 with the response of the frame on a linear elastic soil. The response of the frame on nonlinear soil is reduced after about 2 seconds due to the further period shift and energy dissipation by the plastic deformation of the soil. The nonlinear deformation in the elements along the energy transmitting boundary is smaller than that in the elements underneath the foundation. Pore water pressure generation in elements A and B are shown in Fig. 8.34 and Fig. 8.35. Failure is imminent for element B because of the small initial confined stresses. The shear stress of element A is shown Fig. 8.36.

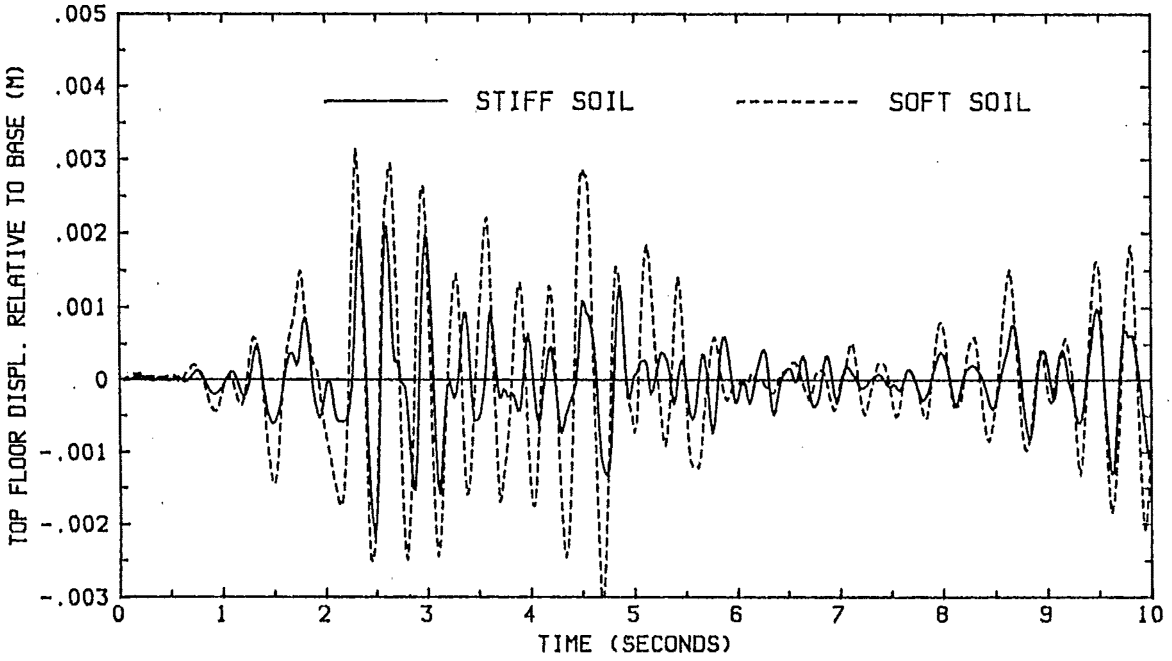

Fig. 8.32 Response of the Frame on Stiff Soil and Soft Soil

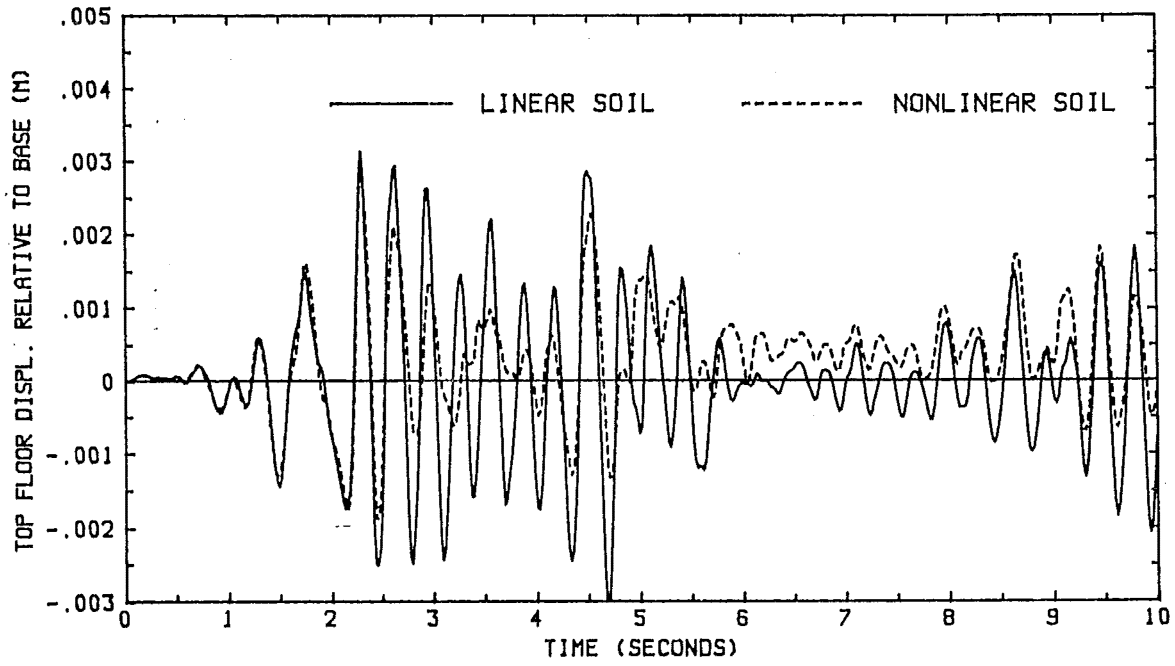

Fig. 8.33 Response of the Frame on Linear and Nonlinear Soil

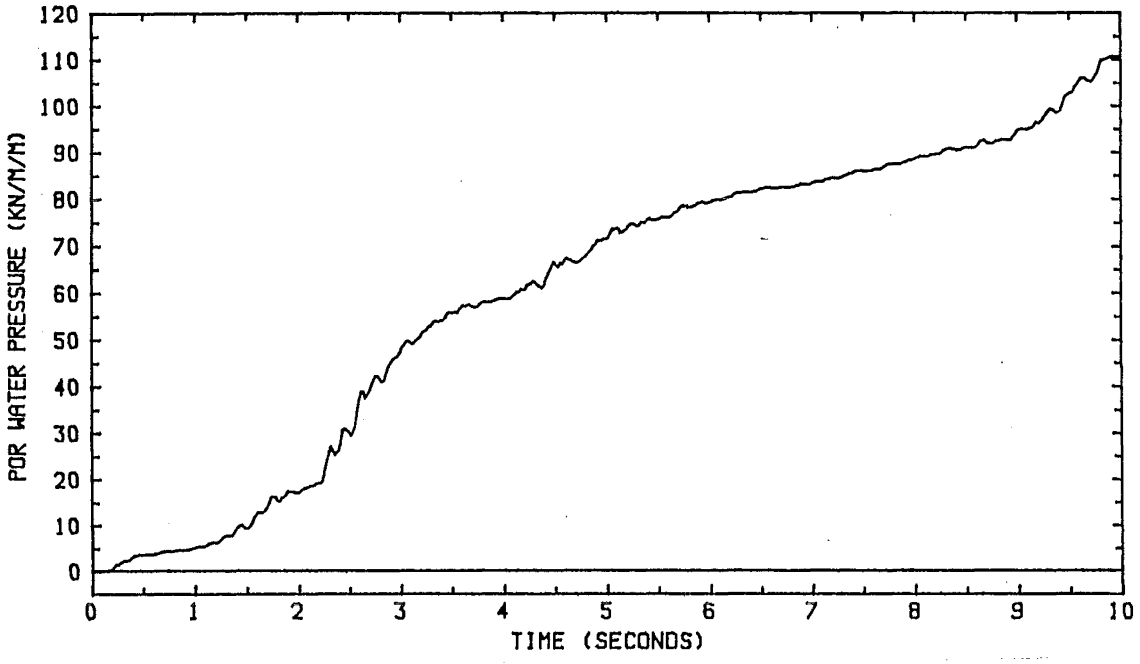

Fig. 8.34 Pore Water Generation in Element A

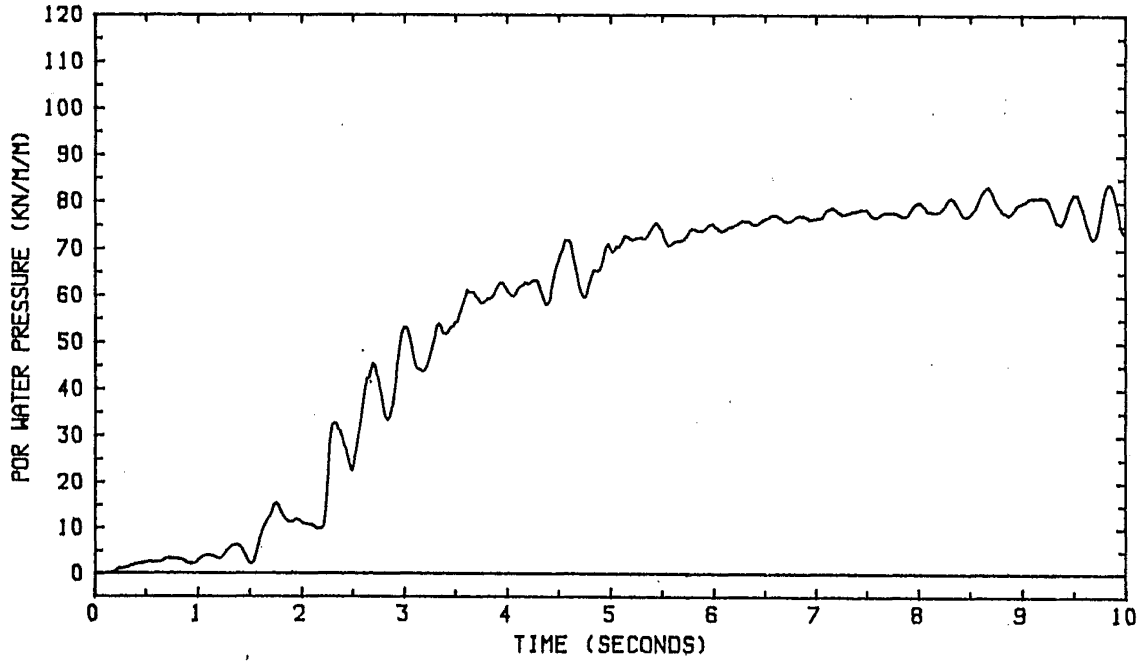

Fig. 8.35 Pore Water Generation in Element B

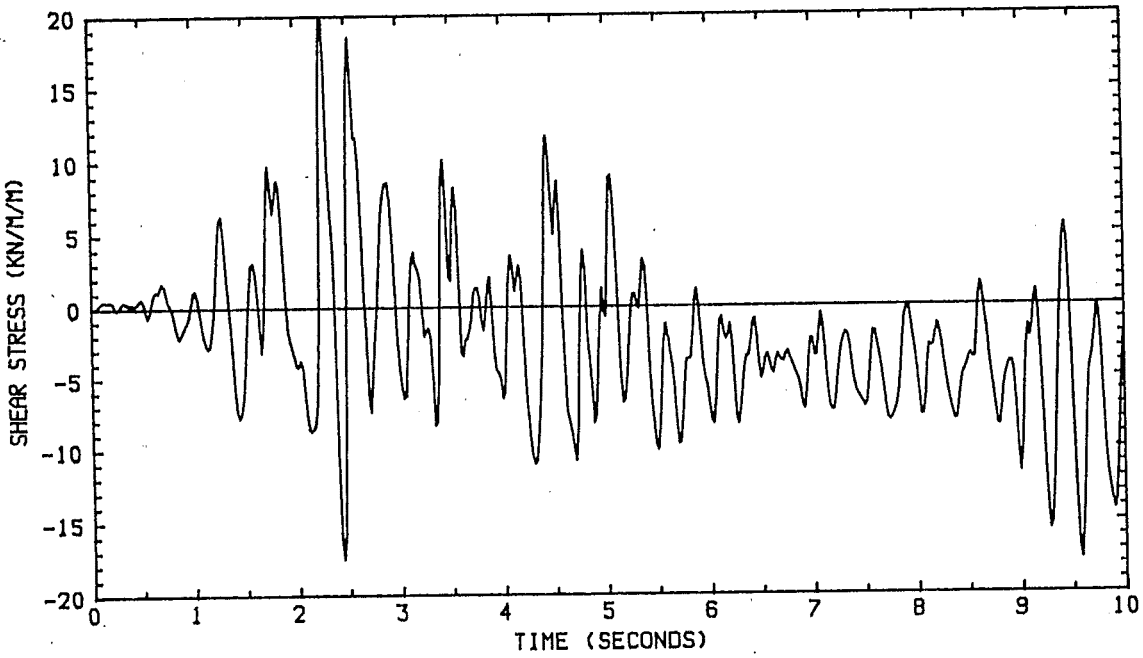

Fig. 8.36 The Shear Stress in Element A

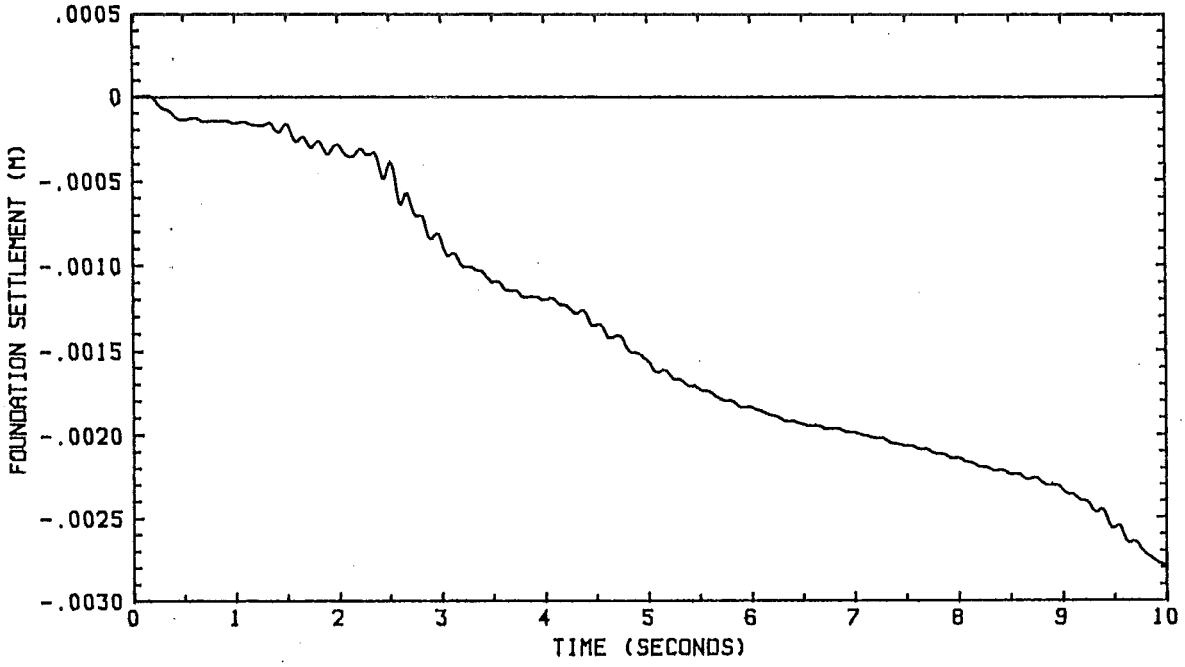

Fig. 8.37 The Vertical Displacement of the Frame Base

The settlement of the foundation is large for the frame on the nonlinear soil even though the site is only excited by vertical propagating shear waves. Linear analysis can not be used to evaluate the foundation settlement in this case. The settlement-time history is shown in Fig. 8.37. The maximum base horizontal displacement and rotation is smaller for the nonlinear soil than for the linear soil.

8.5 Summary

A primary investigation has been carried out on soil-structure interaction. The ground motion amplification by the flexible soil has been shown in the two cases studied. The numerical results have shown that soil-structure interaction has a significant influence on the structural response. When the fundamental frequency of a soil-structure system is greater than the natural frequency of the site for the fundamental mode, radiation damping may reduce the response of the structure. It has been found that, in most cases, the period shift is the more important factor affecting the structural response than is the energy dissipation by plastic deformation in the upper structure and radiation by the flexible soil. Taking soil-structure interaction into account may either increase or reduce the structural response depending on the fundamental period of the soil-structure system and the fundamental period of the site. In general, if the fundamental period of the structure is less than the fundamental period of the site, ignoring the soil-structure interaction may sometimes be dangerous while if the fundamental period of the structure is longer than the fundamental period of the site, the soil-structure interaction effects would reduce the structural responses even though radiation damping does not exist for an undamped site. If fundamental period of the soil-structure system is in the range of the fundamental period of the site, the displacements of the structure relative to the free field are generally very large and they may be responsible for the pounding of adjacent structures which was a major failure factor in the 1985 Mexico City earthquake. More damage would occur at the upper levels of the structure resting on flexible soil due to the foundation rocking. The embedment of the foundation will stiffen the soil-structure system and the period-shift is smaller than that for the surface structure but the radiation damping increases considerably. Nonlinear soil behaviour may reduce the structural

response because of the energy dissipation. Large foundation settlement may result from the nonlinear soil deformation. Pore water pressure generation is large in the soil underneath the foundation and failure may first occur at the edge of the foundation.

The examples given above are deliberately designed to show the influence of soil-structure interaction effects rather than normal design practice. The surface foundation may not be the most practical example since pile foundations may be more likely to be used for many structures. The soil-structure interaction would still affects the dynamic characteristics of the structure even when pile foundations are used.

Chapter 9

Conclusion

This research has mainly covered the analysis procedure and computer implementation of theoretical models for seismic soil structure interaction which involves three aspects: the energy transmitting boundary, the finite element modelling and the dynamic solution procedure.

In Chapter 2, the boundary element method was presented. The evaluation of the Green's functions for both surface foundation and embedded foundation has been given for the two dimensional problem. An analytical solution to evaluate the local response of a homogenous layer and the global reaction due to the local load was derived from which better accuracy can be achieved over the numerical procedure. The inefficiency of the boundary element for a large near-field finite element mesh is avoided by developing the simplified vertical boundary for the horizontally layered half space. The exact surface wave mode shapes have been used and the error due to discretization was minimized. The computational cost of the simplified boundary was small compared with the boundary element model and good accuracy has been achieved. The Rayleigh viscous boundary given by Lysmer and Kuhlemeyer (L6) may be considered as a special case of the simplified boundary for a homogenous half space in which the displacement compatibility of the near-field and the far-field is not imposed. It has also been found that for high frequencies, the frequency independent viscous boundary can be used with the simplified vertical boundary to achieve a slightly better accuracy.

Soil models based on plasticity theory are briefly discussed in Chapter 3. The finite element implementation of the bounding surface soil model has been given. The model has shown a good agreement with experiment for both monotonic and cyclic loading and is relatively simple to implement. The bounding surface model has been also used for the beam element to simulate the nonlinear moment-curvature relationship and may be suitable to simulate the interaction between the axial forces, shear forces and the bending moments of the beam. For the bending problem, the model has some advantages over the

most commonly used Romberg-Osgood nonlinear model and is very simple to implement.

In Chapter 4, the computer implementation of the energy transmitting boundaries has been given. The numerical transform is also briefly discussed. The formulae for symmetric and antisymmetric foundations are given.

Some approximate models of the far-field for time domain analysis are briefly discussed in Chapter 5. An approximate model is proposed in which the far-field dynamic stiffness matrix is specified at the fundamental frequency of the soil-structure system. For a better accuracy on the high frequency mode, an added mass matrix may also be used. For most structures, specifying the far-field dynamic stiffness matrix at the fundamental frequency of the soil-structure system without the added mass matrix can give reasonably good accuracy. Numerical examples are given for surface foundations to verify the approximate model. The finite element mesh may be equipped with a simplified vertical boundary and a viscous horizontal boundary specified at the fundamental frequency of the soil-structure system. The instability arising from the negative diagonal elements of the stiffness and damping matrices from the vertical boundaries can be overcome by converting the negative diagonal element in the stiffness matrix to an added mass at the fundamental frequency of the soil-structure system and replacing the negative diagonal element in the damping matrix with the viscous damping coefficient of the corresponding degree of freedom. The modification affects only the higher modes which is less important for the seismic structural response.

The methods for free-field analysis are discussed in Chapter 6. The need for the evaluation of the scattering motion can be avoided. It has been proposed that for a finite element mesh with energy transmitting boundaries, the equivalent nodal forces evaluated from the stresses of the free-field motion may be used as the input loading for the soil-structure system if inclined seismic waves are travelling in the free-field. For the vertically propagating waves, the input loading may be obtained by applying the dynamic free-field displacements statically to the finite elements along the boundary. For a site underlain by a rigid rock at a depth modelled by finite element mesh, the relative displacement can be used to solve the nonlinear problem.

In Chapter 7, the partitioned analysis procedures are discussed. The stability and the accuracy of each algorithm are evaluated numerically. Some

stability limits have been found for those procedures reported as unconditionally stable in the literature. The Node-by-Node implicit partition has been found to be the only one unconditionally stable procedure with proper predictors.

In Chapter 8, a primary investigation of the soil-structure interaction has been carried out for two hypothetical sites. The components of the input waves with the period near to the fundamental period of the site are amplified thus the spectral acceleration has a sharp peak at this period. The ground motion at a site with a soft soil has very different characteristics from the motion on the stiff soil and the equal displacement principle may not be applied to the nonlinear structure. It has been found that if the fundamental period of the soil-structure system is less than the period of the site for the fundamental wave mode, ignoring soil-structure interaction in the dynamic analysis could lead an unsafe design while if the fundamental period of the soil-structure system is larger than that of the site, the soil-structure interaction effects will reduce the structural response. The period shift due to inelastic deformation or flexible soil has a much larger influence on the structural response than the energy dissipation by plastic deformation in the upper structure and radiation damping by soil do. For the period evaluation of the structure on a flexible soil it is very important to take into account the soil flexibility. Possible foundation failure may have to be evaluated by nonlinear modelling of the near-field soil. Large settlements can arise for a structure on a soft soil even when subjected to only vertical propagating shear waves. The failure of the foundation soil may start at the edge of the foundation first due to the stresses concentration and small confined stresses. Large pore water pressures are generated and this may lead to soil liquefaction underneath the structure. It seems that the energy dissipation by the soil has considerable effect on the structural responses.

The models proposed here are for the soil-structure interaction under seismic loading. For other types of loading, such as blast loading and machine generated loading, further modification would have to be carried out.

References

A1 Aboim, C.A. and Roth, W.H., Bounding-Surface-Plasticity Theory Applied to Cyclic Loading of Sand. Numerical Models in Geomechanics, Edited by R. Dungar, G.N. Pande and J.A. Stunder, A.A. Balkema/Rotterdam, 1982.

A2 Atkinson, J.H., The Mechanics of Soils, An Introduction to Critical State Soil Mechanics, McGraw-Hill Book Company (UK) Limited, 1978.

B1 Banerjee, P.K. and Stipho, A.S., An Elastoplastic Model for Heavily Over-consolidated Clays. International Journal for Numerical and Analytical Methods in Geomechanics, Vol. 3, 1979, pp 97-103.

B2 Banerjee, P.K. and Stipho, A.S., Associated and Non-associated Constitutive Relations for Undrained Behaviour of Isotropic Soft Clays. International Journal for Numerical and Analytical Methods in Geomechanics, Vol. 2, 1978, pp 35-56.

B3 Bathe, K.J. and Wilson E.L., Numerical Method in Finite Element Analysis, Prentice-Hall, Inc., Englewood Cliffs, New Jersey, 1976.

B4 Bayo, E. and Wilson, E.L., Numerical Techniques for the Evaluation of Soil-Structure Interaction Effects in the Time Domain. Earthquake Engineering Research Centre, University of California, Berkeley, Report No. UCB/EERC-83/04, December 1983.

B5 Belytschko, T. and Mullen, R., Mesh Partition of Explicit-Implicit Time Integration. Formulations and Computational Algorithms in Finite Element Analysis, edited by Bathe, K.J., Oden, J.T. and Wunderlich, W., MIT Press,Cambridge, MA, 1976, pp 673-690.

B6 Belytschko, T. and Mullen, R., Stability of Explicit-Implicit Mesh Partition in Time Integration. International Journal of Numerical Methods in Engineering Vol. 12, 1978, pp 1575-1586.

B7 Belytschko, T., Yen, H.J. and Mullen, R., Mixed Methods for Time Integration, Computer Methods in Applied Mechanics and Engineering Vol. 27, 1981, pp 139-154.

B7 Bertero, V.V., Observations on Structural Pounding. Proceedings of the International Conference, The Mexico Earthquakes-1985, Factors Involved and Lessons Learned. Edited by M.A. Cassaro and E.M. Romero, the American Society of Civil Engineers, 1987, pp 264-278.

B8 Borja-Navrrete, G., Diaz-Canales, M., Vazquez-Vera, A. and Valle-Calderon, E. del, Damage Statistics of the September 19, 1985 Earthquake in Mexico City. Proceedings of the International Conference, The Mexico Earthquakes-1985, Factors Involved and Lessons Learned. Edited by M.A. Cassaro and E.M. Romero, the American Society of Civil Engineers, 1987, pp 70-77.

B9 Brebbia, C.A., Telles, J.C.F., and Wrobel L.C., Boundary Element Techniques, Theory and Applications in Engineering. Springer-Verlag Berlin, Heidelberg, 1984.

B10 Burland, J.B., The Yielding and Dilation of Clay. Correspondence, Geotechnique, Vol. 15, 1965, pp 211-214.

C1 Cheung, K.C., Behaviour of Axially Loaded Piles. Research Report 88-10, Department of Civil Engineering, University of Canterbury, Christchurch, New Zealand, December, 1988.

C2 Clough, R.W. and Penzien, J., Dynamics of Structures, McGraw-Hill Inc., 1975.

C3 Cohen, M. and Jennings, P.C., Silent Boundary Methods for Transient Analysis. Computational Methods for Transient Analysis, edited by T. Belytschko and T.J.R Hughes, Elsevier Science Publishers B.V., 1983, pp 301-360.

C4 Cooley, J.W. and Tukey, J.W., An Algorithm for the Machine Calculation of Complex Fourier Series. Mathematics of Computation, Vol. 19, 1965, pp 297-301.

D1 Dafalias, Y.F., Bounding Surface Plasticity. I: Mathematical Foundation and Hypoplasticity, Journal of Engineering Mechanics, ASCE, Vol. 112, EM9, 1986, pp 966-987.

D2 Dafalias, Y.F. and Anandarahah, A., Bounding Surface Plasticity. III: Application to Anisotropic Cohesive Soils, Journal of Engineering Mechanics, ASCE, Vol. 112, EM12, 1986, pp 1292-1318.

D3 Dafalias, Y.F. and Herrmann L.R., A bounding Surface Soil Plasticity Model. Proceedings on the International Symposium on Soils under Cyclic and Transient Loading, edited by G.N. Pande and O.C. Zienkiewicz, A.A. Balkema/Rotterdam, Vol. 1, 1980, pp 334-343.

D4 Dafalias, Y.F. and Herrmann L.R., A bounding Surface Formulation of Soil Plasticity. Soils Mechanics-Transient and Cyclic Loads, edited by G.N. Pande and O.C. Zienkiewicz, John Wiley & Sons Ltd, 1982, pp 253-282.

D5 Dafalias, Y.F. and Herrmann L.R., Bounding Surface Plasticity. II: Application to Isotropic Cohesive Soils. Journal of Engineering Mechanics, ASCE, Vol. 112, EM12, 1986, pp 1263-1291.

D6 Dafalias, Y.F. and Popov, E.P., A Model for Nonlinear Materials for Complex Loading. Acta Mechanica, Vol. 21, 1975, pp 173-192.

D7 Dafalias, Y.F. and Popov, E.P., Plastic Internal Variables Formalism of Cyclic Plasticity. Journal of Applied Mechanics, Vol. 43, 1976, pp 645-651.

D8 Davis P.J. and Rabinowitz, P., Methods of Numerical Integration. 2nd edition, Academic Press Inc., 1984.

D9 Desai, C.S. and Siriwardane, H.J., Constitutive Laws for Engineering Materials with Emphasis on Geologic Materials, Prentice-Hall, Inc., Englewood Cliffs, New Jersey, 1984.

D10 DiMaggio F.L. and Sandler I.S., Material Model for Granular Soils. Journal of Engineering Mechanics Division, ASCE, Vol. 97, EM3, 1971, pp 935-950.

F1 Felippa, C.A. and Park, K.C., Direct Time Integration Methods in Nonlinear Structural Dynamics. Computer Methods in Applied Mechanics and Engineering, Vol. 17/18, 1979, pp 277-313.

F2 Felippa, C.A. and Park, K.C., Staggered Solution Transient Analysis Procedures for Coupled Mechanical Systems:Formulation, Computer Methods in Applied Mechanics and Engineering, Vol. 24, 1980, pp 21-111.

G1 Ghaffar-Zadeh, M. and Chapel, F., Frequency-Independent Impedances of Soil-Structure Systems in Horizontal and Rocking Models. Earthquake Engineering and Structural Dynamics, Vol. 11, 1983, pp 523-540.

G2 Girault, P.D., Analysis of Foundation Failures. Proceedings of the International Conference, The Mexico Earthquakes-1985, Factors Involved and Lessons Learned. Edited by M.A. Cassaro and E.M. Romero, the American Society of Civil Engineers, 1987, pp 178-192.

G3 Graham, C.J., Nonlinear Soil Modelling, Report No. 294, Department of Civil Engineering, School of Engineering, University of Auckland, 1982.

H1 Hardin, B.O., Plane Strain Constitutive Equations for Soils. Journal of Geotechnical Engineering, ASCE, Vol. 109, 1983, pp 388-407.

H2 Houbolt, J.C., A Recurrence Matrix Solution for the Dynamic Response of Elastic Aircraft. Journal of Aeronautical Science, Vol. 17, 1950, pp 540-550.

H3 Hughes, T.J.R. and Liu, W.K., Implicit-Explicit Finite Element in Transient Analysis: Stability Theory, Journal of Applied Mechanics, Vol. 45, 1978, pp 371-374.

H4 Hughes, T.J.R. and Liu, W.K., Implicit-Explicit Finite Element in Transient Analysis: Implementation and Numerical Examples, Journal of Applied Mechanics, Vol. 45, 1978, pp 375-378.

I1 Idriss, I.M., Lysmer, J., Hwang, R. and Seed, H.B., Quad-4 A Computer Program for Evaluating the Seismic Response of Soil Structures by Variable Damping Finite Element Procedures. Earthquake Engineering Research Centre, University of California, Berkeley, Report No. UCB/EERC-73/16, December 1973.

I2 Ishida, K., Dynamic Characteristics of Soil-Foundation Interaction System Detected from Forced Vibration Test and Earthquake Observation. Earthquake Engineering and Structural Dynamics, Vol. 13, 1985, pp799-825.

J1 Joyner, W.B. and Chen, A.T.F., Calculation of Nonlinear Ground response in Earthquakes, Bull. Seismological Soc. Amer., Vol. 65, 1981, pp 1315-1336.

K1 Kanaan, A. and Powell, G.H., General Purpose Computer Program for Inelastic Dynamic Response of Plane Structures. Earthquake Engineering Research Centre, University of California, Berkeley, Report No. UCB/EERC-73/6, 1973.

K2 Kausel E. and Roesset J.M., Stiffness Matrices for Layered Soils. Bull. Seismological Soc. of Amer., Vol. 71, 1981, pp 1743-1767.

K3 Kobori, T., Setogawa, S., Hosatoku, T. and Nagase, T., Nonlinear Uplift Response of Soil-Structure-Interaction System Considering Dynamic Ground Compliance. Proc. 7th Eur. Conf. Earthquake Engr., Athens 2, 1982, pp647-654.

K4 Krieg, R.D., A Practical Two-Surface Plasticity Model. Journal of Applied Mechanics, Vol. 42, 1975, pp 641-646.

L1 Larkin, T.J., Propagation of Seismic Waves Through Non Linear Soil Media, Report No. 144, School of Engineering, University of Auckland, 1976.

L2 Liao, Z.P. and Wong, H.L., A Transmitting Boundary for the Numerical Simulation of Elastic Wave Propagation. Soil Dynamics and Earthquake Engineering, Vol. 3, 1984, pp 174-183.

L3 Liu, W.K. and Belytchko, T., Mixed-Time Implicit-Explicit Finite Elements for Transient Analysis, Computers & Structures, Vol. 15, 1982, pp 445-450.

L4 Luco, J.E., Soil-Structure Interaction Effects on the Seismic Response of Tall Chimneys. Soil Dynamics and Earthquake Engineering, Vol. 5, 1986, pp 170-177.

L5 Lysmer, J., Analytical Procedures in Soil Dynamics. Earthquake Engineering Research Centre, University of California, Berkeley, Report No. UCB/EERC-78/29, December, 1978.

L6 Lysmer, J. and Kuhlemeyer, R.L., Finite Dynamic Model for Infinite Media. Journal of Engineering Mechanics Division, ASCE, Vol. 98, 1969, pp 859-877

M1 Medina, F., Modelling of Soil-Structure Interaction by Finite and Infinite Elements. Earthquake Engineering Research Centre, University of California, Berkeley, Report No. UCB/EERC-80/43, December 1980.

M2 Meli, R., Evaluation of Performance of Concrete Buildings Damaged by the September 19, 1985 Mexico Earthquake. Proceedings of the International Conference, The Mexico Earthquakes-1985, Factors Involved and Lessons Learned. Edited by M.A. Cassaro and E.M. Romero, the American Society of Civil Engineers, 1987, pp 308-327.

M3 Mroz, Z., On the Description of Anisotropic Work Hardening. J. Mech. Phys. Solids, Vol. 15, 1967, pp 163-175.

M4 Mroz, Z., Norris, V.A. and Ziekiewicz, O.C., Application of an Anisotropic Hardening Model in the Analysis of Elasto-plastic Deformation of Soils. Geotechnique, Vol. 29, 1979, pp 1-34.

N1 Naylor, D.J., Stresses in Nearly Incompressible Materials by Finite Elements with Applications to the Calculation of Excess Pore Water Pressures. International Journal for Numerical Methods in Engineering, Vol. 8, 1974, pp 443-460.

N2 Nelson I. and Baron M.L., Application of Variable Moduli Models to Soil Behaviour. Int. J. Solids Structures, Vol. 7, 1971, pp 399-417.

N3 Newmark, N.M., A Method of Computation for Structural Dynamics. Journal of Engineering Mechanics Division, ASCE, Vol. 85, 1959, pp 67-94.

O1 Okamoto, S., Introduction to Earthquake Engineering, University of Tokyo Press, 1973.

P1 Pande, G.N. and Pietruszczak, S., A Critical Look at Constitutive Models for Soils. Geomechanical Modelling in Engineering Practice, edited by R. Dungar and J.A. Studer, A.A. Balkema/Rotterdam/Boston, 1986, pp 369-395.

P2 Park, K.C., Felippa, C.A. and DeRuntz, J.A., Stabilization of Staggered Solution Procedures for Fluid Structure Analysis. Computational Methods for Fluid-Structure Interaction Problems, edited by Belytschko T. and Geers T.L., ASME Applied Mechanics Symposia Series. AMD-Vol. 26, 1977, pp 94-124.

P3 Park, K.C., Partitioned Transient Analysis Procedures for Coupled Field Problems: Stability Analysis, Journal of Applied Mechanics, Vol. 47, 1980, pp 370-376.

P4 Park, K.C. and Felippa, C.A., Partitioned Transient Analysis Procedures for Coupled Field Problems: Accuracy Analysis, Journal of Applied Mechanics, Vol. 47, 1980, pp 919-826.

P5 Park, K.C. and Felippa, C.A., Partitioned Analysis of Coupled Systems. Computational Methods in Transient Analysis, edited by Belytchko, T. and Hughes, T.J.R.. Elsevier Science Publishers B.V., 1983, pp 157-219.

P6 Park, K.C. and Felippa, C.A., Recent Development in Coupled Field Analysis Method. Numerical Method in Coupled Systems, edited by Lewis, R.W., Bettess, P., Hinton, E.. John Wiley & Sons Ltd., 1984, pp 327-351.

P7 Park, R. and Paulay, T., Reinforced Concrete Structures, John Wiley & Sons Inc., 1975.

P8 Patterson, T.N.L., On High Precision Methods for the Evaluation of Fourier Integrals with Finite and Infinite Limits. Numer. Math., Vol. 24, 1976, pp 41-52.

P9 Prevost, J.H., Mathematical Modelling of Monotonic and Cyclic Undrained Clay Behaviour. International Journal for Numerical and Analytical Methods in Geomechanics, Vol. 1, 1977, pp 195-216.

P10 Prevost, J.H., Two-Surface versus Multi-Surface Plasticity Theories: A Critical Assessment. International Journal for Numerical and Analytical Methods in Geomechanics, Vol. 6, 1982, pp 323-338.

R1 Riggs, H.R. and Wass, G., Influence of Foundation Flexibility on Soil-Structure Interaction. Earthquake Engineering and Structural Dynamics, Vol. 13, 1985, pp 597-615.

R2 Roscoe, K.H. and Burland, J.B., On the Generalized Stress-Strain Behaviour of 'Wet Clay'. Engineering Plasticity, Cambridge University Press, 1968.

R3 Roscoe, K.H. and Schofield, A.N., Mechanical Behaviour of an Idealized 'Wet Clay'. Proc. 2nd European Cof. Soil Mech., 1963, pp 47-54.

R4 Roscoe, K.H., Schofield, and Thurairajah, A. Yielding of Clays in States Wetter Than Critical. Geotechnique, Vol. 13, 1963, pp 211-240.

S1 Scawthorn, C., Celebi, M. and Prince, J., Performance Characteristics of Structures, 1985 Mexico City Earthquake. Proceedings of the International Conference, The Mexico Earthquakes-1985, Factors Involved and Lessons Learned. Edited by M.A. Cassaro and E.M. Romero, the American Society of Civil Engineers, 1987, pp 217-232.

S2 Schnabel, P.B., Lysmer, J. and Seed, H. B., SHAKE—A Computer Program for Earthquake Response Analysis of Horizontally Layered Sites. Earthquake Engineering Research Centre, University of California, Berkeley, Report No. UCB/EERC-72/12, 1972.

S3 Seed, H.B. and Idriss, I.M., Soil Moduli and Damping Factors for Dynamic Response Analyses. Earthquake Engineering Research Centre, University of California, Berkeley, Report No. UCB/EERC-70/10, 1970.

S4 Seed, H.B. Wong, R.T., Idriss, I.M. and Tokimatsu, K., Moduli and Damping Factors for Dynamic Analyses of Cohesionless Soils. Earthquake Engineering Research Centre, University of California, Berkeley, Report No. UCB/EERC-84/14, 1984.

S5 Seed, H.B. Lysmer, J. and Hwang, R., Soil-Structure Interaction Analyses for Evaluating Seismic Response. Earthquake Engineering Research Centre, University of California, Berkeley, Report No. UCB/EERC-74/6, 1974.

S6 Seed, I.B., Method of Earthquake Resistant Design of Earthdams. Journal of Soil Mechanics and Foundation Division, ASCE, Vol 92, SM 1, 1967, pp 13-41.

S7 Seed, H.B. and Idriss, I.M., The Influence of Soil Conditions on Ground Motions During Earthquakes. Journal of the Soil Mechanics and Foundations Engineering Division, ASCE, Vol. 94, SM1, 1969, pp 93-137.

S8 Seed, H.B., Romo, M.P., Sun, J., Jaime, A., and Lysmer, J., Relationship Between Soil Conditions and Earthquake Ground Motions in Mexico City in the Earthquake of Sept. 19, 1985. Earthquake Engineering Research Centre, University of California, Berkeley, Report No. UCB/EERC-87/15, 1987.

S9 Siriwardane, H.J. and Desai, C.S., Computational Procedures for Non-linear Three-Dimensional Analysis with Some Advanced Constitutive Laws. International Journal for Numerical and Analytical Methods in Geomechanics, Vol. 7, 1983, pp 143-171.

S10 Smith, I.M., Programming the Finite Element Method with Applications to Geomechanics, John Wiley & Sons Ltd, 1982.

S11 Smith, W.D., A Nonreflection Plane Boundary for Wave Propagation Problems. J. Computational Physics, Vol. 15, 1974, pp 492-503.

S12 Spyrakos, C.C. and Beskos, D.E., Dynamic Response of Rigid Strip-foundations by a Time-Domain Boundary Element Method. International Journal for Numerical Methods in Engineering, Vol. 23, 1986, pp1547-1565.

S13 Stricklin, J.A. and Walter, E.H., Formulation and Solution Procedures for Nonlinear Structural Analysis. Computers & Structures, Vol. 7, pp 125-136.

T1 Traub, J.F., Iterative Method for the Solution of Equations. Printice-Hall, Inc., Englewood Cliff, N.J., 1964.

T2 Tzong, Tsair-Jyh and Penzien, J., Hybrid Modelling of Soil-Structure Interaction in Layered Media. Earthquake Engineering Research Centre, University of California, Berkeley, Report No. UCB/EERC-83/22, 1983.

W1 White, W., Valliappan, S. and Lee, I.K., Unified Boundary for Finite Dynamic Models. Journal of Engineering Mechanics Division, ASCE, Vol. 103, EM5, 1977, pp 949-964.

W2 Wilson E.L. and Dovey H.H., Solution or Reduction of Equilibrium Equations for Large Complex Structural Systems. Advances in Engineering Software, Vol. 1, 1978, pp 19-25

W3 Wolf, J.P. and Darbre, G.R., Dynamic-Stiffness Matrix of Soil by the Boundary Element Method: Conceptual Aspects. Earthquake Engineering and Structural Dynamics, Vol. 12, 1984, pp 385-400.

W4 Wolf, J.P. and Darbre, G.R., Dynamic-Stiffness Matrix of Soil by the Boundary Element Method: Embedded Foundation. Earthquake Engineering and Structural Dynamics, Vol. 12, 1984, pp 401-416.

W5 Wolf, J.P. and Somaini, D.R., Approximate Dynamic Model of Embedded Foundation in Time Domain. Earthquake Engineering and Structural Dynamics, Vol. 14, 1986, pp 683-703.

W6 Wolf, J.P. and Darbre, G.R., Non-linear Soil-Structure Interaction Analysis Based on the Boundary Element Method in Time Domain with Application to Embedded Foundation. Earthquake Engineering and Structural Dynamics, Vol. 14, 1986, pp 83-101.

W7 Wolf, J.P., Dynamic Soil-Structure Interaction, Prentice-Hall, Englewood Cliffs, New Jersey, 1985.

W8 Wolf, J.P., Soil-Structure Interaction Analysis in Time Domain, Prentice Hall, Englewood Cliffs, New Jersey, 1988.

W9 Wolf, J.P., A Comparison of Time Domain Transmitting Boundaries. Earthquake Engineering and Structural Dynamics, Vol. 14, 1986, pp 655-673.

W10 Wolf, J.P. and Obernhuber, P., Non-linear Soil-Structure Interaction Analysis Using Green's Function of Soil in Time Domain. Earthquake Engineering and Structural Dynamics, Vol. 13, 1985, pp 213-223.

W11 Wolf, J.P. and Obernhuber, P., Non-linear Soil-Structure Interaction Analysis Using Dynamic Stiffness or Flexibility of Soil in Time Domain. Earthquake Engineering and Structural Dynamics, Vol. 13, 1985, pp 195-212.

W12 Wolf, J.P., Seismic Analyses of Cooling Towers. Engineering Structures, Vol. 8, 1986, pp 191-198.

W13 Wong, H.L. and Luco, J.E., Dynamic Interaction Between Rigid Foundations in a Layered Half-Space. Soil Dynamics and Earthquake Engineering, Vol. 5, 1986, pp 149-158.

Z1 Zhao, X., Carr, A.J. and Moss, P.J., Soil-Structure Interaction Using Boundary Elements in the Time-Domain. Proceedings of The Eleventh Australasian Conference on the Mechanic of Structures and Materials, Auckland, New Zealand, 1988, pp 27-32.

Z2 Zienkiewicz, O.C., The Finite Element Method, 3rd ed., McGraw-Hill, London, 1977.

Appendix

Dynamic Stiffness Matrices for In-plane Motion

The displacements of a homogenous layer under a harmonic loading can be written as (from Eq.2.26)

$$u(z) = L(e^{ikrz}A_p + e^{-ikrz}B_p) - Ms(e^{iksz}A_{sv} - e^{-iksz}B_{sv}) \quad (A.1a)$$

$$w(z) = Lr(-e^{ikrz}A_p + e^{-ikrz}B_p) - M(e^{iksz}A_{sv} + e^{-iksz}B_{sv}) \quad (A.1b)$$

where L and M are the cosines of the incident angle for P-wave and S-wave respectively and r and s are defined in Eq.2.25. The wave amplitudes are defined as the constants A and B for the wave travelling in the negative and positive z-direction respectively. The subscripts p and sv indicate the P-wave and S-wave respectively. The wave number k is defined in Eq. 2.25b. For the convenience and simplicity, the following variables are introduced

$$A_1 = L(A_p + B_p) \quad (A.2a)$$

$$A_2 = L(A_p - B_p) \quad (A.2b)$$

$$A_3 = M(A_{sv} + B_{sv}) \quad (A.2c)$$

$$A_4 = M(A_{sv} - B_{sv}) \quad (A.2d)$$

and

$$e^{ikrz} = cos(krz) + isin(krz) \quad (A.2e)$$

$$e^{iksz} = cos(ksz) + isin(ksz) \quad (A.2f)$$

Eq. A.1 can be rewritten as

$$u(z) = A_1 cos(krz) + iA_2 sin(krz) - s[iA_3 sin(ksz) + A_4 cos(ksz)] \quad (A.3a)$$

$$w(z) = -r[iA_1 sin(krz) + A_2 cos(krz)] - A_3 cos(ksz) - iA_4 sin(ksz)] \quad (A.3b)$$

If the origin of the coordinate is set at the top surface of the layer and the positive z-direction is downwards, setting z = 0 and z = d in Eq. A.3, the displacements at the top and the bottom surface are defined as

$$U_1 = A_1 - sA_4 \quad (A.4a)$$

$$W_1 = -. rA_2 - A_3 \quad (A.4b)$$

$$U_2 = A_1 cos(krd) + iA_2 sin(krd) - isA_3 sin(ksd) - sA_4 cos(ksd) \quad (A.4c)$$

$$W_2 = -irA_1 sin(krd) - rA_2 cos(krd) - A_3 cos(ksd) - iA_4 sin(ksd) \quad (A.4d)$$

where d is the depth of the layer and U and W are the displacements at the boundary in horizontal and vertical direction respectively. The subscript 1 for the displacements indicates the top surface while 2 indicates the bottom surface. A_2 and A_4 can be eliminated from Eq. A.4 so that A_1 and A_3 can be solved as

$$\begin{aligned} A_1 = \{&[rs(1 - cos(krd)cos(ksd)) + sin(krd)sin(ksd)]U_1 - \\ &is[sin(krd)cos(ksd) + rscos(krd)sin(ksd)]W_1 + \\ &rs[cos(krd) - cos(ksd)]U_2 + is[sin(krd) + rssin(ksd)]W_2\}/D \end{aligned} \quad (A.5a)$$

$$\begin{aligned} A_3 = \{&-is[cos(krd)sin(ksd) + rssin(krd)cos(ksd)]U_1 - \\ &[rs(1 - cos(krd)cos(ksd)) + sin(krd)sin(ksd)]W_1 + \\ &is[sin(ksd) + rssin(krd)]U_2 + rs[cos(krd) - cos(ksd)]W_2\}/D \end{aligned} \quad (A.5b)$$

Eliminating A_1 and A_3 from Eq. A.4 and A_2 and A_4 can be solved for as

$$A_2 = \{i[cos(krd)sin(ksd) + rssin(krd)cos(ksd)]U_1 - s[1 - cos(krd)cos(ksd) + rssin(krd)sin(ksd)]W_1 - i[sin(ksd) + rssin(krd)]U_2 - s[cos(krd) - cos(ksd)]W_2\}/D \quad (A.5c)$$

$$A_4 = \{-r[1 - cos(krd)cos(ksd) + rssin(krd)sin(ksd)]U_1 - i[sin(krd)cos(ksd) + rscos(krd)sin(ksd)]W_1 + r[cos(krd) - cos(ksd)]U_2 + i[sin(krd) + rssin(ksd)]W_2\}/D \quad (A.5d)$$

where

$$D = 2rs[1 - cos(krd)cos(ksd)] + (1 + r^2s^2)sin(krd)sin(ksd) \quad (A.5e)$$

Eq. A.3 can be rearranged in terms of the boundary displacements as

$$u(z) = E^uU_1 + F^uW_1 + G^uU_2 + H^uW_2 \quad (A.6a)$$

$$w(z) = E^wU_1 + F^wW_1 + G^wU_2 + H^wW_2 \quad (A.6b)$$

where

$$E^u = \{rs[1 - cos(krd)cos(ksd)][cos(krz) + cos(ksz)] + sin(krd)sin(ksd)[cos(krz) + r^2s^2cos(ksz)] - [cos(krd)sin(ksd) + rssin(krd)cos(ksd)][sin(krz) + rssin(ksz)]\}/D \quad (A.6c)$$

$$F^u = is\{[cos(krd)cos(ksd) - 1][sin(krz) - rssin(ksz)] + sin(krd)sin(ksd)[sin(ksz) - rssin(krz)] - [sin(krd)cos(ksd) + rscos(krd)sin(ksd)][cos(krz) - cos(ksz)]\}/D \quad (A.6d)$$

$$G^u = \{rs[cos(krd) - cos(ksd)][cos(krz) - cos(ksz)] + [sin(ksd) + rssin(krd)][sin(krz) + rssin(ksz)]\}/D \quad (A.6e)$$

$$H^u = is\{[sin(krd) + rssin(ksd)][cos(krz)-cos(ksz)] - [cos(krd) - cos(ksd)][sin(krz) + rssin(ksz)]\}/D \quad (A.6f)$$

$$E^{v} = ir\{-[cos(krd)sin(ksd) + rssin(krd)cos(ksd)][cos(krz) - cos(ksz)] + [1 - cos(krd)cos(ksd)][sin(ksz) - rssin(krz)] - sin(krd)sin(ksd)[sin(krz) - rssin(ksz)]\}/D \qquad (A.6g)$$

$$F^{v} = \{-[sin(krd)cos(ksd) + rscos(krd)sin(ksd)][sin(ksz) + rs\, sin(krz)] + rs[(1 - cos(krd)cos(ksd)][cos(krz) + cos(ksz)] + sin(krd)sin(ksd)[cos(ksz) + r^2s^2cos(krz)]\}/D \qquad (A.6h)$$

$$G^{v} = ir\{-[cos(krd) - cos(ksd)][sin(ksz) + rssin(krz)] + [sin(ksd) + rssin(krd)][cos(krz) - cos(ksz)]\}/D \qquad (A.6i)$$

$$H^{v} = \{[sin(krd) + rssin(ksd)][sin(ksz) + rssin(krz)] + rs[cos(krd) - cos(ksd)][cos(krz) - cos(ksz)]\}/D \qquad (A.6j)$$

The first order derivatives of the displacement shape functions with respect to z are

$$\frac{\partial E^{u}}{\partial z} = \frac{kr}{D}\{s[cos(krd)cos(ksd) - 1][rsin(krz) + ssin(ksz)] - sin(krd)sin(ksd)[sin(krz) + rs^3sin(ksz)] - [cos(krd)sin(ksd) + rssin(krd)cos(ksd)][cos(krz) + r^2cos(ksz)]\} \qquad (A.7a)$$

$$\frac{\partial F^{u}}{\partial z} = \frac{iks}{D}\{r[cos(krd)cos(ksd) - 1][cos(krz) - s^2cos(ksz)] + ssin(krd)sin(ksd)[cos(ksz) - s^2cos(krz)] + [sin(krd)cos(ksd) + rscos(krd)sin(ksd)][rsin(krz) - ssin(ksz)]\} \qquad (A.7b)$$

$$\frac{\partial G^{u}}{\partial z} = \frac{kr}{D}\{-s[cos(krd) - cos(ksd)][rsin(krz) - ssin(ksz)] + [sin(ksd) + rssin(krd)][cos(krz) + s^2cos(ksz)]\} \qquad (A.7c)$$

$$\frac{\partial H^{u}}{\partial z} = \frac{iks}{D}\{-[sin(krd) + rssin(ksd)][rsin(krz) - ssin(ksz)] - r[cos(krd) - cos(ksd)][cos(krz) + s^2sin(ksz)]\} \qquad (A.7d)$$

$$\frac{\partial E^v}{\partial z} = \frac{ikr}{D}\{[cos(krd)sin(ksd) + rssin(krd)cos(ksd)]$$
$$[rsin(krz) - ssin(ksz)] +$$
$$s[1 - cos(krd)cos(ksd)][cos(ksz) - r^2cos(krz)] -$$
$$rsin(krd)sin(ksd)[cos(krz) - s^2cos(ksz)]\} \quad (A.7e)$$

$$\frac{\partial F^v}{\partial z} = \frac{ks}{D}\{-[sin(krd)cos(ksd) + rscos(krd)sin(ksd)]$$
$$[cos(ksz) + r^2cos(krz)] -$$
$$r[(1 - cos(krd)cos(ksd)][rsin(krz) + ssin(ksz)] -$$
$$sin(krd)sin(ksd)[sin(ksz) + r^3ssin(krz)]\} \quad (A.7f)$$

$$\frac{\partial G^v}{\partial z} = \frac{ikr}{D}\{-s[cos(krd) - cos(ksd)][cos(ksz) + r^2cos(krz)] +$$
$$[sin(ksd) + rssin(krd)][rsin(krz) - ssin(ksz)]\} \quad (A.7g)$$

$$\frac{\partial H^v}{\partial z} = \frac{ks}{D}\{[sin(krd) + rssin(ksd)][cos(ksz) + r^2cos(krz)] -$$
$$r[cos(krd) - cos(ksd)][rsin(krz) - ssin(ksz)]\} \quad (A.7g)$$

The stresses of the layer may be obtained from

$$\sigma_{zz} = (\lambda + 2G)\frac{\partial w}{\partial z} + \lambda \frac{\partial u}{\partial x} \quad (A.8a)$$

$$\tau_{xz} = G(\frac{\partial w}{\partial z} + \frac{\partial u}{\partial x}) \quad (A.8b)$$

where the Lame constant λ can be related to the shear modulus G by

$$\lambda + 2G = \frac{1 + s^2}{1 + r^2} G \quad (A.9a)$$

$$\lambda = \frac{s^2 - 2r^2 - 1}{1 + r^2} G \quad (A.9b)$$

Substituting Eq. A.6a, A.6b and A.9 into Eq. A.8 the stresses can be obtained as

$$\sigma_z = G\frac{1+s^2}{1+r^2}\left(\frac{\partial E^w}{\partial z}U_1 + \frac{\partial F^w}{\partial z}W_1 + \frac{\partial G^w}{\partial z}U_2 + \frac{\partial H^w}{\partial z}W_2\right) -$$

$$ikG\frac{s^2-2r^2-1}{1+r^2}\left(E^uU_1 + F^uW_1 + G^uU_2 + H^uW_2\right) \qquad (A.10a)$$

$$\tau_{xz} = G\left(\frac{\partial E^u}{\partial z}U_1 + \frac{\partial F^u}{\partial z}W_1 + \frac{\partial G^u}{\partial z}U_2 + \frac{\partial H^u}{\partial z}W_2\right) -$$

$$ikG\left(E^wU_1 + F^wW_1 + G^wU_2 + H^wW_2\right) \qquad (A.10a)$$

Setting $P_1 = -\tau_{xz}$ and $R_1 = -\sigma_{zz}$ at $z = 0$ and $P_2 = \tau_{xz}$ and $R_2 = \sigma_{zz}$ at $z = d$, the nodal stress and displacement relationship can be obtained as

$$\begin{Bmatrix} P_1 \\ iR_1 \\ P_2 \\ iR_2 \end{Bmatrix} = \frac{krs(1+s^2)G}{D}\begin{bmatrix} S_{11} & S_{12} & S_{13} & S_{14} \\ S_{21} & S_{22} & S_{23} & S_{24} \\ S_{31} & S_{32} & S_{33} & S_{34} \\ S_{41} & S_{42} & S_{43} & S_{44} \end{bmatrix}\begin{Bmatrix} U_1 \\ iW_1 \\ U_2 \\ iW_2 \end{Bmatrix} \qquad (A.11a)$$

in which the stiffness matrix is symmetric and where

$$S_{11} = \frac{1}{s}cos(krd)sin(ksd) + rsin(krd)cos(ksd) \qquad (A.11b)$$

$$S_{12} = \frac{3-s^2}{1+s^2}[1-cos(krd)cos(ksd)] + \frac{1+2r^2s^2-s^2}{rs(1+s^2)}sin(krd)sin(ksd) \qquad (A.11c)$$

$$S_{22} = \frac{1}{r}sin(krd)cos(ksd) + scos(krd)sin(ksd) \qquad (A.11d)$$

$$S_{13} = -rsin(krd) - \frac{1}{s}sin(ksd) \qquad (A.11e)$$

$$S_{23} = - \cos(krd) + \cos(ksd) \tag{A.11f}$$

$$S_{33} = S_{11} \tag{A.11g}$$

$$S_{14} = \cos(krd) - \cos(ksd) \tag{A.11h}$$

$$S_{24} = - \frac{1}{r}\sin(krd) - s\sin(ksd) \tag{A.11i}$$

$$S_{34} = - S_{12} \tag{A.11j}$$

$$S_{44} = S_{22} \tag{A.11k}$$

An imaginary unit i is used to multiply the vertical nodal displacements and stresses to achieve the symmetry of the dynamic stiffness matrix.

For a half space, no incoming waves from infinity exist and thus A_p and A_{sv} equal zero. If the following parameters are introduced

$$B_1 = LB_p \tag{A.12a}$$

$$B_2 = MB_{sv} \tag{A.12b}$$

Eq. A.1 may be written for the half space as

$$u(z) = B_1 e^{-ikrz} + sB_2 e^{-iksz} \tag{A.13a}$$

$$w(z) = rB_1 e^{-ikrz} - B_2 e^{-iksz} \tag{A.13b}$$

for which the origin is at the surface and the positive z-direction is downwards. If the displacements at the surface of the half space are U_0 and W_0 for x-direction and z-direction respectively, setting $z = 0$ in Eq. A.13, the constants B_1 and B_2 can be solved as

$$B_1 = \frac{1}{1 + rs}(U_0 + sW_0) \tag{A.14a}$$

$$B_2 = \frac{1}{1 + rs}(rU_0 - W_0) \tag{A.14b}$$

Substituting Eq. A.14 into Eq. A.13, Eq. A.13 can be written in terms of the surface displacements as

$$u(z) = \frac{1}{1 + rs}[(e^{-ikrz} + rse^{-iksz})U_0 + s(e^{-ikrz} - e^{-iksz})W_0] \tag{A.15a}$$

$$w(z) = \frac{1}{1 + rs}[r(e^{-ikrz} - e^{-iksz})U_0 + (rse^{-ikrz} + e^{-iksz})W_0] \tag{A.15b}$$

The first order derivatives with respect to z are

$$\frac{\partial u}{\partial z} = \frac{-ik}{1 + rs}[r(e^{-ikrz} + s^2e^{-iksz})U_0 + s(re^{-ikrz} - se^{-iksz})W_0] \tag{A.16a}$$

$$\frac{\partial w}{\partial z} = \frac{-ik}{1 + rs}[r(re^{-ikrz} - se^{-iksz})U_0 + s(r^2e^{-ikrz} + e^{-iksz})W_0] \tag{A.16b}$$

At the origin z = 0, the derivatives can be obtained as

$$\left.\frac{\partial u}{\partial z}\right|_{z=0} = \frac{-ik}{1 + rs}[r(1 + s^2)U_0 + s(r - s)W_0] \tag{A.17a}$$

$$\left.\frac{\partial w}{\partial z}\right|_{z=0} = \frac{-ik}{1 + rs}[r(r - s)U_0 + s(1 + r^2)W_0] \tag{A.17b}$$

Substituting Eq. A.17 and A.9 into A.8 and setting $P_0 = -\tau_{xz}$ and $R_0 = -\sigma_{zz}$ at the surface of the half space, the surface tractions and the surface displacements are related by

$$\begin{Bmatrix} P_0 \\ iR_0 \end{Bmatrix} = kG \begin{bmatrix} \frac{ir(1 + s^2)}{1 + rs} & 2 - \frac{1 + s^2}{1 + rs} \\ 2 - \frac{1 + s^2}{1 + rs} & \frac{is(1 + s^2)}{1 + rs} \end{bmatrix} \begin{Bmatrix} U_0 \\ iW_0 \end{Bmatrix} \tag{A.18}$$

For vertically propagating waves, the wave number k = 0, or high frequency waves, for which the frequency ω tends to ∞, kr and ks converge to ω/c_p and ω/c_s respectively. The parameter r and s both converge to ∞. Eq. A.11a becomes

$$\begin{Bmatrix} P_1 \\ iR_1 \\ P_2 \\ iR_2 \end{Bmatrix} = G\frac{\omega}{c_s}\begin{bmatrix} ctg(\omega d/c_s) & 0 & -csc(\omega d/c_s) & 0 \\ 0 & ctg(\omega d/c_p)c_p/c_s & 0 & -csc(\omega d/c_p)c_p/c_s \\ -csc(\omega d/c_s) & 0 & ctg(\omega d/c_s) & 0 \\ 0 & -csc(\omega d/c_p)c_p/c_s & 0 & ctg(\omega d/c_p)c_p/c_s \end{bmatrix}$$

$$\begin{Bmatrix} U_1 \\ iW^1 \\ U_2 \\ iW_2 \end{Bmatrix} \tag{A.19}$$

and Eq. A.18 becomes

$$\begin{Bmatrix} P_0 \\ iR_0 \end{Bmatrix} = iG\frac{\omega}{c_s}\begin{bmatrix} 1 & 0 \\ 0 & c_p/c_s \end{bmatrix}\begin{Bmatrix} U_0 \\ iW_0 \end{Bmatrix} \tag{A.20}$$

For static loading or very large wave number, r and s both converge to -i. Noticing that

$$sin(ix) = isinh(x) \tag{A.21a}$$

$$cos(ix) = cosh(x) \tag{A.21b}$$

Eq. A.11 can be written as

$$\begin{Bmatrix} P_1 \\ iR_1 \\ P_2 \\ iR_2 \end{Bmatrix} = \frac{2kG}{E}\begin{bmatrix} S_{11} & S_{12} & S_{13} & S_{14} \\ S_{21} & S_{22} & S_{23} & S_{24} \\ S_{31} & S_{32} & S_{33} & S_{34} \\ S_{41} & S_{42} & S_{43} & S_4 \end{bmatrix}\begin{Bmatrix} U_1 \\ iW_1 \\ U_2 \\ iW_2 \end{Bmatrix} \tag{A.22a}$$

where

$$S_{11} = (1 + \frac{c_s^2}{c_p^2})sinh(kd)cosh(kd) - (1 - \frac{c_s^2}{c_p^2})kd \tag{A.22b}$$

$$S_{12} = -(1 + \frac{c_s^2}{c_p^2})sinh^2(kd) + E \tag{A.22c}$$

$$S_{22} = (1 + \frac{c_s^2}{c_p^2})sinh(kd)cosh(kd) + (1 - \frac{c_s^2}{c_p^2})kd \tag{A.22d}$$

$$S_{13} = (1 - \frac{c_s^2}{c_p^2})kdcosh(kd) - (1 + \frac{c_s^2}{c_p^2})sinh(kd) \tag{A.22e}$$

$$S_{23} = -kd(1 - \frac{c_s^2}{c_p^2})sinh(kd) \tag{A.22f}$$

$$S_{33} = S_{11} \tag{A.22g}$$

$$S_{14} = kd(1 - \frac{c_s^2}{c_p^2})sinh(kd) \tag{A.22h}$$

$$S_{24} = -(1 - \frac{c_s^2}{c_p^2})kdcosh(kd) - (1 + \frac{c_s^2}{c_p^2})sinh(kd) \tag{A.22i}$$

$$S_{34} = -S_{12} \tag{A.22j}$$

$$S_{44} = S_{22} \tag{A.22k}$$

$$E = \left[1 + \frac{c_s^2}{c_p^2}\right]^2 sinh^2(kd) - \left[1 - \frac{c_s^2}{c_p^2}\right]^2 k^2d^2 \tag{A.22l}$$

Eq. A.18 becomes

$$\begin{Bmatrix} P_0 \\ iR_0 \end{Bmatrix} = 2kG \begin{bmatrix} \frac{1}{1 + c_s^2/c_p^2} & \frac{1}{1 + c_p^2/c_s^2} \\ \frac{1}{1 + c_p^2/c_s^2} & \frac{1}{1 + c_s^2/c_p^2} \end{bmatrix} \begin{Bmatrix} U_0 \\ iW_0 \end{Bmatrix} \tag{A.23}$$

For the static loading with zero wave number, kr and ks both converge to zero. Setting $\omega = 0$ in Eq. A.19 and A.20, the following equations can be obtained

$$\begin{Bmatrix} P_1 \\ iR_1 \\ P_2 \\ iR_2 \end{Bmatrix} = \frac{G}{d} \begin{bmatrix} 1 & 0 & -1 & 0 \\ 0 & c_p^2/c_s^2 & 0 & -c_p^2/c_s^2 \\ -1 & 0 & 1 & 0 \\ 0 & -c_p^2/c_s^2 & 0 & c_p^2/c_s^2 \end{bmatrix} \begin{Bmatrix} U_1 \\ iW^1 \\ U_2 \\ iW_2 \end{Bmatrix} \tag{A.24}$$

$$\begin{Bmatrix} P_0 \\ iR_0 \end{Bmatrix} = \begin{bmatrix} 0 & 0 \\ 0 & 0 \end{bmatrix} \begin{Bmatrix} U_0 \\ iW_0 \end{Bmatrix} \tag{A.25}$$

If material damping is present, the shear modulus G and the wave velocities c_s and c_p can be replaced with the complex ones defined in Eq. 2.38.